The Design and Synthesis of Imidazo-Phenanthridinium based Ligands.

Philip Joseph Kitson

A thesis submitted to the University of Glasgow
for the degree of Doctor of Philosophy

Department of Chemistry
May 2009

This Thesis is dedicated to my wife Katie,

for all her support over the past three years.

Acknowledgements

This project was carried out between October 2005 and December 2008 in the Department of Chemistry at the University of Glasgow, during which time I received the help and advice of many people, in particular:

Professor Lee Cronin, for giving me the opportunity to work on such an interesting and enjoyable project and for the constant encouragement throughout.

Dr. De-Liang Long, for his help with all the X-Ray Crystallography in this thesis.

Dr. Yufei Song, for giving me a million ideas for my work and sharing his experience of both ligand design and inorganic synthesis with me.

Dr. Alexis Parenty, for being my mentor in the ways of organic chemistry, and not least for discovering the DIP reaction in the first place. Also **Dr. Louise Smith** and **Craig Richmond** for their research into DIP and its analogues upon which the work in this thesis builds.

Professor Makoto Fujita for giving me the opportunity to work in his Lab at the University of Tokyo.

Dr. Graham Newton and for numerous scientific (and not so scientific) discussions, his expertise with the Cryospray Mass Spectrometer, his proof reading of this thesis and also for sharing his knowledge of coordination chemistry, crystallisation techniques, cookery and ornithology.

The technical staff of the University of Glasgow Chemistry Department, for the help they give all the students in the department, in particular; **Jim McIver**, for all his technical support with my work, **Jim Gall** and **Dr David Adam** for help with NMR and **Kim Wilson** for elemental analysis.

All the members of the Cronin Group, past and present, who have made this such an enjoyable and interesting time, both scientifically and socially. In addition to those above I would like to mention: **Dr. Geoff Cooper, Dr. Carsten Streb, Dr. Chris Ritchie, Dr. Hamera Abbas, Scott Mitchell, Mali Husby Rosnes, Neus Corella Ochoa, Johannes Thiel, Jennifer Mathieson, Thomas McGlone and Rob Thatcher.**

Above all, I would like to thank my Mum and Dad and all my family for the constant support and encouragement they have given me over the last three years, I couldn't have done it without them.

Table of Contents

Abbreviations

aq.	Aqueous
Boc	*tert*-butoxycarbonyl
CI	Chemical ionisation
conc.	Concentrated
DIP	Dihydro-imidazo-phenanthridinium
DPP	Dihydro-pyrrolo-phenanthridine
DMF	Dimethylformamide
DMSO	Dimethyl sulfoxide
DNA	Deoxyribonucleic acid
EI	Electron impact
eq.	Equivalent
ES	Electrospray
FAB	Fast atom bombardment
MHz	Megahertz
mp	Melting point
MS	Mass spectrometry
NA	Not applicable
NAD+/ NADH	Nicotinamide adenine dinucleotide
NBS	*N*-Bromosuccinimide
NMR	Nuclear magnetic resonance
PP	Propyl phenanthridinium
rp	Room pressure
rt	Room temperature
TEA	Triethylamine

THF	Tetrahydrofuran
TIP	Tetrahydro-Imidazo-Phenanthridine
TLC	Thin layer chromatography
Ts	Tosyl

Troughout this thesis crystal structures are coloured by atom using the following colouring scheme except where otherwise stated:

Bromine	Dark red
Carbon	Grey
Chlorine	Green
Cobalt	Pink
Copper	Orange
Hydrogen	White
Nitrogen	Blue
Oxygen	Light red
Palladium	Teal
Silver	Purple
Sulfur	Yellow

Abstract

Two isomeric, pyridyl based ligands with Dihydro-1H-Imidazo-(1,2-F)-Phenanthridinium (DIP) moieties have been designed, synthesised and complexed with a range of Cu^{II} salts and their coordination products crystallised both in the presence and absence of bridging anions. The π stacking interactions of the DIP regions of these ligands have been shown exhibit a limited number of geometries due to the cationic nature of the DIP framework and to link the resulting complexes into 1D, 2D or 3D networks in the crystalline phase.

In addition, a third DIP based ligand has been designed and synthesised based on a 1,3,5-triazine core incorporating two dipyridylamine based coordinating moieties. Upon complexation with $Pd(OAc)_2$ this ligand is observed to undergo a hydrolytic transformation leading to a new penatnuclear palladium complex which exhibits an unusual C-H···π···*lone pair* motif in the crystalline phase. A second dinuclear, *bis*-ligand complex is formed upon complexation of this ligand with $Cu(ClO_4)\cdot 6H_2O$ in which the designed ligand undergoes no transformation.

The design and synthesis of a new Imidazo-Phenanthridinium (IP) based ligand is described. Complexations of this new ligand lead to the formation of four new coordination complexes with a variety of transition metals. The coordination and supramolecular interactions of these new coordination complexes are investigated in the crystalline phase.

Furthermore, the synthetic methodology used to generate these new ligands has been extended resulting in the discovery of a new C-C bond forming annulation reaction based on the DIP synthetic methodology leading to the synthesis of chiral 2,3-Dihydro-12bH-Pyrrolo[1,2-f]Phenanthridine (DPP) derivatives which exhibit a reversible, pH dependant, cyclisation process.

Introduction

1 SUPRAMOLECULAR CHEMISTRY

1.1 Definition of Supramolecular Chemistry

Despite the fact that intermolecular interactions have been recognised and studied by chemists for over 100 years, introduced by Emil Fisher's "*lock and key*" concept of host-guest interactions,[1] it is really only in the last 20-25 years that the field of supramolecular chemistry has seen major expansion and has attained the status of a discrete field of study amongst such previously defined fields as organometallic chemisty and organic synthesis. The reasons for this are varied, but not least among them is the fact that the interactions that concern the supramolecular chemist are so ubiquitous that their effects within other fields were well known and supramolecular chemistry grew from a realisation by chemists working in these various fields that these forces could be harnessed to achieve functionality in chemical systems vastly beyond that found in the realm of molecular chemistry. Coupled to this, advances in organic synthesis have opened the prospect of the design of molecular architectures which can be used to systematically direct and exploit these interactions in a pre-determined or at least partially predictable fashion.

Supramolecular chemistry has been defined by Nobel Laureate Jean-Marie Lehn as "*Chemistry of molecular assemblies and of the intermolecular bond*"[2]. Such a broad definition leaves the field of study very open and supramolecular chemistry can encompass such wide ranging fields as the synthesis of artificial enzymes,[3,4] crown ethers,[5] cryptands[6,7] and related structures[8] and crystal engineering[9,10] to the construction of supramolecular devices, such as the rotaxanes of Stoddart[11,12] which rely on the motion of one component of the system relative to others conferring a functionality on the assemblies. The one feature that such disparate fields of study have in common is the understanding and utilisation of the way discrete molecules interact with each other *via* bonds weaker than the typical covalent interaction.[13]

1.2 Supramolecular interactions

Supramolecular chemistry as a field of study is intimately bound up with the study and manipulation of non-covalent interactions it is important first of all to define these interactions. These forces vary greatly in both their strength and directionality of action. The main supramolecular interactions discussed in the current research are coordination bonds and the interactions of π electron systems.

1.2.1 Electrostatic Interactions and Coordinative Bonds

Electrostatic interactions are attractive interactions between oppositely charged species. The obvious example of this type of interaction is that between a cation and an anion, one of the simplest cases being the cubic lattice of NaCl where each Na^+ ion is surrounded in the lattice by six Cl^- ions to form the familiar rock salt structure. Such ion – ion interactions are comparable in strength to a covalent bond (with energies up to 350 kJ mol^{-1})[13] and are, for the most part, not thought of as supramolecular interactions.

Weaker than ion – ion bonds and more often associated with supramolecular chemistry are ion – dipole interactions where an ion experiences an attractive interaction with some polar molecule. Of interest to us in the current research are the coordinative interactions between ligands and transition metal centres which can be understood in terms of crystal field theory[14] where coordinative interactions are described as ion-dipole interactions between the Lewis basic electron pairs of the ligand and the positively charged metal ion. Conversely, ligand field[15] and molecular orbital theory predict a significant degree of covalent character to these interactions, arising from the mixing of the ligand orbitals and metal *d* orbitals, however the strength and kinetic lability of these interactions is such that they are often considered to be essentially supramolecular in nature, and are the focus of much active research into the construction of polydentate ligands to act as pre-organised supramolecular building blocks (see section 1.3). The coordination chemistry of main group transition metals varies widely and is largely dependant on the *d*-electron configuration of the particular metal involved. The coordination chemistry of the metals of particular interest to this thesis are introduced briefly below.

1.2.1.1 Coordination Chemistry of Copper, Cobalt, Palladium and Silver

Due to its single *s* electron outside the filled *3d* orbital copper is the only one of the first row main group transition metals to exist in a stable +1 oxidation state (d^{10} electron configuration), however coordination complexes in this oxidation state are readily oxidised to the +2 state. Copper is most commonly found in coordination complexes in a +2 (d^9) or +3 (d^8) oxidation state.[16] In the +2 oxidation state copper complexes can exhibit an extremely large array of coordination numbers (from 3 to 8, although 4, 5 and 6 predominate in N- and O- donor systems) and a correspondingly large variation in coordination geometries, especially square planar, square based pyramidal, trigonal bipyridyl and octahedral. Due to its d^9 electron configuration Cu^{II} complexes exhibit Jahn-Teller distortions when placed in regular tetrahedral or octahedral symmetry. Copper is also a significant component in many biological systems, being present in proteins such as haemocyanins and enzymes such as cytochrome oxidase.[14]

In coordination chemistry cobalt is most often found in either the +2 or +3 oxidation state, with *d* electron configurations of d^7 and d^6 respectively. While complexes of Co^{III} are usually octahedral, low spin and kinetically inert, complexes of Co^{II} are generally more kinetically labile can exhibit a wider range of geometries, often dependant on the geometrical constraints of the ligand, for example in the case of polydentate ligands. [14,16]

In the second row of the *d* block, palladium is most often found in the +2 oxidation state (d^8 electronic configuration) and what few Pd^{IV} coordination complexes exist are normally formed by the oxidation of corresponding Pd^{II} species. Pd^{II} generally forms low spin, diamagnetic square planar complexes and favours the formation of complexes with amines and other large donor atom ligands.[14,16]

In the same group as copper discussed above, silver also forms a stable +1 oxidation state, and it is in this state that silver is usually encountered as a coordination complex. Ag^{I} complexes favour soft donor atoms, exhibiting a wide variety of complexes with sulfur and phosphorous based ligands, coordinations ranging from 2 to 6 are common and tetrahedral and linear geometries are favoured.[14,16]

1.2.2 Interactions of π-Electron Systems

The delocalised π electron systems of olefinic, alkynic and aromatic organic molecules provide another fertile ground for supramolecular interactions which play a vital role in many natural and artificial systems.[14,16] It has long been known that the π systems of various components interact favourably with certain transition metals as established early in the case of Zeise's Salt and later on with the isolation of ferrocene.[17] These interactions have a high degree of covalency to them and are generally considered to be a separate effect to the majority of intermolecular π interactions observed due to the degree of mixing between the π orbitals of the ligands and the *d* orbitals of the metal centres. Of more general interest to the supramolecular chemist are the interactions in which electrostatic and other weaker forces predominate to promote binding both between molecules with π electron systems and with other species.

It is well known that cations experience favourable interactions with polar molecules such as H_2O, however it is less well known that aromatic systems also experience relatively strong interactions with the same cations.[18,19] It has been shown that the interaction of benzene with K^+ ions in the gas phase has a magnitude of 19 kcal mol^{-1}, which is stronger even than the interaction between K^+ and H_2O (18 kcal mol^{-1}),[20] potassium salts are more soluble in water than benzene, however, as the steric bulk of the benzene molecule allows much fewer molecules to be involved in solvation than is the case in aqueous systems. The mode of interaction between cations and π systems is a complex mix of factors, not least among them the polarisability[21] of the aromatic electrons leading to induced dipole – cation interactions.[22,23] Other factors which have an influence over the overall binding energy are donor-acceptor, charge transfer and dispersion forces. It apperars, however that these factors remain fairly constant for aromatic-π interactions and variations in the binding energy of such systems come from the electrostatic contribution to the binding energy.[24] The understanding of the nature of the cation-π interaction has lead to the design of several synthetic hosts for cations to further probe and utilise this supramolecular interaction. It has also been suggested that electron deficient aromatic

systems can form attractive interactions with anions, and evidence for these interactions exist in a number of crystal structures.[25-27]

Along with interactions with charged species the delocalised electron cloud of aromatic systems also provides a focus for interaction with other, formally neutral, species and with other π electron systems. The two major motifs of interaction encountered between aromatic rings are the edge or point-to-face type arrangement associated with C-H···π interactions[28] and the face-to-face interactions associated with π stacking where there is direct interaction between the π electrons of both species, a true π···π interaction. These modes of interaction have been extensively studied[29-31] although the fundamental nature of the interactions of these systems is complex and a matter of some discussion to this day.

The edge-to face type arrangement of C-H···π interactions have been described as weak hydrogen bonds between the electron deficient hydrogen of one species and the partially negatively charged aromatic electron system of the other species.[32] Theoretical calculations on these types of interactions have shown that, while always attractive, these interactions are characterised by shallow energy potential allowing a wide variety of binding arrangements, and the softness of the interaction allows many different binding geometries of similar energies.[33] C-H···π interactions represent an extremely large class of motifs which play a vital structural role in systems ranging from coordination chemistry[34, 35] to protein structures.[36,37]

The face-to-face motif observed in some π electron interacting systems is probably the best known π electron system interaction, the π stacking interaction. This weak interaction is vital in numerous biological systems[36,38,39] as well as crystal engineering (see section 1.4.1) and supramolecular coordination chemistry (see section 1.3) and as such is the focus of major investigations into its magnitude, geometry and modes of interaction.

Many different binding geometries are associated with the face-to-face arrangement of aromatic moieties observed in π···π interactions. As with the cation···π interactions discussed above, the overall attraction experienced in this situation is a combination of a

variety of contributing factors: dipole-dipole interactions, electrostatic interactions, and London dispersion forces all play a roll[40,41] along with such system dependant factors as solvophobic effects[42] and polarisation of the π electron system due to substituents on the aromatic ring or inclusion of non-carbon atoms in aromatic heterocycles.

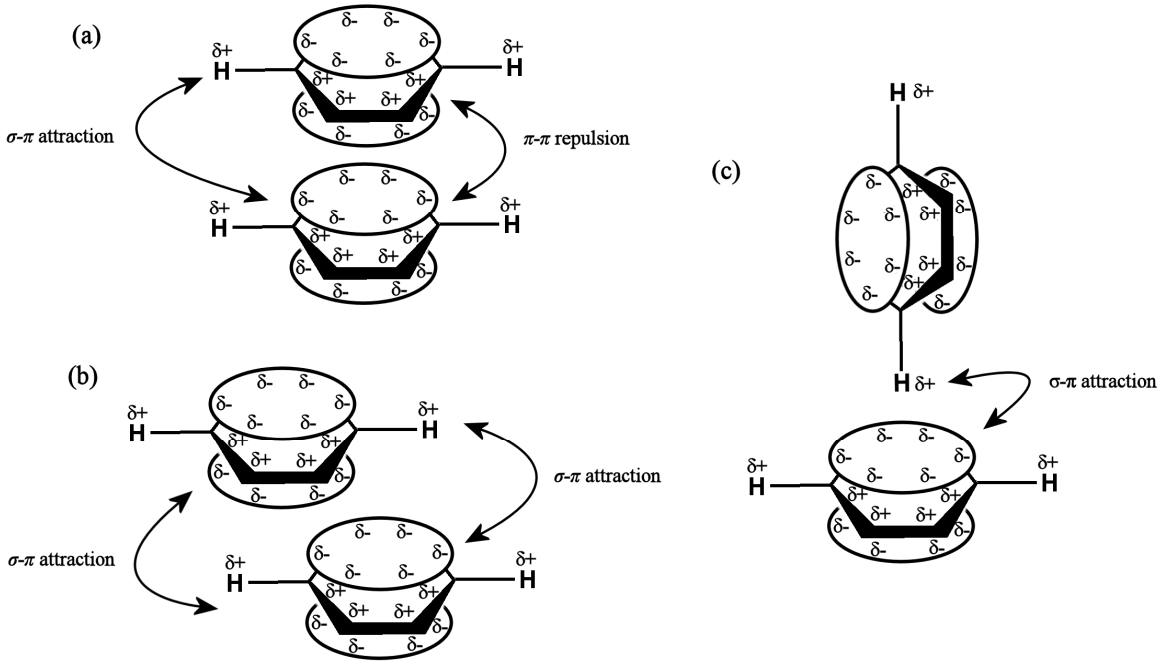

Figure 1: Schematic representation of the electrostatic interactions between the σ framework and the π systems of an ideal aromatic in an (a) face-to-face π stacked, (b) offset face-to-face π stacked and (c) edge-to-face C-H···π type arrangement.

In the early nineties Hunter and Sanders[43] proposed a simple model for the understanding of $\pi\cdots\pi$ interactions where the charge distribution between the $\delta+$ σ framework and the $\delta-$ π system of the aromatic molecules is used to explain the geometrical requirements for such interactions (see Figure 1). Hunter and Sanders introduced a series of rules to aid in the qualitative prediction of the geometry of various π interacting systems. The work recognised that the overall strength of the $\pi\cdots\pi$ interaction is a combination of many forces at work simultaneously, however it ascribes the peculiar geometric features often observed in such systems to an electrostatic attraction between the $\delta-$ charge of the π electron cloud and the $\delta+$ charge of the σ-bonded framework. This formula therefore predicts a "*slipped*" or "*off-set"* motif in $\pi\cdots\pi$ interacting systems where the σ framework experiences some electrostatic access to the π electron cloud of the

interacting aromatic system. The limiting case of this interaction, therefore, is the T-shaped C-H···π interaction described above. This prediction is born out by statistical analysis of the CSD database of crystal structures which shows that in systems which exhibit perfect face-to-face π stacking interactions are relatively rare.[44]

The Hunter and Sanders model has not gone uncriticised, however, and it has been argued that the Hunter and Sanders model suffers from an arbitrariness in assigning π charges and π-σ charge splitting. This criticism points out that consideration of the interactions of the quadrupoles of aromatic systems are enough to understand the attractive and repulsive interactions in these systems.[31,45] The Hunter and Sanders model however remains a useful empirical model for the illustration of these systems.

1.2.3 Other Supramolecular Interactions

Although π-π interactions are of most relevance to the present work, they are by no means the majority of, or often the most significant, non-covalent interactions which the supramolecular chemist can take advantage of in the construction of functional molecular assemblies. In almost every supramolecular system the above attractive and repulsive forces combine with a variety of other interactions such as; hydrogen bonding interactions,[46-48] other dipole-dipole interactions, solvophobic effects and crystal close packing effects in the solid state.[13,49-52] The interplay of all these forces leads to a very complex situation in which it is often not clear which is the predominating factor and it the great challenge of supramolecular chemistry to understand and utilise not just the individual components of intermolecular interactions, but also the overall effect that the combination of these factors has in a system.

1.3 Ligand Design

One of the principle ways in which the supramolcular chemist can direct the formation of supramolecular materials and molecular assemblies based on coordination chemistry is by the judicious use of ligands to perform a particular structural role. The realisation of this

has lead to a great deal of interest in the field of directed ligand design, whereby the geometry of the product is dependant on the coordination geometry of the metal ion and the geometry of the ligand.[53-56] If a ligand can be thought of as a simple molecular species containing a free electron pair available for coordination to a metal centre,[15] then the use of ligands with more than one available lone pair can act as bridging ligands between metal centres, and therefore be seen as structural elements in the formation of larger species.

The number of donor atoms of a ligand, however, is not the only aspect of ligand structure that is important, as the geometry of the possible binding sites of a multidentate ligand, along with its structural rigidity is also important. If a multidentate ligand has coordinating atoms which can orient themselves in a convergent manner, these atoms will often be found to coordinate to the same metal ion in a chelating fashion. The entropically unfavourable bridging coordination mode is normally only encountered when the coordination sphere of the metal is blocked by other, more tightly bound, ligands or when the ligand atoms are prevented from coming close together by an inflexible or bulky ligand core.

Several approaches to the design and selection of ligands for use in supramolecular synthesis have been developed over the last few decades, one example being a molecular library approach developed by Stang[57] amongst others[58,59] where the interaction of various multidentate building blocks with well defined geometries is considered, with each subunit representing either an edge or vertex of the resulting polyhedron (see Figure 2).

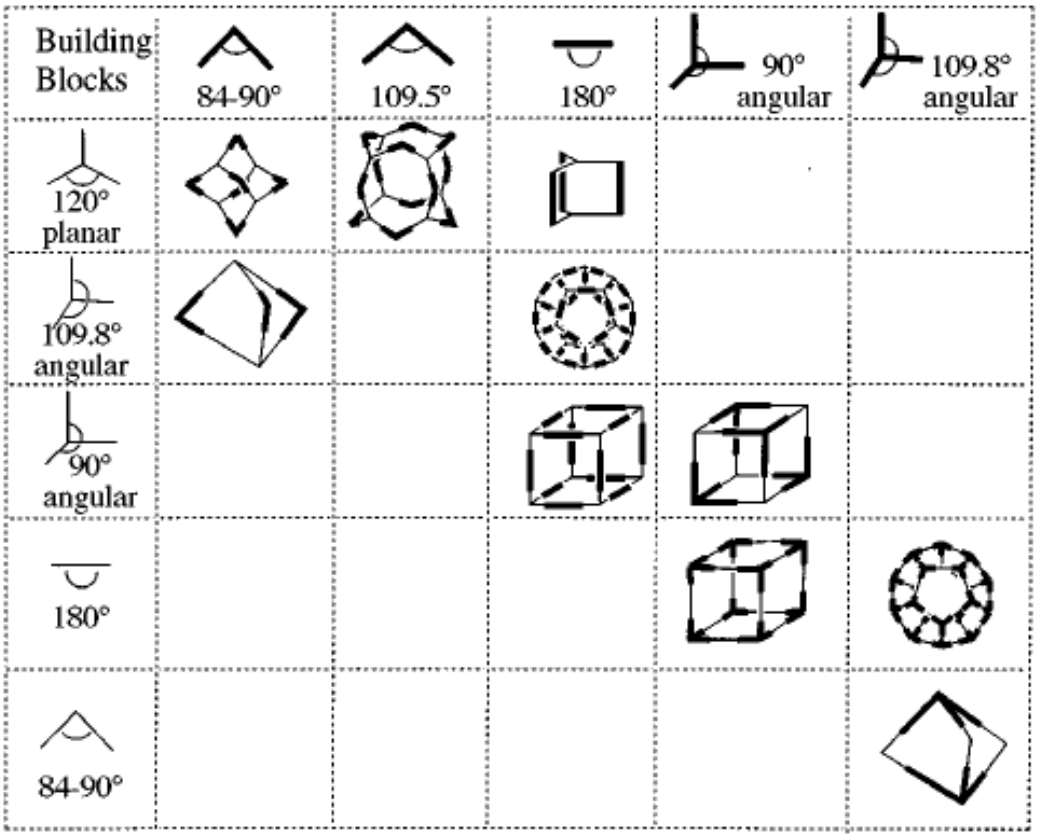

Figure 2: Part of a combinatorial library for the construction of supramolecular polyhedra illustrating the possible 3-D products of possible combinations of rigid building blocks (figure reproduced without permission).[57]

As transition metal ions exhibit coordination behaviour with generally well defined coordination geometries, this approach and others[54,60] rely on the use of transition metal ions as acceptor units which can be linked together by building blocks which form the rigid framework of the resulting structure. For this approach, the rigidity of the ligand units is vital to the predictability of the system, and therefore lends itself well to use with aromatic, often pyridyl, based coordinating ligands to provide the predictable coordination and geometrical features required by this model.

Another approach to the synthesis of supramolecular coordination structures uses a "*molecular panelling*" strategy developed by Fujita[61] which links planar 2-D organic components *via* metal coordination. This approach has proved successful in the

construction of polyhedral cages with the ability to encapsulate small organic compounds in an aqueous environment and act as nanoscale reaction vessels.[62-64]

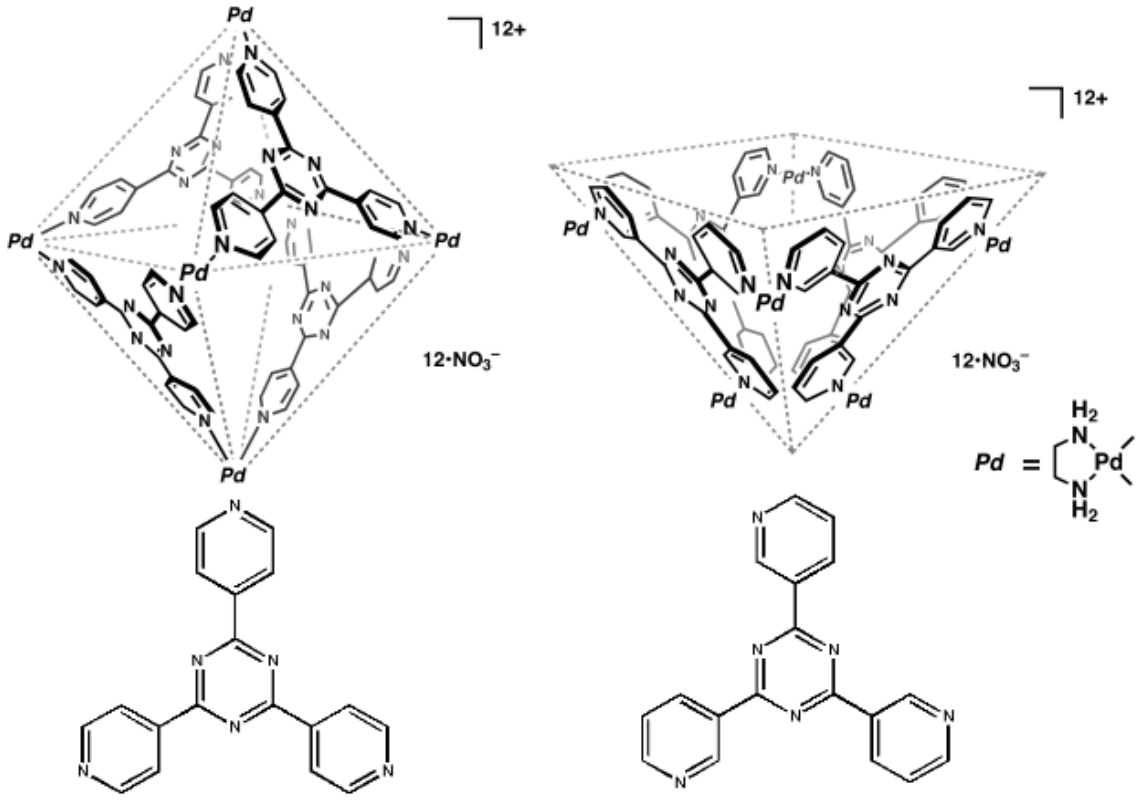

Figure 3: A molecular cage (left) and bowl (right) constructed *via* a molecular panelling approach to ligand design. The trivalent ligands used are shown below in each case. The ligands are connected by a $[(en)Pd]^{2+}$ cation providing a 90º linking unit (figure adapted from reference [62] and reproduced without permission).[62]

In the above example we see a molecular panelling ligand based on a triazine core with different directionality of coordination sites introduced by using either 3- or 4-pyridyl substituents to create the desired connections to the 90º linking unit of the ethylene diamine (en) capped square planar palladium complex. The use of triazine in the design of ligands for supramolecular chemistry is well established and structures based on a triazine core have been used extensively to produce a wide range of supramolecular achitectures, from the primitive trivalent ligand of 1,3,5-triazine itself to the much more complicated ligands with a degree of flexibility built into the system (see Figure 4).[65-69]

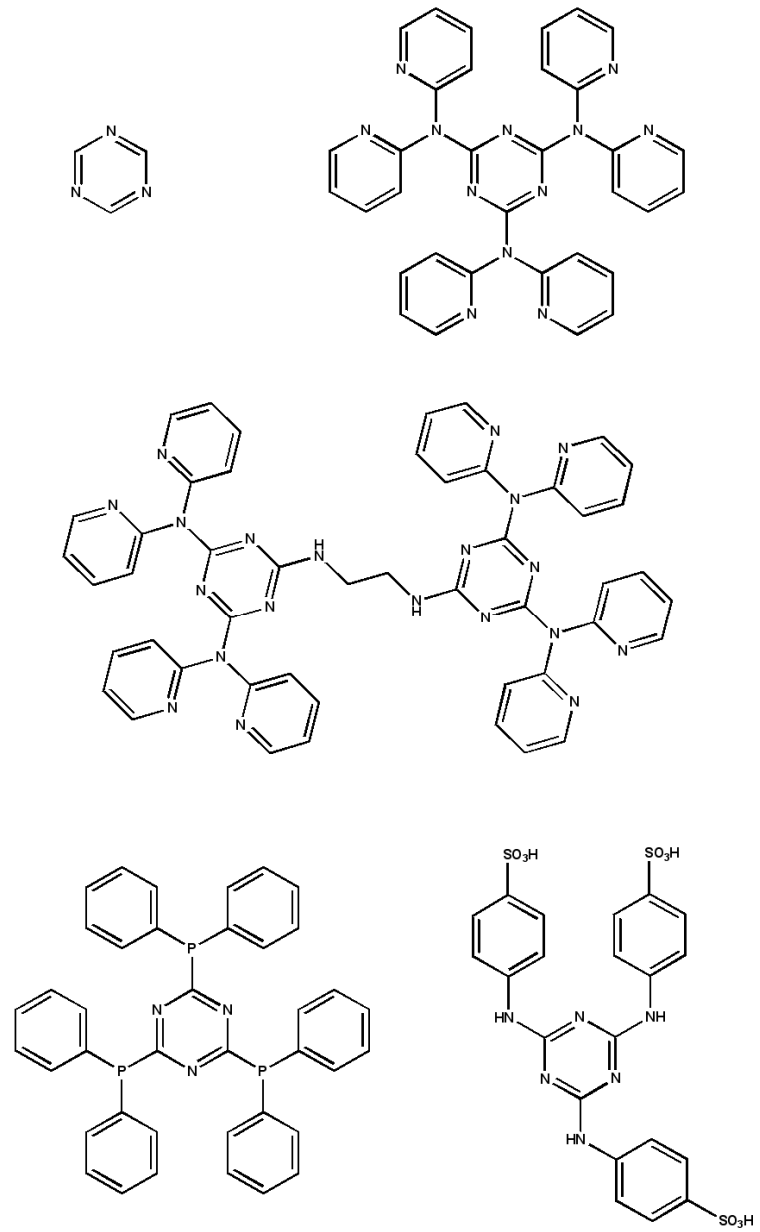

Figure 4: Some examples of 1,3,5-triazine based ligands for supramolecular synthesis.[66-69]

In the design of ligands it is important to remember, however, that it is not only the coordinative interactions which have an influence over the resulting supramolecular frameworks produced and many ligands are designed not only with their coordinative properties in mind, but also their ability to form other supramolecular interactions such as hydrogen bonded structures and π interactions. These interactions are especially important in the crystalline phase where weak interactions which may be insignificant in the dynamic

environment of the solution phase can play an important role in the formation of long range architectures.

1.4 Supramolecular Interactions in the Crystalline Phase

The crystalline phase has been described by Dunitz as "*a supermolecule par excellence*",[70] as it is essentially an infinitely ordered supramolecular system which has the added advantage that modern techniques in X-Ray crystallography can give the chemist unsurpassed resolution to study the 3-D arrangement of atoms in the system and ability to study the supramolecular interactions which influence the structure's formation. The study of crystal structures has an influence not only on the understanding of the solid state structure of supramolecular systems but can give valuable insight into their functions in solution as well.[71] The study of crystal structures of the active sites of biological enzymes, for example, has provided detailed structural information which has allowed the design of drugs which target the particular interactions found in the crystal structure.[72] To this end there are a number of databases which store the available crystal structures such as, among others, the Protein Data Bank (PDB),[71] the Cambridge Structural Database (CSD)[73] and the Inorganic Crystal Structure Database (ICSD)[74] which deals with small molecules and so has a more general use to the non-biological chemist. Although one must always be careful of extrapolation of structural features in the crystalline phase to other situations as there are fundamental differences which have to be taken into account such as the maximisation of dispersive forces and minimisation of repulsive forces to enable crystal close packing.[75]

The study of supramolecular interactions in the crystalline phase has lead recently to great advances in the separate but related fields of crystal structure prediction[76] and crystal engineering.[9,10,53] While crystal structure prediction remains a significant challenge, even with modern computational methods being applied to simple systems,[77] the field of crystal engineering has used the knowledge obtained from the study of supramolecular interactions in the crystalline phase to enable the rational design of crystalline systems. It is worth noting, however, that crystal engineering still remains a challenging discipline as the number of factors affecting the crystal structure of even the simplest systems can be very large indeed involving complex interplay of such factors as temperature, pressure and

crystal growth conditions[78] as well as the designed features of the crystallising components.

1.4.1 π Electron interactions in the Crystalline Phase

The ability of aromatic components in a crystallising system to interact *via* their π electron systems has long been understood to be a factor governing their crystal structures, as can be seen in the classical example of benzene where C-H···π interactions gives the crystal structure a herringbone-like pattern.[79] The simplest organic π interacting systems, that of fused-ring aromatic hydrocarbons, have been classified by Disiraju[80] into four distinct packing types, distinguished by the length of their shortest crystallographic axis (s.a.), in the crystalline phase. This classification forms the basis of a predictive model for the packing of these simple hydrocarbons taking into account the relative contribution of carbon and hydrogen to the molecules surface area. The classifications are:

1. Simple herringbone; nearest neighbours non-parallel; 5.4 Å < s.a. < 8.0 Å (e.g. naphthaline).
2. Sandwich herringbone; herringbone motif is made up of sandwich like diads; s.a. > 8.0 Å. (e.g. pyrene).
3. γ-type; main interactions are between parallel translated molecules; 4.6 Å < s.a < 5.4 Å. (e.g. coronene).
4. β-type; graphitic planes; s.a < 4.2 Å. (e.g. tribenzopyrene).

Using fused-ring polyaromatic hydrocarbons as a structural motif to encourage the formation of π interactions is a strategy that is often encountered in crystal engineering, whether by introducing the aromatic hydrocarbon region by covalently grafting it to a non aromatic molecule,[81] or by using the polyaromatic hydrocarbon as a co-ligand with other aromatic groups[82] to encourage π interactions.

It has been an active area of research, therefore to design components of supramolecular systems which can interact *via* their π electron systems, to exploit these interactions to form interesting architectures in the crystal phase, and also to use these interactions to vary the properties of individual systems. Some examples of these are given below.

The study of π interactions in organic systems has come a long way from the classification of purely hydrocarbon materials and organic chemists can now take a more crystal engineering inspired approach by the introduction of non carbon atoms to influence the electronic properties of the aromatic system, and thereby engineer both electron-deficient and electron-rich aromatic regions to encourage the formation of face to face π stacking interactions.[83] A recent example of this type of strategy is seen in the work of Chao *et al.* who incorporate electron-rich thieno[2,3-*b*]thiophene units and electron deficient pyrimidine or benzothiazole units into a single molecule, thereby encouraging π stacking with very little offset across the short molecular axis and moderate offset along the long molecular axis, following the pattern of the donor-acceptor regions of the molecules. This arrangement has produced favourable theoretical values for uses as organic semiconductors (see Figure 5).[84]

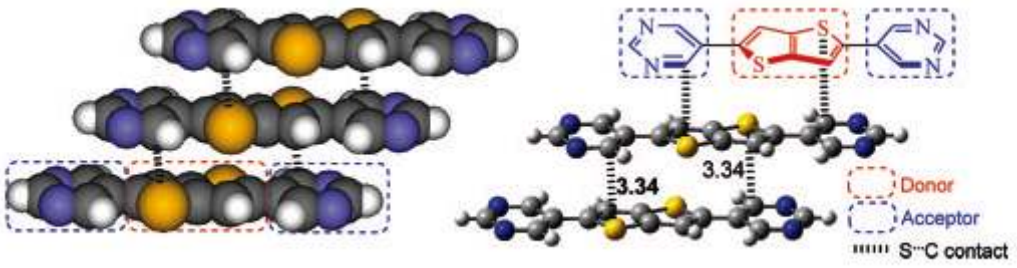

Figure 5: Crystal engineering strategy of introducing electron-rich and electron-deficient regions in a molecule to encourage face-to-face π stacking interactions(figure reproduced without permission).[84]

The above example also provides an illustration of the influence π electron interactions in the solid state can have on the bulk properties of a material. These properties are not restricted to organic semiconductors and the π electron interactions in the crystalline phase have also been linked to the physical properties of the resulting material.[85]

While the use of purely organic components in a crystal system is sufficient for the presence of π interactions, in the field of crystal engineering it is more often the case that π interacting units are incorporated into ligands for coordination chemistry. Coordination chemistry allows the supramolecular chemist to take advantage of the rational design of ligands (see section 1.3) to exploit the directional properties of metal coordination to gain control over the supramolecular system. The introduction of aromatic regions to these ligands is a very popular way of tuning the supramolecular interactions these systems experience.

A good example of this is the work of Dai *et al.*[86,87] who have synthesised a mononuclear Cu^{I} complex based on 1-aminopyrene, where the copper centre has a coordination number of 3, and the crystal structure shows both intra- and intermolecular stacking of the pyrene moieties extending the structure in two dimensions(see Figure 6).

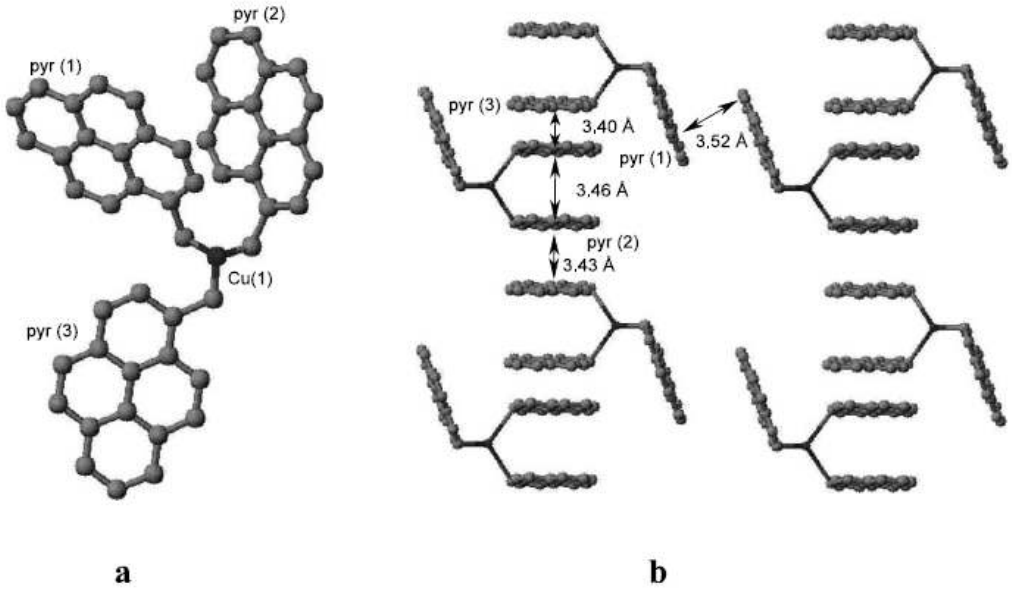

Figure 6: (a) Molecular structure of $[Cu(apyr)_3]^+$ cation. (b) Packing of the [Cu(apyr)3]+ unit showing intermolecular stacking of the pyrene units and the formation of 2D sheets *via* intermolecular stacking interactions.[87](figure reproduced without permission from Reference [86])

The above example illustrates how π interactions can link discrete molecular units into larger, supramolecular, structures. The use of ligands which can bind to more than one metal centre in a controlled fashion gives the supramolecular chemist the opportunity to design both molecular polyhedra, as in the example of Fujita's molecular cages described above, and extended coordination polymers. One of the most common ligands for this work is the 4,4'-bipyridine molecule[88] which can be seen as a molecular rod for the formation of structures such as chains, ladders, and helical motifs.[89] The aromatic nature of these types of ligands, however, leads to the possibility of their interacting with each other *via* non-coordinative interactions, influencing both the coordination environment of the metal centre and the intermolecular interactions. These species also have the ability to act as either non-coordinated guest molecules, bridging ligands or terminal ligands depending on the situation. As an example of all of these types of behaviour of 4,4'-bipyridine we have the synthesis of a "*molecular railroad*" by Yaghi *et al.*,[90] where the railroad-like double chains are linked into 2D sheets by π interactions between terminal 4,4'-bipyridine ligands on either side of the chain. The structure forms large 1D pores which are filled by uncoordinated 4,4'-bipyridine molecules (see Figure 7).

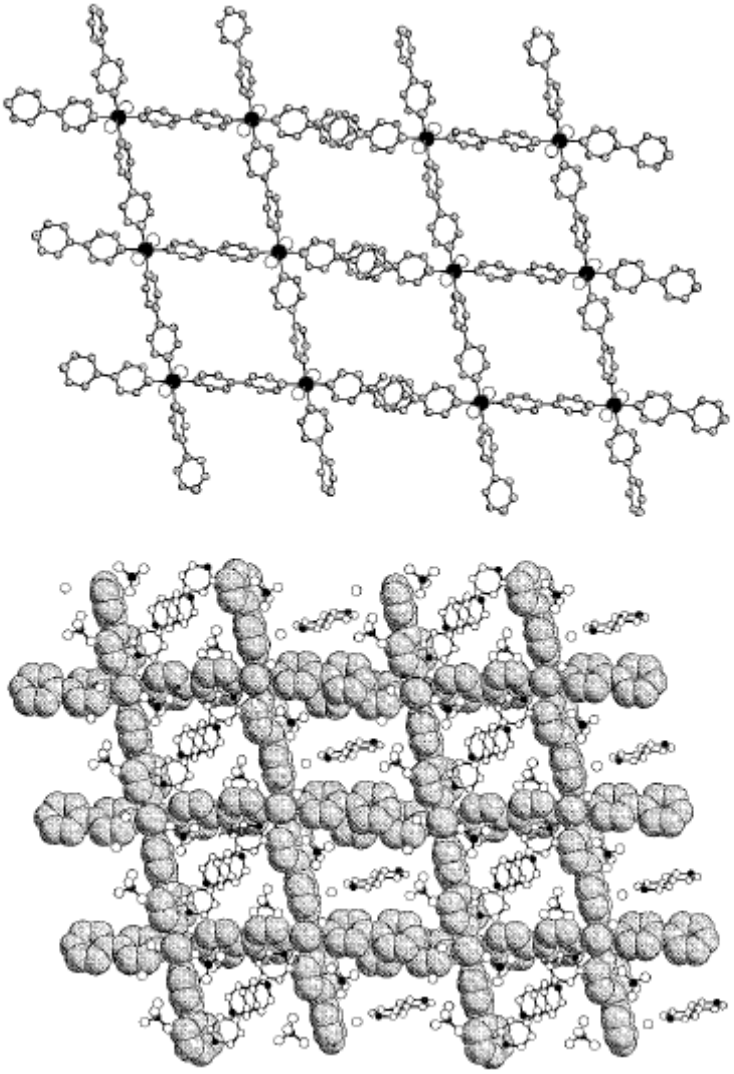

Figure 7: "*Molecular railroad*" of Yaghi *et al.* (Top) ball and stick representation showing π interactions between the railroad units to form a 2D sheet, and (bottom)space filling representation of the framework showing the large pores filled with uncoordinated 4,4'-bipyridine (figure reproduced without permission).[90]

Non-bridging aromatic ligands have also been used to influence the supramolecular interactions of coordination complexes in the crystalline phase. The use of such terminal, chelating ligands as 2,2'-bipyridine or 1,10-phenanthroline along with bridging ligands can direct the formation of interesting supramolecular structures. In a recent example[91] these two ligands along with bridging dicarboxylate ligands (isophthalate, 4,4'-oxybis(benzoate) and ethylenedi(4-oxybenzoate)) were used to construct double-stranded helices and

molecular "*zippers*" *via* the supramolecular interactions of the aromatic chelating ligands on Cu^{II} metal ions. In this case the π interactions link the helical structures of the bridged coordination polymers into more complex supramolecular structures (see Figure 8).

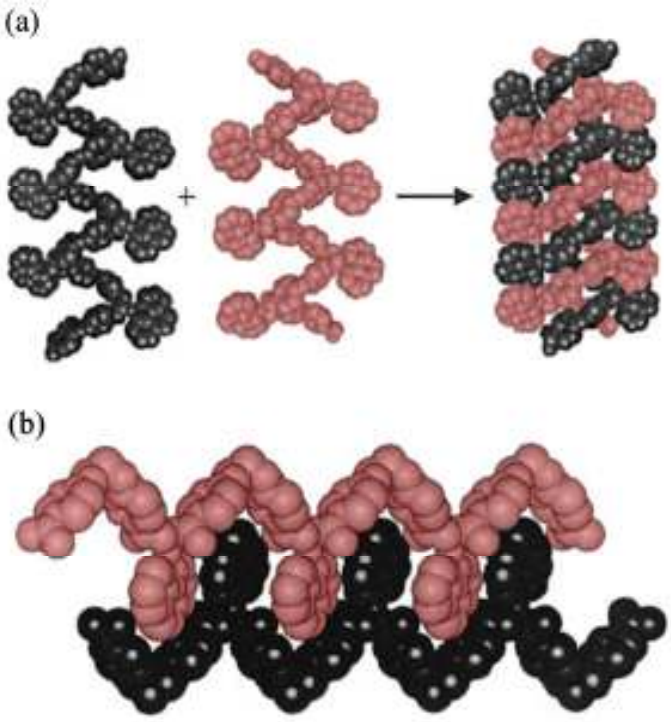

Figure 8: (a) Formation of double helical structures by the intertwining of single stranded helical coordination polymers stabilised by π interactions. (b) Linking of two helical coordination polymers in a "*zipper*" arrangement (figure reproduced without permission).[91]

All of the above examples have depended to a greater or lesser degree on the use of organic ligands to direct the formation of supramoleular systems. Supramolecular chemistry therefore can be seen as depending to a large extent upon ability of chemists to synthesise species with the desired properties to act as efficient ligands for supramolecular interactions. Given the prevalence of pyridyl and heterocyclic aromatics in ligands for supramolecular chemistry the synthesis and derivatisation of organic heterocycles is of critical interest to the supramolecular chemist.

2 HETEROCYCLIC CHEMISTRY

In addition to their uses in coordination chemistry, aromatic heterocyclic rings are present in the skeletons of more than half of the biologically active compounds found in nature[92] and as such have been employed by humans for various purposes for centuries. Synthetic heterocycles have widespread uses as herbicides, fungicides, insecticides and dyes as well as modern pharmaceutical drugs to treat conditions as varied as fevers, ulcers and cancer.[93]

Any organic ring system containing at least one heteroatom can be described as a heterocycle, encompassing both aromatic and aliphatic heterocycles, however in this thesis we will be principally concerned with aromatic heterocycles and therefore it is worth considering the effect that the introduction of a heteroatom has on an aromatic system. The aromaticity of a heterocycle is greatly influenced by the type of heteroatom present and its ability to contribute electrons to the delocalised system. The simplest illustration of this is the difference between the two aromatic heterocycles pyridine (C_5H_5N) and pyrrole (C_4H_4NH). Both of these molecules are aromatic, but the requirements of the Hückel criteria for aromaticity of cyclic polyenes to contain ($4n+2$) electrons in filled p orbitals capable of overlap mean that the nitrogen lone pair of a pyrrole molecule is delocalised in the π electron system, whereas the lone pair of the nitrogen in pyridine is not. This difference has a large effect on the chemical properties of the two structures. As the lone pair of the pyrrole is delocalised it is therefore not available to act as a base in organic reactions (pK_{aH} = -4) or to interact with metal ions to form coordination complexes. Protonation of pyrrole results in the loss of aromaticity in the system and is therefore energetically unstable. Pyridine, by contrast, can be seen as an analogous structure of benzene in which one of the C-H groups has been replaced with a nitrogen and it is not necessary for the lone pair to participate in the aromatic system and pyridine is therefore much more basic (pK_{aH} = 5.2) and coordinates to metal ions much more readily than pyrrole.[94]

The introduction of a heteroatom into an aromatic system does not just effect the ability of that moiety to participate in chemical reactions, it also has an influence on the supramolecular behaviour of the aromatic system. The introduction of a more electronegative atom than carbon results in polarisation of the aromatic system leading to the existence of a dipole within the molecule (pyridine has a dipole moment of 2.3[95]). The polarisation of heteroaromatic moieties such as pyridine can be further increased upon complexations to a metal ion (see Figure 9).

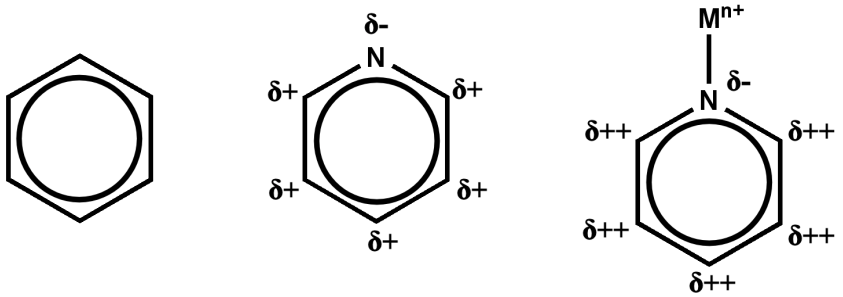

Figure 9: Effect of substitution of an electronegative heteroatom such as nitrogen and metal complexations on the polarisation of an aromatic system.

Although pyridine and its analogues have found a great deal of use in the area of coordination chemistry it has been their uses in the field of medicine and their prevalence in natural products which has driven massive efforts to discover and optimise new reactions to synthesise and to functionalise heterocycles. There is therefore a vast reservoir of knowledge which the synthetic chemist can draw upon for the design of new ligands.

2.1 Methodologies for the derivatisation of pyridine and Benzo-fused analogues

The simplest method for the derivatisation of pyridine and related heterocycles is by the use of the lone pair of the nitrogen to perform a nucleophilic substitution reaction leading to the formation of a quaternary ammonium salt, although it should be noted that pyridine

nitrogens are significantly less basic than saturated amines which will react much more readily.

Due to the electronegative character of the nitrogen in pyridine and its analogues, these species are virtually inert to aromatic electrophilic substitution, the nucleophilic lone pair of the nitrogen will preferentially attack the electrophile in question, forming a quaternary pyridinium salt and making the ring even less reactive towards electrophilic substitution. Exhaustive reaction of pyridine with an electrophile will generally produce only very poor yields of the C3 substituted product, and so reactions like electrophilic nitration or Friedel-Crafts acylation or alkylation are generally not preparitively useful. Only substituted pyridines with electron donating substituents like amino or methoxy groups perform electrophilic aromatic substitution in reasonable yields (see Scheme 1). The electrophilic substitution of benzo-fused analogues of pyridine such as quinoline or iso-quinoline generally proceed on the benzoid ring of the heterocycle, as under electrophilic conditions the lone pair of the pyridine ring becomes substituted as in the example of pyridine discussed above. This deactivates the pyridine ring towards substitution and directs any reaction onto the non-heterocyclic ring.

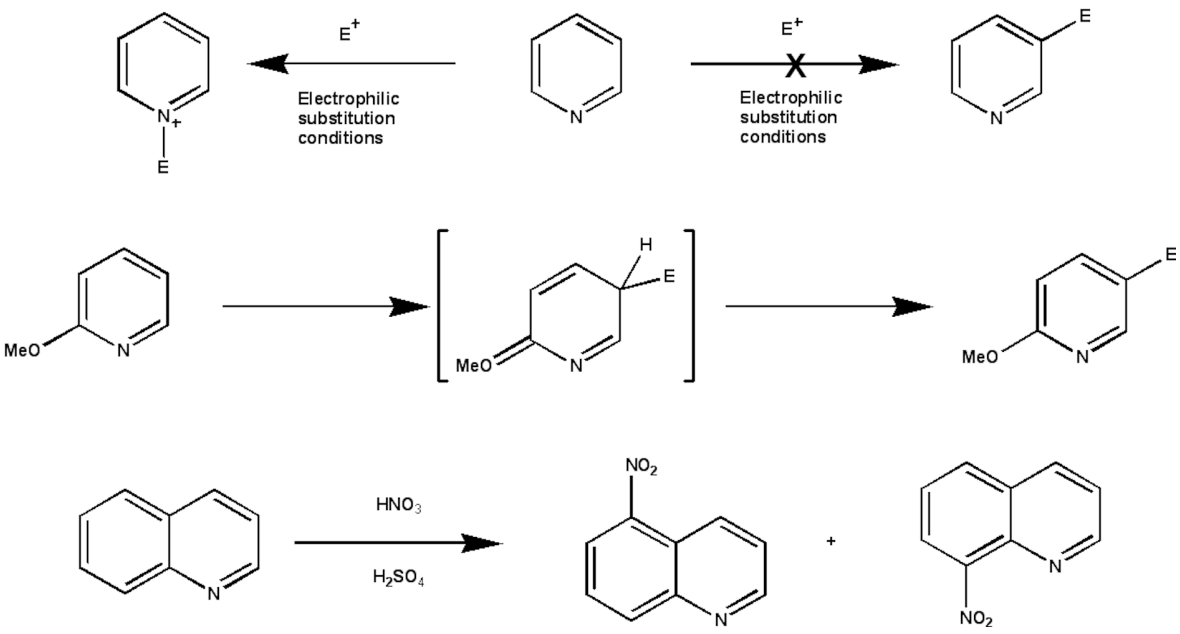

Scheme 1: Electrophilic substitution of pyridine (top), pyridines with electron donating substituents (middle) and the electrophilic nitration of the benzo-fused pyridine quinoline (bottom).

One way of activating pyridine-like heterocycles towards electrophilic substitution is by the conversion to the pyridine N-oxide[96] which, although it also produces a quaternary pyridinium nitrogen, allows the negative charge of the oxygen atom to be delocalised around the aromatic ring to activate it towards electrophilic substitution. Such substitution occurs generally at the C4 position of the pyridine ring due to electrostatic repulsion between the electrophile and the positively charged quaternary nitrogen atom. The conversion to the N-oxide has the added advantage of being easily reversible, once the desired transformation has been accomplished the N-oxide can be converted back to the pyridine by reduction with PCl_3, producing the substituted pyridine and phosphorous oxychloride.

The same effect which gives rise to the deactivation of the pyridine ring towards electrophilic substitution activates the ring toward attack by nucleophiles, generally at the C2 or C6 position of the ring, analogous to nucleophilic attack of a carbonyl group at the 1,2 or 1,4 positions. Attack at these positions results in the loss of aromaticity of the heterocyclic ring, and while under certain conditions the intermediate anion can

rearomatise by loss of hydrogen as a hydride anion (as illustrated by the Chichibabin reaction, see Scheme 2) the nucleophilic substitution of pyridine rings is more favourable when better leaving groups are present, such as halogen atoms which can leave as halide anions, at the C2 or C6 position.

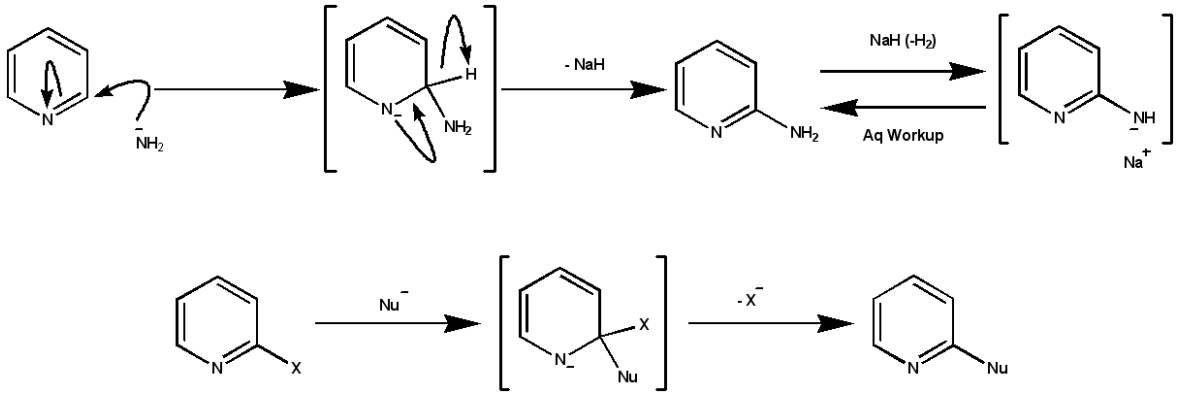

Scheme 2: Simplified reaction mechanism of the Chichibabin reaction (top) and Nucleophilic substitution of pyridine substituted at the 2- position with a leaving group X (where X = halogen,[97] methoxy,[98] tosyl or mesyl[99]) (bottom).

Halopyridine derivatives can also take part in metal-catalysed cross coupling reactions such as Heck or Sonogashira and so are central intermediates in the formation of derivatised pyridine and benzo-fused pyridine heterocycles. Such intermediates can be prepared form their pyridone analogues, or by radical substitution by bromine or chlorine at high temperatures.

Formation of the pyridine N-oxide,[96] as well as encouraging electrophilic substitution of the pyridine ring, also activates the ring towards nucleophilic substitution by stabilisation of the negative charge of the nucleophilic substitution intermediate by the cationic nitrogen of the pyridine N-oxide. This motif is also observed in the reactivity of N-substituted pyridinium cations towards nucleophilic reagents.

Pyridinium derivatives are susceptible to nucleophilic attack at the 2- and 4- positions because the negative charge can be delocalised onto the cationic nitrogen resulting in the

dearomatisation of the system yielding a neutral reaction product. This can be seen in the reaction of N-alkylpyridinium cations with hydroxide anions to produce a "*pseudobase*" addition product, which can then be oxidised to form an N-alkyl pyridone.[100] This reaction can be synthetically useful as nucleophiles such as Grignard reagents can be used to functionalise the ring at the 2- or 4- position, followed by oxidative rearomitastion to the pyridinium using reagents such as silver nitrate to yield the product nitrate salt (see Scheme 3).

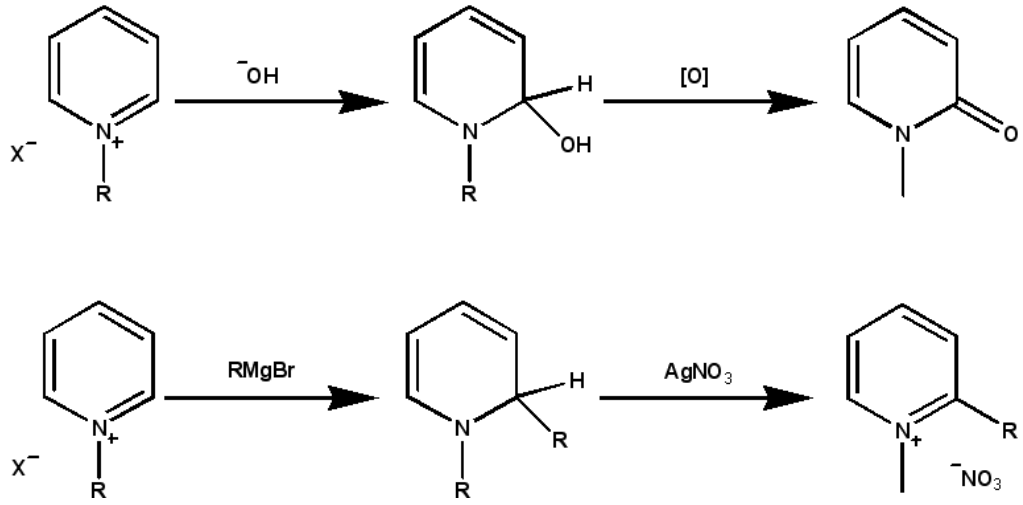

Scheme 3: (Top) Addition of hydroxide to alkyl pyridinium cations followed by oxidation by, for example, $K_3Fe(CN)_6$,[100] to yield the corresponding N-alkyl pyridone. (Bottom) Use of Grignard reagent followed by oxidation by $AgNO_3$ to yield the alkyl pyridinium nitrate salt.[101]

Pyridinium derivatives are also susceptible to reduction by a variety of methods such as catalytic reduction with hydrogen at room temperature and pressure,[102] reduction with complex metal hydrides such as $NaBH_4$[103] and also by formate. The reduction of alkyl pyridinium derivatives can be seen as an analogue to the biological activity of the coenzyme nicotinamide adenine dinucleotide (NAD+) which is important in biological redox reactions.[104]

Heterocyclic chemistry represents an important area of the development of organic chemistry with the fundamentals of reactivity relatively well understood. Because of the importance of these structures to medicinal chemistry the development of new methodologies for the construction of heterocyclic systems will always be an area of active research. In particular the search for methodologies which can introduce increased structural complexity in the fewest possible synthetic steps is active area of modern research.

2.2 The Synthesis of Dihydro-1H-imidazo-(1,2-F)-phenanthridinium (DIP) cations and related structures.

Because of the biological significance of π interactions, especially in terms of interactions with the DNA macromolecule (see section 2.2.3) there is a great deal of active research into the derivatisation of large polyaromatic systems.[105-108] One such polyaromatic system which has seen very few ring extensions around the core of the ring system and none on the central heteroaromatic ring is that of phenanthridine. Previous work in the Cronin group has led to the discovery of a number of new methodologies for the extension of this ring system by the exploitation of its pyridyl like reactivity combined with the judicious introduction of reactive alkyl groups on the heteroaromatic nitrogen. The main heteraromatic platform used in the present thesis is that of the Dihydro-1H-Imidazo-(1,2-F)-Phenanthridinium (DIP) cation.

2.2.1 DIP

The DIP cation is a large polyaromatic cation consisting of a dihydro-imidazole ring fused onto the central ring of a phenanthidine moiety (**5**, see Scheme 4) which is synthesised from *N*-bromoethyl phenanthridinium bromide **3** by reaction with a primary amine under basic conditions.

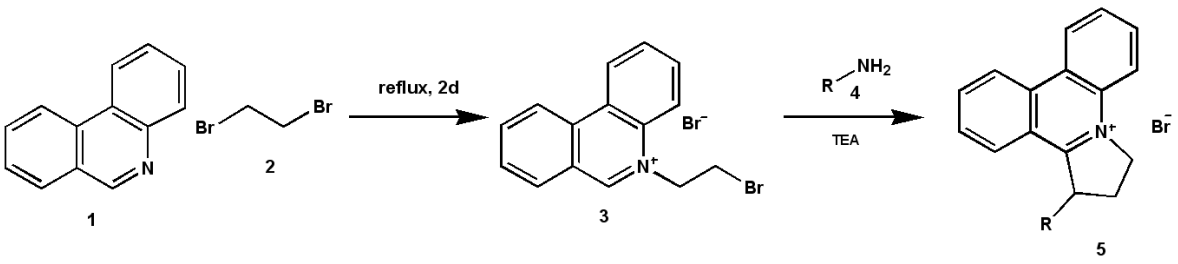

Scheme 4: Synthesis of Dihydro-1H-Imidazo-(1,2-F)-Phenanthridinium (DIP) cation.

Mechanistic investigations into this reaction identified two possible pathways *via* which this reaction could proceed (see Scheme 5). One possible reaction mechanism (Path A) could be designed where the primary amine initially adds nucleophilically to the *α* position of the phenathridinium ring follwed by a second nucleophilic substitution onto the bromoethyl side chain of the phenanthridinium moiety. This would lead to a favourable *5-exo-tet* cyclisation to give intermediate **7** which is then oxidised by a second equivalent of the starting material to yield the rearomatised DIP product **5**. An alternative pathway (Path B) was invisioned where the initial nucleophilic attack of the primary amine takes place on the bromoethyl side chain leaving the phenanthridinium moiety unaffected until the second step in the reaction where the amine attacks the *α* position of the phenanthridinium ring leading to an unfavourable *5-endo-trig* cyclisation to give **7**. The pure product precipitates from solution as the reaction proceeds and can be isolated by simple filtration and washing with an appropriate solvent.

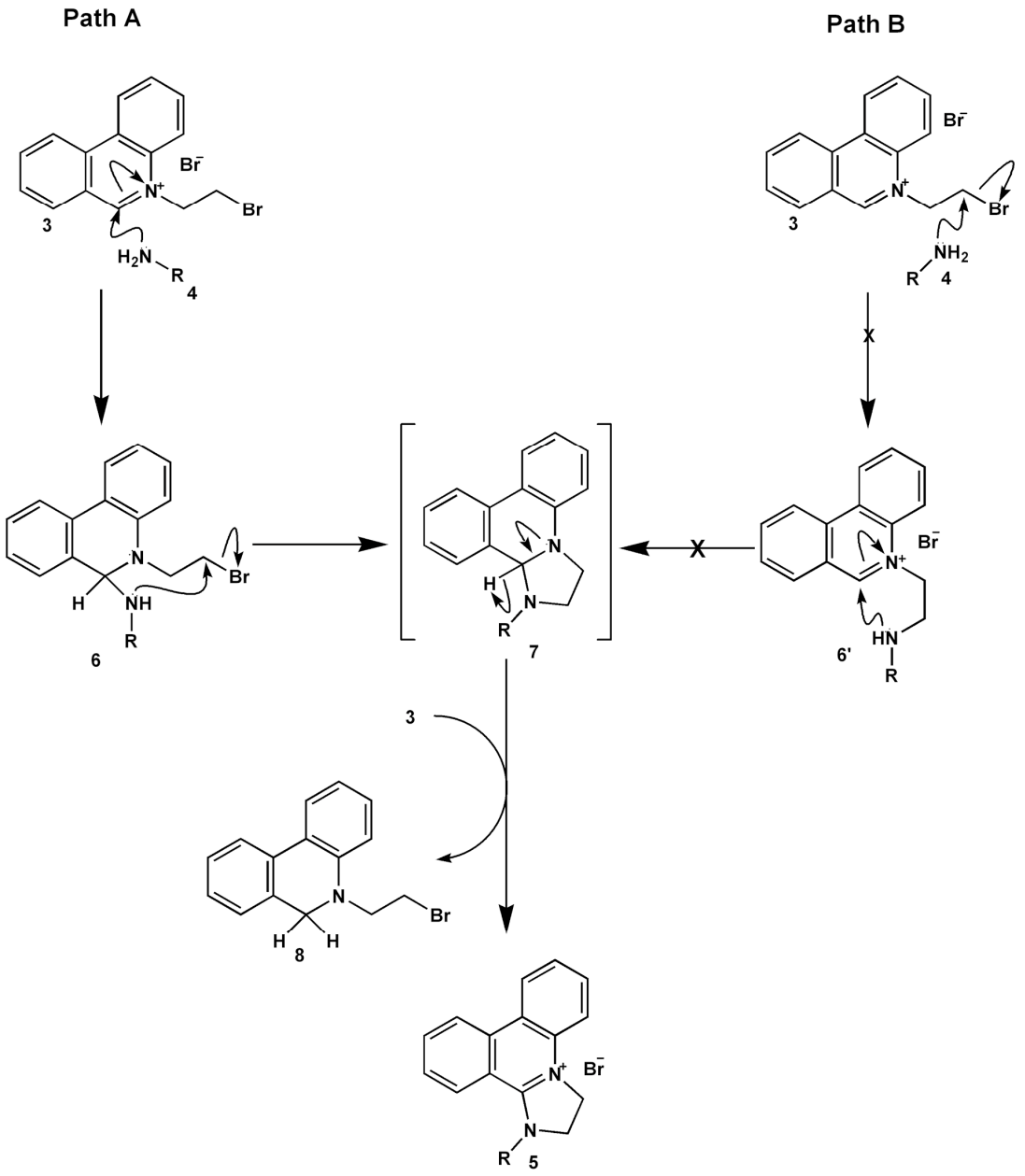

Scheme 5: The two possible reaction pathways in the mechanism of the DIP synthesis reaction.

The oxidation product **8**, common to both reaction pathways, was isolated and characterised in accordance with the oxidative step of the proposed pathways, and electrochemical investigations in acetonitrile showed this *in situ* oxidation step to be irreversible. The efficiency of this oxidation can be explained by the delocalisation of the positive charge of the phenanthridinium between the two nitrogens of the dihydro-

imidazole ring, this is shown in crystal structures of DIP compounds where the bond lengths indicate significant double bond character to both of the carbon-nitrogen bonds (see Scheme 6).

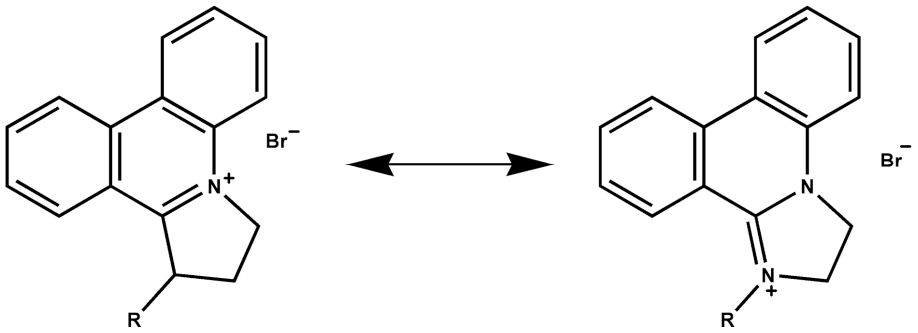

Scheme 6: Resonance structure of DIP cation showing delocalisation of the positive charge over the two nitrogens.

The intermediate **7** was characterised by a biphasic reaction performed in an NMR tube in a $D_2O/CDCl_3$ solvent system where the organic soluble **7** is isolated from the water soluble oxidising agent **3**. The presence of a singlet at δ 4.81 ppm confirms the presence of the hydrogen which is lost as a hydride during the oxidation step.

Intermediate **6** has also been isolated by the use of sterically hindered primary amines which cannot undergo the required cyclisation step, to further investigate this step the bromine of the bromoethyl side chain was replaced with non-leaving groups such as fluorine or hyrdroxyl. Reactions of these analogues of the DIP starting material did not show cyclisation, however, the α-addition product was formed almost instantaneously. The accumulation of such mechanistic evidence as well as the requirement of Path B for an unfavourable *5-endo-trig* cyclisation strongly suggest that Path A is the mechanism for the DIP reaction.

2.2.2 Imidazo Phenanthridine (IP) Derivatives

This methodology has been extended by work within the *Cronin* group to produce larger conjugated aromatic systems with a fully oxidised imidazo-ring. Oxidation of the DIP to the corresponding Imidazo-Phenanthridinium (IP) proved to be impossible using conventional oxidising agents, probably due to the high stability of the aromatic ring. The procedure was adapted by the use of liquid ammonia (see Scheme 7), which allows the loss of aromaticity simply by deprotonation of the intermediate **11**, giving a route to the formation of the imidazole ring from a less stable intermediate. This then leads to a neutral imidazo phenanthridine moiety which can be further functionalised by nucleophilic substitution of a range of electrophiles to give a family of Imidazo-Phenanthridinium (IP) derivatives analogous to the DIP structure.

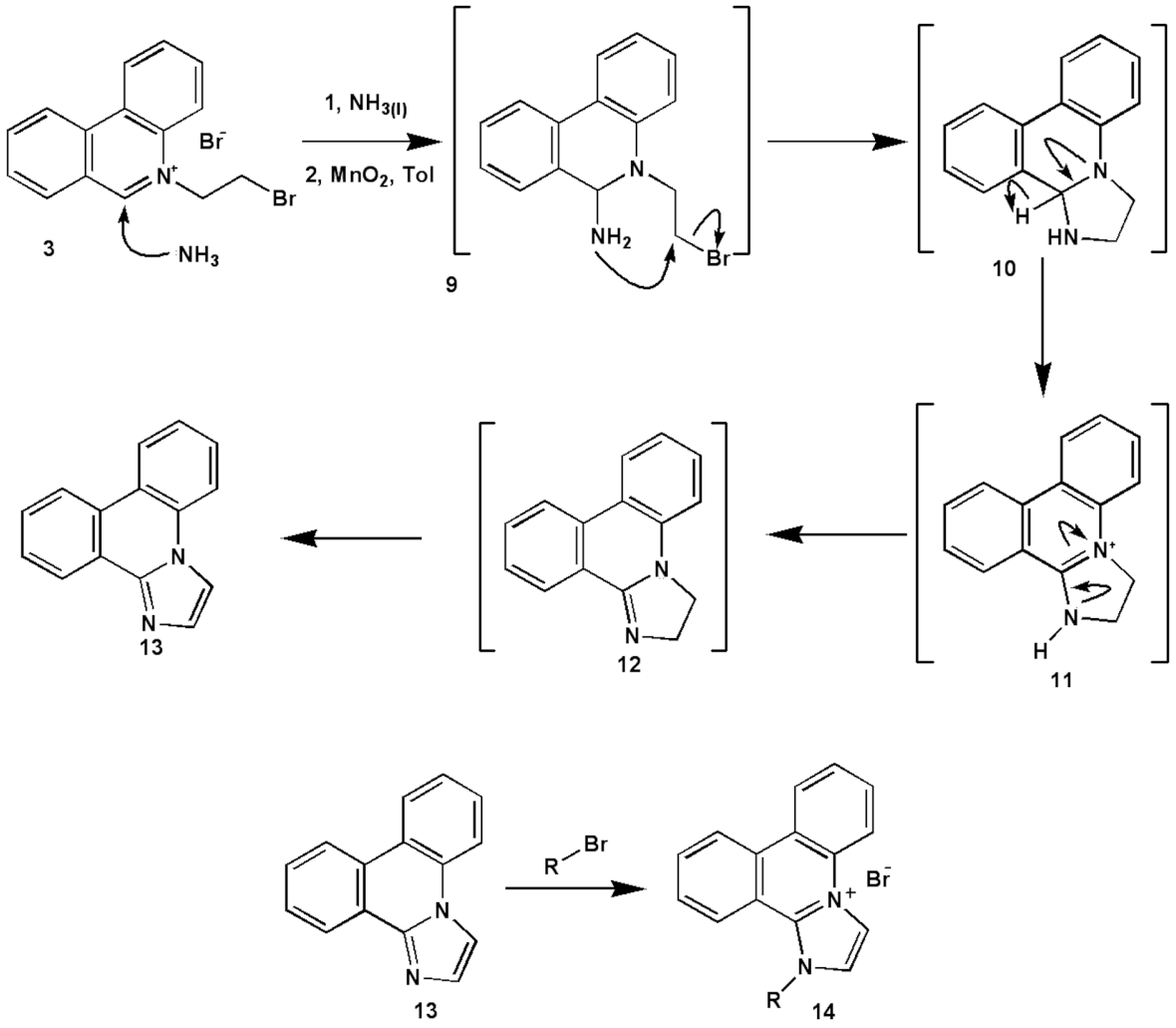

Scheme 7: (Above) 5-step-one pot synthesis of imidazo-phenanthridine (13) and (Below) derivatisation of 13 by reaction with a suitable electrophile.

A variation of this procedure provides a route to the synthesis of IP derivatives which are functionalised on the carbon atoms of the imidazole ring of the framework (see Scheme 8). Reacting a substituted α-bromo carbonyl compound with phenanthridine provides a starting material of structure **16**. In this case use of liquid ammonia is impossible as the carbonyl moiety increases the acidity of the adjacent methylene position and leads to the formation of a stabilised ylide that undertakes cycloaddition side reactions. In this procedure therefore, ammonium acetate is used as a mild source of ammonia. The initial nucleophilic addition is then followed by a condensation reaction which closes the five membered ring and introduces the first C=N double bond. Under acidic conditions this

imine (**19**) isomerises to an enamine and the resulting dihydroimidazole is oxidised by MnO_2 to form the substituted Imidazo-Phenanthridine compound **21**.

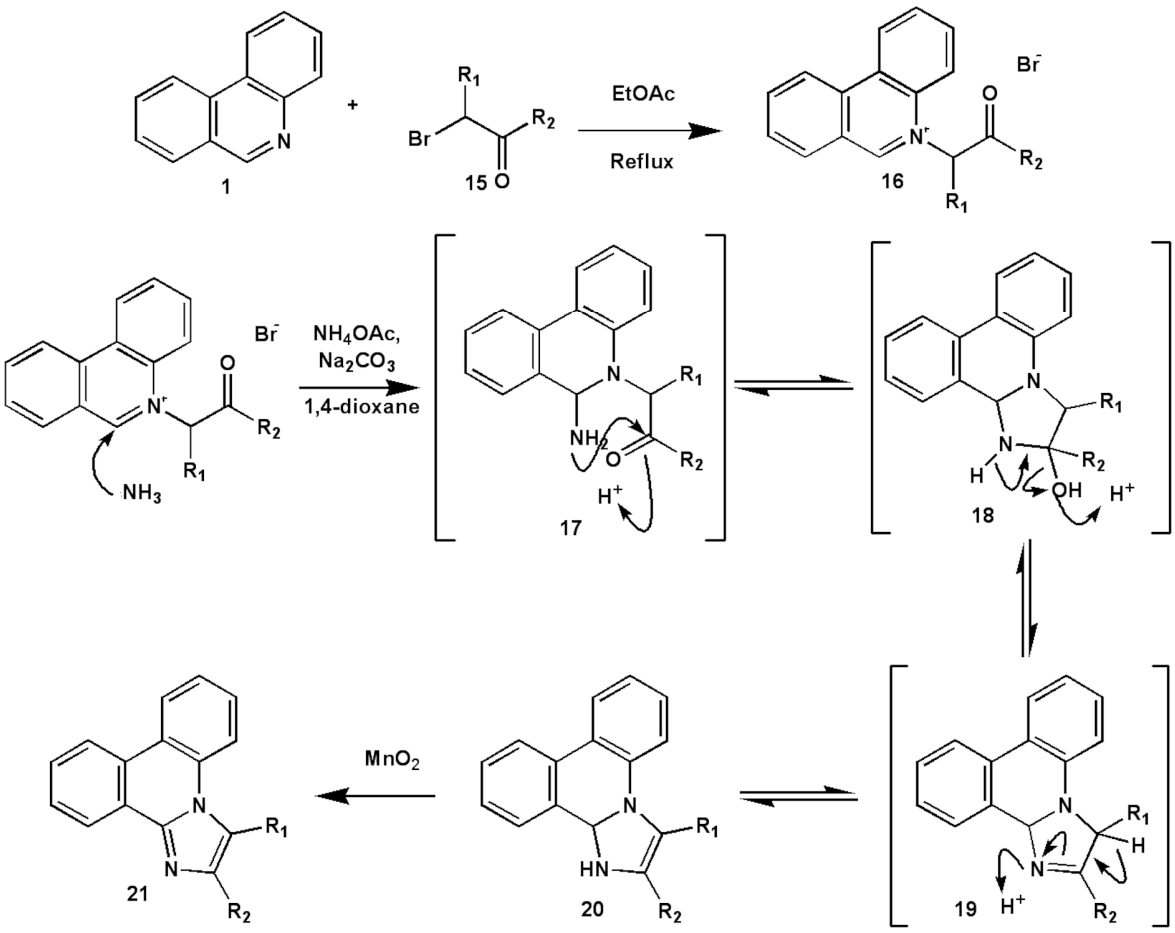

Scheme 8: (Top) Synthesis of IP derivative starting material (16). (Bottom) Mechanism of formation of derivatised IP (21).

2.2.3 Biological activity of DIP and Related Structures

As discussed above, heterocyclic compounds have an important role in biological processes, and one of the most important targets for interaction of compounds is the molecule of DNA, especially for the fight against cancer. There are several ways in which small molecules can interact with DNA such as through binding in the major or minor grooves of the double helical B-DNA structure, or by alkylating one of the Watson-Crick

base pairs of the DNA molecule and forming a covalently linked DNA adduct. Another important mode of interaction with DNA is that of an intercalative mode, first suggested by Lerman in the 1960's,[109] whereby an aromatic moiety can stack between the base pairs and bind by π stacking interactions in a similar fashion to the base pairs themselves. Aromatic cations are particularly well suited to this task as they take advantage of an electrostatic attraction with the anionic phosphate backbone of the DNA molecule.

Both DIP and IP derivatives posses DNA binding properties with binding constants in the order of $K = 10^4\ M^{-1}$. These molecules have been shown by viscometry studies to bind to DNA *via* an intercalative mode. DIP cations in particular have shown cytotoxicity on ovarian cancer cell line A2780 using a tetrazolium dye based microtitration (MTT) based assay. The cytotoxicity of DIP compounds has been shown to be highly dependant on the structure, especially the hydrophobicity, of the non-DIP region of the molecule, and as such exhibit tunable biological activity. DIP cations also show significantly more cytotoxic activity on some cis-platin resistant cell lines. These biological properties point to this category of polyaromatic heterocyclic moieties being of great interest to medicinal chemistry, and all the biological properties of the compound arise from the ability of the structures to participate in supramolecular interactions *via* their π electron systems.

Aims

The ability to controllably direct the solid state structures of coordination compounds *via* the non-covalent interactions of the coordinated ligand molecules is an area of much active reseach in the field of crystal engineering. Therefore the generation of new ligands which can act as directing building blocks in the synthesis of such supramolecular architectures is vital to the growth of this field. The aim of this work is the design and synthesis of new ligands for transition metal coordination chemistry which can take part in supramolecular π stacking interactions to form extended architectures in the crystalline phase.

The recent development of phenanthridine heterocyclic chemistry within our group represents the opportunity to utilise a new class of polyaromatic heterocycles, specifically DIP and IP related frameworks, as supramolecular building blocks in crystal engineering. This research will aim at the design and synthesis of a number of new ligands which incorporate DIP or IP regions. These new ligands will then be coordinated with a variety of transition metals to produce new complexes. These complexes will be crystallised and their supramolecular interactions in the crystalline phase will be investigated *via* their X-Ray crystal structure.

In order to further develop the phenanthridine chemistry which has led to these frameworks, a new organic reaction will also be investigated focussing on the use of carbon based nucleophiles in DIP-like reactions to develop new synthetically useful organic reactions and functional organic materials.

Results and Discussion

3 COMPLEXES OF DIP PYRIDYL LIGANDS

3.1 Ligand Design: Pyridyl DIPs

As the DIP structure itself is cationic in nature, the parent molecule of the DIP family does not lend itself well to coordination with metal salts as the positive charge of the metal ion will repel the cationic DIP, and the degree of conjugation between the nitrogen atoms in the structure means that neither atom possesses a suitable lone pair for the coordination of metal ions. In order to obtain suitable DIP ligands for complexations it is therefore necessary to exploit the ease with which the DIP moiety can be synthesised with a variety of R groups to suit a particular purpose (see Scheme 9). This has been seen in previous work where the R group of the DIP structure has been tuned to increase the cytotoxicity of the resulting compound.[110] In this work however the aim of producing ligands for coordination chemistry containing DIP moieties required the choice of an R group with a lewis basic lone pair of electrons in a suitable position for metal complexation. To that end it was decided to incorporate a pyridyl group into the DIP structure which would have a free lone pair available for metal coordination that would be sufficiently separated from the cationic region of the DIP structure that metal coordination would not be hampered. Two such ligands were designed and synthesised using the standard DIP synthesis procedures[111] from 2-methylaminopyridine and 4-methylaminopyridine to form compounds **22**·Br and **23**·Br respectively (see Scheme 9).

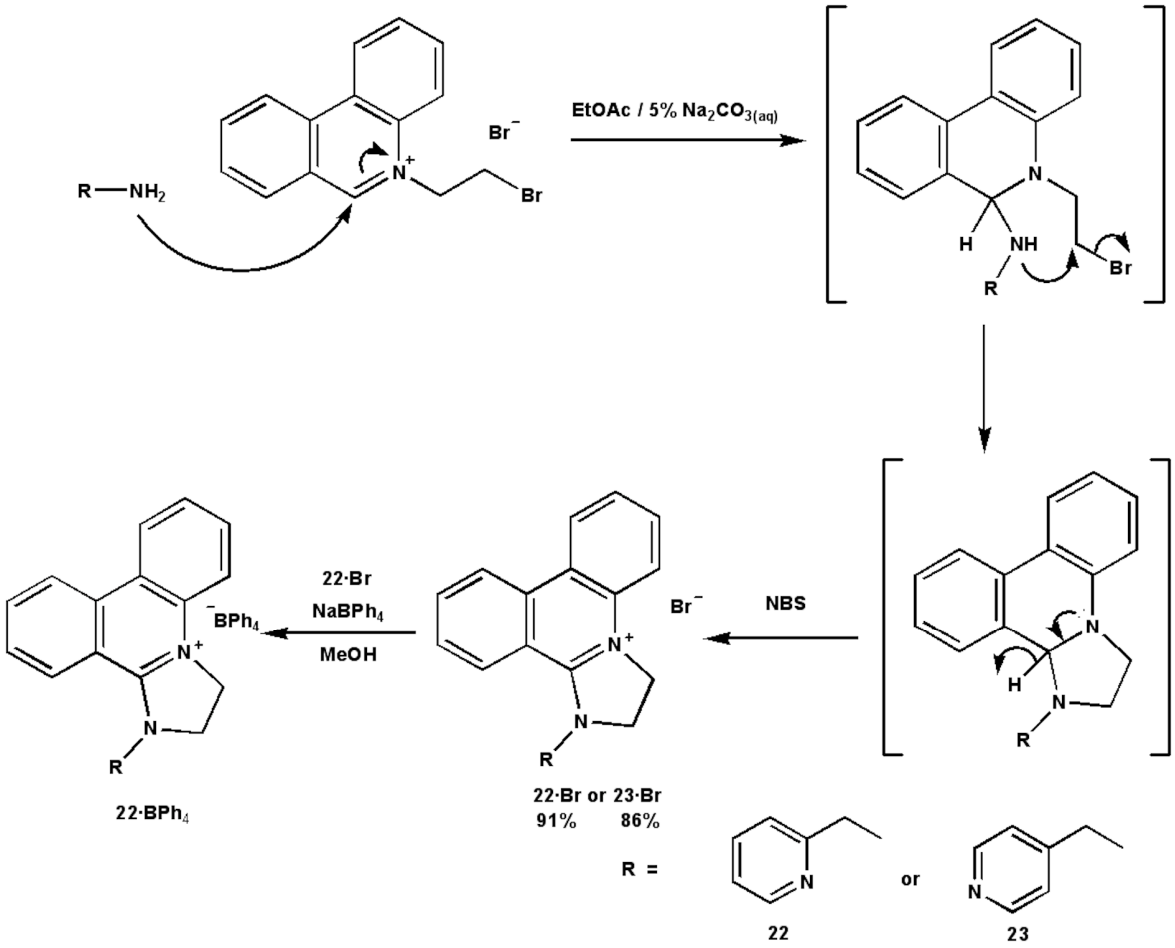

Scheme 9: Synthesis of pyridyl functionalised DIP compounds 22·Br and 23·Br.

Compounds **22**·Br and **23**·Br were synthesised *via* a biphasic methodology whereby the initial *α* addition of the primary amine to the BEP starting material, **3**, was carried out in a mixture of ethyl acetate and 5% aqueous sodium carbonate solution. In the absence of an oxidising agent the *α* addition product moves to the organic layer where it cyclises to give the trihydro-imidazo-phenanthridine (TIP) intermediate. The organic layer is then separated, washed with deionised water to remove any salts present and then the oxidising agent N-bromosuccinimide (NBS) is added to the organic layer to yield the oxidised DIP structure which precipitates out of the organic solvent. This procedure was used in preference to the monophasic conditions described in the introduction (see Section 2.2.1) as that procedure uses a second equivalent of the bromoethyl phenanthridinium starting material as an oxidising agent and therefore is less atom efficient. The compounds **22**·Br and **23**·Br were designed to interact with metal ions in a similar fashion, however the use

of the 2-pyridyl moiety in **22** and the 4-pyridyl moiety in **23** give the two compounds significantly different binding environments for metal ions, with **22** predicted to be significantly more sterically hindered than **23**.

By carrying out ion exchange from bromide to tetraphenyl borate, crystals of the **22** cation were obtained that were of sufficient quality for X-Ray crystallographic analysis. The tetraphenyl borate salt of the **22** cation crystallises from methanol in a monoclinic $P2_1/n$ system. The asymmetric unit of the crystal structure includes one DIP cation and one BPh_4 anion. The pyridine ring of the ligand structure is located in such a way as to be almost perpendicular to the plane described by the phenanthridinium ring system, describing a dihedral angle of 88.3(1)º. This almost perpendicular arrangement represents the possibility of this ligand forming two orthogonal sets of π interactions per ligand molecule (see Figure 10). The ligands used in this study have very limited structural flexibility, with only one CH_2 unit linking the rigid DIP ring system with the coordinating pyridyl moiety. This rigidity has major implications for the interaction of the ligand molecules both in metal coordination and in interactions with other ligands in the crystalline phase. With a restricted access to different conformations, the coordination geometry and supramolecular interactions of the ligand will be predominantly influenced by the perpendicular arrangement of the aromatic systems, with the proximity of the steric bulk of the DIP system exerting a strong influence on the coordination geometry of other ligands to the metal ions.

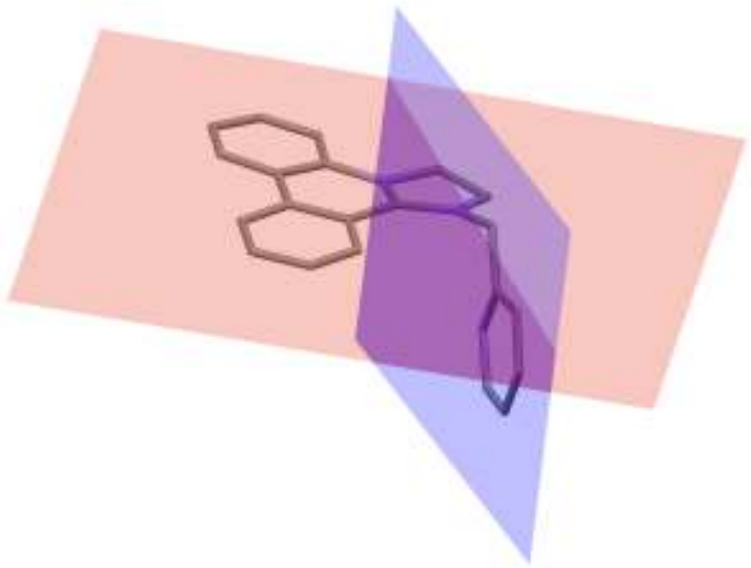

Figure 10: X-Ray crystal structure of 22·BPh_4 showing the almost perpendicular arrangement of the planes of the pyridyl and DIP moieties.

As the DIP ring system is not symmetrical and contains both quinoline and isoquinoline-like rings attached to the central pyridyl-like ring of the phenanthridinium moiety, it will be useful for the following discussion of the supramolecular interactions of this ligand in the crystalline phase to define the rings of the DIP system. In this discussion, the isoquinoline-like peripheral aromatic ring of the DIP system will be referred to as ring **X**, the central aromatic ring as ring **Y**, the quinoline-like aromatic ring as ring **Z** and the non-aromatic dihydro-imidazo ring as ring **I** (see Figure 11).

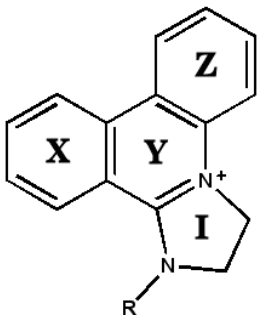

Figure 11: Designation of the individual rings of the DIP moiety that will be used in this discussion.

3.2 Mononuclear Complexes of DIP-Pyridyl Ligands with Cu^{II} Salts

3.2.1 Complexation of 22·Br with $Cu(BF_4)_2·6H_2O$

The reaction of one equivalent of **22**·Br with two equivalents of $Cu(BF_4)_2·6H_2O$ and subsequent slow evaporation from methanolic solution yielded green, needle shaped crystals of compound **24** of suitable quality for X-Ray crystallographic analysis.

The asymmetric unit of **24** is made up of one $[Cu_{0.5}Br(\mathbf{22}\text{-}Br_{0.05})]^+$ cation with the coordinating ligand partially brominated at the C4 position, an uncoordinated **22**-$Br_{0.45}$ molecule which has been partially brominated at the C25 position and two BF_4^- anions as noncoordinating counterions. The crystal structure shows that the Cu^{II} ion is coordinated by two **22**-$Br_{0.05}$ molecules *via* the pyridyl region of the ligands as expected. The Cu^{II} ion is further coordinated by two Br^- anions giving the copper an overall coordination environment of CuN_2Br_2 with a square planar geometry. The Cu-N bond distance is 1.959(4) Å and the Cu-Br bond distance is 2.453(1) Å. The Cu-N and Cu-Br bond lengths and the bond angles around the Cu^{II} ion are all within the normal ranges expected for such a CuN_2Br_2 donor set when compared to comparable complexes from the CSD database.

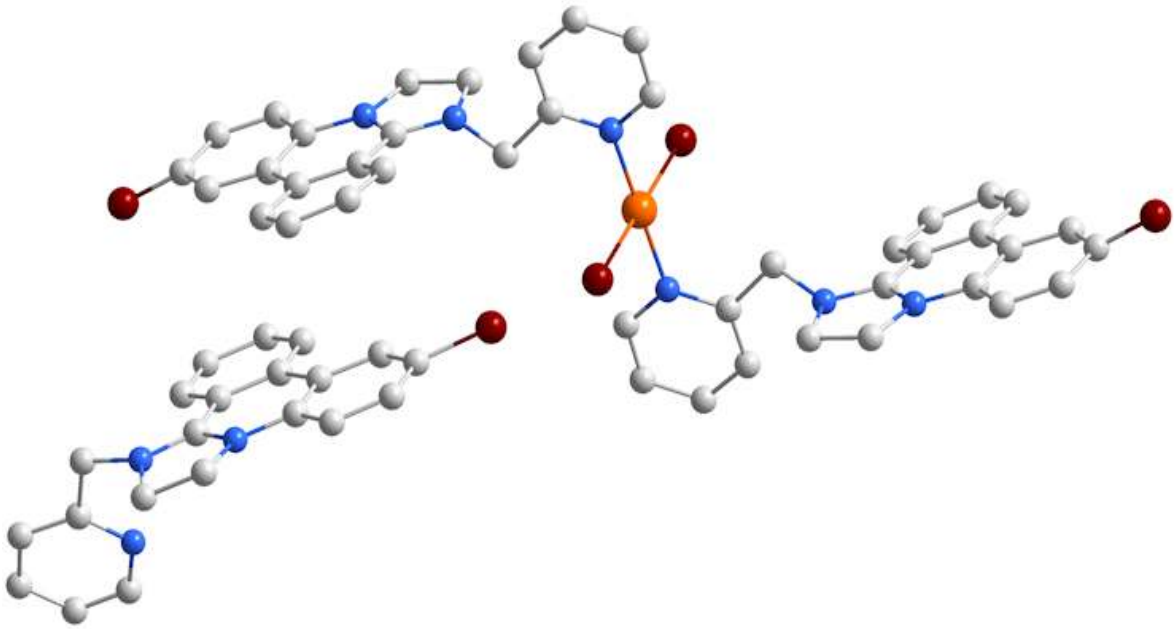

Figure 12: Ball and Stick representation of the asymmetric unit of 24 showing both the coordinated and uncoordinated ligand molecules. Uncoordinated anions and hydrogen atoms have been removed for clarity.

Recent work by Hauser *et al.*[112] has introduced the concept of a new four coordinate geometry index, τ_4, which is similar in principle to the standard τ_5 parameter which is used to describe trigonal distortion of a five coordinate species from square pyramidal geometry.[113] Like τ_5, τ_4 is defined using the two largest θ angles (α and β) in the four coordinate species ($\tau_4 = [360-(\alpha+\beta)]/141$) and ranges from 0 for a square planar geometry to 1 for tetrahedral geometry. In the case of **24**, with a N-Cu-Br angle of 89.20(14)^o, this formula gives a τ_4 value of 0 indicating a high degree of square planar character for the Cu^{II} ion.

It should be mentioned here that there is partial bromination at the C4 position of the coordinated **22**-$Br_{0.05}$ with a C-Br distance of 1.739(7) Å (the occupancy of bromine atom is about 5%) and the uncoordinated **22**-$Br_{0.45}$ is also partially brominated with a 50% occupancy at the C25 position. Some examples of oxybromination of aromatic compounds have been reported, in which different types of catalysts,[114, 115] or biphasic media[116, 117] have been utilized in order to achieve the brominated products. In contrast, the copper(II)-

mediated bromination reaction seen here is a very unusual result (the reaction mixture contains only the ligand and copper salt).

In this structure the plane of the pyridyl ring of the coordinated ligand makes a dihedral angle of around 79.4(1)º with the plane described by the phenanthridinium moiety, which is slightly smaller than that observed in the crystal structure of the BPh_4^- salt of the ligand alone (see section 3.1), but larger than the angle described by the same features of the ucoordinated molecule of **22** present in the crystal structure; 69.4(1)º. This ligand flexibility highlights the influence exerted on the conformation of the molecule by the intermolecular forces experienced in the crystal phase. The planes of the phenanthridinium moieties of the coordinated and the uncoordinated ligands in this crystal structure are almost parallel describing a dihedral angle of around 1.63º. In the crystalline phase, **24** can be seen to form supramolecular sheets *via* π stacking interactions (see Figure 13).

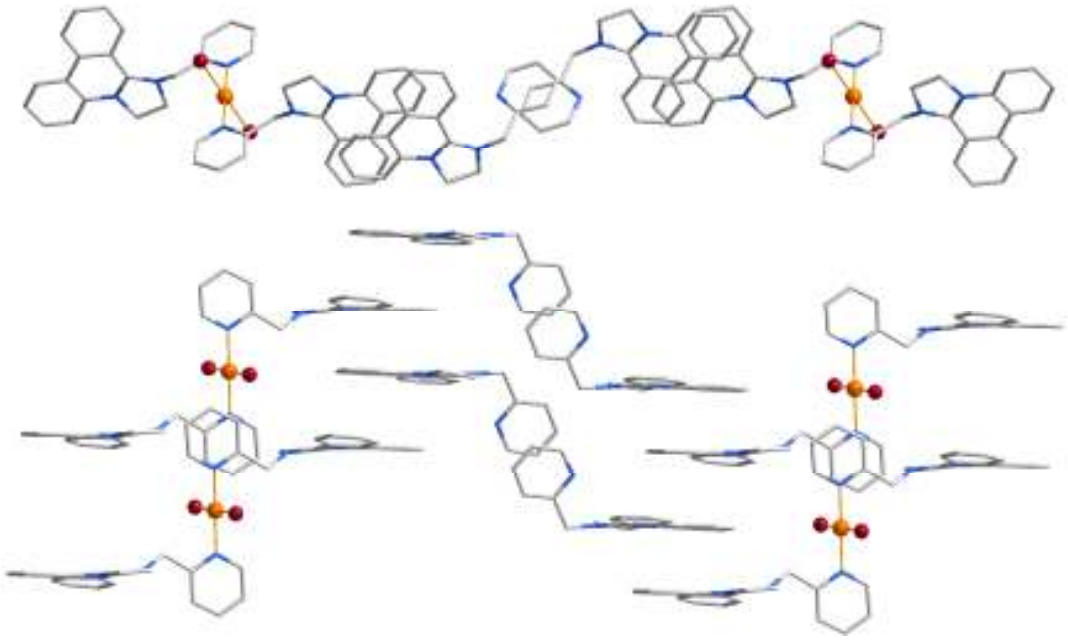

Figure 13: Crystal structure of 24 shows π-π interactions between the phenanthridinium moieties of adjacent molecules forming 2D supramolecular sheets through the crystal structure. Structure is viewed along the crystallographic *b* axis (top) and the (+*b*+*c*) crystallographic vector (bottom); counter ions and partially occupied bromines are omitted for clarity.

The coordinated **24** molecules in the crystal structure experience π stacking interactions with the uncoordinated **22** molecules above and below them. These interactions are arranged such that the majority of the interaction takes place between the peripheral benzoid rings of the DIP ring system, with each **X** ring interacting with the corresponding **Z** ring in order that the distance between the cationic charges residing on the nitrogen atoms is maximised. The distances between centroids defined by each of the peripheral rings of DIP region of the structure are in the range 4.03(1) – 4.45(1) Å. The uncoordinated DIP molecules experience a second, orthogonal set of π stacking interactions between their pyridyl ring systems with a centroid-centroid distance of 3.56(1) Å. The structure is therefore made up of infinite 1D chains consisting of a repeating unit of uncoordinated ligand molecules (A) linked through π stacking interactions to a central diligand metal complex (B) in an ···ABAABAABA··· arrangement (see Figure 13, top). These chains are then linked into two dimensional sheets along the crystallographic *b* axis by π stacking interactions between the DIP regions of the coordinated and uncoordinated ligands.

3.2.2 Complexation of 22 with $Cu(NO_3)_2 \cdot 3H_2O$

By changing the Cu^{II} salt used in the reaction from BF_4^- to NO_3^- a second compound, **25** was synthesised. **25** is a five coordinate Cu^{II} complex with a $CuBr_2NO_2$ donor set, of which the two bromide anions come from the initial **22**·Br ligand used in the complexation (see Figure 14). The cationic charges of the Cu^{II} and DIP moiety are entirely compensated for by the coordinated anions leading to a formally neutral complex with the formula $CuBr_2(NO_3)$(**22**).

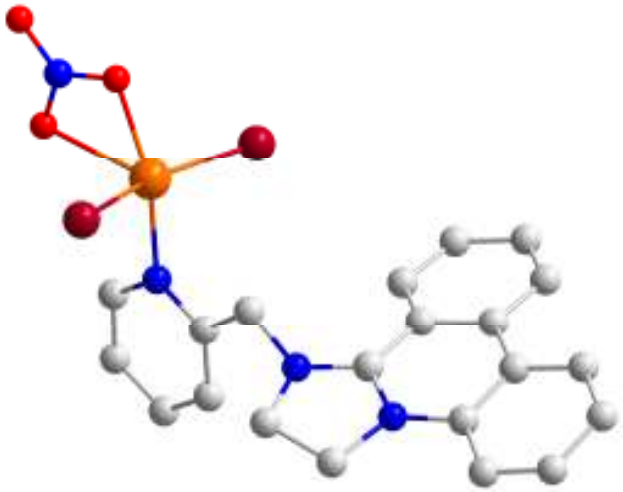

Figure 14: Ball and stick representation of the asymmetric unit of 25.

25 crystallises in a triclinic P-1 system with the Cu^{II} in a distorted square pyramidal geometry, with the basal plane made up of one pyridyl nitrogen, two bromide anions and one of the oxygens from the nitrate ligand. The τ_5 parameter (used to describe the degree of trigonal distortion from a square pyramidal geometry where a value of 0 indicates square pyramidal geometry and 1 indicates trigonal bipyramidal) for this compound is 0.07. This does not, however represent an ideal square pyramidal geometry as the apical oxygen is significantly off centre as a result of the bite angle of the chelating nitrate group the O-Cu-O angle is 56.6(4) º. The Cu-N bond length in the complex is 1.986(4)Å, the Cu-Br bond length are 2.4035(9) and 2.4097(8)Å, and the Cu-O bond lengths are 1.989(4) Å for the basal oxygen and 2.492(4) Å for the apical oxygen. These bond lengths are again in the normal range for such a $CuBr_2NO_2$ donor set. The crystal packing of **25** is again highly influenced by the supramolecular interactions of the DIP moieties (see Figure 15).

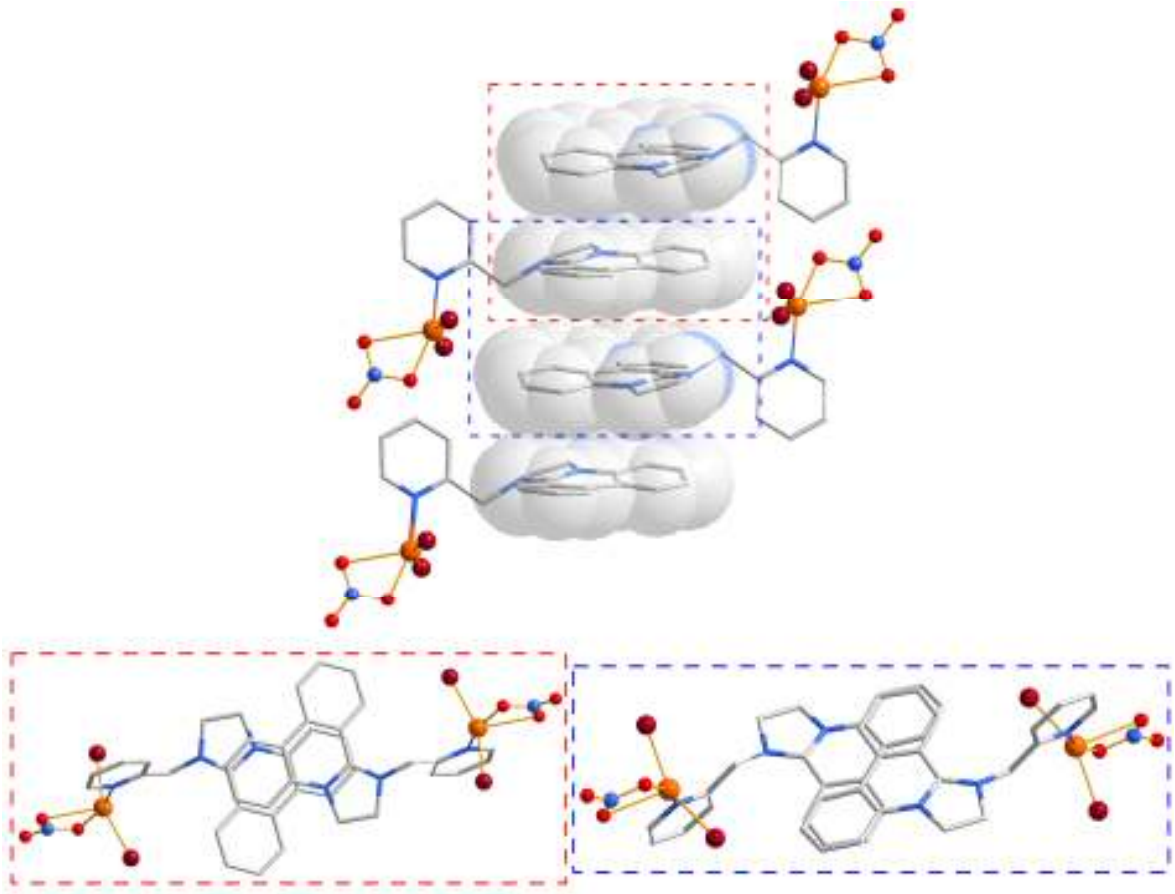

Figure 15: Supramolecular interactions of 25. (Top) 1D columns formed by supramolecular interactions showing two distinct interactions between the DIP ligands. (bottom, left) offset π stacking interactions (bottom, right) longer range interactions.

In contrast to the crystal structure of **24**, above, the pyridyl region of the ligand does not experience any interactions with neighbouring π systems, however the DIP regions of the ligand again exhibit π stacking interactions. In this structure each DIP unit experiences two sets of π interactions with neighbouring DIP moieties the first of which sees the overlap of two of the phenanthride rings in an offset fashion where the central **Y** ring of the DIP is interacting with the peripheral **Z** ring of the corresponding moiety (see Figure 15, bottom left). The distance between the planes described by the phenanthridinium moiety in this case is 3.51(1) Å and the distances between the centroids described by the individual interacting rings are 3.71(1) Å.

Along with these interactions each DIP moiety experiences a second set of interactions on the other side of the ring system (see Figure 15, bottom right). These interactions are considerably longer and are further offset than the previous example. The distance between the phenanthride planes is comparable to that shown above, indeed the planes are closer together with a separation of 3.45(1) Å. However, the degree of overlap between the ring systems is significantly less than in the first instance. In the case of this interaction the central ring of the phenanthridine system does not experience the π interaction and a motif similar to that observed in the π stacking of compound **24** is observed where the peripheral **X** and **Z** rings of the phenanthridinium systems interact. The lack of significant overlap in the system is shown by the long centroid-centroid distance between the interacting rings, of 4.58(1) Å. These distances would seem to preclude the existence of a π stacking interaction in this case, however, it has often been observed that in the case of ring slipped systems a better measure of the existence of π interactions is the atom to atom distance.[44] In this case the shortest C-C distance between the interacting rings is 3.51(1) Å, which is within the range which can be defined as a π interaction. The combination of these two interactions leads to the formation of 1D π stacked columns of complexes through the crystal structure (see Figure 15, top).

3.2.3 Complexation of 22 with $CuBr_2$

Reaction of **22** with $CuBr_2$ in a methanolic solution followed by slow evaporation yields another monoligand Cu^{II} complex with the formula $CuBr_3$(**22**) (**26**, see Figure 16). Once again the cationic charge of the Cu^{II} and DIP regions of the complex are completely compensated for by the anions coordinated to the Cu^{II} centre, giving a formally neutral molecular species. **26** crystallises in a triclinic crystal system with a *P*-1 space group and the asymmetric unit of the crystal structure comprises two crystallographically distinct complexes which have slightly different coordination geometries, but the same stoichiometry. As these two species have differing coordination geometries and experience differing supramolecular interactions, they have been arbitrarily labelled here as species A and species B to aid discussion.

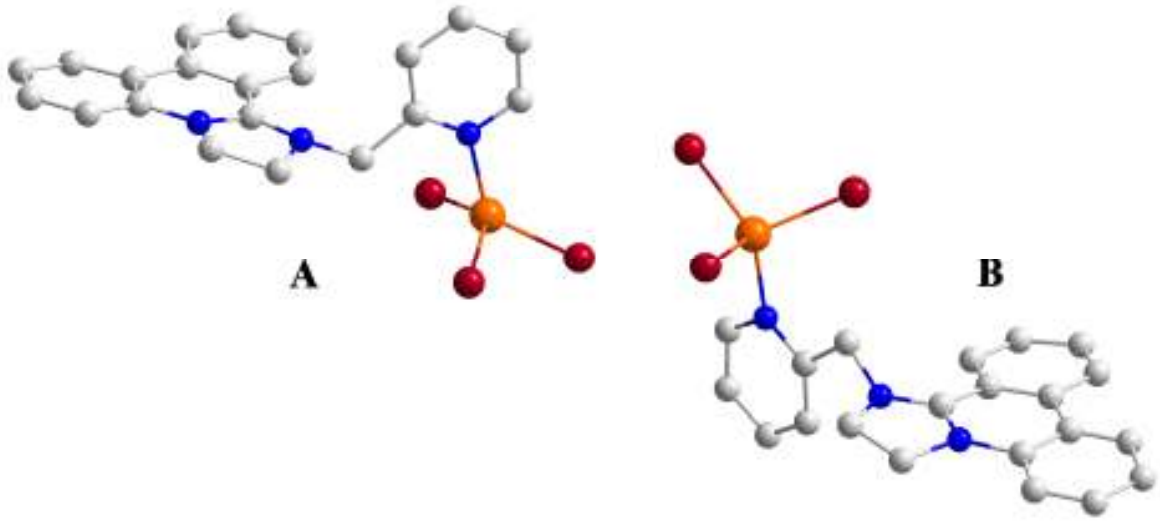

Figure 16: Ball and stick representation of the assymetric unit of 26 indicating the two crystallographically distinct species A and B. Atom colours as above.

Both species have a $CuNBr_3$ Donor set with C-N bond distances of 2.024(15) Å for complex A and 2.019(16) Å for complex B and C-Br distances ranging from 2.334(3) to 2.409(3) Å. The two complexes in the asymmetric unit have similar but slightly different coordination geometries, however they both show a quite unusual tetrahedral geometry for a Cu^{II} complex. The dihedral angles between the Br-Cu-Br and Br-Cu-N planes in the complexes are 89.90(1)º for species A and 63.00(1)º for species B and the calculated values for the τ_4 parameter described above are 0.662 and 0.663 respectively. This tetrahedral geometry is likely due to the steric environment of the Cu^{II} where the steric bulk of the large bromide anions and the CH_2 group in the *ortho* position of the ligand molecule prevent coordination of further ligands to the metal centre, and force the Cu^{II} ion to take up a tetrahedral geometry.

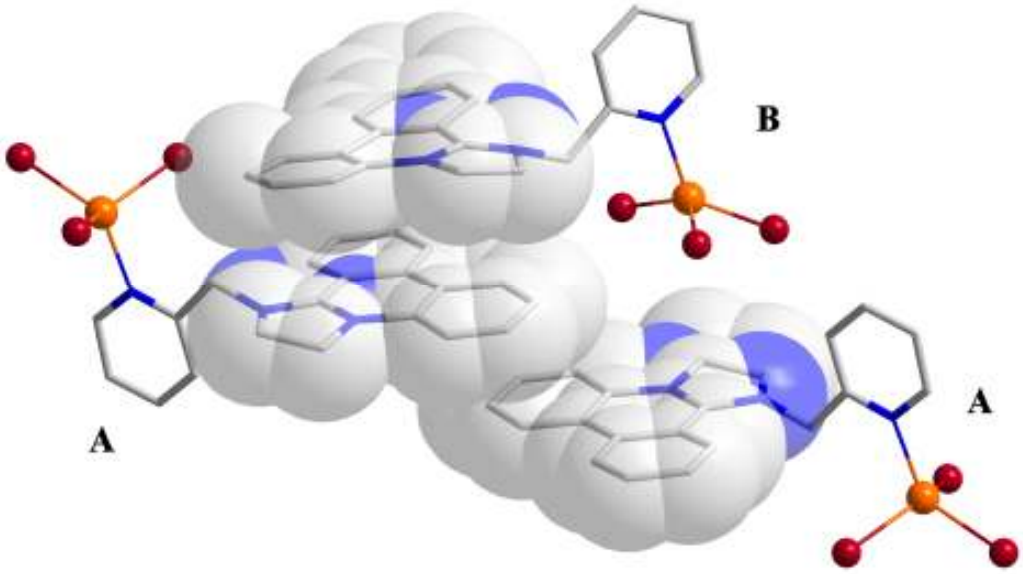

Figure 17: π interactions of species A in the crystal structure of 26.

The two distinct species in the asymmetric unit also experience differences in their supramolecular interactions, with each species experiencing different sets of interactions with their π systems. Species A exhibits two sets of π interactions in the crystal structure of compound **26** (see Figure 17), both of which are experienced through the DIP region of the ligand molecule; the pyridyl region does not interact with any other π system in the crystal structure. The DIP region of the ligand experiences, first of all, an interaction with the π system of a B type complex in which there is significant overlap of the ring systems. The central rings of the DIP systems are directly above each other with a centroid-centroid distance of 3.65(1) Å and each DIP system rotated and inverted with respect to the other in a manner such that the imidazo ring, **I**, of each ligand is directly above the peripheral **Z** phenanthridinium ring of the interacting system. These two ring systems are close to parallel with a dihedral angle between planes described by the phenanthridinium atoms of around 6.34(1)º.

On the other face of species A's DIP ring system there is an interaction with the π system of a second A complex which, by contrast, exhibits very little ring overlap. The two A species interact *via* only the peripheral **Z** phenanthride ring, and the centroid-centroid distance between these rings is 3.94(1) Å. The interplanar distance between these two ring

systems is 3.20(1) Å, and the shortest carbon to carbon distance between the two systems is 3.37(1) Å.

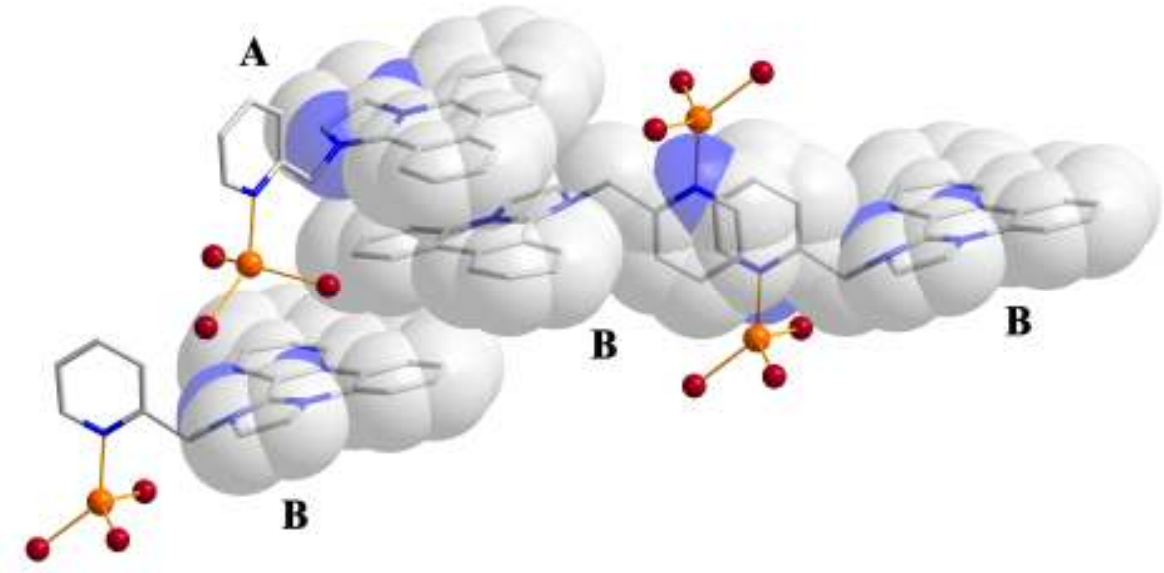

Figure 18: π interactions of species B in the crystal structure of 26.

As mentioned above species B experiences significantly different intermolecular forces in the crystal phase to species A. Species B interacts with a second B molecule *via* a π stacking interaction of its pyridyl region with the pyridyl region of a neighbouring complex (see Figure 18). As would be expected of this interaction the pyridyl rings are arranged such that the coordinating nitrogen atoms are at opposite sides to each other. As well as allowing the two pyridyl regions to come close together by avoiding steric clashes with the coordinated $CuBr_3$ moiety, this arrangement minimises the π–π repulsion experienced between the π systems and ensures that the areas of least electron density of one pyridyl ring interact with the regions of most electron density of the corresponding ring due to the polarising effect of the electronegative nitrogen atom and its coordination to the Cu^{II} centre (see Figure 19). This results in a relatively strong π interaction with the shortest carbon-carbon distance between rings being 3.37(1) Å. There is a degree of ring-slippage in this interaction as the two rings are not perfectly aligned and the distance between the centroids of the two rings is slightly longer with a value of 3.70(1) Å.

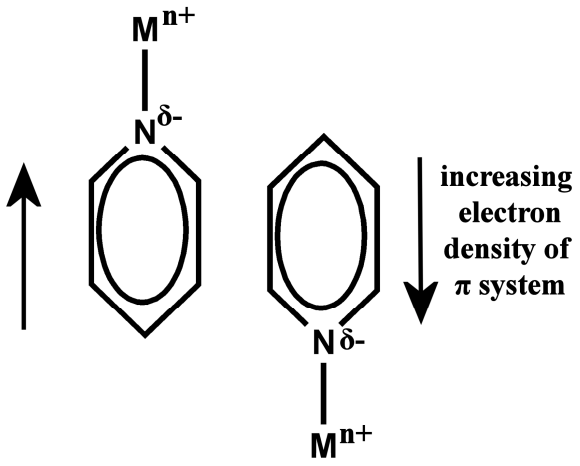

Figure 19: Effect of polarisation by metal coordination on π stacking of pyridyl moieties.

Along with this pyridyl interaction, the B complex also takes part in π interactions *via* its DIP region. Along with the interaction with a neighbouring A complex, as described above, the DIP region of the B complex experiences an interaction with the DIP region of a neighbouring B complex as well. As with the A complex, this second interaction does not display a comparable degree of ring overlap as is the case with the A-B interaction. The π interaction takes place only between the peripheral **X** and **Z** rings of the phenanthridinium system, with a centroid-centroid distance of 3.99(1) Å and separation of the closest two carbon atoms in the interacting ring system of 3.30(1) Å.

These supramolecular interactions combine to produce a two dimensional network of complexes in the crystal structure which is held together by π stacking interactions (see Figure 20). These interactions work in two different directions, with the interactions of the DIP regions forming columns of complexes which are then linked in a second direction *via* π stacking interactions between the pyridyl rings of the B type complexes within the crystal structure.

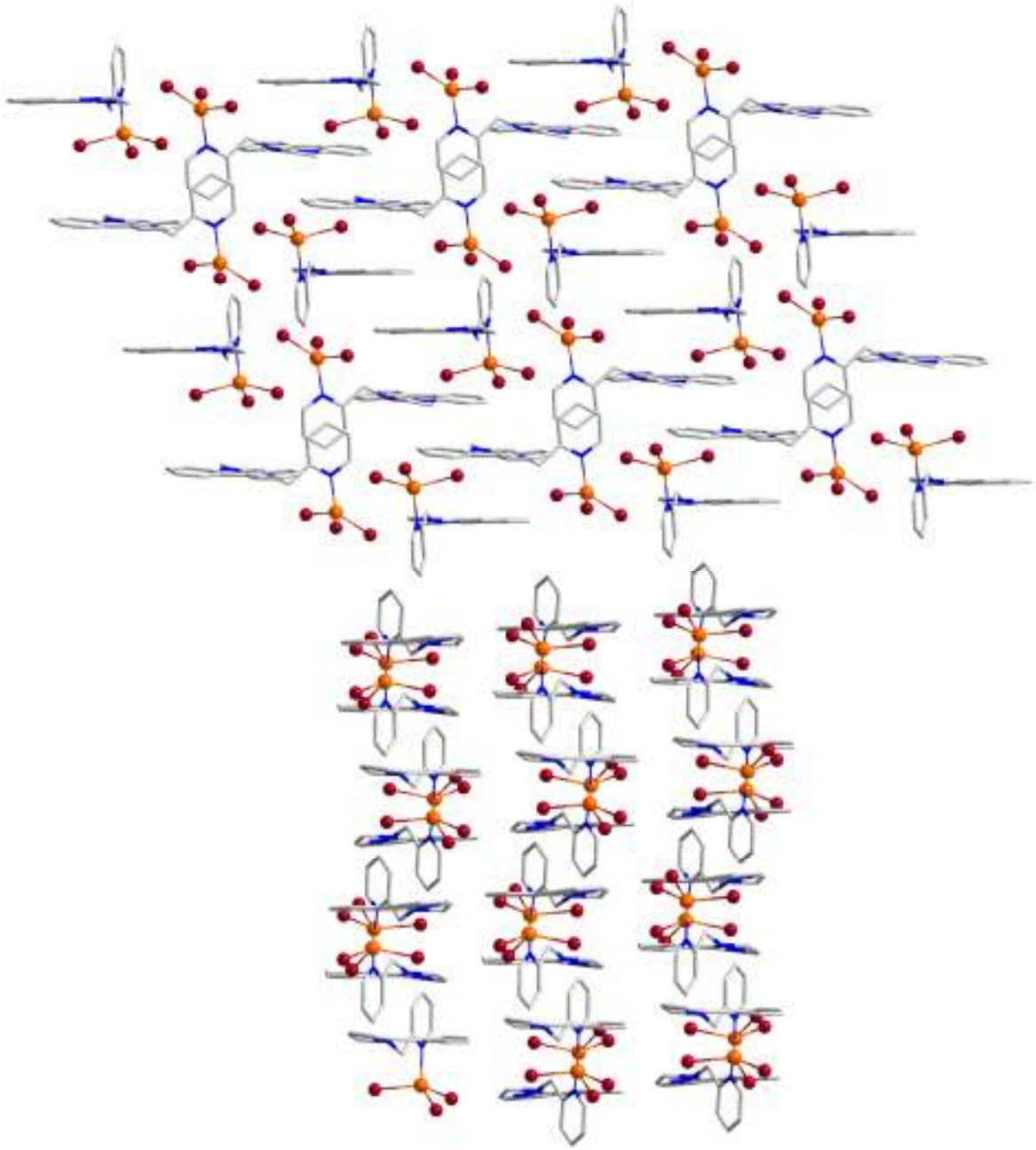

Figure 20: Packing diagram of 26. (top) View along the crystallographic *a* axis showing the intermolecular *π* stacking interactions. (bottom) View along the crystallographic (+*a*+*b*) vector, along the 2D sheets formed by these interactions.

3.2.4 Complexation of 23 with $CuBr_2$

Complexation of the **22** analogue **23**, where the pyridyl group is attached at the *para* rather than the *ortho* position, with $CuBr_2$ in methanol followed by recrystallisation from a water/methanol mixture yields yellow crystals of compound **27**. Compound **27** comprises a mononuclear, diligand complex with the formula $[CuBr_3(\mathbf{23})_2]Br{\cdot}H_2O$. **27** crystallises in a monoclinic *C*2/*c* system and the Cu^{II} ion is five coordinate with a CuN_2Br_3 donor set (see Figure 21).

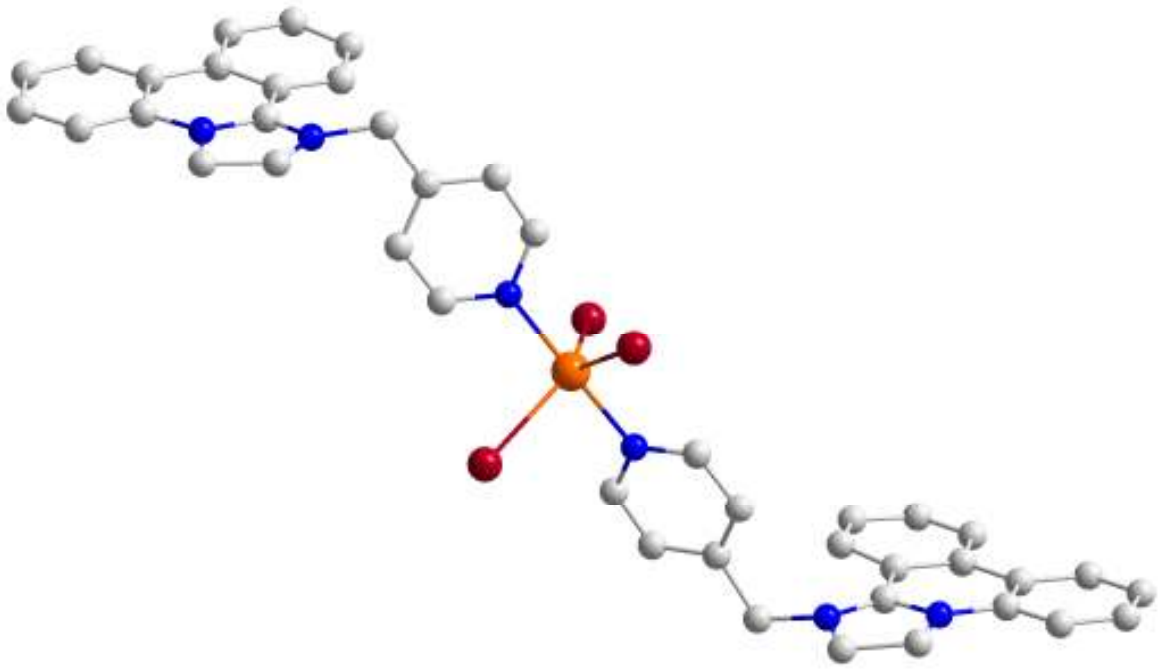

Figure 21: Crystal structure of one molecule of 27, noncoordinated counterions, solvent molecules and hydrogen atoms have been removed for clarity.

The Cu^{II} centre is in a trigonal bipyramidal coordination environment, with a τ_5 value of 0.78, where the equatorial positions are taken up by bromide anions, with an average Cu-Br bond length of 2.53(1) Å and the nitrogen donor atoms of the ligand occupy the apical position with a Cu-N bond length of 2.010(6) Å.

The pyridyl rings of the complex form a dihedral angle of 37.2(1)º with each other and of 76.40(1)º with the plane of the phenanthridinium moiety. Unlike both **26** and **25**, the cationic charge of the Cu^{II} and the DIP ligand in **27** is not completely compensated for by coordinated anions, leading to the formation of a complex cation which is balanced by an uncoordinated bromide anion. The crystal structure of **27** also contains uncoordinated water molecules in the crystal lattice. Again the DIP regions of the ligand moieties experience π stacking interactions in the crystal structure (see Figure 22).

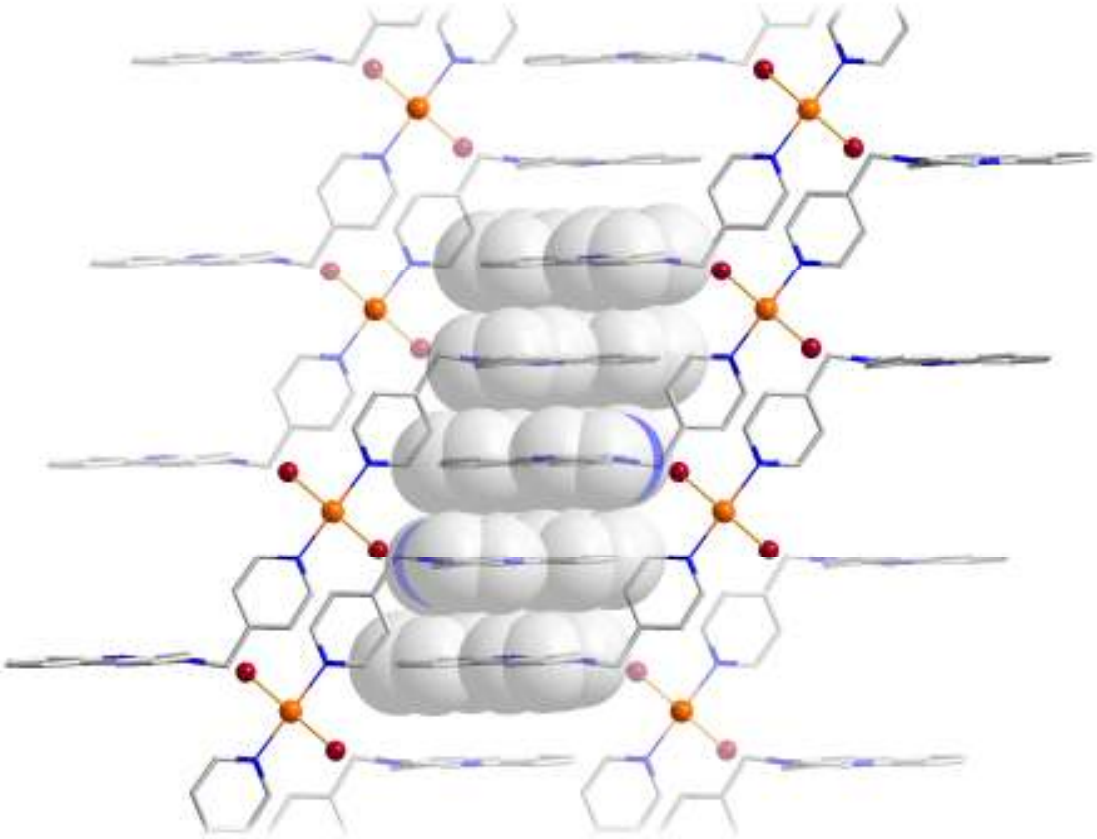

Figure 22: 2D arrangement formed from π stacking interactions in the crystal structure of 27.

Each DIP moiety experiences π stacking interactions on both faces of the DIP ring system. These interactions are arranged such that the peripheral **Z** ring of the phenanthridinium system is oriented above the central, **Y**, ring of the corresponding DIP system, and vice versa with centroid-centroid distances of 3.62(1) Å and shortest C-C

contacts of 3.40(1) and 3.30(1) Å. This arrangement of supramolecular interactions means that the central ring of each DIP moiety experiences a π stacking interaction on both of its faces, with each peripheral ring experiencing one interaction with a DIP moiety either above or below the plane of the ring. This leads to the formation of columns of π stacking interactions through the crystal structure. As each **27** cation has two coordinated ligands pointing in opposite directions these interactions also link the complexes in a second direction forming supramolecular sheets through the crystal lattice (see Figure 23).

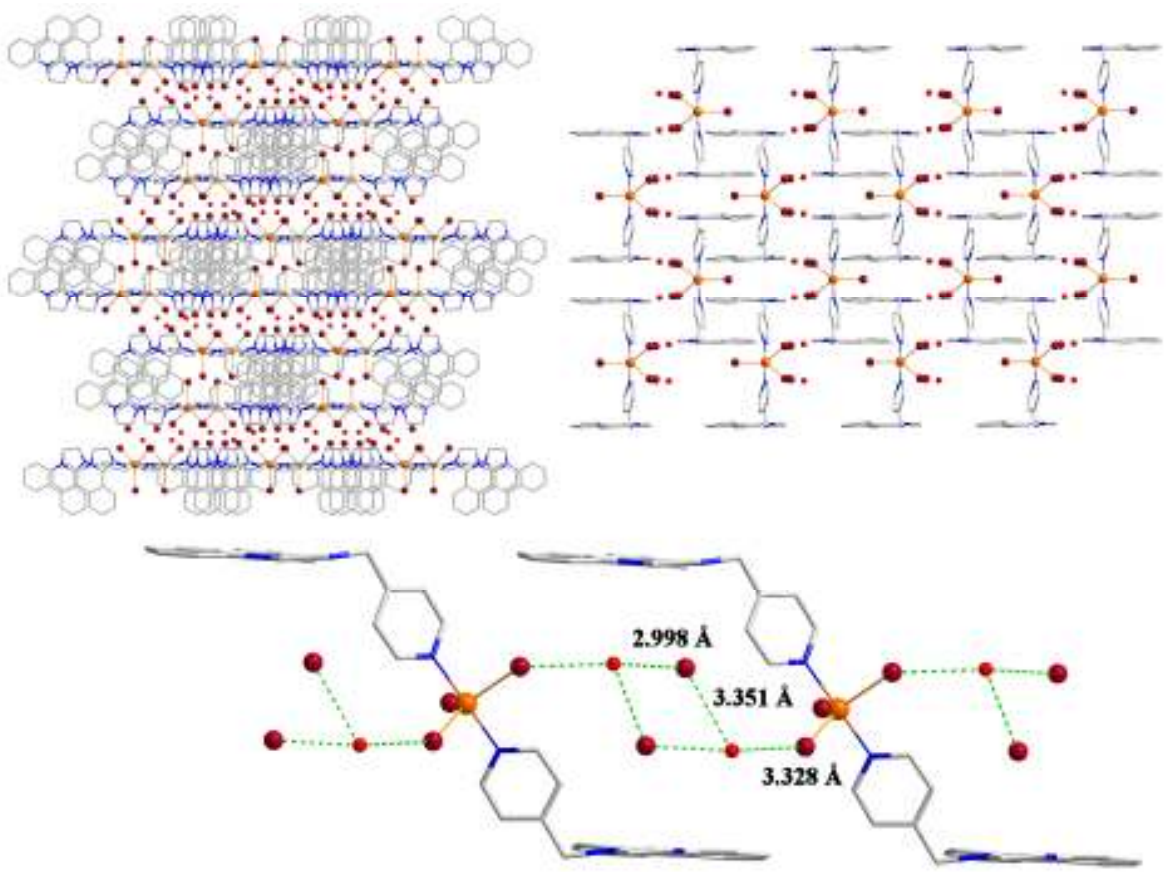

Figure 23: Packing of 27 in the crystalline phase (top left) viewed along the crystallographic *c* and *a* (top right) axes, and view of the hydrogen bonded chains running along each sheet (bottom).

These sheets are also linked by a chain of hydrogen bonded interactions between the coordinated bromide anions, the uncoordinated bromide counterions and the lattice water molecules. These interactions have Br-O distances of 3.33(1), 3.35(1) and 3.00(1) Å (see

Figure 23), with each water molecule partaking in three hydrogen bonded interactions, due to disorder in the hydrogen positions in the crystal structure. This chain of interactions runs along the sides of the sheets formed by the π stacking interactions of the DIP moieties, running in the direction the crystallographic *a* axis. These hydrogen bonded interactions bridge between adjacent complexes within the same sheet, but do not link the sheets together.

3.3 Dinuclear Complexes of DIP-Pyridyl Ligands with Cu^{II} Salts and bridging ligands

3.3.1 Complexation of 22 with $Cu(NO_3)_2 \cdot 3H_2O$ and NaN_3

Reaction of ligand **22**·Br with $Cu(NO_3)_2 \cdot 3H_2O$ in a 1:2 ratio yields compound **25** as described above, however addition of eight equivalents of NaN_3 to this reaction mixture, followed by recrystallisation from a MeOH/DMF solvent system results in the formation of brown crystals of the formula $Cu_2(\mathbf{22})_2(N_3)_6$ (**28**). **28** crystallises in a monoclinic *C*2/c crystal system and comprises a dinuclear Cu^{II} complex (see Figure 24).

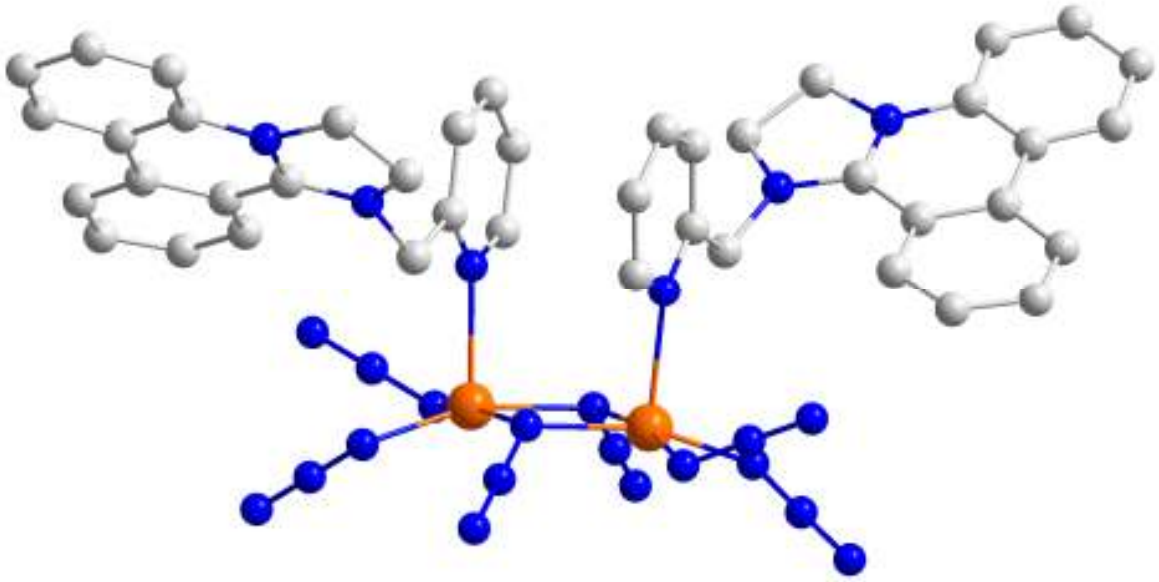

Figure 24: Crystal structure of 28. The structure has a C_2 axis resulting in a *syn* arrangement of the two ligand moieties.

Each Cu^{II} centre in the structure is five coordinate with a slightly distorted square pyramidal geometry, where the τ_5 parameter is 0.12. The Cu^{II} centres have a CuN_5 donor set with the basal positions of the square pyramid occupied by two terminal azido ligands, with Cu-N bond lengths of 1.981(3) and 1.987(2) Å and two μ_2-N atoms from bridging azido ligands with bond lengths of 2.027(2) and 2.055(2) Å. This arrangement leads to a Cu-Cu distance of 3.143(2) Å, and Cu-N-Cu angles of 100.70(10) º. The apical position is occupied by the pyridyl nitrogen of the **22** ligand, which bonds to the Cu^{II} ion with a bond length of 2.294(2) Å. This azido bridged dinuclear core represents, to the best of our knowledge, only the second example of its kind reported and if the apical nitrogen atoms are neglected there are only another three examples reported in the CSD database.[118,119] Again in this case we see that the positive charge from the metal centres and ligand groups is compensated for by anions coordinated to the Cu^{II} cation, yielding a neutral species.

The pyridyl regions of the two coordinated **22** ligands are situated in an almost parallel arrangement, with a dihedral angle of 4.01(1)º between planes described by the atoms in the pyridyl rings, with a centroid-centroid distance of 3.76(1) Å, and the shortest atom-

atom contact between the pyridyl nitrogens 3.55(1) Å. When compared to the pyridyl-pyridyl π stacking observed in previous complexes of this ligand this appears to be quite a long range interaction. This may be a result of the orientation of the pyridyl rings with relation to each other; in this case the rings are oriented such that the π systems of the coordinating nitrogens are directly interacting with each other. Considering the polarization of the π system of the pyridyl ring this means that the distribution of electron density in the interacting pyridyl systems is not as favourable as in the previous cases, with the regions of most electron density interacting with each other, increasing the π–π repulsion in this system. Despite this the intramolecular interaction of the pyridyl π systems may contribute to the overall stability of the *syn* arrangement of the ligand moieties in the structure of **28**.

The planes defined by the phenanthridinium atoms of the two DIP regions of **28** form a dihedral angle of 69.8(1)º, and once again the DIP regions of the ligand moieties experience π stacking interactions with those of neighbouring complexes (see Figure 25).

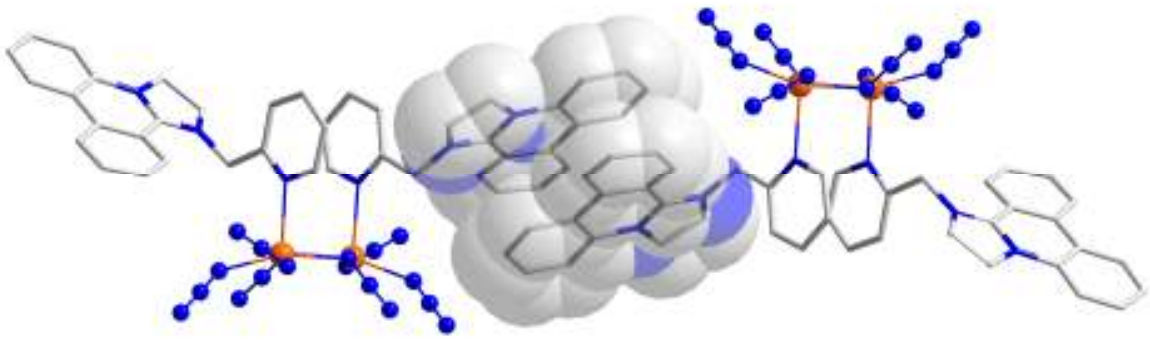

Figure 25: π stacking interactions between neighbouring 28 molecules.

Each ligand DIP system interacts with the neighbouring complex *via* π stacking interactions between the peripheral **X** and **Z** rings of the DIP system. This arrangement of the ring systems maximises the distance between the cationic regions of the DIP structures, thus minimising their electrostatic repulsion. The distance between planes described by the

phenanthridinium framework is 3.42(1) Å and the centroid-centroid distance of the rings is 3.66(1) Å indicating a relatively large degree of ring overlap in this system.

This π stacking interaction of the DIP moieties in **28** leads to the formation of supramolecular chains of complexes through the crystal structure where the units of **28** interlock in an alternating up/down arrangement (see Figure 26).

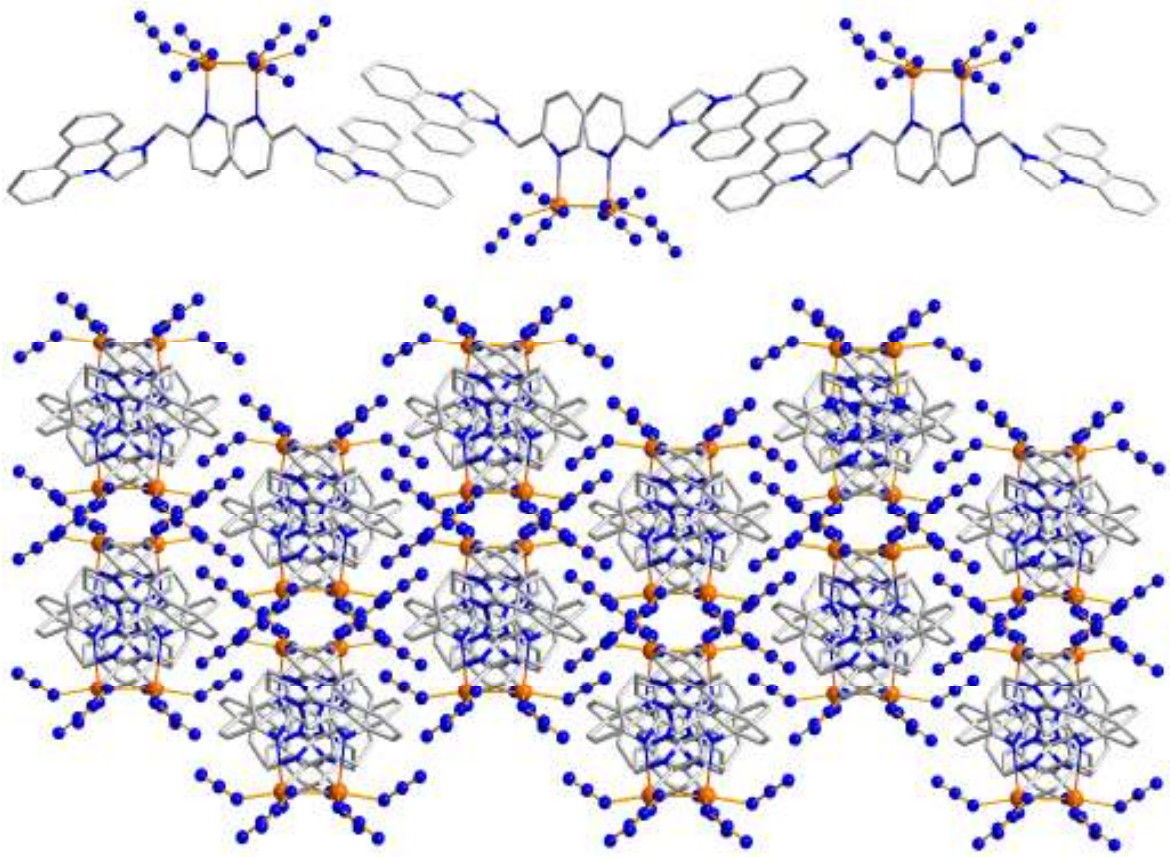

Figure 26: Packing diagrams of 28 showing the chains formed by the π interacting DIP systems (top) and a view down these chains along the crystallographic (+*a*+*c*) vector (bottom).

3.3.2 Complexation of 22 with $Cu(NO_3)_2 \cdot 3H_2O$ and NaSCN

Complexation of **22** with $Cu(NO_3)_2 \cdot 3H_2O$ and sodium thiocyanate in the presence of triethylamine forms a different complex which can be formalised as $Cu_2(\mathbf{22})_2(NCS)_4(OMe)_2$ (**29**). this complex crystallises in a triclinic *P*-1 crystal system (see Figure 27).

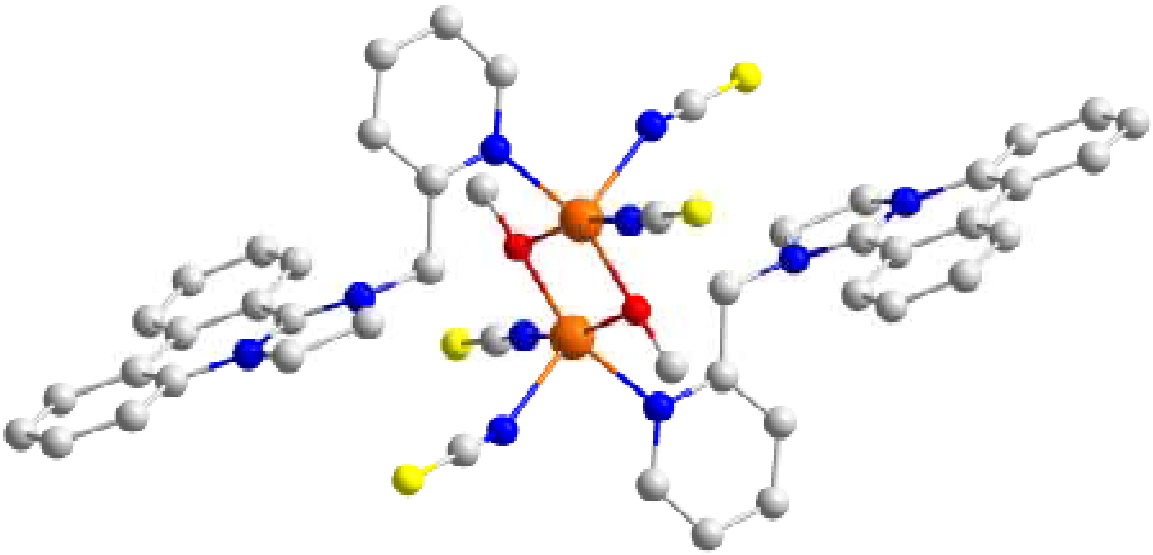

Figure 27: Crystal structure of 29.

The crystal structure of **29** consists of a bis-(μ_2-methoxo)-bridged Cu^{II} complex where each Cu^{II} ion is five coordinate with an almost ideal square pyramidal geometry (the τ_5 value for this complex is 0.016) and a CuN_3O_2 donor set. The bridging methoxo ligands form a Cu-O-Cu angle of 78.22(13) ° and Cu-O bond lengths of 1.946(3) and 1.948(3) Å giving a Cu-Cu distance of 3.02(1) Å. The remaining basal positions are occupied by one of the thiocyanate ligands coordinated *via* its nitrogen atom with a Cu-N bond length of 1.951(4) Å and the pyridyl nitrogen with a bond length of 2.038(3) Å. The apical position of the square pyramidal geometry is occupied by the remaining thiocyanate ligand also coordinating *via* nitrogen with a Cu-N distance of 2.236(5) Å. This unusual coordination core around the Cu^{II} ion represents, to our knowledge, the first example of a methoxy

bridged dinuclear Cu^{II} complex with four coordinating thiocyanate anions. The crystal structure of **29** also contains a disordered methanol molecule as solvent of crystallization. The cationic charge of the Cu^{II} metal centre and the DIP ligand is compensated for by the coordinated thiocyanate and methoxy anions, making the resulting complex formally neutral.

Unlike the structure of **28** the bridging ligands of this complex arise from the deprotonation of the reaction solvent, methanol and the thiocyanate ligands appear in only a terminal mode. The second major difference between **28** and **29** is the orientation of the DIP ligand **22**. Whereas in the structure of **28** these ligands appear in a *syn* configuration, in **29** they take up an *anti* arrangement with respect to its neighbouring ligand. It is possible that the interactions of the π systems of the pyridyl regions contribute to this difference in coordination. In complex **29** we observe a slightly smaller Cu-Cu distance than is the case for **28** and it could be argued that this would bring the pyridyl rings too close together, were they to adopt a *syn* configuration. It has already been noted that in the above situation the interaction of the π systems is less favoured by the polarization of the pyridyl π system when they are arranged in such a way that the nitrogens of the pyridyl rings are directly above each other as they would have to be for a *syn* conformation to be adopted.

In its crystal structure **29** can be observed to take part in several intermolecular interactions, not only through interactions of the DIP π systems. Intermolecular S···S interactions can be observed with a S-S distance of 3.41(1) Å between two of the thiocyanate ligands in the complex and the corresponding thiocyanate ligands in the neighbouring complex (see Figure 28).

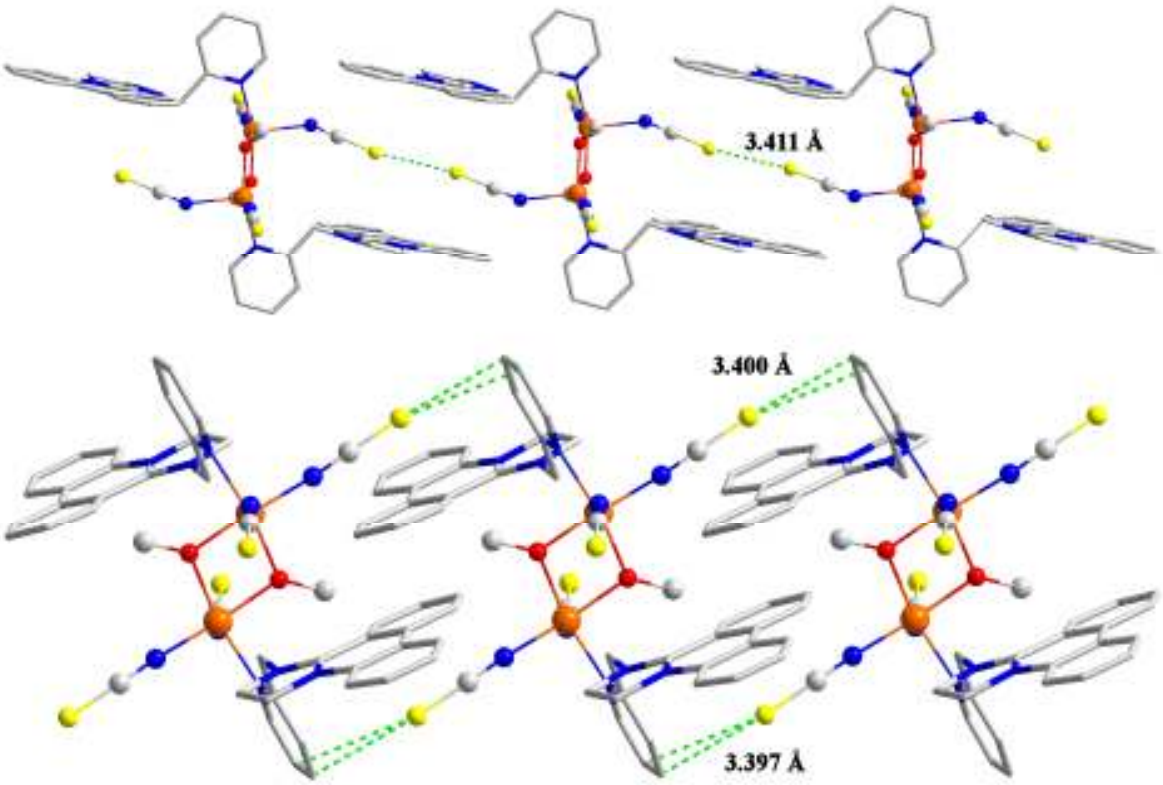

Figure 28: Supramolecular interactions of the thiocyanate ligands in 29. (top) S···S interactions. (bottom) Orthogonal S···π interactions with the pyridyl rings of the 22 ligands.

Along with these S···S interactions, the remaining two thiocyanate ligands of each complex can be observed to pariticipate in an orthogonal set of interactions with the π system of the pyridyl ring of the **22** ligand of a neighbouring complex. The shortest contacts observed between the sulfur atoms and the carbon atoms of the pyridyl ring are 3.40(1) Å and 3.40(1) Å, however the thiocyanate group does not point directly at the center of the π system with a S-centroid distance of 3.60(1) Å. The interaction of sulfur atoms with π systems is well known to be an important factor in biological systems such as protein structures.[30,120] The interactions of coordinated thiocyanate ions with the π systems of aromatic moieties has also been noted as a structural feature in coordination compounds.[121]

In addition to the interactions of the sulfur atoms of the thiocyanate anions, we again see interactions of the DIP regions of the ligands with each other linking the complexes a third direction (see Figure 29).

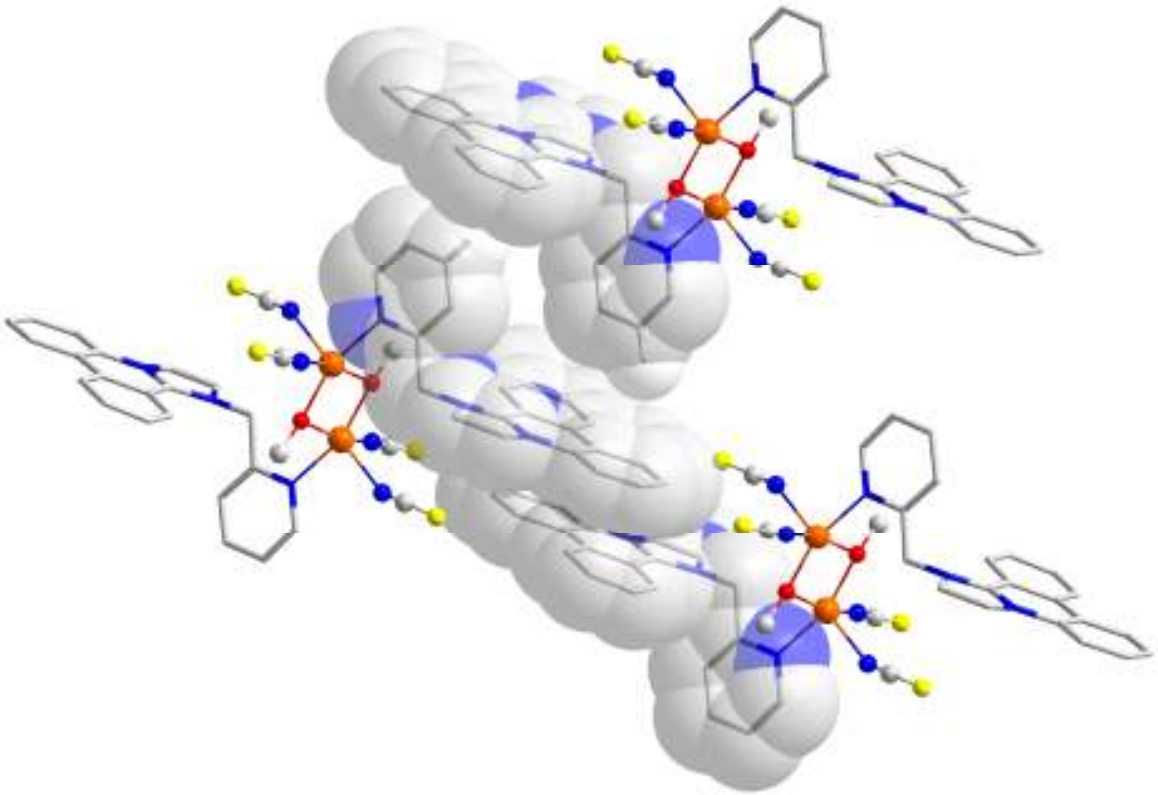

Figure 29: π interactions of ligand 22 in the crystal structure of compound 29.

Each DIP region of the coordinated **22** experiences, on one face, a π stacking interaction with a neighbouring DIP moiety, where the rings are arranged such that the peripheral **X** and **Z** rings of the phenanthridinium system are above each other with a reasonable degree of ring overlap, where the centroid-centroid distance of these rings is 3.84(1) Å and the closest atom-atom distances are 3.32(1) Å and 3.67(1) Å. On the other face of the DIP ring system, each complex experiences an interaction with a hydrogen atom from the pyridyl ring of an adjacent complex in a T-shaped C-H···π interaction. This interaction is centred over the DIP ring which is *para* to the phenanthridinium nitrogen, with a H-centroid distance of 2.53(1) Å, and H-C distances ranging from 2.80(1) to 2.90(1) Å. The combination of these two sets of interactions leads to the linking of the **29** complexes into

one dimensional chains through the structure *via* alternating C-H···π and π stacking interactions (see Figure 30). The combination of the intermolecular interactions of the thiocyanate groups and the DIP moieties of the **22** ligand links this moiety into a three dimensional network of supramolecular interactions in the crystalline phase.

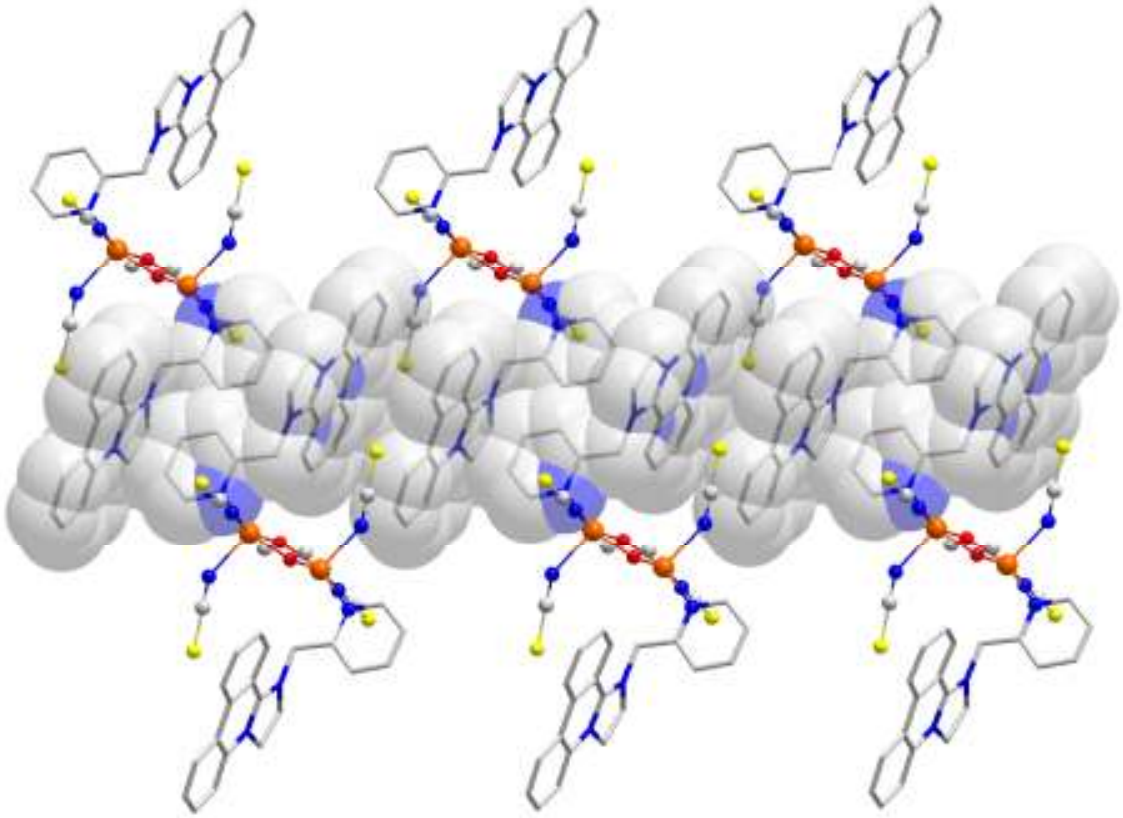

Figure 30: 1D chains of 29 complexes in the crystalline phase, linked by alternating C-H···π and π stacking interactions.

3.4 The Supramolecular Interactions of Pyridyl DIP ligands.

3.4.1 Coordination of DIP Pyridyl Ligands

In all cases, the DIP moiety is quite rigid and only the pyridine nitrogen is involved in the coordination with the Cu^{II} centres (see Table 1), the Cu-N bond distances in all cases are within the normal range for such Cu-Pyridyl coordination. With $Cu(BF_4)_2$, compound **23**, the copper ion is coordinated by two **22** DIP moieties through pyridine nitrogen and two Br^- anions coming from the ligand salt, while the BF_4^- remains as a noncoordinating counterion. With $CuBr_2$, bromide anions coordinate with the Cu^{II} centre and a relatively unusual tetrahedral geometry is observed (compound **26**). Three structures were obtained by complexation with $Cu(NO_3)_2{\cdot}3H_2O$, two dinuclear species and one mononuclear complex. In the mononuclear complex **25** the nitrate anion chelates with the Cu^{II} centre and two bromide anions from **22**, resulting in a distorted square-pyramidal geometry. When additional bridging ligands such as N_3^- and SCN^- were added to the mixture of **22**·Br and $Cu(NO_3)_2$ no coordination of the $(NO_3)^-$ groups is observed and these are replaced by bridging groups or solvent molecules in the coordination around the Cu^{II} ion.

Compound	Pyridyl N-Cu Distance (Å)	Other coordinating atoms	Cu Geometry
24	1.959(4)	Br	Square Planar
25	1.986(4)	Br, O	Distorted Square Pyramid
26	2.024(15), 2.019(16)	Br	Tetrahedral
27	2.010(6)	Br	Trigonal Bipyramid
28	2.294(2)	N	Sqare Pyramid
29	2.038(3)	N, S	Sqare Pyramid

Table 1: Coordination of the Pyridyl Nitrogen to Cu^{II} in complexes of 22 and 23.

Four-coordinate Cu^{II} complexes, varying from square planar to novel tetrahedral geometries are observed with BF_4^- and Br^-, respectively. With NO_3^-, N_3^- and SCN^- as anions, five-coordinate Cu^{II} structures have been observed. Comparing the $CuBr_2$ complexes, two different geometries of copper complexes have been obtained. The difference of the coordination environment around Cu^{II} ion results from the difference in position of the pyridine nitrogen in **22** and **23**, respectively with the less sterically hindered **23** ligand forming a biligand complex in contrast to the monoligand **22** product. Compounds **28** and **29** also represent Cu^{II} complexes with unusual dinuclear cores.

3.4.2 π Interactions of the DIP Moiety

From analysis of the crystal structures of the above compounds we can see that the intermolecular forces which direct their packing in the crystalline phase are largely dependant on the ability of the DIP moieties to participate in interactions *via* their DIP π systems. Several different modes of interaction of the DIP moiety are observed in the above structures, ranging from interactions between only one of the DIP rings with very little ring overlap, to situations where all four of the DIP rings (including the non-aromatic dihydro imidazo ring, **I**) are situated above one another with a maximum possible overlap. The cationic nitrogen of the DIP structure exerts a similar effect to that observed by the complexation of a pyridyl moiety to a metal cation leading to an overall electron deficient aromatic system for the DIP structure encouraging the formation of π stacking interactions. Electrostatic attractions between the cationic charge of the DIP system and the partially negatively charged π electron systems of other aromatic moieties would tend to encourage an orientation whereby the cationic charge of the nitrogen would be interacting directly with the π system of the adjacent molecule, and this motif can indeed be seen amoungst the synthesised compounds. Interactions between two cationic DIP structures, however, must also contend with a mutual repulsion of the cationic charges on each of the species. By far the most common motif observed in the structures above, therefore, is that where the peripheral **X** and **Z** rings interact with the ring systems pointing in opposite directions (see Figure 31), leading to the introduction of directionality to the system. This orientation of the DIP ring system minimises both the steric interaction of the bulky, non aromatic ring, **I**, and also maximises the distance between the cationic centres of the ligand. Consideration

of the polarisation of the aromatic system is also important, with which has a balancing effect on the electrostatic repulsions of the cationic nitrogen. The effect of polarisation is likely to be most pronounced in interactions between with the central, **Y**, rings. It is probable therefore that it is a combination of these factors at work in the favouring of this arrangement. Comparison of the distances observed between the cationic nitrogen atoms in interacting DIP systems show that this balance of factors is a fine one, with distances ranging from 3.89(1) Å (in **27**) to 8.36(1) Å (in **25**), most of these distances are greater than 6 Å, indicating that the electrostatic repulsions are a major factor in the orientation of DIP π interactions, favouring the motif described above.

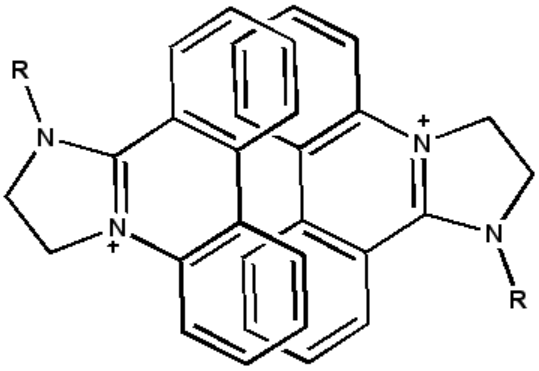

Figure 31: Most common mode of interaction of DIP moieties.

This motif of interaction can be observed in all the above crystal structures, with the exception of **27**, where the only interactions observed are between the central **Y** and quinoline-like **Z** ring of the DIP system. Whilst this motif can be identified in the majority of crystal structures studied, a variety of distances and degrees of ring overlap are observed, with centroid-centroid distances for the interacting rings of the DIP moieties ranging from 3.66(1) Å to 4.45(1) Å. The DIP regions of the ligand systems do not, in general, interact with the pyridyl regions of neighbouring complexes, with the exception of compound **29**, where a C-H···π interaction is observed. This leads to the existence essentially of two orthogonal π systems which will interact with other π systems of the same type, but not with π systems of the opposite type.

3.4.3 π Interactions of the Pyridyl Moiety.

The pyridyl regions of the above ligands can be seen to interact in a face-to-face manner with other pyridyl regions in both an inter- and intra-molecular mode, with different interacting orientations in each case. In the case where there is an intramolecular π interaction the rings were necessarily arranged with the pyridyl nitrogens pointing in the same direction resulting in a slight lengthening of the interaction compared to the intermolecular examples. In the intermolecular examples, we can see that the pyridyl region adopts an orientation where the pyridyl nitrogens point in opposite directions, a situation which minimises both the steric interaction of the coordinated metal centres, and the repulsion of the π electron systems between the polarised ring systems.

4 TRIAZINE BASED DIP LIGAND

4.1 Ligand Design and Synthesis

In order to increase the ability of DIP moieties to function effectively as supramolecular building blocks, it was decided to extend the coordinating region of DIP containing ligands to include ligands with the potential to bind more than one metal centre at the same time, i.e. which had the potential to act as bridging ligands. One attractive candidate for the construction of multifunctional architectures which has been used extensively to synthesise a variety of ligands for use in supramolecular chemistry is the 1,3,5-triazine moiety (see section 1.3).

The 1,3,5-triazine unit offers a particularly convenient basis for the synthesis of supramolecular building blocks due to the ease with which it can be functionalised to form a variety of sophisticated derivatives from the cheap and readily available starting material 2,4,6-trichloro-1,3,5-triazine (cyanuric chloride, **30**). This starting material undergoes successive nucleophilic substitutions at each of its chloro positions at progressively higher temperatures, with the first position being replaced at 0 ºC, the second at 25 ºC and the third at 65 ºC (see Figure 32). These temperatures are ideal for the synthetic chemist as they represent easily accessible conditions for the stepwise building of a tri-functionalised architecture.

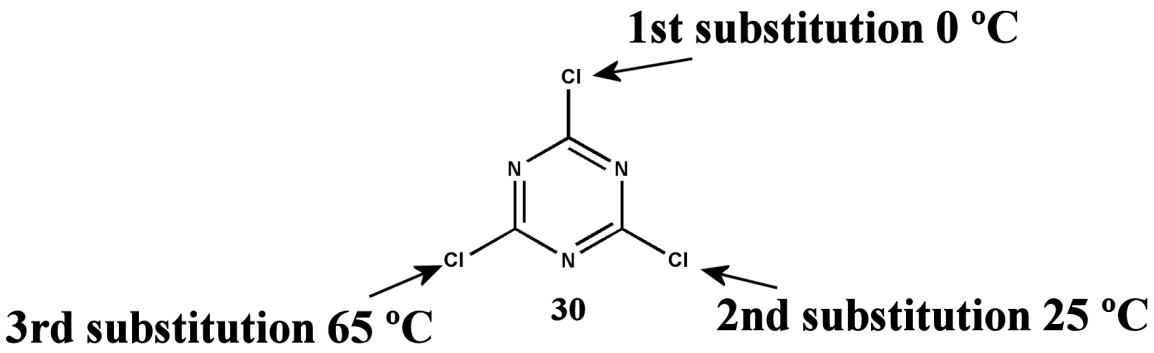

Figure 32: Successive substitutions of 2,4,6-trichloro-1,3,5-triazine.

It was therefore decided that the triazine unit would be used as the basis of a DIP containing ligand which could complex more than one metal centre simultaneously. To this end two coordinating 'arms' and one DIP containing arm would be successively substituted onto the triazine ring. The coordinating unit used in this design is that of dipyridin-2-yl amine (**31**) which provides a bidentate chelating coordination centre. The substitution of two of these moieties onto the triazine ring allows the ligand to coordinate two separate metal centres in a bridging fashion. In the third position of the triazine ring it was decided to substitute a DIP containing moiety, however as the DIP structure does not contain a nucleophilic centre with which to undergo the nucleophilic substitution reaction, it was necessary to design a suitable 'linker' region that would allow the DIP to be attached to the triazine core. To this end the following convergent synthetic scheme was designed (see Scheme 10).

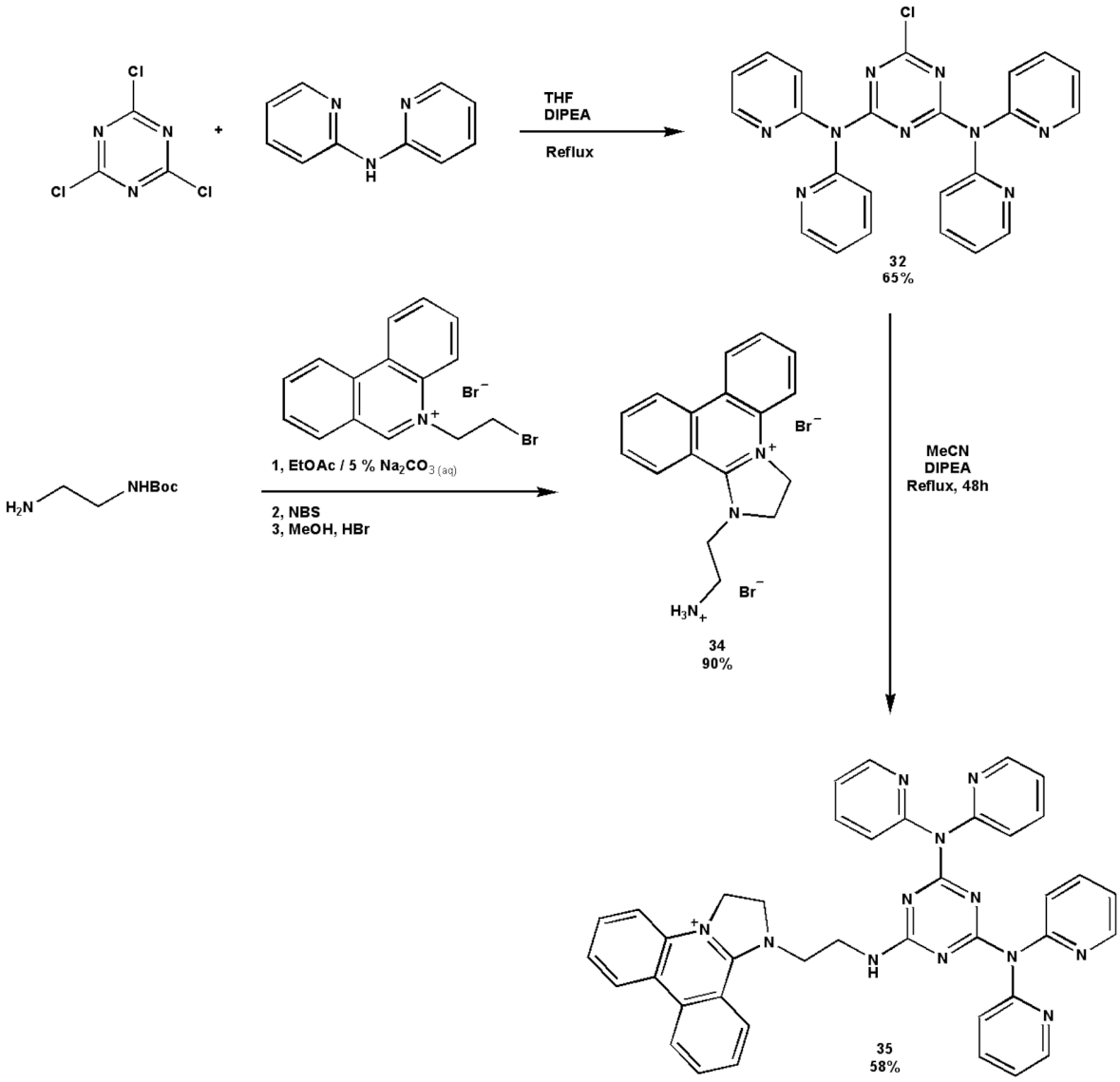

Scheme 10: Synthesis of DIP-Trazine ligand 35.

In order to introduce a simple ethylene diamine linker unit between the DIP moiety of the ligand and the triazine core it was necessary to use a mono-protected ethylene diamine species to avoid the formation of the DIP dimer, which would take place under normal reaction conditions with the unprotected amine. It was decided to use the mono-N-*tert*-butoxycarbonyl protected amine (**33**) as this protecting group cleaves easily under relatively mild acidic conditions to which the DIP group is stable. Using a base-labile protecting group would have been unsuitable for this reaction as the DIP can react under basic conditions to form a *pseudobase* moiety discussed in the introduction (see section 2.1).

The DIP reaction on the protected ethylene diamine was carried out according to the same biphasic reaction procedure described in the synthesis of the previous ligands **22** and **23**, and the resulting protected DIP species was deprotected by suspending the DIP species in methanol and adding concentrated HBr until the solid had completely dissolved. The solution was then allowed to stir and after one hour the deprotected product had precipitated from solution as the DIP ethylene diamine hydrobromide salt (**34**). A small amount of diethyl ether was added to the solution to ensure complete prectipitation and the product could be isolated in good (90%) yield by simple filtration followed by washing with diethyl ether.

Comound **34** was then reacted with the di-substitiuted triazine moiety **32** (which had been synthesised by literature procedures)[122,123] in dry acetonitrile using diisopropyl ethylamine (DIPEA) as a bulky organic base to facilitate the nucleophilic substitution. The reaction mixture was heated for 48 hours to ensure maximum possible substitution on the triazine ring. The product was isolated by removing the reaction solvent and washing the residue with diethyl ether and acetone. The yield in this reaction is moderate (58%), this is most likely due to degradation of the DIP moiety under the basic conditions of the reaction. The isolated ligand (**35**) was then used in complexation reactions with metal salts.

4.2 Complexation of 35 with Metal salts

4.2.1 Complexation of 35 with $Pd(OAc)_2$

By successively layering a solution of **35** in toluene over THF and a solution of $Pd(OAc)_2$ in dichloromethane and allowing the solutions to slowly diffuse together over the course of two weeks yellow, needle shaped single crystals of a new compound, **36** were formed. Single crystal X-Ray analysis of these crystals yielded the following structure (see Figure 33).

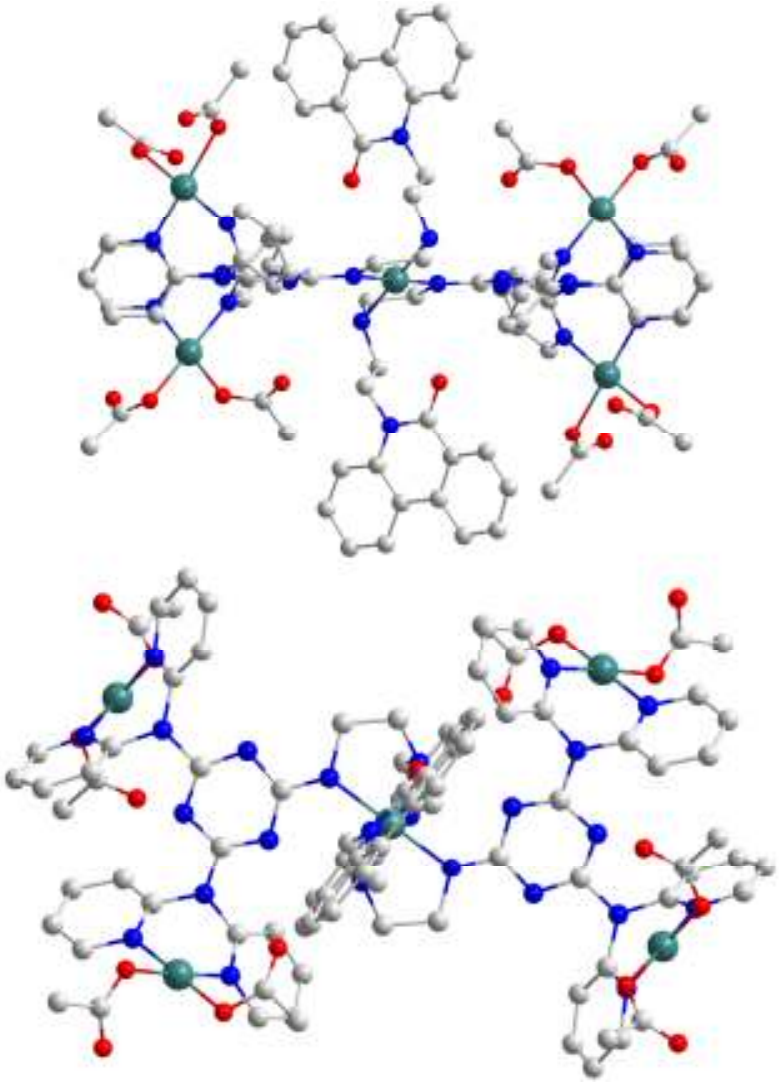

Figure 33: Crystal structure of 36 viewed along the plane of the triazine moieties (top) and along the plane of the phenanthridinone moieties (bottom). Uncoordinated counterions and solvent molecules are omitted for clarity.

The structure of **36**, which crystallises in the *P*-1 space group, is a pentanuclear Pd^{II} complex containing two new ligands, **35**', which can be formulated as $[Pd_5(\mathbf{35}')_2(OAc)_8]Br_2$. The crystal structure of compound **36** contains three distinct palladium positions; Pd1, Pd2 and Pd3. Pd1 and Pd2 are coordinated in the dipyridyl region of the ligand and are coordinated by the two pyridyl nitrogens and two acetate ligands, giving each one a PdN_2O_2 donor set. Both Pd1 and Pd2 exhibit almost ideal square planar geometry typical of d^8 palladium (II) centres with N-Pd-N angles of 88.7(3)º and 87.8(3)º and O-Pd-O angles of 88.4(3)º and 90.4(3)º. The pyridyl nitrogens of the ligand

coordinate to the Pd^{II} with bond lengths ranging from 2.002(8) Å to 2.026(9) Å, and the two acetate ligands with Pd-O distances of between 1.999(7) and 2.179(9) Å. These bond lengths and bond angles are in normal ranges when compared to analogous compounds.[124,125] The cationic charge of the Pd1/Pd2 metal centres is compensated for by the coordinated acetate anions.

The third palladium metal centre, Pd3, is coordinated by four amine nitrogen atoms belonging to two different **35**' ligands (see Scheme 12), thus connecting two Pd1/Pd2 entities to form the overall $\{Pd_5\}$ structure. The coordinating ethylene diamine units are formed in the alteration of the original **35** compound upon complexation with $Pd(OAc)_2$. The amine nitrogens are coordinated to the Pd^{II} metal centre with bond lengths of 2.025(7) and 2.035(7) Å, which are in the normal range for the coordination of bidentate amine ligands in such an environment.[126,127] Pd3 is in a square planar geometry where there is significant distortion within the plane of the coordinated atoms from the ideal. This distortion is most likely due to the small bite angle of the chelating ethylene diamine group, which has a N-Pd-N angle of 80.2(3)º combined with steric hindrance due to the phenanthridinone moieties. As the Pd3 centre is coordinated entirely by neutral donor atoms, this gives the pentanuclear complex an overall 2+ charge, which is compensated for by two uncoordinated bromide anions which are disordered over eight bromide positions in the asymmetric unit. The crystal structure of **36** also contains three dichloromethane molecules and several water molecules as uncoordinated solvent of crystallization.

The first thing to note about the structure of **36** is that during the complexation reaction the ligand has undergone a transformation from the initial DIP based ligand **35** to a new, ring-opened structure **35**'. The DIP structure of the initial ligand has undergone a hydrolysis reaction at the α position of the phenanthridinium ring system and the imidazo ring of the DIP moiety has opened to give a phenanthridinone moiety linked to the triazine core *via* a bis-ethylene diamine chain (see Scheme 11). By analysis of the bond lengths of the phenanthridinone moiety in the crystal structure of **36**, it can be seen that the central ring of the new phenanthridinone moiety exhibits a loss of aromaticity compared with the original DIP structure. The carbonyl C-O bond length is 1.222(10) Å, and there is a significant lengthening of the non-aromatic bond lengths in the central ring to 1.40(1) –

1.46(1) Å, indicating much less aromatic character of this ring than is the case in the parent DIP structure. The loss of aromaticity of this central ring in the aromatic system would be expected to have a significant impact on the ability of this region to participate in supramolecular interactions *via* its π electron system.

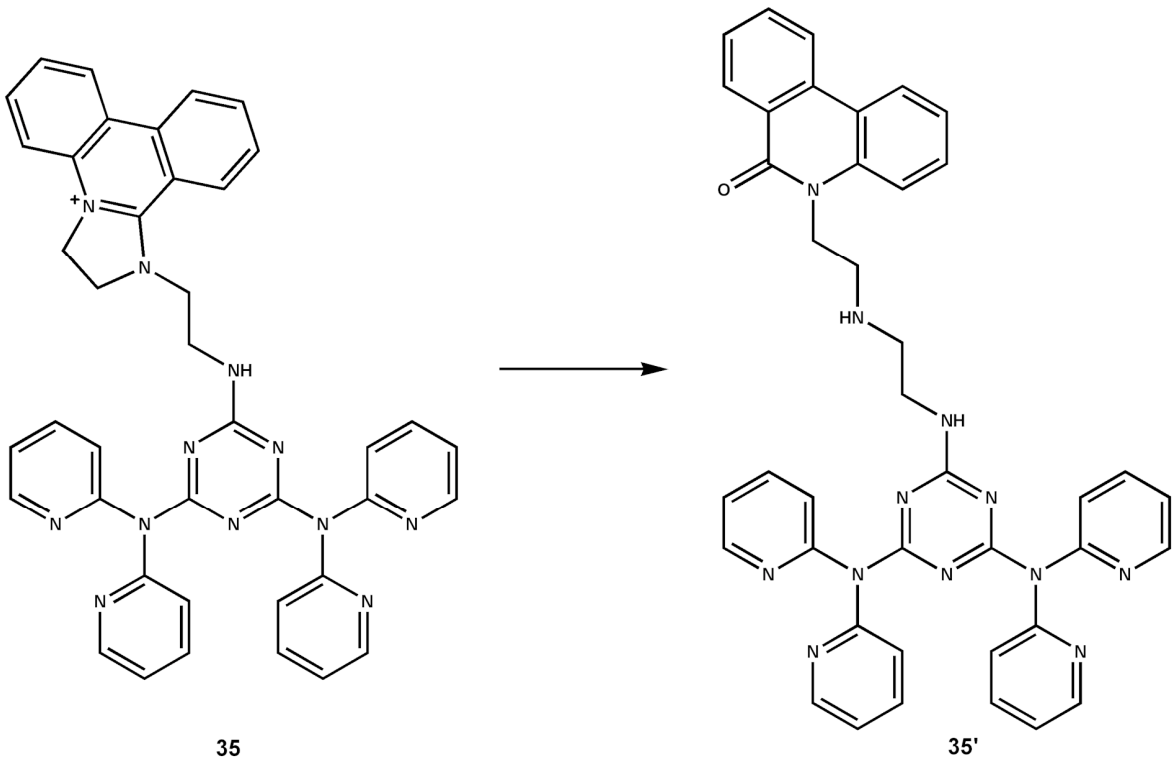

Scheme 11: Transformation observed on complexation with $Pd(OAc)_2$ from 35 to 35'.

35' forms from compound **35** (see Scheme 11) via a ring opening process with the introduction of a carbonyl group to give the ligand observed in the crystal structure upon coordination to $Pd(OAc)_2$. Whilst future work will seek to determine the precise mechanism of this ligand transformation through detailed experimental and theoretical investigation, one's first thought turns to a hydrolytic process during coordination (see Scheme 12).

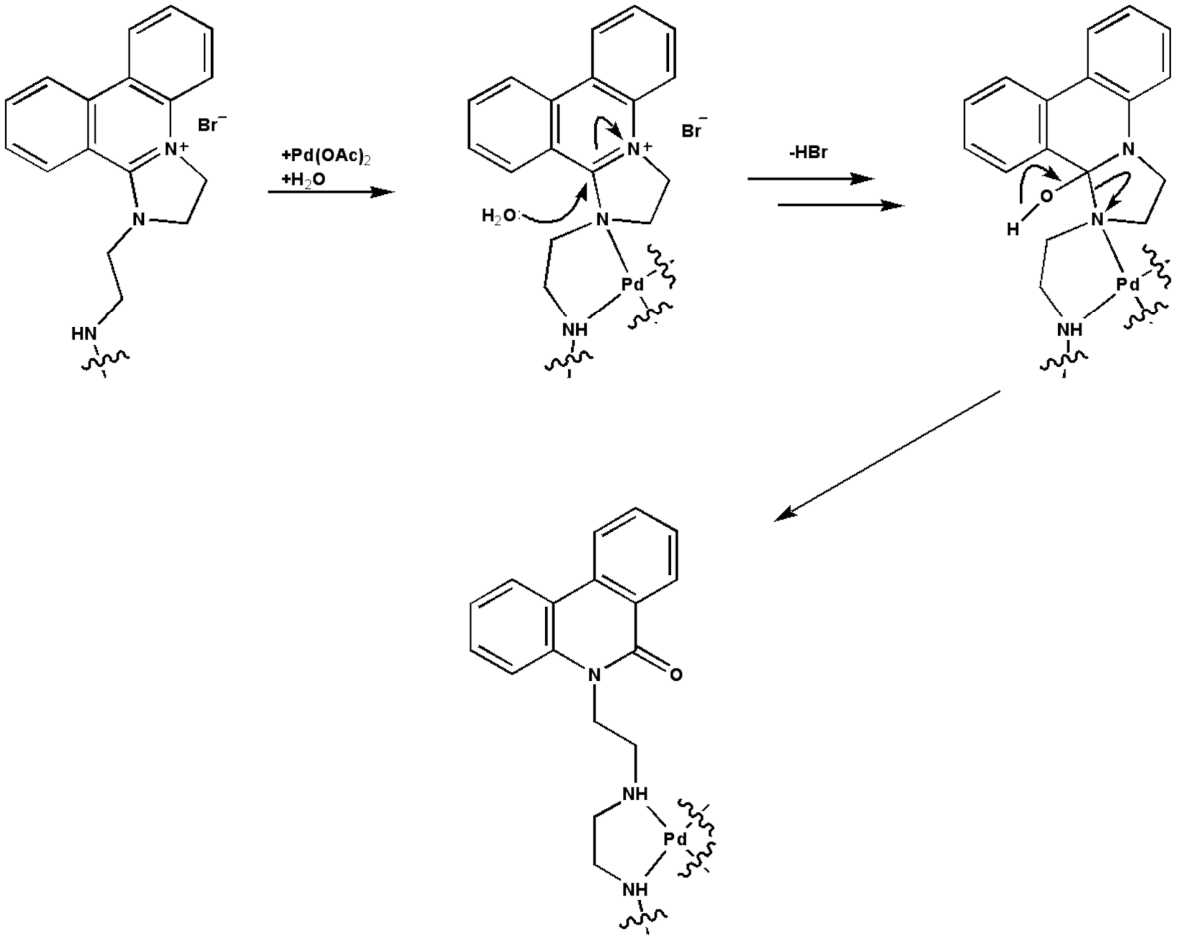

Scheme 12: Possible mechanism for the transformation of ligand 35 upon coordination with $Pd(OAc)_2$.

A possible reaction mechanism for the transformation of ligand **35** into the crystallographically observed **35**' is suggested where the Pd^{II} cation acts as a lewis acid which, upon coordination to the DIP nitrogen, activates the α-position of the phenanthridinium moiety to nucleophilic attack from ambient water molecules in the reaction solvents. Elimination of HBr from this intermediate results in the formation of a neutral hydroxy-DIP pseudobase molecule which then undergoes a ring-opening rearrangement to form the crystallographically observed phenanthridinone moiety. This ring opening significantly reduces the steric bulk around the Pd^{II} coordination environment, which may contribute to the driving force for this transformation.

The crystal structure of **36** shows interesting supramolecular interactions with the major intermolecular interactions arising from the relationships between the π systems of the aromatic moieties in the structure (see Figure 34).

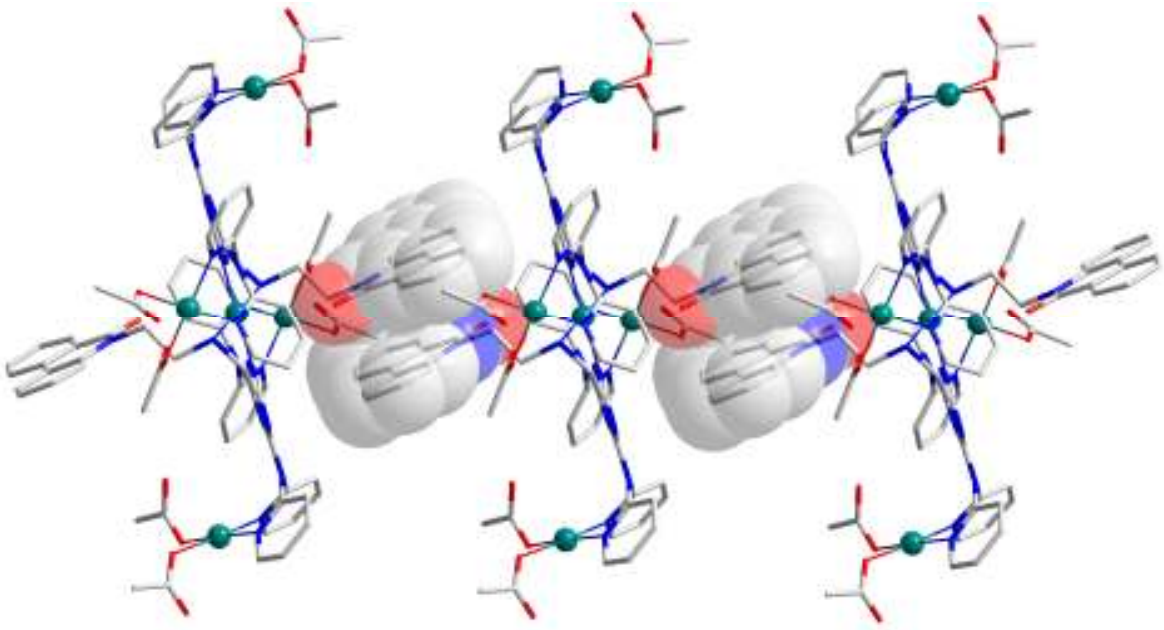

Figure 34: 1D chains formed by interactions of the phenanthridinone π systems.

The phenanthridinone moieties, while exhibiting much less aromaticity than is the case in the DIP structure, show a greater degree of overlap of the ring systems than has been previously seen in the case of DIP ligands (see section 3.4.2). This may be due to the loss of the cationic charge of the ring system, allowing the ring systems to overlap to a greater extent without experiencing electrostatic repulsions. The loss of aromaticity does have an effect on this interaction, and even though the ring overlap of the system is much greater, the strength of the interaction is weakened by the lack of a central aromatic ring, and this can be seen in the distance of the interaction.

The distance between the two planes described by the phenanthridinone moieties amounts to 3.40(1) Å, but the interaction between individual atoms is longer than those seen for interacting DIP moieties, for example (see Chapter 3). The interaction takes place with the central, non-aromatic, ring of one complex directly over the quinolinone-like ring

of the neighbouring complex, with a centroid-centroid distance of 3.82(1) Å. However, the closest atom-atom distances observed are between the carbon atoms shared between the isoquinolinone-like and central rings of one complex and the quinolinone-like ring of the corresponding complex, with C-C distances of 3.77(1) and 3.79(1) Å indicating a very long π stacking interaction, approaching the borderline between π interactions and merely close packing effects. The chains produced by these interactions are further stabilised by a C-H···π interaction between phenanthride hydrogens and the electron deficient triazine ring, with a H-centroid distance of 2.69(1) Å (see Figure 35). Such C-H···π interactions are well known for the triazine ring moiety.[128-130]

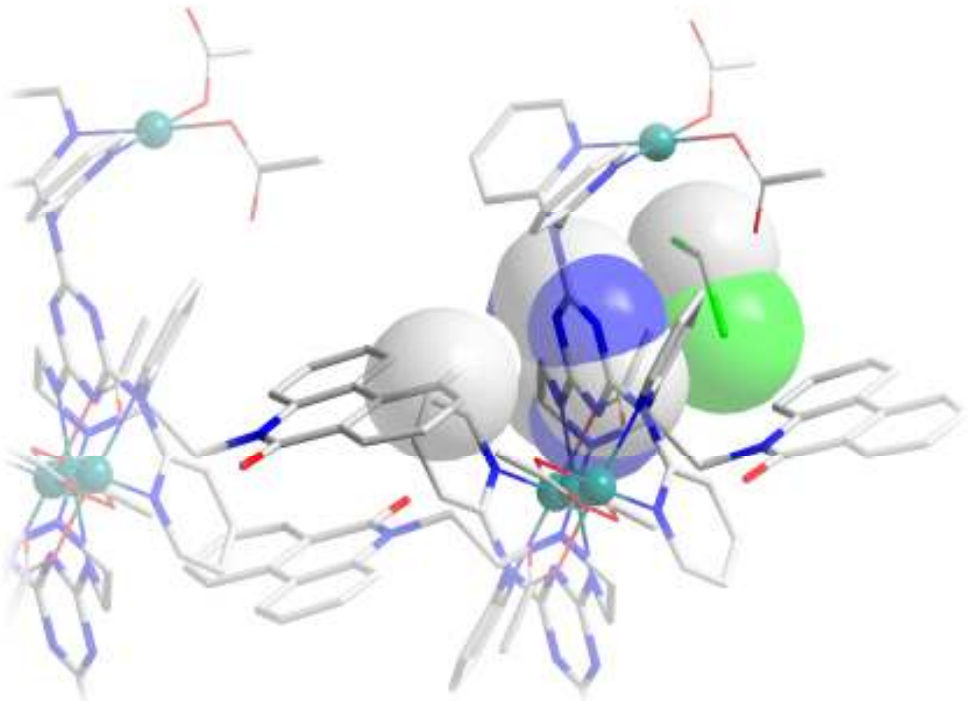

Figure 35: Representation of C-H···π···*l.p.* interaction stabilising 1D chains in the crystal structure of 36.

Another interesting feature of this crystal structure is that there appears to be an interaction on the opposing face of the triazine aromatic ring with a chlorine atom from a molecule of dichloromethane present in the lattice as solvent of crystallisation. The distance between the chlorine atom and the centroid of the triazine ring is 3.50(1) Å. This

interaction could be thought of as an interaction between the lone pair (*l.p.*) of the chlorine atom and the π system of the triazine ring which could be formulated as a C-H···π···*l.p.* (*i.e* a δ+···π···δ-) motif. A search of the CSD indicates that the observation of such a motif is unique, and as the interplay between cation···π, π···π and anion···π interactions[129] has been clearly demonstrated by DFT calculations which predict such interactions could exist.[130] This could be seen as the first crystallographic example of such a C-H···π···*l.p.* supramolecular complex, corroborating the recent results of Frontera and Deyà.[131]

Using the relatively new technique of cryospray mass spectrometry[132, 133] it is possible to observe the central Pd_5(**35**')$_2$ unit of this compound as the $[Pd_5(\mathbf{35'})_2(CH_3CO_2)_5Cl_6]^-$ anion, where the chloride anions originate from NaCl added to the solvent mixture. The mass spectrum of **36** is complex and is characterised by a series of overlapping isotopic envelopes, and while it was possible to observe the core unit of **36**, it was not possible to fully assign the mass spectrum (see section 8.6 for full mass spectrum).

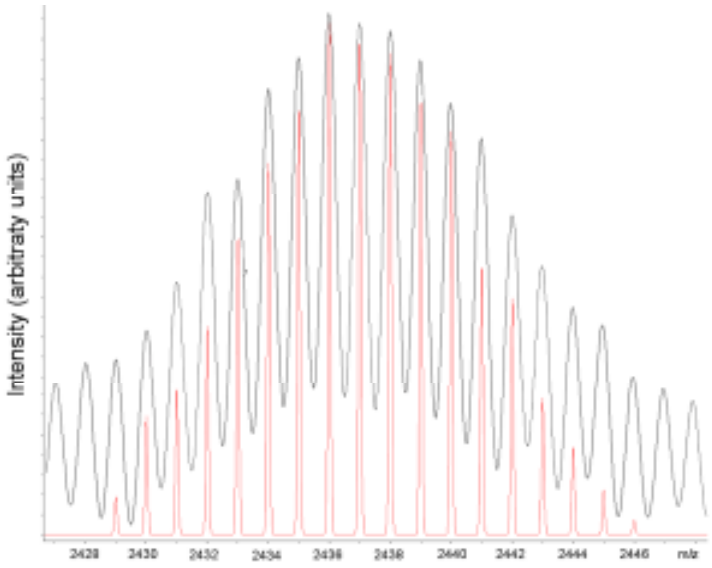

Figure 36: Selected peak from the cryospray mass spectrum (negative ion mode) of 36 in a DCM:MeCN (1:1) mixture at -40 ºC (black). The simulated spectrum for $[Pd_5(35')_2(CH_3CO_2)_5Cl_6]^-$ is shown in red.

4.2.2 Complexation of 35 with $Cu(ClO_4)_2.6H_2O$.

Reaction of DIP triazine ligand **35** with two equivalents of $Cu(ClO_4)_2.6H_2O$ in an acetonitrile solution, followed by slow diffusion of diethyl ether yields blue needle crystals of a new complex, with the formula $Cu_2(\mathbf{35})_2Br_2$, **37**.

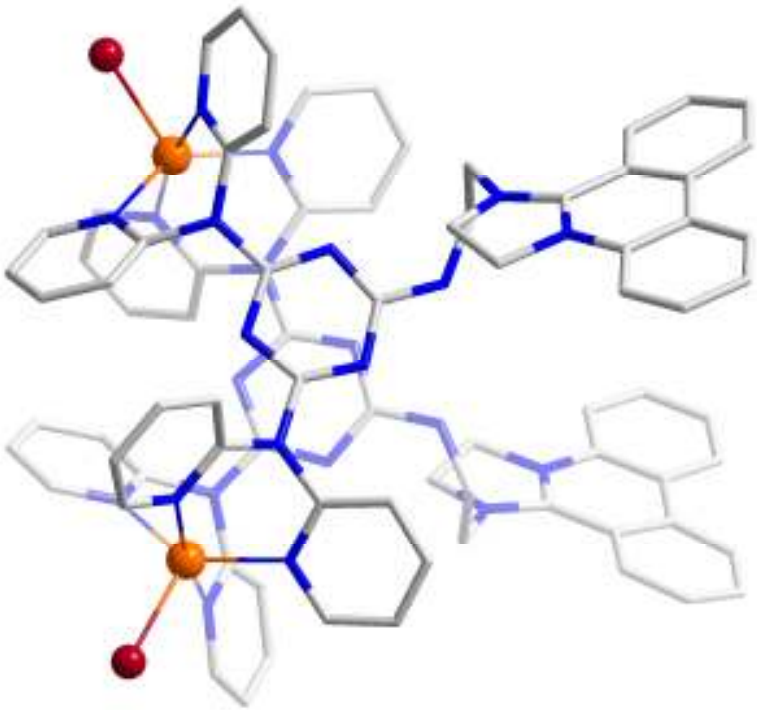

Figure 37: Structure of complex 37. Hydrogen atoms, uncoordinated anions and solvent molecules have been omitted for clarity.

Complex **37** consists of two **35** ligand molecules which have remained unchanged through the complexation process in contrast to those in **36**. Each **35** ligand is coordinated to two Cu^{II} metal centres *via* the chelating dipyridyl regions of the triazine based ligand creating six-membered chelate rings with Cu-N bond lengths between 1.993(4) and 2.047(4) Å. These Cu^{II} centres are coordinated by two different ligands simultaneously producing a dinuclear, biligand complex. The Cu^{II} centres in the **37** complex are five coordinate and display an extremely distorted trigonal bipyramid coordination geometry, with a τ_5 value for the Cu^{II} ion of 0.51, indicating a geometry which appears to be halfway

between trigonal bipyramid and square based pyramid. The copper centres in the structure have a CuN_4Br donor set, with the coordinated bromide anion originating from the **35** DIP ligand, with a Cu-Br bond length of 2.4746(10) Å. The cationic charge of the ligand is partially compensated for by the charge of the coordinated bromide anions, giving the complex an overall charge of 4+, which is balanced by uncoordinated perchlorate anions in the crystal lattice. Also present in the crystal structure are disordered acetonitrile molecules as solvent of crystallisation.

The structure of the **37** complex is arranged such that the triazine rings from each of the ligand moieties are located directly above each other; in an almost parallel arrangement (the dihedral angle between the two ring systems is 6.4(1)º). This indicates the existence of a stabilizing π stacking interaction between the two electron deficient triazine rings, with a centroid-centroid distance of 3.42(1) Å. It is also worthy of note that the coordination of the two ligand moieties with the two Cu^{II} centres forms a 20 membered macrocyclic ring through the coordinating pyridyl groups (see Figure 38).

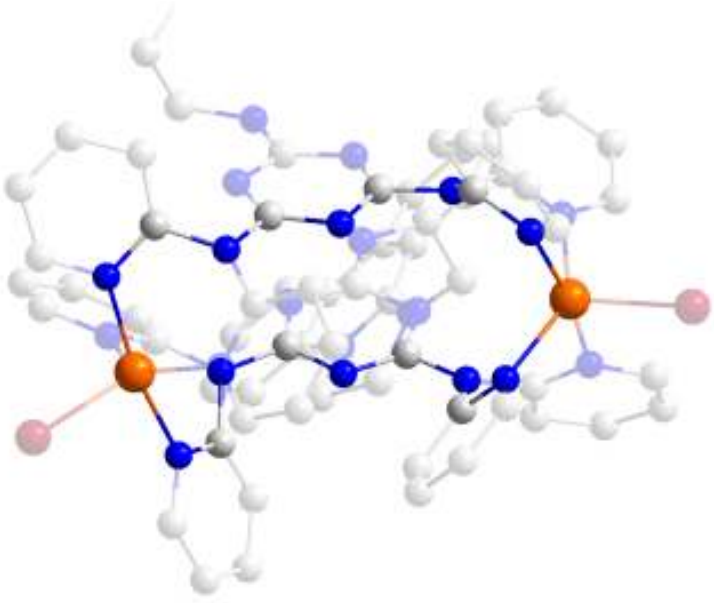

Figure 38: 20-membered macrocyclic structural motif present in the 37 complex.

The DIP regions both extend out from the triazine core of the complex in the same direction in a diverging fashion, with an angle of 22.2(1)º between the planes described by the phenanthridine rings of the DIP systems. The DIP sections of the two coordinated ligands have a large distance between them with a distance between the corresponding phenanthride carbon atoms of the order of 10-15 Å, allowing enough space between the DIP regions for the complex to interlock with a neighbouring complex *via* π stacking interactions between the DIP rings and two of the coordinating pyridyl regions of a neighbouring complex (see Figure 39). These π stacking interactions take place between one of the pyridyl regions of each ligand moiety on one **37** complex and the isoquinoline-like ring of the DIP regions of one of the ligand moieties on the neighbouring complex, with a centroid-centroid distance of 3.40(1) Å between the interacting ring systems.

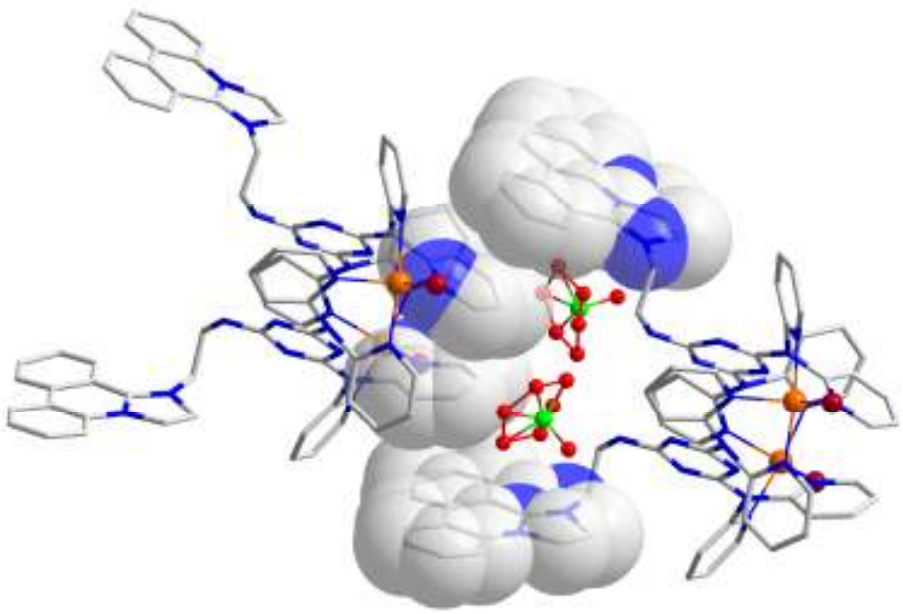

Figure 39: π stacking of DIP regions of 37 with the pyridyl groups of a neighbouring complex.

Also situated between the DIP moieties on each complex are two of the perchlorate counterions which balance the charge of the cationic DIP ring systems. On the opposing face of the DIP system are a second set of intermolecular interactions between the DIP

regions of two neighboring complexes, linking the molecules in a second direction (see Figure 40). These interactions take place between the peripheral rings of the DIP regions of adjacent complexes, where the DIP rings are arranged in an antiparallel fashion with the isoquinoline-like ring of one ligand interacting with the quinoline like ring of the corresponding ligand, with a centroid-centroid distance of 3.81(1) Å. These intermolecular interactions combine to link each **37** complex in two dimensions through the crystal structure leading to the formation of π interacting sheets of complexes in the crystallographic *bc* plane. These sheets are separated by uncoordinated solvent molecules, with the final perchlorate counterions located within each sheet, above and below each complex.

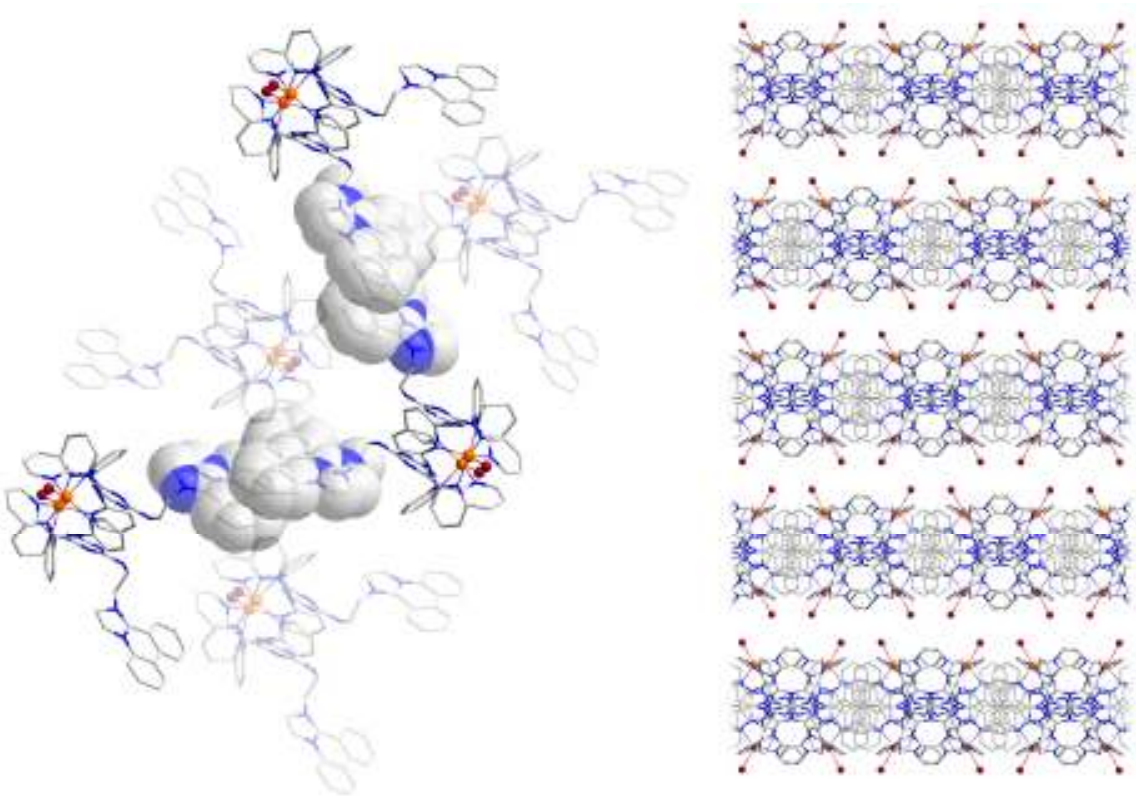

Figure 40: (left) π stacking interactions between DIP regions of ligand moieties in 37 leading to the formation of 2D sheets in the crystal structure. (right) View along the crystallographic *c* axis of the 2-D sheets. Uncoordinated anions and solvent molecules omitted for clarity.

5 IMIDAZO PHENANTHRIDINIUM BASED LIGANDS

5.1 Ligand Design and Synthesis

The bipyridine moiety has been described as "*the most widely used ligand*"[134] in coordination chemisty, and one of the most important types of bypyridine ligand is the 2,2'-bipyridine molecule and its analogues. Such a motif is ubiquitous in coordination chemistry, with a search of the CSD giving over 8000 hits for 2,2'-bipyridine analogues with the vast majority of these structures (7000+) cases where the 2,2'-bipyridine coordinates to a transition metal atom in a chelating mode *via* its two pyridine like nitrogen atoms. The bipyridine moiety has also been extensively decorated by extending the aromatic ring system to enhance certain desired properties of the resulting compounds, such as their luminescence[135,136] or use in transition metal catalysts for organic synthesis.[137,138] Significantly less common, however, are ligands in which one of the pyridine rings of a 2,2'-bipyridine molecule is replaced with a different aromatic heterocycle such as a pyrrole or imidazole type ring, while still retaining the chelating mode seen in the original bipyridine ligand.

The development of phenanthridine chemistry in our group[139,140] has recently opened a route to the facile synthesis of imidazo-phenanthridine derivatives, which lend themselves to the construction of such aromatic heterocyclic ligands. As discussed previously, the nature of the DIP structure has several limits to its use in coordination chemistry, which can be illustrated by the difference between the DIP and IP parent structures (see Figure 41).

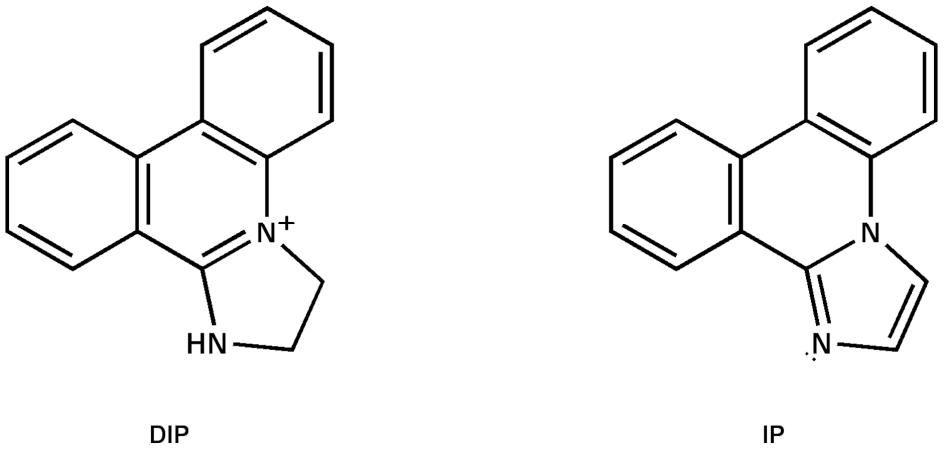

Figure 41: Parent DIP and IP structures.

The main difference between the DIP and IP structures is that the imidazo- ring of the IP structure has two less hydrogen atoms and is therefore fully oxidised and the aromatic system extends over all four rings of the heterocyclic structure with a total of 18 electrons in conjugated *p* orbitals satisfying Hückel's criterion for aromaticity. In contrast the aromaticity of the DIP framework which extends over only the phenanthridinium rings (although significant conjugation exists between the two nitrogen atoms). The imidazole-like ring of the IP structure can arrange in such a way that this parent structure becomes a neutral moiety, which is much more favourable for use in coordination chemistry than the cationic structure of DIP, which experiences electrostatic repulsions with the positively charged metal ions. In common with imidazole, the two nitrogen atoms in the IP structure play different roles in the aromaticity of the overall structure in that the lone pair of one nitrogen is delocalised in the aromatic π system whereas the lone pair of the other nitrogen atom is not and therefore gives this nitrogen a much more basic and nucleophilic character. In previous work by the *Cronin* group[139-141] this aspect of the reactivity of the IP has been used as a means of functionalising the IP structure to produce cationic N- derivatives analogous to those seen in DIP structures. However, the basicity of this lone pair also means that it can act as a coordination group for inorganic chemistry.

IP structures can be synthesised with substituents on the imidazole carbons by judicious use of α- bromo carbonyl type starting materials. With the aim of producing a bipyridyl-

like ligand for coordination chemistry, the following reaction scheme was designed and carried out to afford compound **40** as an IP-pyridyl type ligand (see Scheme 13).

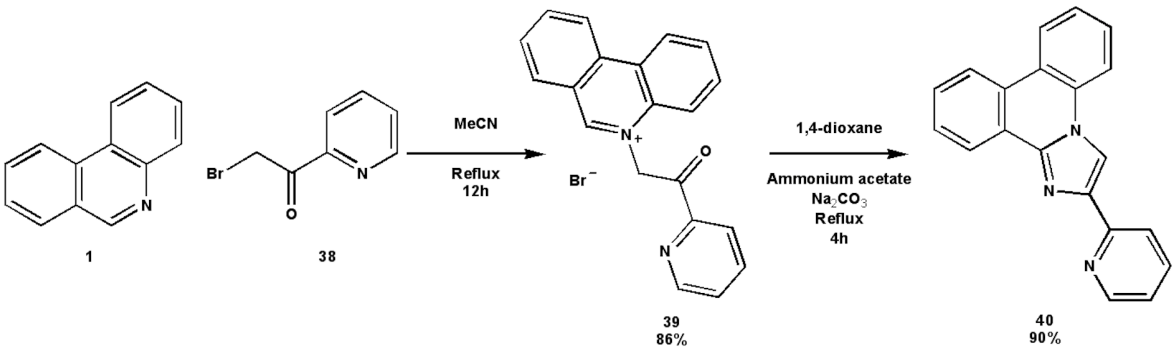

Scheme 13: Synthesis of IP-pyridyl ligand 40.

This ligand was synthesised by reacting phenanthridine with 2-bromo-1-pyridin-2-yl-ethanone (**38**) under refluxing conditions in acetonitrile to form the 5-(2-oxo-2-pyridin-2-yl-ethyl)-phenanthridinium bromide intermediate **39**. This intermediate was then cyclised by reaction with ammonium acetate, sodium carbonate and magnesium(IV) oxide under reflux in 1,4-dioxane to yield the product **40**. The reaction proceeds *via* a mechanism discussed in the introduction (see Section 2.2.2)

This ligand has a bidentate binding site similar to that of 2,2'-bipyridine, however, it is an asymmetric ligand in which one side contains a much larger aromatic system than the other, and this will significantly effect this ligands ability to form supramolecular architectures through interactions of its π electron systems. This ligand was therefore used in complexations with a number of transition metals to investigate its coordination and supramolecular chemistry.

5.2 Complexations of IP-Pyridyl Ligand with Transition Metal Salts

5.2.1 Reaction of 40 with $CuBr_2$

Reaction of **40** with two equivalents of $CuBr_2$ in a methanol/DMF solvent mixture yielded, after slow evaporation over the course of two weeks, yellow block crystals of compound **41** which has the formula $CuBr_2$(**40**)(DMF). X-Ray analysis of suitable single crystals of **41** allowed the elucidation of its crystal structure (see Figure 42).

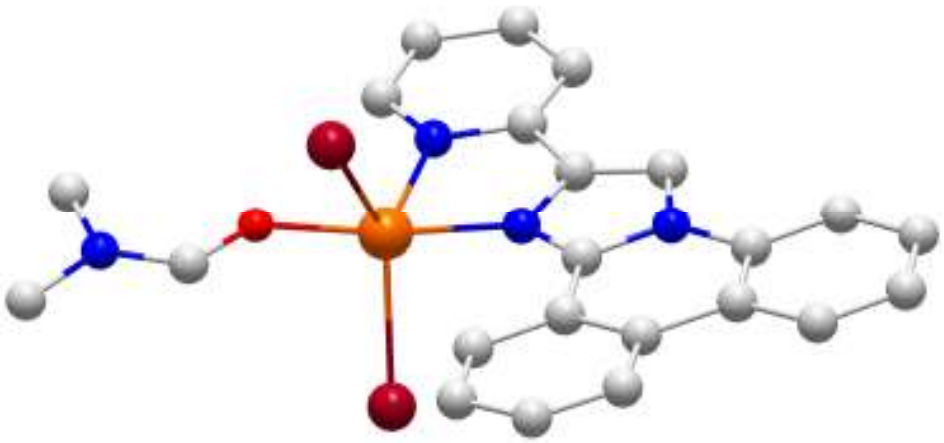

Figure 42: Crystal structure of compound 41.

Compound **41** crystallises in a triclinic *P*-1 space group and consists of a five coordinate copper complex which is coordinated to one **40** ligand, two bromide anions and one coordinated DMF molecule, giving a CuN_2Br_2O donor set. The Cu^{II} anion is in a trigonal bipyrimidal geometry with a τ_5 value of 0.661. The equatorial positions of the trigonal bipyrimidal structure are occupied by two bromide anions with Cu-Br bond lengths of 2.5234(11) and 2.4813(10) Å and the pyridyl nitrogen from the **40**, with a Cu-N bond length of 2.108(5) Å. The apical positions of the structure are taken up by the oxygen of the coordinated DMF solvent molecule (Cu-O bond length 1.962(4) Å) and the imidazole nitrogen from the **40** ligand (Cu-N bond length 1.979(5) Å). The cationic charge of the Cu^{II} is compensated for by the coordinated bromide anions, giving a formally neutral complex.

A search of the CSD reveals that this coordination motif has not been observed in bipyridine based ligands. As expected of the IP based ligand, **41** exhibits a large number of intermolecular interactions through its aromatic π system.

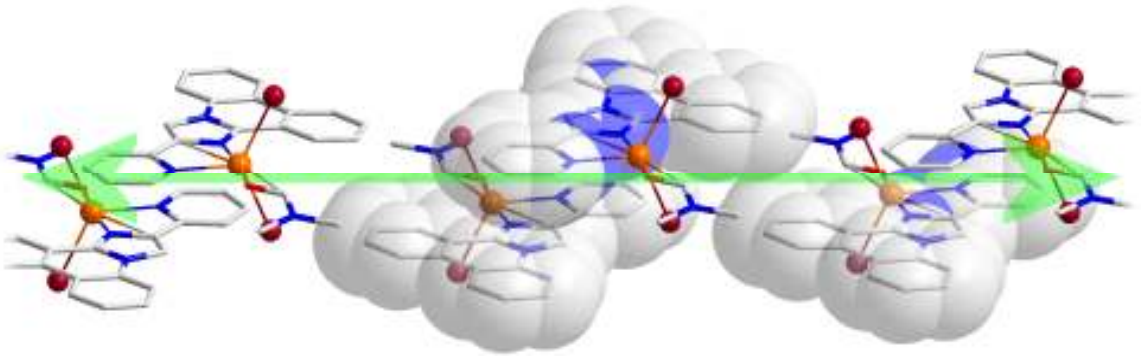

Figure 43: π interactions of one face of 41, showing the direction of the one dimensional chains formed along the crystallographic *c* axis.

The π system of the **40** ligand experiences differing interactions on each face of the complex. On one face the ligand experiences a π stacking interaction with a second complex where there is significant overlap between the two ligand systems, with the IP region of one ligand interacting with the pyridyl region of the second ligand and *vice versa*, with an interplanar distance of 3.54(1) Å between the IP ring systems. This face of **41** also experiences a second π stacking interaction between the isoquinoline like rings of the IP system, which shows significant ring off-set, with a centroid-centoid distance of 4.56(1) Å, and a shortest C-C distance of 3.34(1) Å, linking these molecules into infinite 1D chains along the crystallographic *c* axis (see Figure 43).

Each **41** complex experiences a second set of π interactions on the opposite face of the complex, this time linking the complex in the second and third dimensions (see Figure 44).

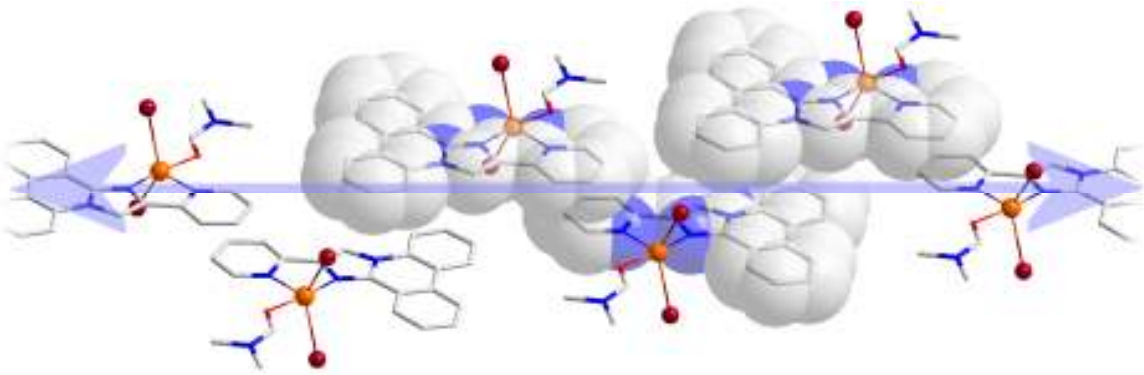

Figure 44: π interactions on the second face of compound 41, showing the one dimensional chains formed along the crystallographic (+*a*+*b*) vector.

In contrast to the previous π interactions where the pyridyl regions of the ligand interacted with the IP regions of a neighbouring complex, on this face of the **41** complex, the ligand IP region interacts with another IP region and the pyridyl with another pyridyl. In the case of the IP interactions, the majority of the interaction takes place between the quinolone-like and central rings of the IP framework and there is very little overlap of the ring system with a centroid-centroid distance of 4.07(1) Å and closest atom-atom contacts of 3.40(1) Å. The interaction between the pyridyl regions, however, exhibits more ring overlap, with a centroid-centroid distance of 3.79(1) Å, and closest atom-atom interactions of 3.28(1) Å. These interactions link the **41** complexes into a second set of 1D chains running in the direction of the crystallographic (+*a*+*b*) vector. As each complex in the structure experiences both sets of these interactions at once, the structure is linked into a 3D network *via* its supramolecular π interactions.

5.2.2 Reaction of 40 with $PdCl_2$

Reaction of equimolar equivalents of ligand **40** with $PdCl_2$ in hot DMSO followed by slow cooling yields, after one week, red block crystals of a new complex, **42** with the formula Pd(**40**)Cl_2. X-Ray crystal analysis of single crystals of compound **42** allowed the determination of its crystal structure (see Figure 45).

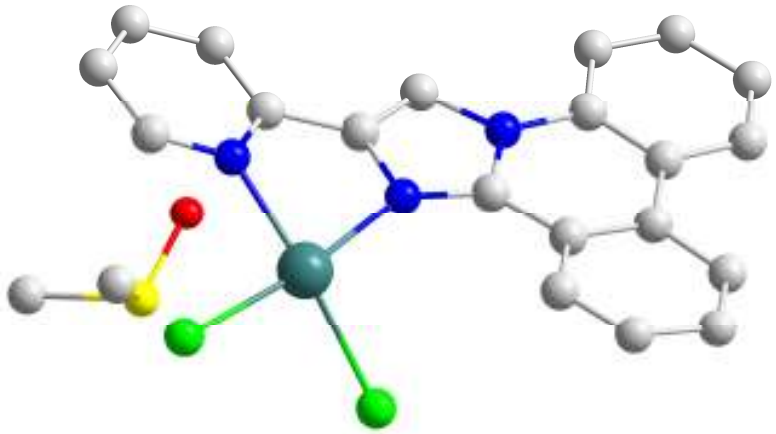

Figure 45: Asymetric unit of the crystal structure of compound 42.

Compound **42** crystallises in a monoclinic $P2_1/c$ space group and consists of a four coordinate Pd^{II} ion which is coordinated by one **40** ligand *via* the expected bidentate binding site of the ligand with Pd-N bond lengths of 2.0404(17) and 2.0571(17) Å, and two chloride anions with Pd-Cl distances of 2.2732(5) and 2.2979(5) Å. The asymmetric unit of the crystal structure also contains an uncoordinated DMSO molecule as solvent of crystallisation. The Pd^{II} ion is coordinated in a square planar geometry typical of d^8 Pd^{II} complexes, however due to the relatively small bite angle of the **40** ligand (80.14(7)º) the geometry of the Pd^{II} is significantly distorted away from ideal square planar geometry. The plane of coordination of the Pd^{II} is tilted with respect to the plane of the ligand, exhibiting a dihedral angle of 30.9(1)º. This arrangement leads to the complex having effectively two faces, a 'top' face with a large angle between the plane of the ligand and the plane of the Pd^{II} (180+30.9(1)º) and a 'bottom' face with the smaller angle. This has a major impact on the supramolecular interactions each face experiences.

Once again we see the IP Ligand involved in extensive intermolecular interactions *via* its aromatic π electrons. On the top face we see a π stacking interaction with the same face of a second **42** complex, where there is extensive overlap of the ring systems, and the peripheral rings of the IP region interact with the pyridyl region with an interplanar distance between the IP ligands of 3.16(1) Å. The top face of the IP region also

experiences a second, longer range, interaction with the 'bottom' face of another neighbouring complex with the quinoline-like ring of one IP unit interacting with the isoquinoline like ring of the neighbouring complex. The arrangement of these interacting species shows very little ring overlap, with a centroid-centroid distance of around 5.04(1) Å. The closest C-C contacts between these two rings are 3.44(1) and 3.32(1) Å. However with such little overlap between the rings, a significant contribution to the stabilising of this geometry is likely due to an electrostatic attraction between the $\delta+$ hydrogen atom of the interacting aromatic system.

The opposite, 'bottom', face of the **42** complexes also experience π interactions, however due to the steric bulk of the $PdCl_2$ unit pointing in the direction of this face, the π stacking interaction between IP ligands only extends over the IP regions of neighbouring complexes, with a centroid-centroid distance of 3.41(1) Å indicating a large degree of ring overlap, and does not include the pyridyl moiety. The isoquinoline-like ring of the IP molecule experiences a long range interaction with the 'top' face of a neighbouring ligand as described above. These interactions on either face of the **42** complex combine to give 2D sheets, with alternating 'top'-'top' and 'bottom'-'bottom' interactions producing π stacked columns which are linked in a second direction by the long range 'top'-'bottom' interactions (see Figure 46).

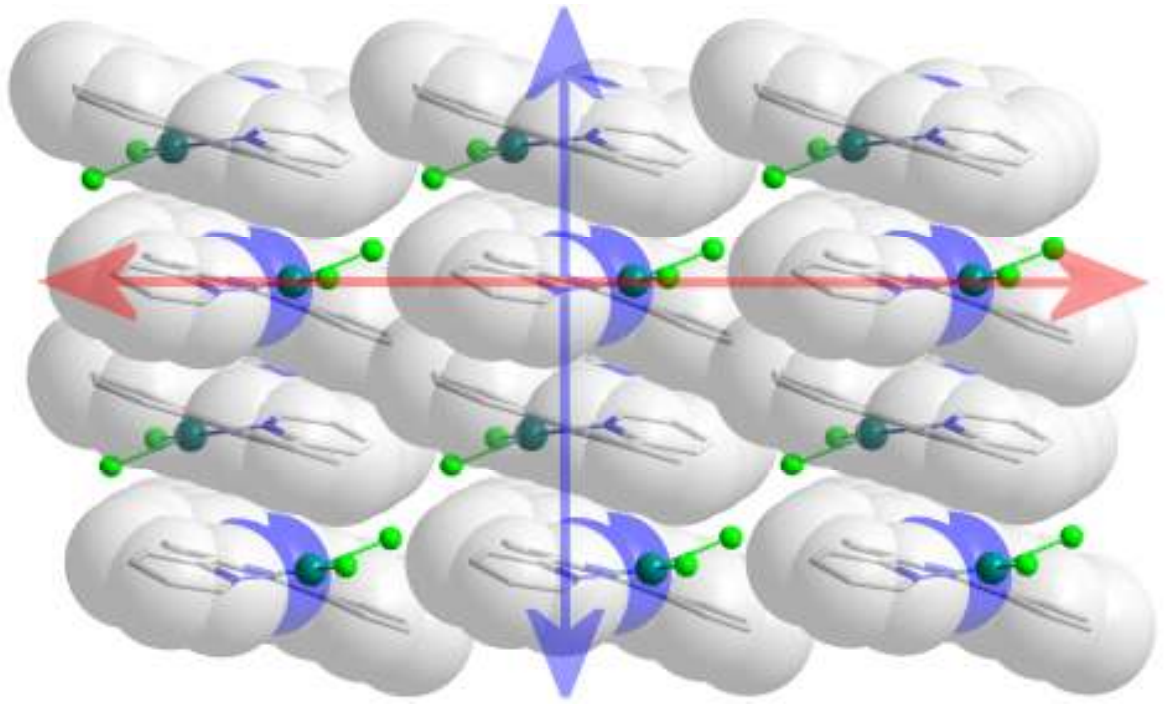

Figure 46: 2D sheets formed by π interactions of complex 42.

These 2D sheets run parallel to the crystallographic *ac* plane and each complex is associated with an uncoordinated DMSO molecule, which form chains in the crystallographic *c* direction. The **42** complexes in neighbouring sheets are arranged in a herring-bone type pattern along the crystallographic *b* axis (see Figure 47)

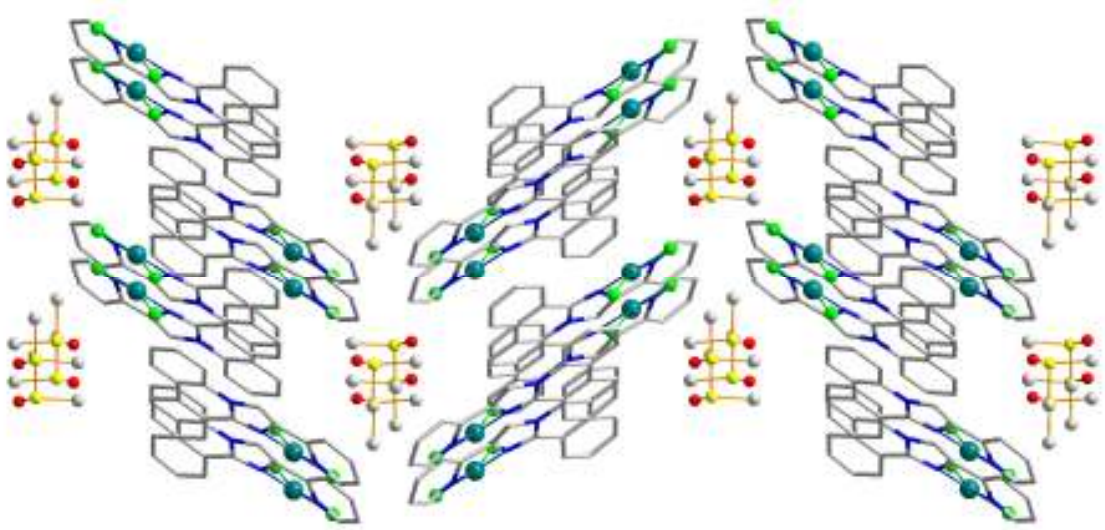

Figure 47: Herring-bone arrangement of 2D sheets in the crystal structure of 42, showing chains of uncoordinated DMSO molecules. Viewed along the crystallographic *c* axis.

5.2.3 Reaction of 40 with Ag(NO_3)

Reaction of equimolar equivalents of ligand **40** with Ag(NO_3) in a methanolic solution followed by slow evaporation yields colourless block crystals of a new compound with the formula Ag(**40**)$_2$(NO_3)·3MeOH (**43**). **43** crystallises in a triclinic *P*-1 space group and comprises a four coordinate Ag^I metal center with a AgN_4 donor set arising from the simultaneous coordination of two molecules of **40** (see Figure 48).

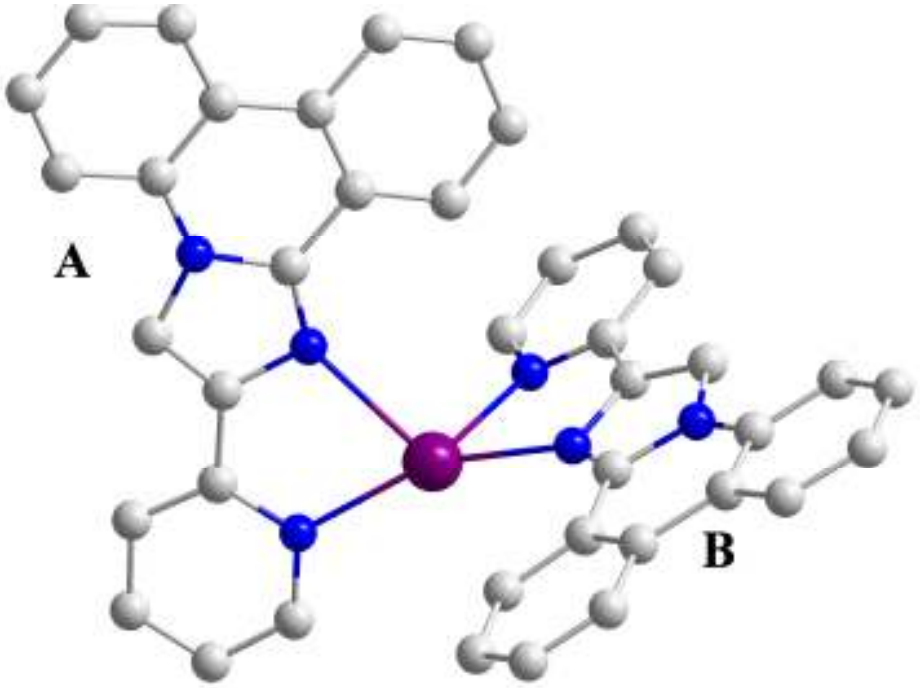

Figure 48: X-Ray crystal structure of 43. Uncoordinated anions, solvent molecules and hydrogen atoms have been removed for clarity.

The Ag^{I} ion in **43** exhibits a significantly distorted *pseudo*-tetrahedral structure, with a dihedral angle of 79.9(1)º between the planes described by the two chelate rings from each of the coordinated ligands. By inspection of the Ag-N bond lengths in this complex we can see that there is a significant degree of linearity to the coordination of the Ag^{I} ion, with two shorter bond lengths of 2.217(8) and 2.233(8) Å exhibiting a N-Ag-N angle of 156.0(3)º, and two Ag-N bonds of 2.402(9) and 2.435(8) Å. There are two similar but distinct ligand coordination modes between the ligands and the Ag^{I} centre in the crystal structure. Each ligand coordinates *via* one short Ag-N bond and one longer Ag-N bond, with one ligand having a shorter bond to the pyridyl nitrogen ('A' type ligands) and the other ligand with a shorter bond to the imidazole nitrogen ('B' type ligands). The ligand molecules in this structure are arranged such that the IP regions are virtually perpendicular to one another, with a dihedral angle between the IP planes of 88.8(1)º. The charge of the Ag^{I} cation is compensated for by one disordered nitrate anion in the crystal structure. Also present in the unit cell are three methanol molecules as solvent of crystallization.

The formation of such a diligand complex gives rise to the possibility of a multitude of intermolecular interactions between ligand moieties to stabilize the crystal structure of **43**. In order to describe these interactions fully it is necessary to distinguish between the two perpendicular ligand units, A and B. The first set of ligand interactions are those between the A ligands, which are linked in two dimensions by π stacking interactions between ligands of the same type (see Figure 49).

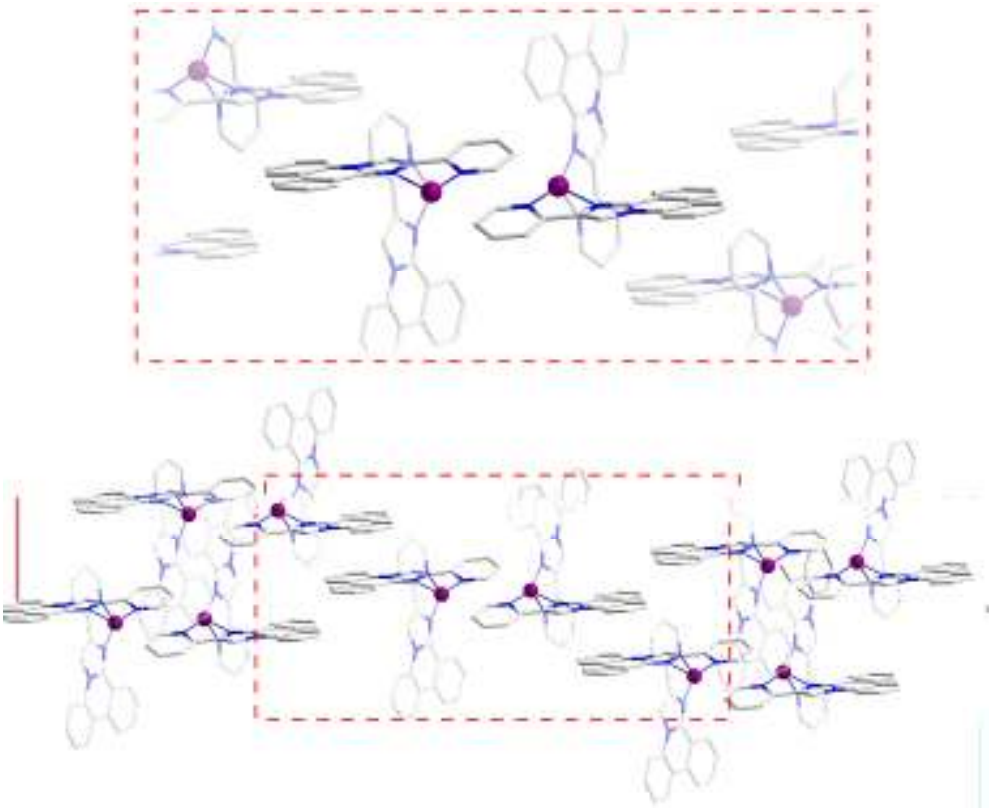

Figure 49: Supramolecular interactions of A type ligand in the crystal structure of 43. (Top) Supramolecular dimers formed by π stacking interactions between pyridyl regions. (Bottom) The linking of these dimers in two dimensions *via* π stacking and long-range π interactions.

The A ligands form supramolecular dimers *via* π stacking interactions between the pyridyl regions of the **40** ligands, with a centroid-centroid distance 3.43(1) Å indicating a large degree of ring overlap. These dimers are then linked into a 2D sheet-like array *via* π interactions on either face of the IP region of the ligand. One of these interactions exhibits

a large degree of ring overlap, with interactions taking place between all three of the phenanthridine rings and an interplanar distance of 3.27(1) Å. On the other face of the IP ring system there is a long range interaction between the quinoline like ring of the IP moiety and that of a neighbouring complex. There is virtually no ring overlap in this interaction (the centroid-centroid distance is 4.82(1) Å and closest C-C distance between rings is 3.36(1) Å) and therefore it is probably best described as a combination of a π-π and C-H···π type interaction as discussed in the case of **42** above. This face of the A ligand also experiences a more traditional 'T-shaped' C-H···π interaction with a B type ligand of a neighbouring complex directly above it in the sheet arrangement, with a distance between the hydrogen atom and the IP plane of 2.66 Å. The combination of these interactions of the A ligands links the **43** complexes of the crystal structure into 2D sheets parallel to the crystallographic *ac* plane.

Projecting out from the sides of the supramolecular sheets formed from the supramolecular interactions of the A type ligands are ligands of the second B type. These ligand moieties experience two sets of π stacking interactions, one on either face of the ligand structure and each stacking interaction is with another ligand of the same type. The complexes stack 'back-to-back' with the maximum possible overlap between the ring systems (i.e. IP stacking over pyridyl and *vice versa*) on the sterically unhindered face of the ligand molecule with an interplanar distance of 3.13(1) Å. On the other face of this ligand molecule this stacking motif is unavailable due to the steric hindrance of the coordinated Ag^{I} and associated ligand, and a second motif is observed whereby the IP regions of two ligands stack antiparallel with each other *via* an interaction between all three of the phenanthridine rings. There is a degree of ring offset, however, shown by the centroid-centroid distances of 3.63(1)–3.87(1) Å between corresponding rings. The average interplanar distance between the two ring systems is 3.36(1) Å.

The interactions between the B type ligands form columns of π stacked complexes along the crystallographic *a* axis which link the sheets formed by interactions of the A ligands on either face of the sheets, forming a three dimensional structure (see Figure 50).

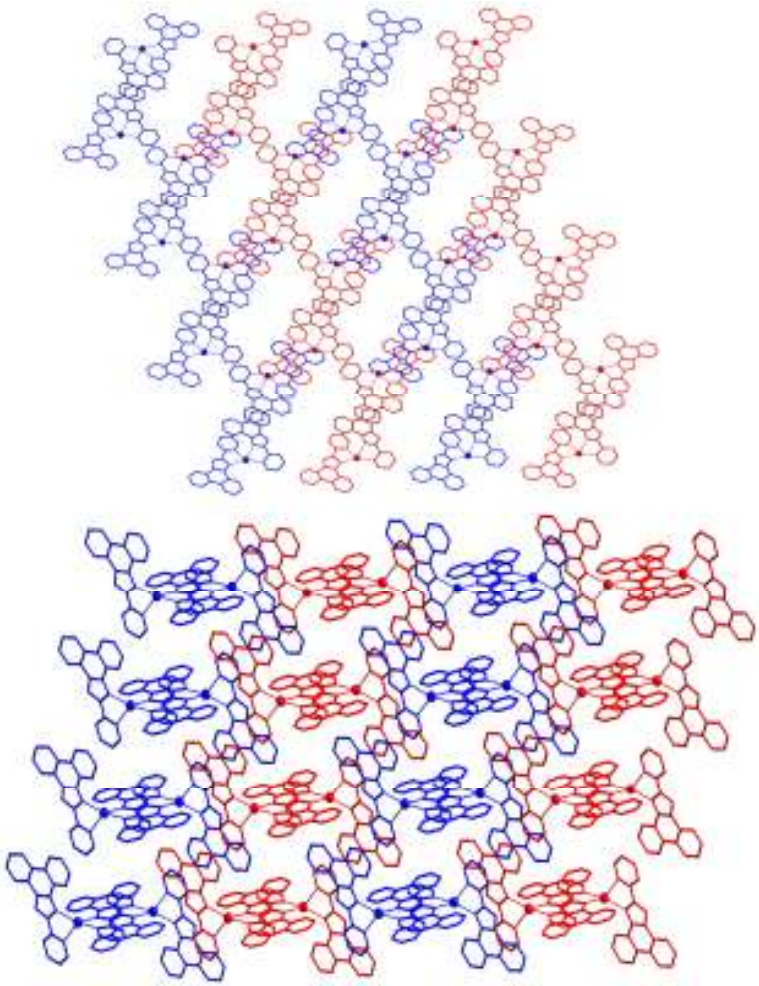

Figure 50: packing diagrams of 43. (Top) View along the crystallographic *a* axis, alternate sheets formed by interactions of type A ligands are coloured red and blue. (Bottom) View of *π* stacking between type B ligands linking adjacent sheets.

This three dimensional network of **43** complexes also forms channels in the crystal structure which run in the direction of the crystallographic *a* axis, these channels are occupied by methanol solvent molecules and nitrate counterions.

5.2.4 Reaction of 40 with $Co(BF_4)_2 \cdot 6H_2O$

Reaction of two equivalents of $Co(BF_4)_2 \cdot 6H_2O$ with one equivalent of ligand **40** in a refluxing acetonitrile solution followed by crystallisation by slow diffusion of diethyl

ether into the reaction mixture yielded red/green block crystals of a new complex with the formula $(Co_2O(\mathbf{40})_4)(BF_4)_3$ **(44)** after two weeks.

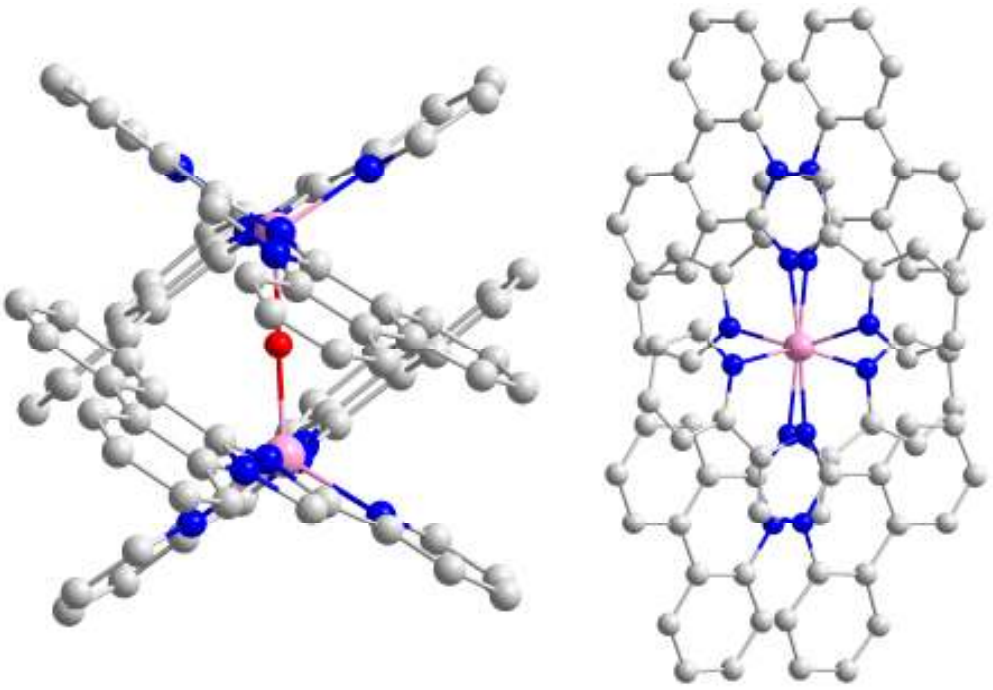

Figure 51: Crystal structure of 44 (left) viewed along one of the Co-N bonds and (right) viewed along one of the Co-O bonds.

The crystal structure of **44** shows it to consist of a dinuclear, tetraligand complex with a bridging μ_2-hydroxo ligand linking the two Co^{II} centres. Each Co^{II} ion is five coordinate with a CoN_4O donor set and an almost ideal trigonal bipyrimidal geometry, with τ_5 values of 0.902 and 0.845 for the Co^{II} centres. The four coordinated nitrogen atoms originate from the **40** ligands coordinating in both equatorial and apical positions. The apical positions of the cobalt coordination are taken up by the ligand imidazole nitrogens with bond lengths of between 2.134(5) and 2.133(4) Å. The equatorial positions are occupied by the pyridyl nitrogens of the same ligands, with Co-N bond lengths of between 2.056(5) and 2.094(5) Å and the final equatorial position of each cobalt is occupied by a bridging oxygen atom, which can be determined by Bond Valence Sum calculation to be a hydroxo ligand. The Co-O bond lengths are 1.941(3) and 1.954(3) Å and the Co-O-Co bond angle is 176.9(2) º, giving an overall Co-Co distance of 3.90(1) Å. A search of the CSD reveals that this is the

first example of such a coordination motif where there is an almost linear relationship between two trigonal bipyrimidal Co^{II} centres bridged by a μ-hydroxo ligand. A few examples have been reported of such near-linear Co-O-Co relationships in the cases of octahedral cobalt clusters[142] or in the case where the bridging oxygen atom originates from a chelating carbonate ligand.[143, 144] The cationic charge of the Co^{II} centres is partially compensated for by the bridging hydroxo ligand, giving the complex an overall charge of 3+, which is balanced by three uncoordinated BF_4 anions. Also two uncoordinated acetonitrile molecules are present in the crystal structure of **44** as solvent of crystallization.

The coordinated ligands in the structure of **44** take up an antiparallel arrangement with the ligands on different Co^{II} centres, such that the IP regions of each ligand point towards the centre of the complex and the pyridyl regions are positioned at the top/bottom of the complex structure. The **40** ligands are almost parallel to one another, forming dihedral angles of 0.7(1)º and 2.0(1)º between planes described by the IP regions of the corresponding ligands. This parallel arrangement of ligand IP ring systems indicates the existence of a stabilising intramolecular π interaction between **40** ligands on the bridged Co^{II} centres in the **44** structure. This is further supported by the distances of around 3.4 Å between atoms of the IP rings and the plane of the interacting ring systems. It is the influence of these π stacking interactions, along with the steric bulk of the coordinated **40** ligands which forces the μ_2-hydroxo ligand into the observed unusual linear geometry.

The X-Ray crystal structure of this complex is reveals **44** to be a chiral complex, its chirality arising from the helical arrangement of the bidentate **40** ligands around four of the Co^{II} centre's five coordination positions. The chirality of trigonal-bipyrimidally coordinated metal ions is well known[145-147] and can be related to the more common chirality of octahedral metal complexes giving rise to the Δ and Λ enantiomers observed in such complexes (see Figure 52). In the case of a *bis*-trigonal bipyramidal system, such as is seen with complex **44**, there arises the possibility of diastereomers being formed, with each trigonal bipyrimidal centre in the complex adopting the opposite conformation to the other. In the case of **44**, however, the steric bulk of the ligands prevent this situation and only the enantiomeric $\Delta\Delta$ and $\Lambda\Lambda$ forms are observed.

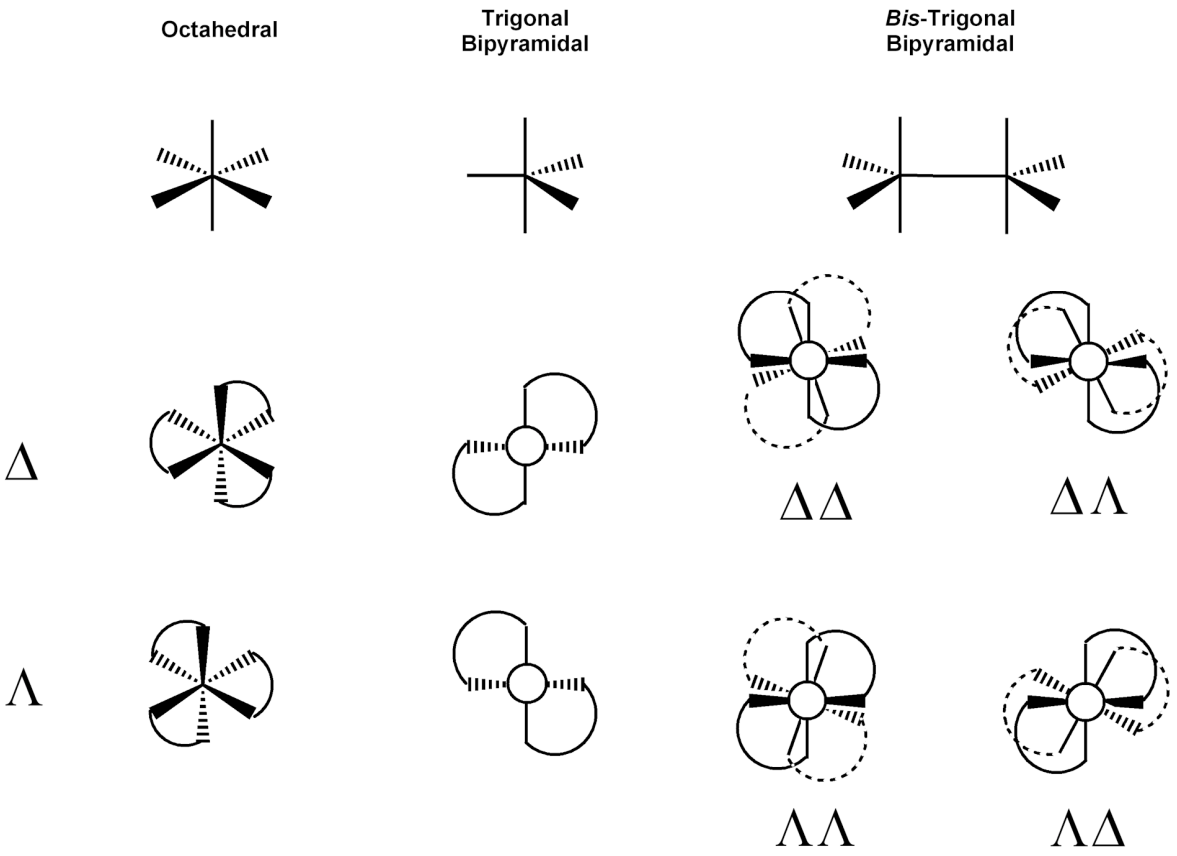

Figure 52: Chirality of octahedral, trigonal bipyrimidal and *bis*-trigonal bipyrimidal coordination geometries with bidentate ligands (trigonal bipyrimidal forms shown as newman projections along one of the equatorial bonds).

44 crystallises as a racemate, with both enantiomeric forms of the complex present in the crystal structure, crystallising in the achiral, polar *Cc* space group. The complex shown in Figure 51 represents the *ΛΛ* form of the **44** structure.

Along with the intramolecular π interactions discussed above, which take up one face of each coordinated **40** ligand, we again see intermolecular π stacking interactions linking the discrete dinuclear clusters into long range structures. Each coordinated ligand moiety experiences a π interaction between its pyridyl ring and the quinoline-like ring of a neighbouring **44** complex of the opposite enantiomeric configuration. These interactions exhibit varying degrees of ring overlap with centroid-centroid distances ranging from 3.6

to 3.9 Å. Each **44** complex is therefore linked to four of its neighbours *via* π stacking interactions of the ligand systems (see Figure 53).

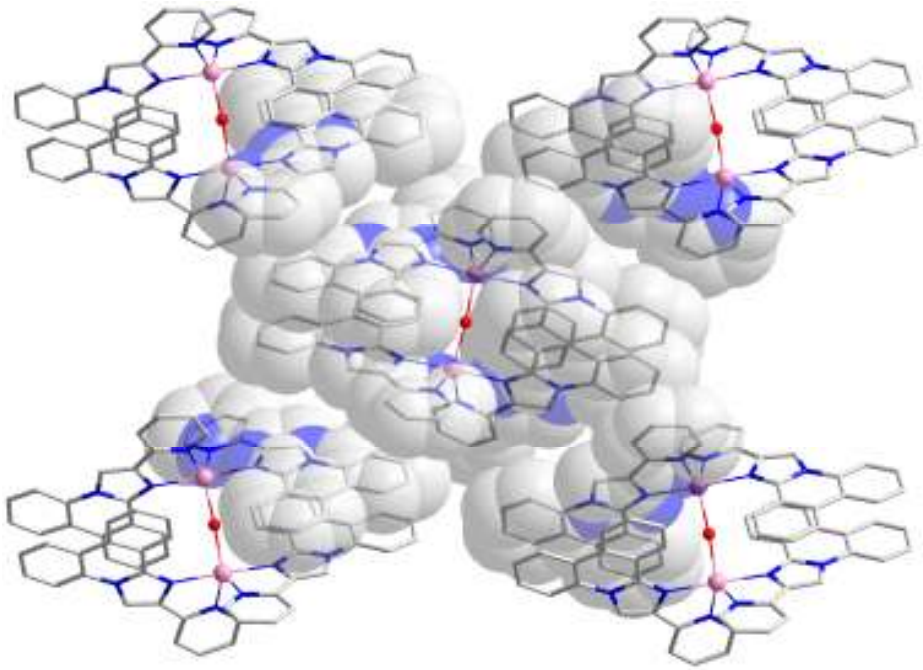

Figure 53: π interactions in the crystal structure of 44.

The result of these π stacking interactions in the crystalline phase is to link the **44** complexes in two dimensions through the crystal structure, giving rise to sheet structures. The π stacking of the **44** complexes takes place between complexes of opposite conformation, giving a situation where each enantiomer is surrounded by four molecules of the opposite enantiomer (see Figure 54).

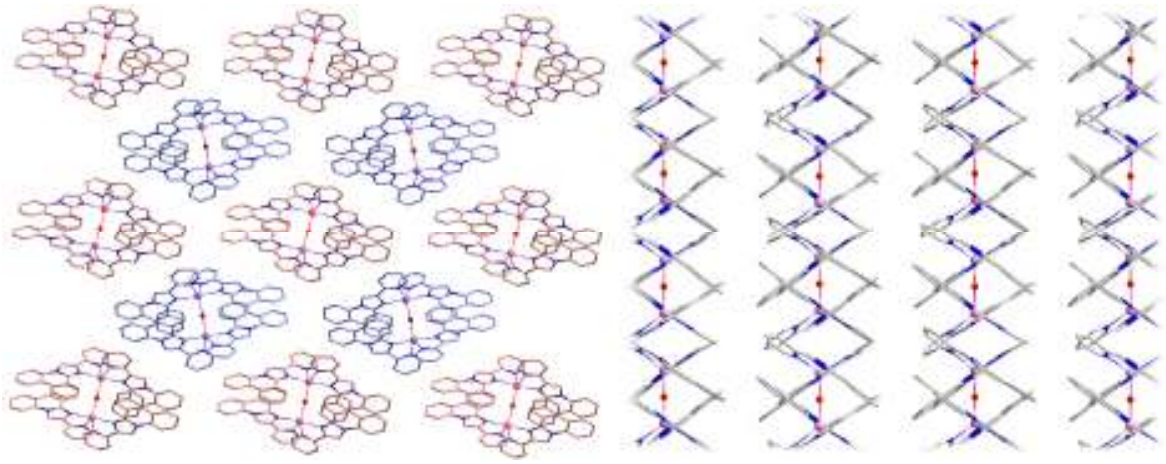

Figure 54: (left) sheets formed by π stacking in the crystal structure of 44, $\Delta\Delta$ enantiomers are shaded blue, $\Lambda\Lambda$ enantiomers are shaded red. (right) View of the two dimensional sheets along the crystallographic *c* axis.

5.3 Supramolecular Interactions of IP-Pyrdiyl ligand 40

The synthesised IP-pyridyl ligand **40** coordinates to metal ions *via* the expected chelating group designed in the ligand and formed both mononuclear and dinuclear complexes where either one or two ligands coordinate to the same metal ion. This shows the versatility of this new ligand when applied to different complexation environments, and, as expected from a ligand with such an extended aromatic ring system, shows a strong tendency for π stacking interactions to influence the long range ordering of complexes in the crystal phase.

5.3.1 π Interactions of Complexed 40 in the Crystalline Phase.

From the four examples here of complexes of the IP-Pyridyl based ligand **40** we can begin to discern a number of common motifs of interactions of this ligand system which will be useful in the design of further architectures based on IP type ligands as π interacting supramolecular building blocks.

The first of these patterns beginning to emerge is that, while the **40** ligand can be seen to form simultaneous π stacking interactions on both faces of the ligand aromatic system, these interactions tend to fall into two types depending on the type of interaction observed on the opposite face of the ligand moiety. The first type of interaction observed between ligand moieties in the crystal structures examined is that where there is an interaction between two ligand molecules across the whole extent of the ligand system, that is that the pyridyl region of one ligand is situated above the IP regions of a second ligand and vice versa (see Figure 55 (a)). One consequence of this mode of interaction is that the relatively small pyridyl region is interacting with the much larger IP region, leaving some of the IP region available for a second interaction on the same face.

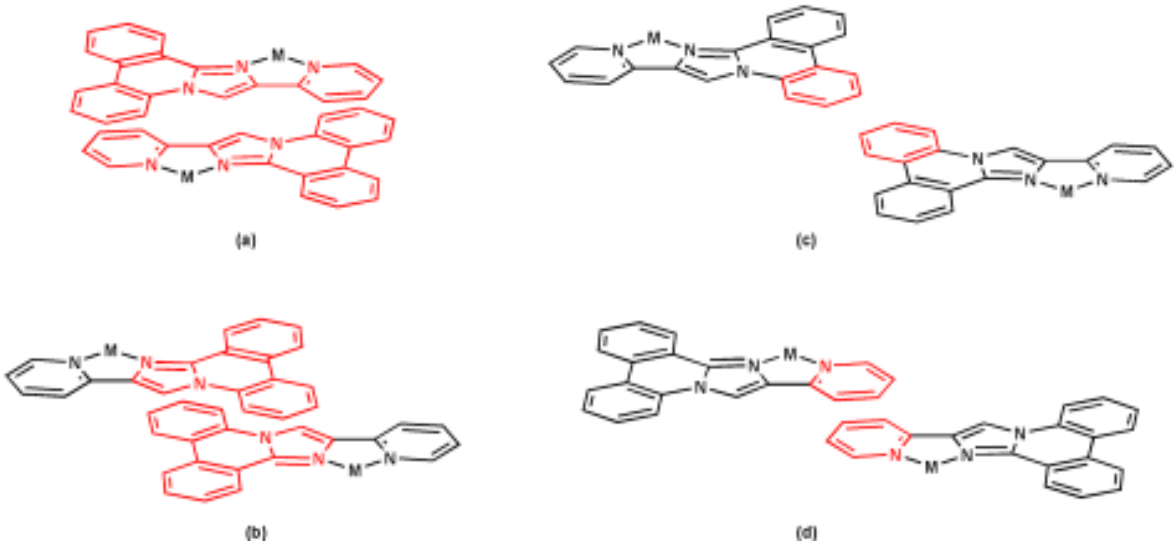

Figure 55: Schematic representation of general types of π interaction observed for the ligand. Interacting regions of the ligand π systems are coloured red.

The second major pattern of interaction of **40** is where the IP regions of two neighbouring complexes interact with each other, with varying degrees of overlap of the extensive IP ring system. In this type of interaction the ligand moieties are arranged in an antiparallel position with respect to each other and this leaves the pyridyl regions of the ligand free for interaction on the same face of the ligand molecule (see Figure 55 (b)).

Along with these modes, we also see longer range π interactions where there is less overlap between the ring systems, the first of these being the situation where one of the peripheral IP rings interacts with a similar peripheral IP ring on a neighbouring complex. This type of π stacking interaction has been seen to adopt a variety of distances between the ring systems, ranging from partial ring overlap to the situation where the interaction would be better described as an unconventional C-H$\cdots\pi$ interaction between the $\delta+$ σ framework of the aromatic ring and the π electrons of the corresponding ring system (see Figure 55c).

The final interaction motif observed in the π stacking of the **40** ligand is the situation where the pyridyl regions of neighbouring ligand molecules interact with each other in an antiparallel fashion analogous to that seen for the IP regions in the (b) type interaction discussed above (see Figure 55d).

These interactions are not mutually exclusive, but inspection of the crystal structres of compounds **41**-**44** reveals that each face of a ligand molecule will generally only experience two of these motifs at any one time. Particularly complimentary are combinations of (a) and (c) interaction motifs and combinations of (b) and (c) motifs on any one face of the ligand system. It is possible to see all these interaction modes in a single crystal structure and this leads to the conclusion that the synthesized **40** ligand can form extremely versatile π stacked interactions in the crystalline phase, but that this versatility is not chaotic and its binding modes can be classified and predicted, hopefully leading to its usefulness as a suitable supramolecular building block in future systems.

6 DIP-TYPE REACTIONS WITH CARBON BASED NUCLEOPHILES.

As discussed in the introduction, the field of heterocyclic chemistry has applications in a wide variety of areas, and as such the development of new methodologies for the synthesis of heterocyclic platforms is of constant interest to chemists. With this in mind it was decided to extend the DIP methodology which has been used extensively in this thesis to synthesise ligands for coordination chemistry. As the DIP reaction is initiated by the nucleophilic attack of a nitrogen atom on the α-position of the phenanthridinium ring of the DIP starting material BEP (**3**, see section 2.2) the obvious choice for an extension of this methodology was to find other nucleophiles which could undertake a similar reaction. While the possibility exists to use group 16 elements such as oxygen or sulfur as nucleophiles in the DIP reaction, these elements offer a limited scope for the facile construction of DIP-like products where the newly formed five-membered ring is functionalised at the initial nucleophilic atom, leading to a wide variety of compounds simply by the choice of nucleophilic starting material. Considering this alongside the importance of C-C bond forming reactions, and specifically annulation reactions, in organic chemistry it was decided to investigate the possibility of using carbon based nucleophiles in DIP-like reactions.

6.1 Choice of Carbon Based Nucleophiles

The three main types of carbon nucleophile used for organic synthesis are alkyl metal halides such as Grignard reagents or organolithium reagents, stabilised carbanions and enol type nucleophiles. Of these three types of carbon based nucleophiles, alkyl metal halides are unsuitable for DIP reactions as the nucleophiles are required to perform a nucleophilic addition followed by a nucleophilic substitution, and the first nucleophilic attack on the phenanthridine ring would quench such a reagent, prohibiting it from carrying out further reaction. The reagents most suitable for this reaction, therefore, are either enol based carbon nucleophiles or species in which a carbanion could be stabilised by electron withdrawing groups on either side of the carbon atom. It was therefore necessary to choose

reagents which had two acidic protons on a single carbon atom, which could participate in successive nucleophilic attacks.

The acidity of carbon based protons is proportional to the degree to which a negative charge on the carbon atom can be stabilised by neighbouring groups or the ability of the negative charge to be delocalised through conjugation with an aromatic system. As the amine based DIP reaction is carried out at ambient temperatures and pressures using convenient bases to effect the reaction such as triethylamine and 5% $Na_2CO_{3(aq)}$ it was decided to use carbon based nucleophiles which were compatible with these reaction conditions, and so the first candidates for this new reaction were malononitrile (**45**)and 1,3-indandione (**46**, see Scheme 14).

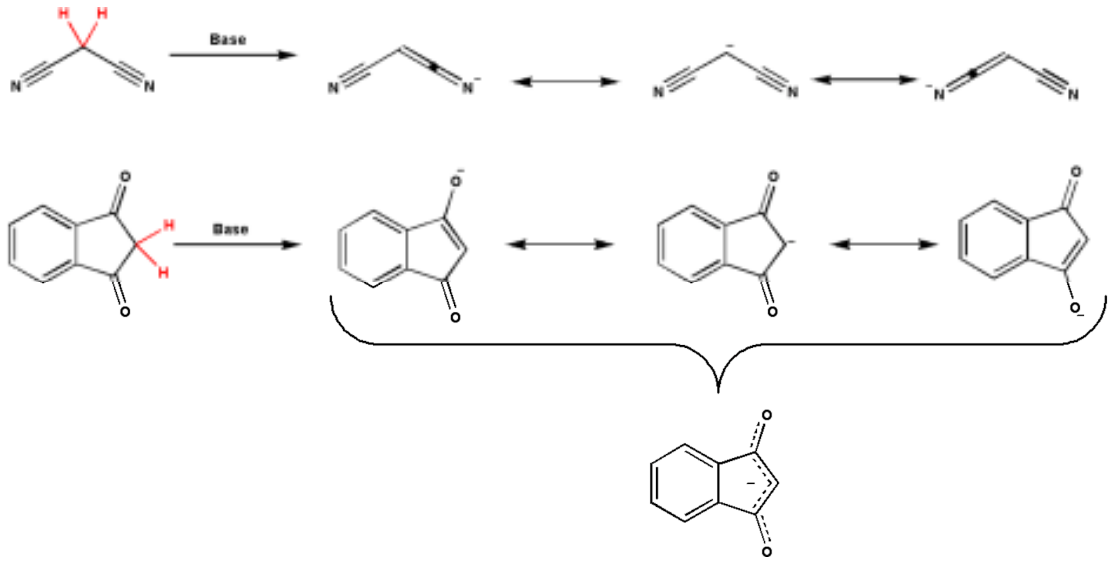

Scheme 14: Deprotonation of (top) malononitrile and (bottom) 1,3-indandione to form carbon based nucleophiles. Acidic protons of the parent structures are shown in red.

Both malononitrile and 1,3-indandione possess two acidic protons and so are suitable to participate in DIP-like reactions. The pKa of malononitrile[148] is 11.2 and has found wide use in organic chemistry as a source of nucleophilic carbon,[149] not least in Knoevenagel[150,151] and related reactions.[152] The deprotonated form of malononitrile is stabilised by inductive effects of the electron withdrawing nitrile moietiesand the ability to

delocalise the negative charge onto the electronegative nitrogen atom. 1,3-Indandione has also been widely studied as a source of nucleophilic carbon in organic chemisty[153,154] and has a much lower pKa of 7.2,[155] as in this case the negative charge of the carbanion is delocalised across two carbonyl moieties in the molecule, indicated by the enolate resonance structure.

Both of these starting materials share the key features necessary for their use in investigating the possibility of performing DIP like reactions with carbon based nucleophiles: they both have two acidic protons which have pKa values in a convenient range for use with common laboratory bases.

6.2 DIP-like Reactions with Carbon Based Nucleophiles: Formation of 2,3-Dihydro-12bH-Pyrrolo[1,2-f]Phenanthridine (DPP) Derivatives

6.2.1 Reaction with Malononitrile

It was found that reaction of one equivalent of malononitrile with one equivalent of DIP starting material BEP in the presence of five equivalents of triethylamine in a methanolic solution leads to precipitation of a colourless microcrystalline product, 2,3-Dihydro-12bH-pyrrolo[1,2-f]phenanthridine-1,1-dicarbonitrile (DPP-dicarbonitrile **47**), within minutes with a yield of 87%.

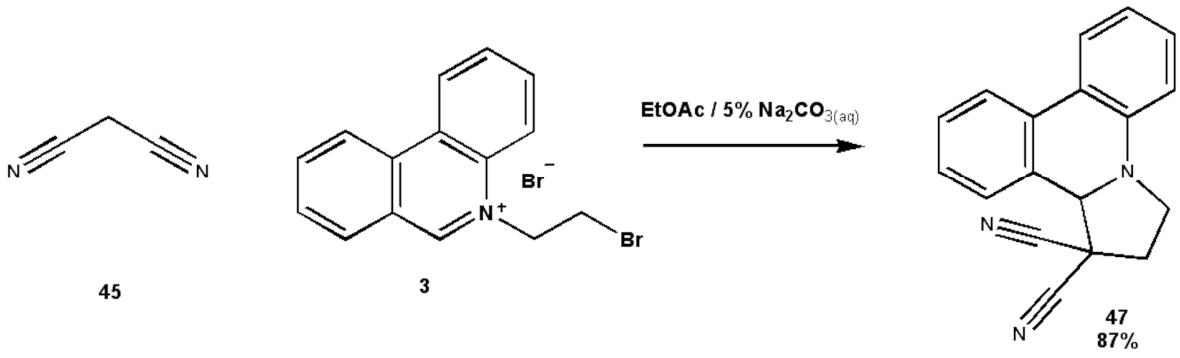

Scheme 15: Reaction of malononitrile with BEP.

Analysis of the ^{1}H NMR of compound **47** proved to be in agreement with the above structure. It is notable that the signal of the phenanthridine *α*-hydrogen, H_a, is shifted significantly up field (compared with the DIP starting material (**3**)) in the **47** product, appearing at a chemical shift of *δ* 5.14 ppm, corresponding to the loss of aromaticity of the central ring of the phenanthridine ring system and the loss of the cationic charge on the neighbouring nitrogen atom leading to a significantly less deshielded environment of this proton. Another consequence of addition onto the *α* position of the phenanthridinium ring is the introduction of a chiral centre to **47** with this *α* position as the stereogenic centre. This chirality significantly affects the signals of the other protons in the five membered ring, desymmetrising their environment, giving four individual proton signals integrating to 1 H at chemical shifts of *δ* 2.82, 3.06, 3.51 and 3.85 ppm and splitting each proton signal into a *ddd* pattern with geminal coupling constants of around 10 Hz for protons H_b and H_c and 13 Hz for protons H_d and H_e (see Figure 56 inset).

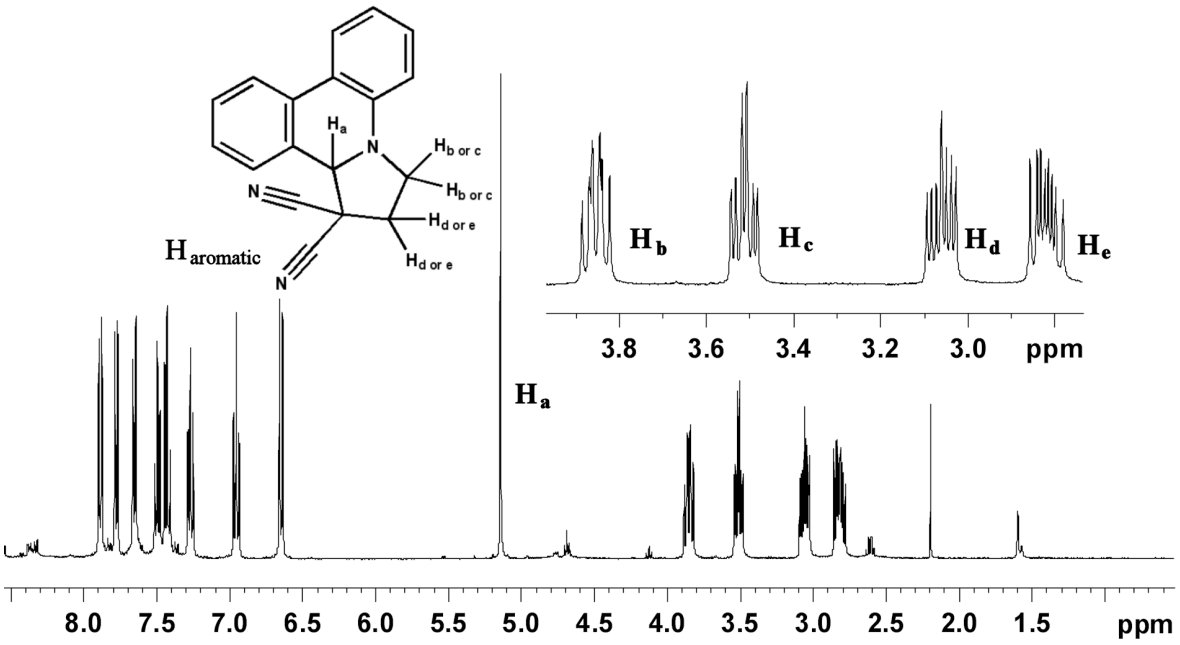

Figure 56: 1H NMR spectrum of 47.

The magnitude of a vicinal NMR proton-proton coupling can be related to the dihedral torsion angle between the coupled protons *via* the Karplus equation[156] (which is of the

form $J_{HH'} = A + B\cos\varphi + C\cos 2\varphi$, where φ is the torsion angle between the coupling protons and A, B and C are experimentally defined constants) which gives maximum coupling constants at torsion angles close to 0º or 180º. With reference to this we can assign protons H_d and H_e with reference to their coupling constants to protons H_b and H_c. Proton H_b couples to H_d, $J_{Hb\text{-}Hd} \approx 8.8$ Hz and to H_e, $J_{Hb\text{-}He} \approx 6.6$ Hz. As the torsion angle between protons H_b and H_d will be much closer to 0º than the torsion angle of H_b and H_e is to 180º this indicates that H_d lies on the same side of the ring system as H_b. This assignation is confirmed by the coupling constants of H_c which has a larger coupling constant ($J_{Hc\text{-}He} \approx 10.0$ Hz) to H_e than it does to proton H_d ($J_{Hc\text{-}Hd} \approx 4.2$ Hz). It is not possible from this spectrum to assign the H_b signal as either the *syn* or *anti* proton with respect to the H_a proton.

47 is sparingly soluble in methanol and slow evaporation of a dilute methanolic solution of **47** yields colourless block crystals suitable for single crystal X-Ray analysis which confirms the structure as that elucidated from NMR data (see Figure 57). **47** crystallises in a monoclinic crystal system with a $P2_1/c$ space group. Although **47** has a chiral centre at the α-carbon of the phenanthride system, the molecule crystallises as a racemate, with the moiety shown in Figure 57 being the *R* configuration. The bond lengths of the central ring of the phenanthridine ring system confirm the loss of aromaticity, with C-C bond lengths of 1.478(3) and 1.508(2) Å for C-C bonds not involved in the peripheral ring systems and C-N bond lengths of 1.391(2) and 1.448(2) Å. The crystal structure of **47** does not show significant π stacking of the molecules.

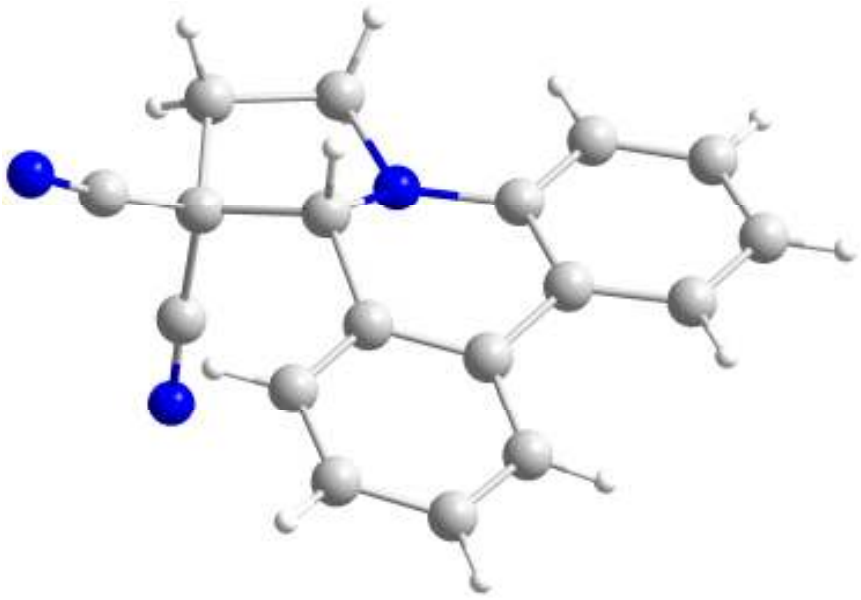

Figure 57: X-Ray crystal structure of 47

By analogy with the reaction mechanism for the standard DIP reaction, the following mechanism can be proposed for the synthesis of **47**. Similar to the DIP reaction, initial addition takes place at the phenanthridinium α- carbon followed by an intramolecular 5-exo-tet cyclisation to form the five membered ring of the product. In contrast to the DIP reaction this product does not then oxidise in the presence of BEP to form the rearomatised cationic species analogous to the DIP structure. Attempts to oxidise **47** using secondary oxidising agents were not successful. The resistance of this species to oxidation relative to the DIP intermediate can be explained by reference to the delocalisation of the positive charge in the DIP structure over two nitrogen atoms, whereas in the structure of **47**, such delocalisation would not be possible and the stabilisation of the system gained by rearomatisation would not be sufficient to offset the energy increase of the introduction of the positive charge. This reaction represents the discovery of a new C-C bond forming annulation reaction related to the Knoevenagel reaction. The reaction products, DPP derivatives have previously only been synthetically available by 1,3-dipolar cycloaddition reactions on suitably functionalised phenanthridine starting materials.[157-159]

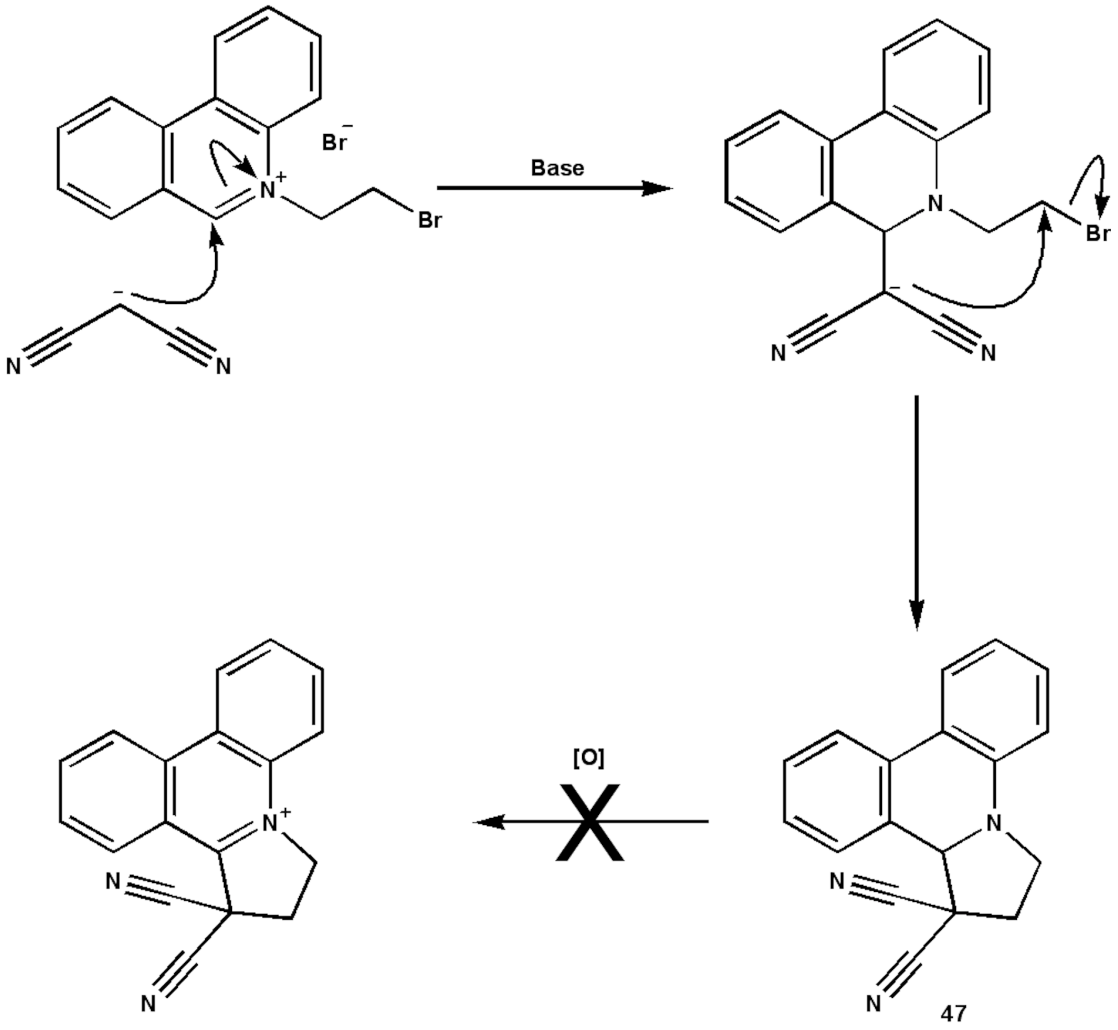

Scheme 16: Possible reaction mechanism for the reaction of malononitrile with BEP

While **47** is stable in the solid state and in methanolic solution, the compound appears to decompose relatively rapidly in other solvents in which it is readily soluble, with the colourless solution rapidly acquiring a yellow colouring. This decomposition can be illustrated by following the ^{1}H NMR spectrum of **47** in $CDCl_3$ over time (see Figure 58). Analysis of these spectra indicates the formation of an as yet unidentified decomposition product.

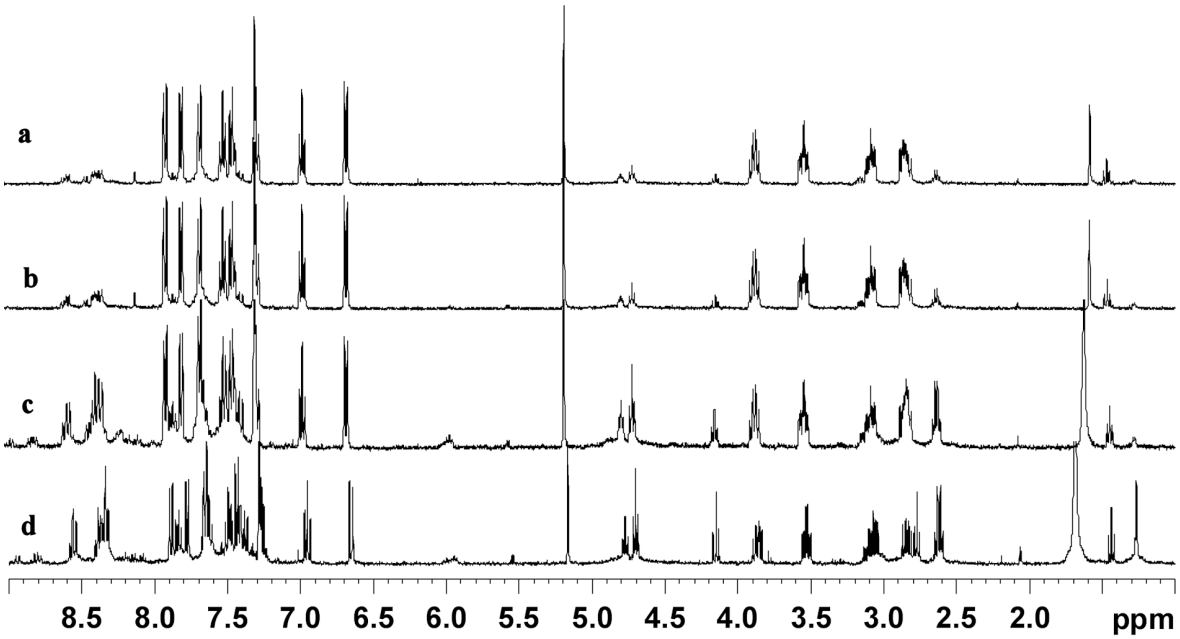

Figure 58: ^{1}H NMR spectrum of 47 (a) 5 minutes, (b) 30 minutes (c) 4 hours and (d) 24 hours after dissolution in $CDCl_3$. Note the appearance and increase in intensity of decomposition product peaks at δ ~4.7 and ~8.5 ppm.

6.2.2 Reaction with 1,3-Indandione

Different reaction conditions were required for the synthesis of the 1,3-indandione DPP product than those employed for the synthesis of **47** due to the solubility properties of the target molecule (i.e. In this case the desired product does not easily precipitate from a methanolic solution of starting materials). Taking as inspiration the biphasic method of DIP synthesis where the TIP intermediate is isolated in an organic phase prior to oxidation by NBS, a biphasic route to the synthesis of the DPP derivative of 1,3-indandione (see Scheme 17) was used. An equimolar mixture of 1,3-indandione and BEP was reacted at room temperature for three hours under a nitrogen atmosphere in a biphasic mixture of EtOAc and 5% aqueous sodium carbonate solution. After this the organic layer was separated, washed with water and brine and the solvent removed under vacuum. Recrystallisation from hot methanol gave the desired 2,3-Dihydro-12H-Pyrrolo[1,2-f]Phenanthridine-1-indandione (DPP-indandione, **48**) as an orange microcrystalline powder in an 73% yield.

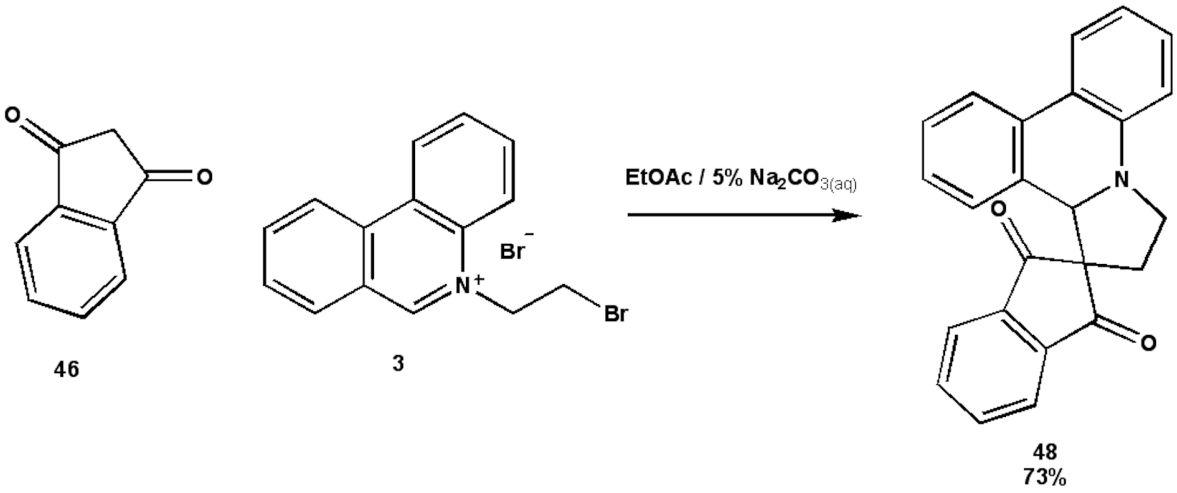

Scheme 17: Reaction of 1,3-indandione with BEP.

The structure of **48** can be seen to be a hexacyclic system with the bicyclic indandione system linked to the DPP framework by a single carbon atom creating a *spiro* structure. The ^{1}H NMR of **48** (see Figure 59) again shows the upfield shift of the α phenanthridine proton when compared to the BEP starting material, appearing at δ 5.36 ppm. In contrast with the spectrum of compound **47** the methylene protons on the DPP five membered ring appear to be in a much more symmetrical environment where the signals from the H_b and H_c cannot de distinguished from each other and appear as a triplet at δ 3.74 ppm, and similarly for the H_d and H_e signals which also appear as a triplet at a chemical shift of δ 2.22 ppm. The ^{1}H NMR of **48** remains unchanged over the course of several weeks, indicating that the structure of the 1,3-indandione moiety confers much more stability on the resulting DPP structure.

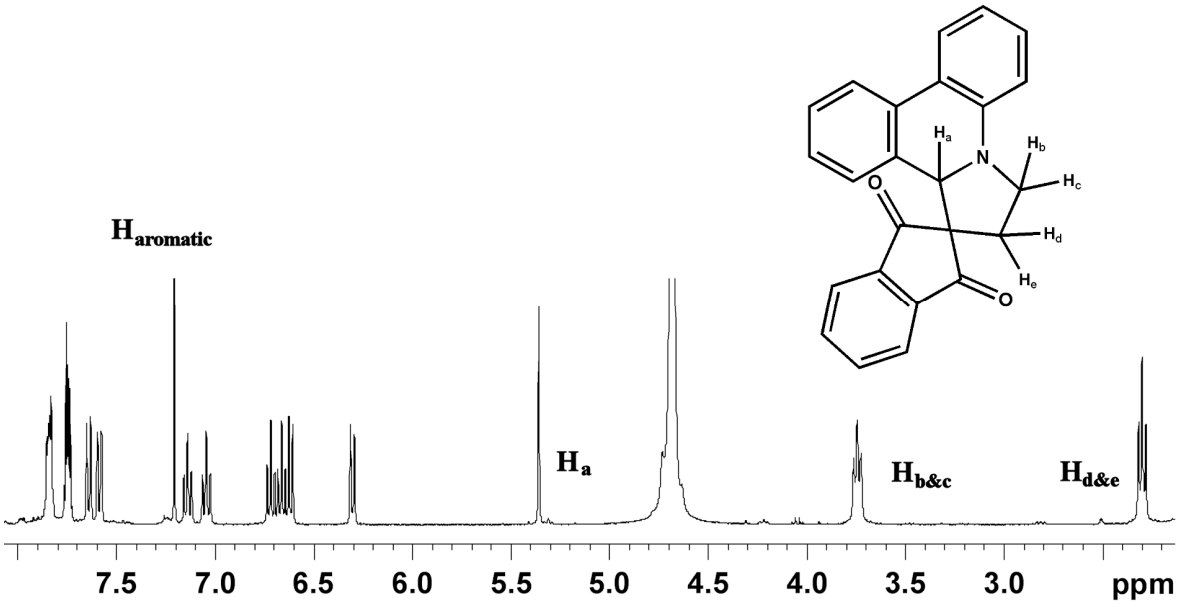

Figure 59: 1H NMR spectrum of 48.

Despite the apparent symmetry of the CH_2 protons observed in the ^1H NMR spectrum the structure of **48** still represents a chiral structure, which was confirmed by a single crystal X-Ray structure of **48** obtained from single crystals grown by slow evaporation of a methanolic solution of **48** (see Figure 60). **48** crystallises in a triclinic crystal system with a *P*-1 space group. As in the case of **47**, **48** crystallises as a racemate with both enantiomers present in the crystal structure (the moiety shown in Figure 60 is the *R* conformation). Once again the bond lengths of the central phenanthride ring confirm the loss of aromaticity in the system.

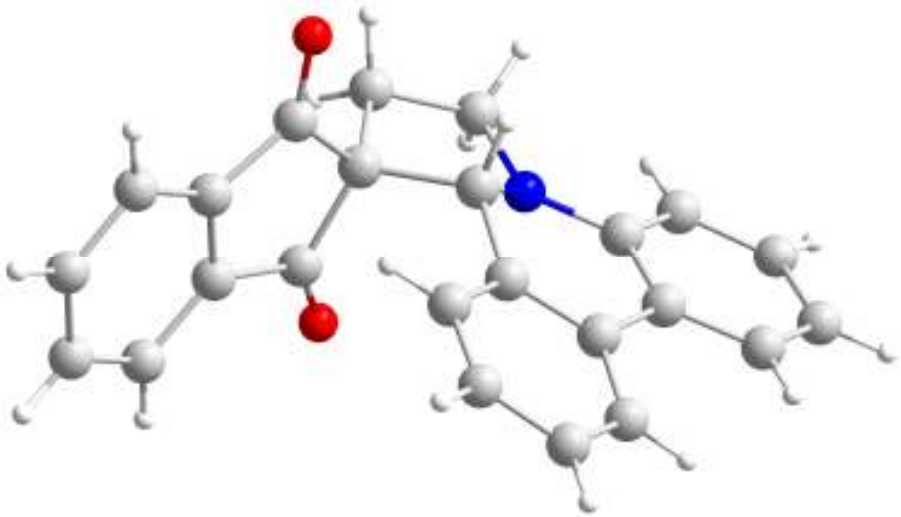

Figure 60: X-Ray crystal structure of 48.

6.3 pH Dependant Behaviour of Synthesised DPP Derivatives.

During attempts to stabilise the structure of the DPP-dicarbonitrile derivative **47** by protonation of the phenanthride nitrogen and hence preventing the lone pair on the nitrogen atom from becoming involved in the rearomatisation of the phenanthridine moiety it was noticed that the reverse was occurring. Rather than protonating the nitrogen, the addition of acid (in this case HCl) promoted the rearomatisation of the phenanthridine system and addition of a proton to the carbon of the malononitrile moiety producing a stable, ring-opened form of the DPP derivative, 5-(3,3-dicyano-propyl)-phenanthridinium chloride **49**. **49** can be synthesised in quantitative yield from a methanolic suspension of **47** by addition of $HCl_{(aq)}$ until all the starting material has dissolved, followed by precipitation of the ring opened product by addition of diethyl ether and isolation of the desired product by filtration. A similar procedure was followed to synthesise the ring opened form of **48** to form a similar open chain 1,3-indandione substituted 5-Propyl Phenanthridinium (PP) product, **50** (see Scheme 18).

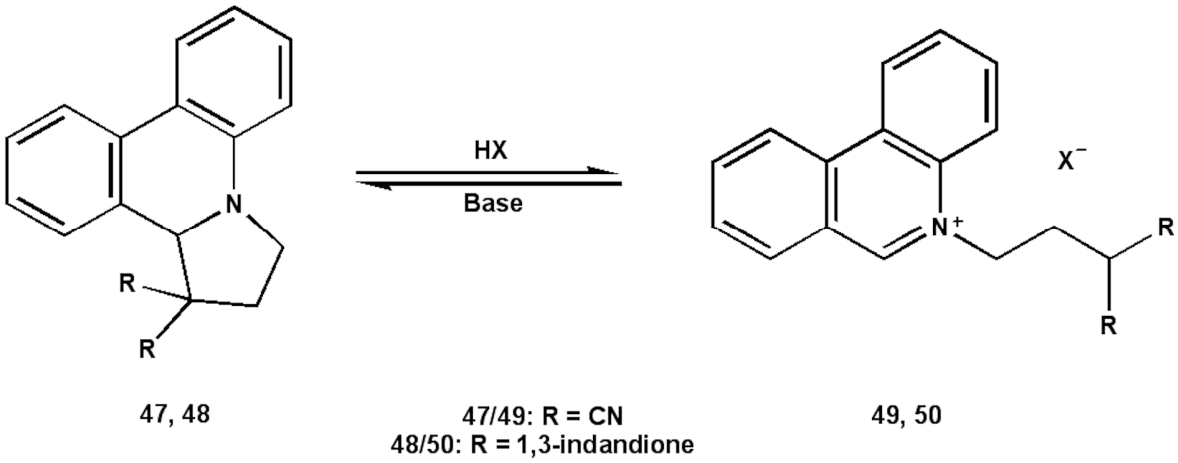

Scheme 18: pH dependant ring-opening/closing of the DPP structures.

During the synthesis of the DPP derivatives discussed above two new C-C bonds are formed and, while rearomatisation of the phenanthridine system and protonation of the electron poor carbon atom provides a driving force for the subsequent breaking of one of these bonds, the second C-C bond does not break, preventing the decomposition of the DPP product. On addition of base this carbon can once again be deprotonated and perform an unusual, intramolecular 5-*endo-trig* cyclisation to reform the original DPP structure. This leads to a reversible, pH dependant, ring-opening/closing step. The reversibility of this reaction has been shown by ^{1}H NMR on **47** (see Figure 61). The ring opened form of the structure is easily distinguishable in the proton NMR by the significant downfield shifting of the aromatic peaks, and in particular that of the α-proton singlet which can be found at δ 10.30 ppm compared to δ 5.24 ppm for the ring closed form. Such a pH dependant ring-opening/closing reaction has also been observed in the case of the Trihydro-Imidazo-Phenanthridine (TIP) intermediate of the standard DIP reaction.[160]

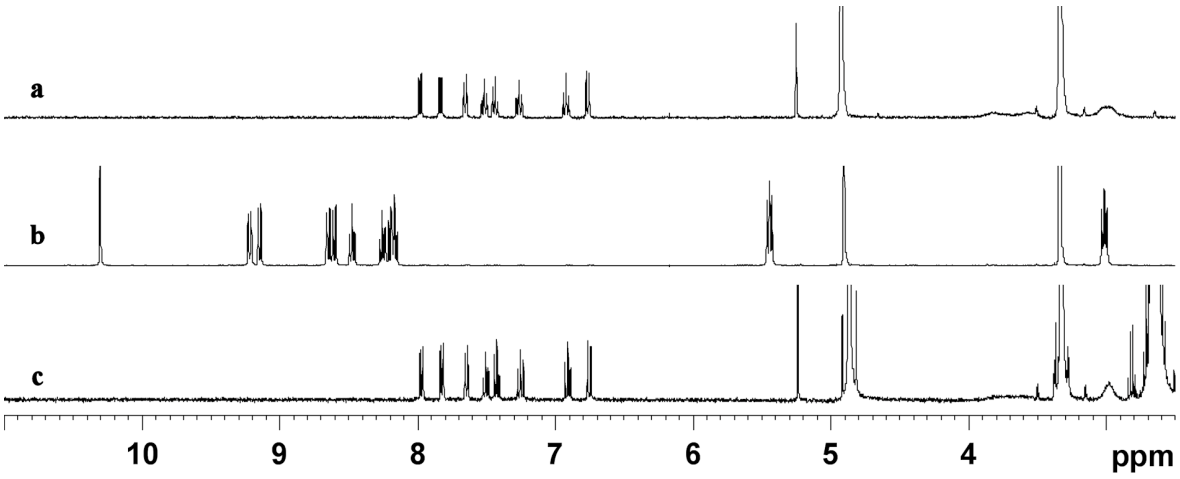

Figure 61: ^{1}H NMR in MeOD of (a) 47, (b) after addition of 1 drop conc. DCl and (c) recyclised product after addition of 2 drops TEA.

The two distinct states of this system can be distinguished not just by ^{1}H NMR of the material, but the significant changes in the chromophore structure of the DPP on conversion to the PP form (i.e. the rearomatisation of the phenanthridine moiety) leads to a difference in the UV spectra and flouresence behaviour of these materials as well. In both of the tested cases the PP form of the molecule leads to a shifting of the maximum absorbance in the UV region to a shorter wavelength, from 343 nm for **47** to 327nm for **49** and from 356 nm for **48** to 326 nm for **50** (see Figure 62).

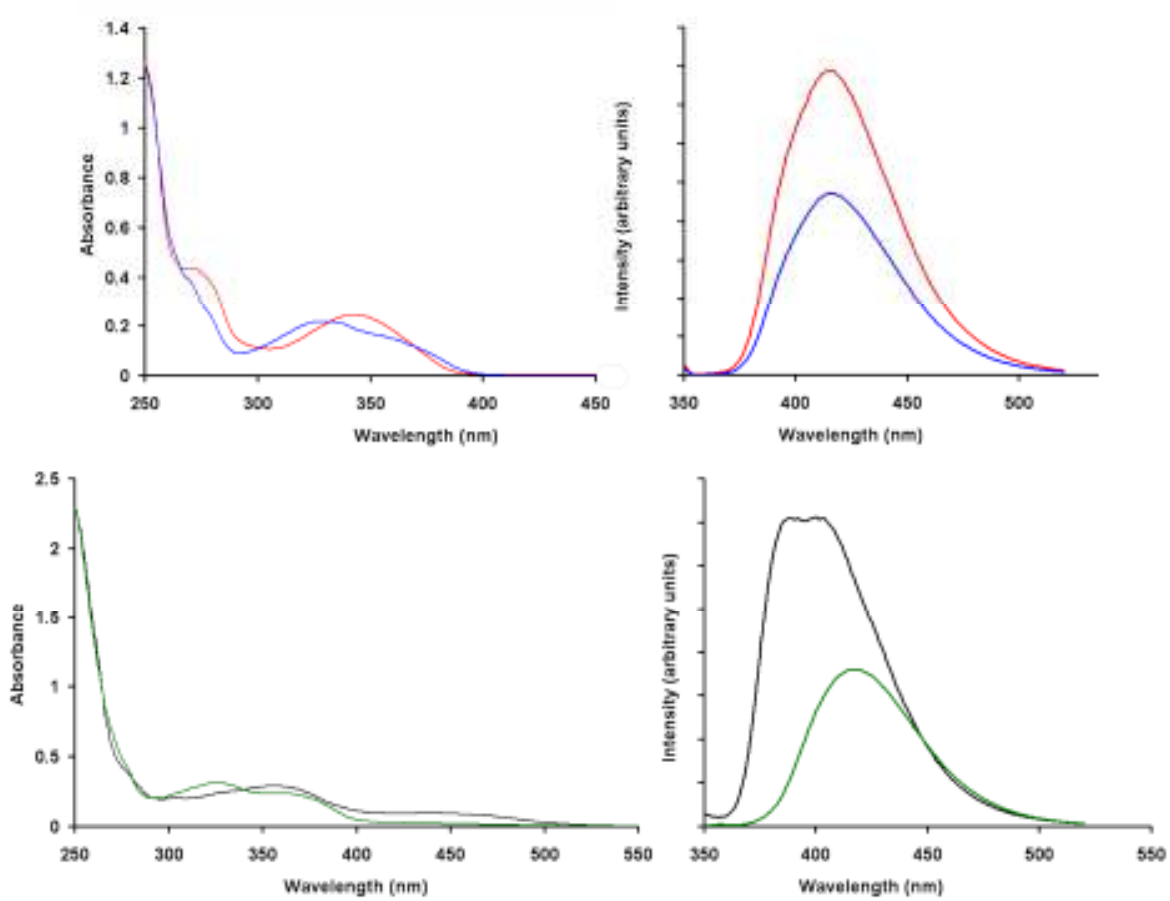

Figure 62: Absorption (left) and emission (right) spectra of 47 (top, red trace), 49 (top, blue trace), 48 (bottom, black trace) and 48 (bottom, green trace).

These changes are most noticeable in the colour of the **48**/**50** system where the ring closed **48** form exists as a bright orange powder, while the ring opened **50** form is bright yellow in colour. The **47**/**49** system also exhibits significant differences in optical properties with UV irradiation of a solution of **47** in methanol producing a large fluorescence emission, which does not appear once the system has been switched to the ring-opened **49** form (see Figure 63). DPP-type compounds therefore represent a promising lead to produce a family of pH switchable systems in which the properties of different switching systems can be tuned by the choice of substituents on the five membered ring of the DPP structure.

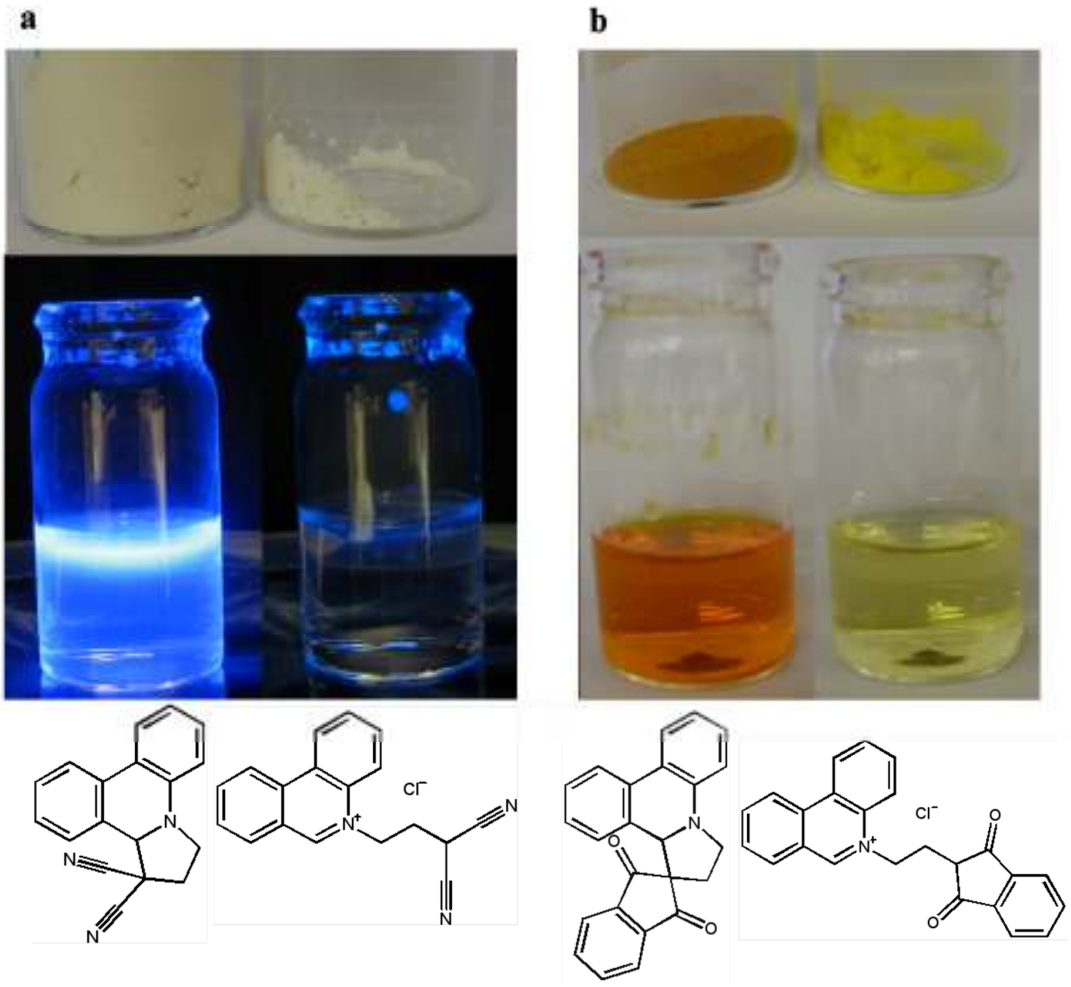

Figure 63: Differing optical appearance of ring-opened and ring-closed forms of the DPP structures. (a) Fluoresence of a solution of 47 under UV irradiation at 365 nm compared with that of 49. (b) Different colours of samples of 48 and 50.

Conclusions and Future Work

7 CONCLUSIONS

The design and synthesis of ligands incorporating Dihydro-Imidazo-Phenanthridinium (DIP) and Imidazo-Phenanthridine (IP) moieties has been described. The complexation behaviour of these ligands with a variety of metal salts has been investigated leading to the synthesis of a number of new coordination compounds, the supramolecular interactions of which in the crystal phase have been described. A new C-C bond forming annulation reaction has been discovered based on the DIP synthetic methodology leading to the synthesis of pH switchable organic materials.

7.1 Complexes of DIP Pyridyl Ligands

Two new ligands were synthesised which incorporated both a metal binding region based on a pyridyl moiety and a DIP region which, as a large polyaromatic heterocycle, has the potential to act as a π stacking motif in supramolecular architectures. These ligands were complexed with several Cu^{II} salts (see Figure 64) in both the presence and absence of other coordinating anions to produce six new compounds, four mononuclear complexes, **24**, **25**, **26** and **27**, and two dinuclear complexes, **28** and **29**, which were characterised by X-Ray crystallography. A great variety of coordination geometries were observed in the six compounds ranging from four coordinate tetrahedral (**26**) and square planar (**24**) geometries to five coordinate trigonal bipyrimidal (**29**, **27**) and square based pyramidal (**25**, **28**) geometries. It is clear from all the crystal structures that the size and coordinating ability of the anions present in the reaction mixture plays a significant role in controlling the geometry of the metal assembly. The use of non-coordinating anions in the metal salts used for complexations often leads to incorporation of the bromide anion from the ligand structure into the coordination sphere of the Cu^{II} ion. The geometry of the ligand itself also proves to be important in the geometry of the resulting complex, as can be seen by the difference between two systems where isomeric ligands were used. In the case where there was a less sterically crowded coordination site available to the metal ion, coordination of

two ligands was observed, while this was prevented in the case where the bulk of the ligand was positioned much closer to the metal centre.

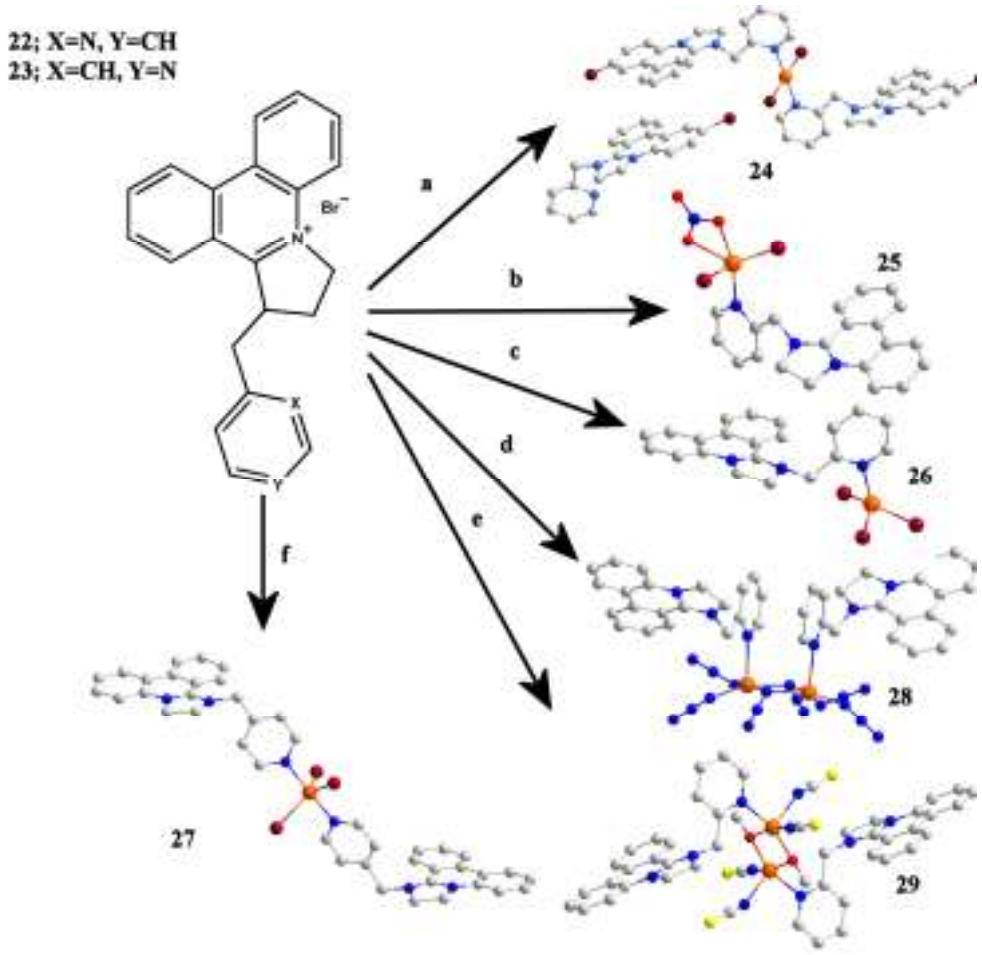

Figure 64: Complexation of ligands 22 and 23 with various Cu^{II} salts: (a) 22, $Cu(BF_4)_2 \cdot 6H_2O$. (b) 22, $Cu(NO_3)_2 \cdot 3H_2O$. (c) 22, $CuBr_2$. (d) 22, $Cu(NO_3)_2 \cdot 3H_2O$, NaN_3, (e) 22, $Cu(NO_3)_2 \cdot 3H_2O$, NaSCN. (f) 23, $CuBr_2$.

The intermolecular forces which determine the packing of the synthesised complexes in the crystalline state are largely dependant on the ability of the DIP region of the ligands to interact with other structural features *via* the phenanthridinium π-system. It has been observed that the DIP regions of the ligands experience π-π stacking interactions with other DIP moieties in every crystal structure obtained, leading to the formation of one and 2D arrays of molecules, with further S···S interactions linking molecules in the third dimension

in one instance (**29**) (see Figure 65). The role played by the pyridyl region of the ligand structures exerts a more subtle influence on the overall structure, with no direct interaction between the π-systems of pyridyl and DIP moieties observed in any of the structures. π stacking is observed only between adjacent pyridyl moieties, whether inter- or intramolecularly, however the pyridyl region of the ligands experience a variety of other interactions, such as S···π interactions with thiocyanate groups or CH···π interactions with DIP aromatic systems.

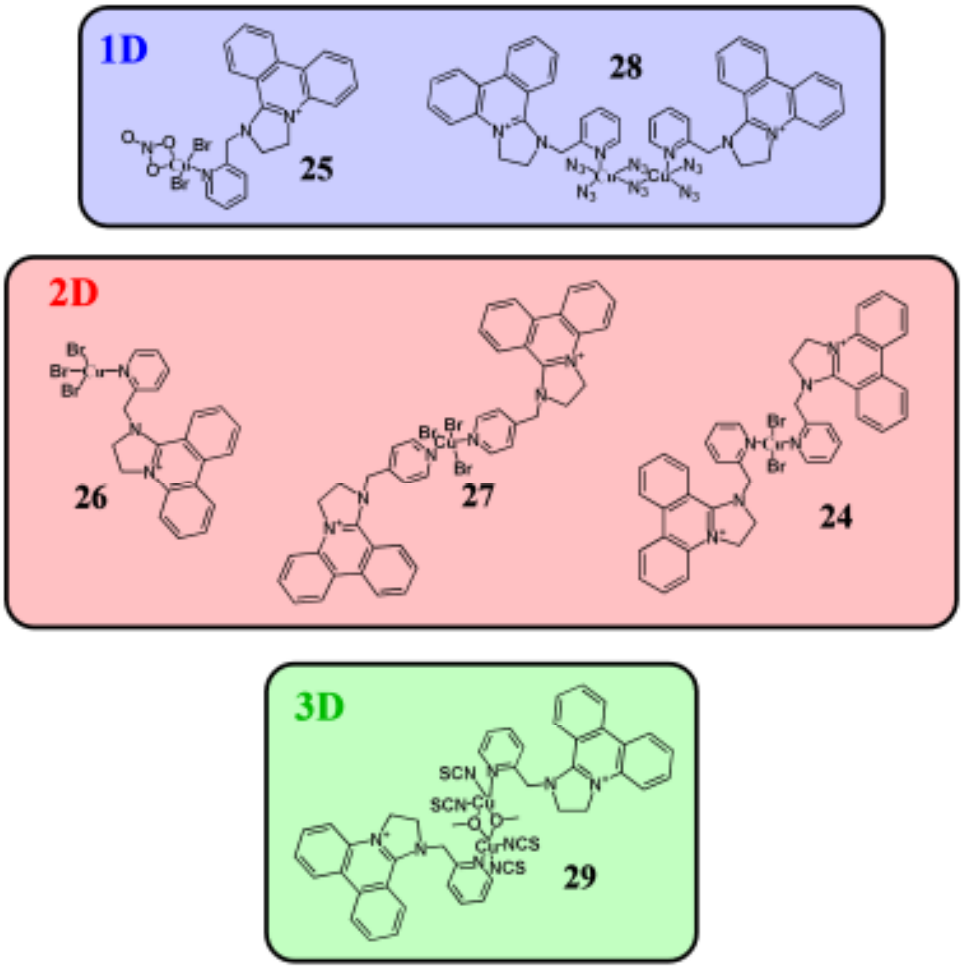

Figure 65: Schematic representations of the reported compounds 24-29, grouped by their intermolecular interactions in the crystalline phase.

The DIP regions of the ligands themselves are large enough to take part in a number of π stacking interactions with the DIP regions of other complexes, however these interactions can be observed to follow a distinct pattern, with a few exceptions, where the interacting DIP rings align themselves in an antiparallel arrangement with the majority of the π stacking interactions taking place between the peripheral benzoid rings of the phenanthridinium system. This arrangement is favoured by the maximising of the distance between the cationic charges on the interacting DIP systems and also by the polarisation of the ring system by the cationic nitrogen which leads to the peripheral ring systems being the most electron deficient. This motif infers a second directionality on the π stacking of these moieties perpendicular to the direction of the π stacking interaction and hence makes DIP based systems a good candidate for the engineering of π stacking interactions in the crystalline phase.

This area of chemistry has several avenues of development open to it, first among them being the use of these synthesised ligands in complexation reactions with other metal ions such as Co or Ni which have fewer easily accessible coordination geometries to introduce a further degree of control to the synthesis of supramolecular architectures based on π stacking interactions.

7.2 Complexation of a Triazine Based DIP Ligand

A new ligand was designed and synthesised based on a 1,3,5-triazine core utilising the synthetic versatility of such a moiety to produce trisubstituted molecules for use in supramolecular chemistry. A bis dipyridyl, monochloro substituted triazine unit was reacted with an ethylene diamine substituted DIP compound to produce a new ligand incorporating both the DIP unit and two bidentate chelating coordination regions, **35**. This new ligand was reacted with both $Pd(OAc)_2$ and $Cu(ClO_4)_2 \cdot 6H_2O$ producing two new coordination complexes.

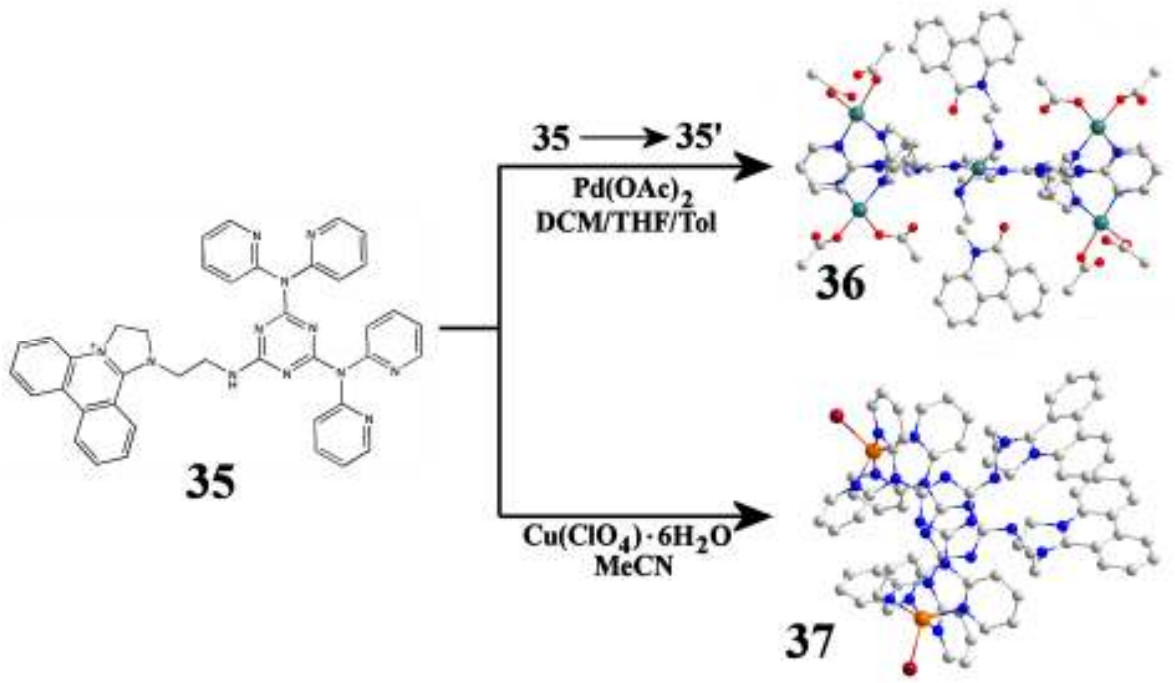

Figure 66: Synthesis of complexes 36 and 37 from ligand 35.

Upon slow reaction over the course of several weeks in a layered solution with $Pd(OAc)_2$, the synthesised ligand **35** is observed to undergo a transformation reaction where the DIP region of the ligand molecules undergo what appears to be a hydrolytic ring opening reaction resulting in the formation of a new phenanthridinone based ligand, **35'**. The mechanism of the ligand transformation in this complexation reaction remains to be fully explored *via* experimental and theoretical investigations; however a proposed mechanism highlights the possible role of complexation as a mediator for the hydrolytic attack of ambient water molecules. The transformed ligand **35'** contains an ethylene diamine linking unit which chelates a bridging Pd atom linking two $\{Pd_2(\mathbf{35'})_2\}$ units to form a discrete cationic pentapalladium complex, **36**, observed crystallographically and by cryospray mass spectrometry.

Supramolecular π interactions link **36** into one dimensional chains in the crystal structure through π stacking interactions of the phenanthridinone moiety. These supramolecular chains are in turn stabilised by C-H···π interactions involving the electron deficient triazine π system. These interactions are also observed to participate in an

unprecedented C-H···π···*l.p.* motif involving the lone pair of a molecule of dichloromethane present in the crystal structure as solvent of crystallisation.

Reaction of **35** with $Cu(ClO_4)_2 \cdot 6H_2O$ produces a dinuclear complex, **37** in which the **35** ligand does not undergo a transformation similar to that observed in the case of **36**. This complex consists of two **35** ligands bridged by two Cu^{II} ions which are coordinated by the dipyridyl chelating units of each of the ligands. These dinuclear complexes are linked into two dimensional sheets in the crystalline phase *via* π stacking interactions of the DIP moieties, which interact with each other in a manner consistent with the π stacking motifs observed in other DIP complexes.

This work represents the development of ligands incorporating both DIP subunits and coordinating regions to produce more complex ligands capable of interacting with each other in a supramolecular fashion. There is scope for the development of this chemistry both in terms of ligand design and the complexation of the synthesised ligand in different systems. The use of a triazine motif as a basis for the development of multifunctional ligands in supramolecular chemistry is well known and the versatility of this chemistry will lend itself well to the synthesis of a wide variety of DIP (and analogous structures) based ligands incorporating, for example, multiple DIP regions in order to further investigate the role of this moiety as a structural unit in crystal engineering. The synthesised ligand represents the beginning of this work; however there remains a vast array of potential systems to investigate using this ligand.

7.3 Complexation of an Imidazo-Phenanthridine Based Ligand

A major disadvantage of DIP based systems in inorganic chemistry is that the cationic nature of the DIP moiety limits its complexation behaviour and necessitates the construction of much more complicated ligands which can coordinate to metal ions through coordinating motifs remote from the polyaromatic ring system. The use of imidazo-phenanthridine based ligands which can be synthesised readily *via* a related synthetic methodology which overcomes this drawback by producing a neutral molecule

with a lewis basic nitrogen atom capable of coordinating directly to metal ions. To this end a new ligand **40** was synthesised as an asymmetric 2,2'-bipyridyl like ligand with a much larger aromatic platform for π stacking interactions. This new ligand was complexed with four metal salts, $CuBr_2$, $PdCl_2$, $Ag(NO_3)$ and $Co(BF_4)_2{\cdot}6H_2O$ giving four new metal complexes, **41**, **42**, **43** and **44** respectively which were characterised by X-Ray crystallography. **40** binds to the metal ion in each of these cases *via* the 2,2'-bipyridyl like chelating region of the ligand structure and forms structures where one (**41**, **42**) or two (**43**, **44**) ligands coordinate to each metal atom. The coordination geometry of the complexes resulting from **40** is largely dependant on the preferred coordination geometry of the metal ion involved, with trigonal bipyrimidal coordination observed for the five coordinate Cu^{II} and Co^{II} species **41** and **44**, square planar coordination to Pd^{II}, **42**, and a *pseudo*-tetrahedral geometry observed on coordination of two ligand molecules to Ag^{I} in **43**.

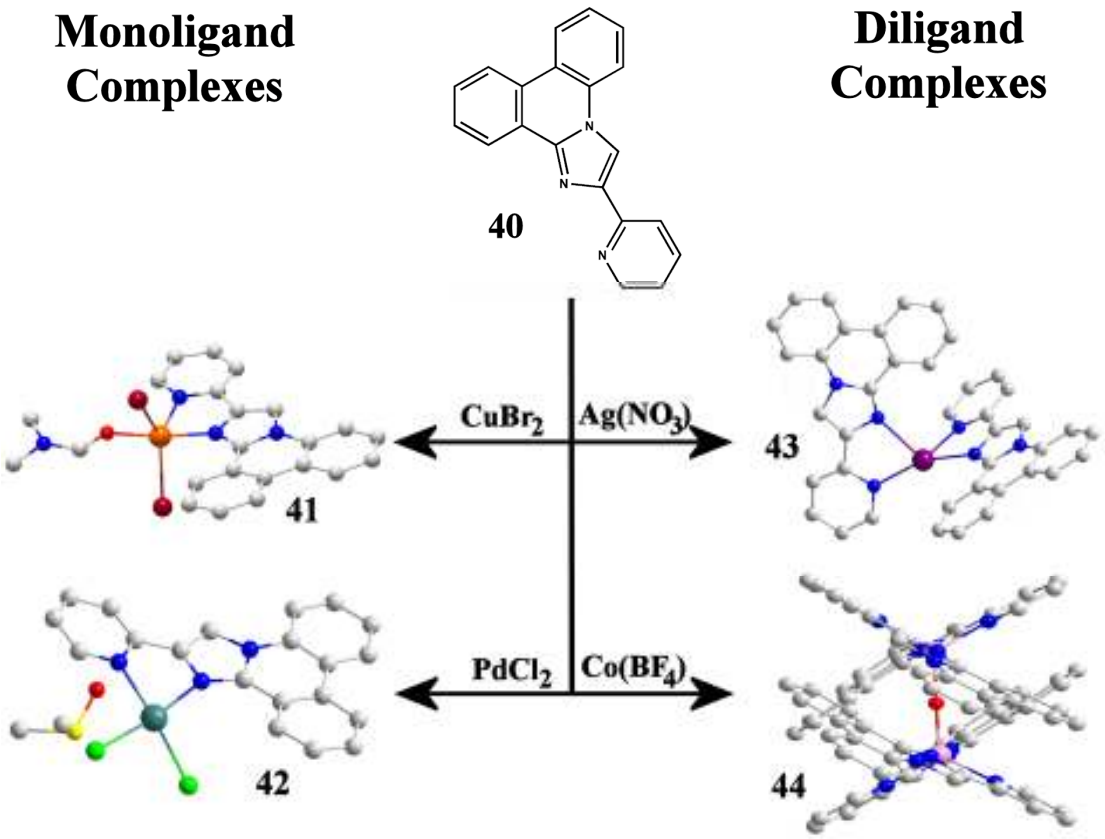

Figure 67: Complexation of 40 with various metal salts allows the formation of complexes 41-44

The steric bulk of the IP region of the ligand, along with its ability to form intramolecular π stacking interactions leads to very unusual coordination observed in the structure of Co^{II} complex **44** which is the first known example of a dinuclear cobalt complex in which two five coordinate cobalt centres are linked by an almost perfectly linear μ_2-hydroxo ligand. The coordination of two bidentate ligands to the trigonal bipyramidal Co^{II} centres leads to an axial chirality in the resulting dinuclear, tetraligand complex which possesses two stereogenic centres. Of the four possible diastereomers of this structure, the steric bulk of the IP ligand molecules allows the formation of only the enantiomeric $\Delta\Delta$ and $\Lambda\Lambda$ forms of the structure, which crystallises as a racemate.

In all the reported complexes of **44** , the ligand molecules experience a wide variety of π stacking interactions linking the complexes into long range structures in the crystalline phase; in one case linking the complexes into a three dimensional network (**43**). The π interactions of the IP ligand are shown to be versatile; displaying a combination of well defined interacting modes in every crystal structure studied. This feature of the IP ligand used here promises to be useful in the synthesis of new materials based on both coordination chemistry and π stacking interactions to a greater degree than traditional 2,2'-bipyridyl based systems.

7.4 DIP-Type Reactions with Carbon Based Nucleophiles

Developed from the DIP synthesis reaction a new C-C bond forming annulation reaction has been discovered which leads to the synthesis of chiral 2,3-Dihydro-12bH-Pyrrolo[1,2-f]Phenanthridine (DPP) based derivatives by attack of a nucleophilic carbon atom on the α position of the phenanthridinium moiety, followed by a 5-*exo*-*tet* cyclisation on the bromoethyl side chain of the starting material. Such fused ring phenanthridine based compounds have previously only been synthesised by 1,3 dipolar addition reactions.[157-159] This reaction has been carried out on two starting materials, malononitrile and 1,3-indandione, which were chosen for their suitability to the reaction conditions, and the

cyclised DPP products, **47** and **48**, were characterised fully and X-Ray crystal structures of the products were obtained.

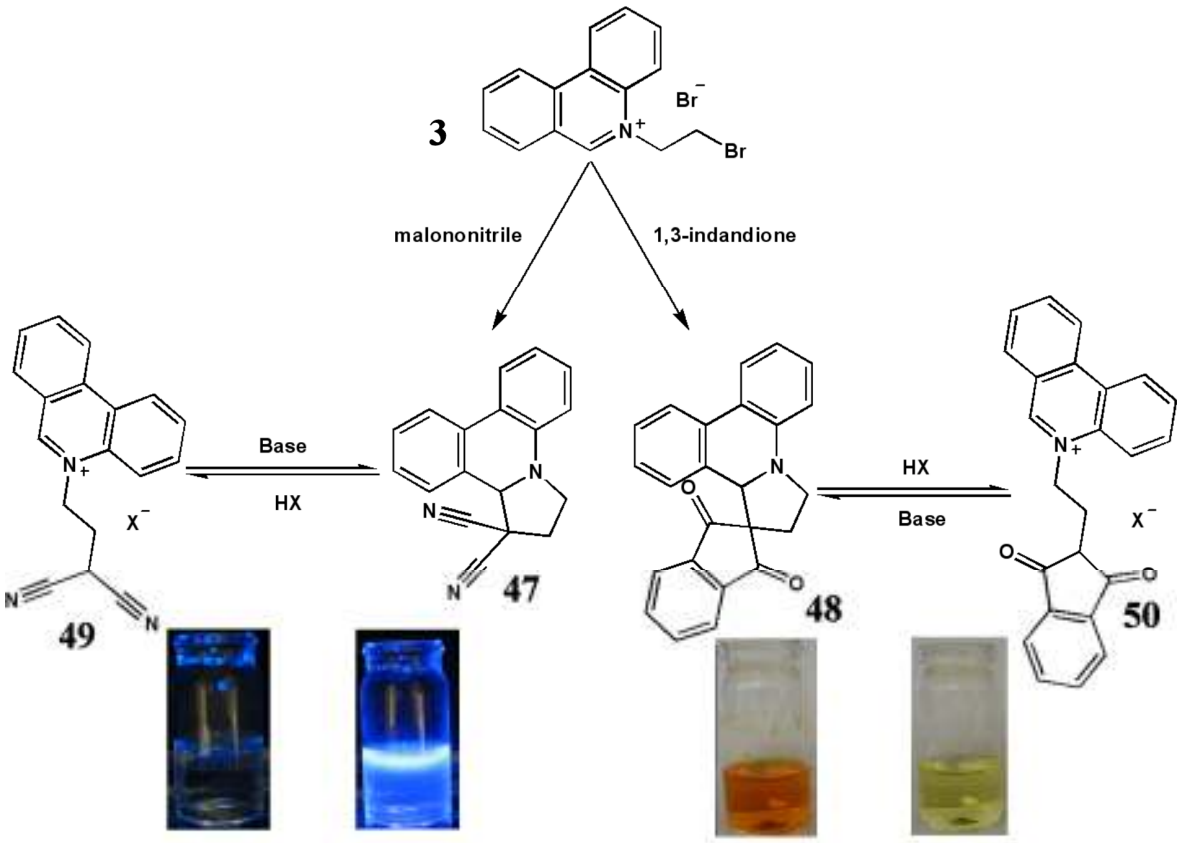

Figure 68: Synthesis and pH sensitive switching behaviour of DPP derivatives, 47 and 48.

The pH dependant behaviour of the DPP products was investigated (see Figure 68)and a reversible ring-opening/closing reaction was discovered, where addition of acid to the DPP material induced protonation of the electron deficient carbon atom and rearomatisation of the phenanthridinium system to produce an open chain 5-Propyl Phenanthridinium (PP) derivative (**49**, **50)**. These PP products were isolated and characterised. The difference in UV and emission spectra of the DPP and PP derivatives has been recorded, indicating that DPP type molecules could be developed into a new type of pH switchable organic material with tunable optical properties.

Experimental

8 EXPERIMENTAL

8.1 Materials

Solvents for synthesis (AR grade) were supplied by *Fisher Chemicals* and *Riedel-de-Haen.* Nitrogen gas was supplied by *B.O.C. Ltd.* and was of commercial grade. Deuterated solvents were supplied by *Aldrich Chemical Company Ltd., Avocado Research Supply* and *GOSS Scientific Instruments Ltd.* All other reagents were supplied by *Aldrich Chemical Company Ltd., Fisher Chemicals* or *Lancaster Chemicals Ltd.* Column Chromatographies were performed on Silica Gel 60 obtained from *Merck*. All commercial starting material were used as supplied, without further purification. Reactions requiring dry conditions were carried out in AR grade previously dried using traditional procedures.[161]

8.2 Instrumentation

Where air sensitive materials were prepared, work was carried out under standard Schlenk line techniques under nitrogen (dried over calcium chloride and oxygen free). The following instrumentation was used to obtain the analytical and spectroscopic data reported herein:

Melting Point:	Electrothermal IA 9000 digital melting point apparatus. The given temperatures are uncorrected.
pH measurements:	Hanna Instruments HI 9025C microcomputer pH meter with a BCH combination pH electrode (309-1065) and HI 7669/2W temperature probe.
Microanalysis:	EA-1110 CHNS, CE-440 Elemental Analyser.
Mass spectrometry:	Bruker microTOFQ Spectrometer used for ESI-MS, and with Cryospray attachment for CSI-MS.
FT-IR spectroscopy:	Shimadzu FTIR-8300 and Jasco FTIR-410 spectrometers, manipulation with Shimadzu HyperIR and JASCO software.
UV-Vis spectroscopy:	Shimadzu UV-3101PC UV-VIS-NIR Scanning Spectrophotometer. Manipulation using Shimadzu software.
NMR spectroscopy:	Bruker DPX-400 and Avance-400 (400 MHz ^{1}H, 100 MHz ^{13}C, 2D experiments). Manipulation with XwinNMR and Mestre-C2.3a.
Single-crystal X-ray:	Nonius Kappa-CCD (Mo-K_α) and Bruker Apex II (Mo-K_α) diffractometers.

All NMR spectra were recorded at room temperature unless otherwise stated. Chemical shifts are reported using the δ-scale, referenced to the residual solvent protons in the deuterated solvent for ^{1}H- and ^{13}C-NMR. The coupling constants (*J*) are reported in Hz as absolute values. Characterisation of spin multiplicities: s = singlet, d = doublet, t = triplet, q = quartet, quint = quintet, m = multiplet, b = broad, *p* = pseudo.

FT-IR spectra of solid materials were measured in KBr pellets unless otherwise stated while all liquid/oil samples were measured as thin film on a diamond anvil. Notation used in the interpretation of FT-IR spectra are as follows: sh = shoulder, w = weak, m = medium, s = strong, vs = very strong. Some peaks identified as OH stretches may have some contribution from residual water in the KBr used in the KBr disc.

8.3 Methods for Crystal Growth

Crystal growth of metal complexes was achieved using two methods; slow evaporation and solvent diffusion. In the first instance, the nascent solution was concentrated nearly to the point of precipitation and placed in a small sample vial fitted with a perforated lid. In the second method, solvent diffusion, the nascent solution was placed into a small vial which is then placed in a larger sealed vial containing the diffusing solvent. A successful diffusion solvent must be sufficiently volatile to diffuse into the small vial as well as being miscible with the nascent solution while causing precipitation of the complex (see Figure 69). The small vial may, in some cases, be fitted with a perforated lid or cotton wool plug to reduce the rate of diffusion and allow slower crystal growth. In both cases, the crystallisations were allowed to stand undisturbed in a crystallisation room with vibration free surfaces which is maintained at a constant temperature of 18 °C.

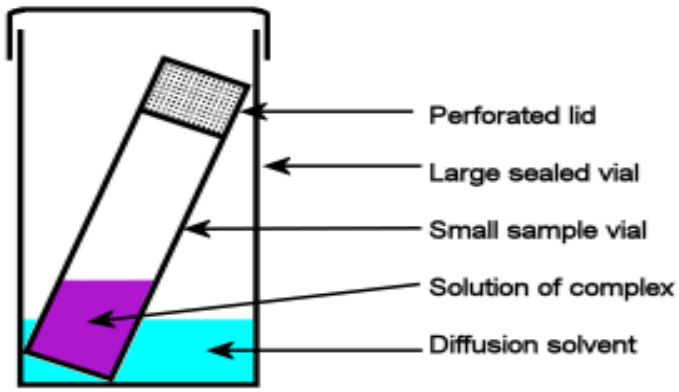

Figure 69: Schematic representation of a solvent diffusion type crystallisation.

8.4 Synthesis and Analytical Data

8.4.1 5-(2-Bromo-ethyl)-phenanthridinium bromide (3)

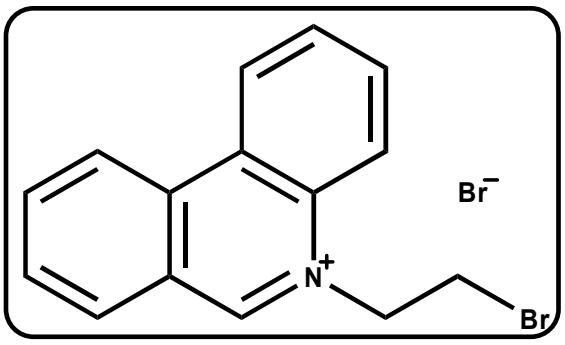

Phenanthridine **1** (5g, 27.9 mmol.) was dissolved in 1,2-dibromoethane (104.96g, 50ml, 558.7mmol.). The solution was stirred at 90°C for three days. During that time a white precipitate was formed and filtered off every periodically. After each filtration the filtrate was rinsed with an additional 5ml 1,2-dibromoethane and the mother liquor was put back stirring at 90°C until the next filtration. The reaction was stopped after three days when no more precipitate formed. The filtrates were combined and washed thoroughly with ethyl acetate to give the title compound as a pale yellow powder (9.56g, 26.0 mmol)

Yield: 93.3%; M.p. 233.2 – 234.7 °C; ^{1}H NMR (D_2O:400MHz) δ 4.00 (t, 2H, *J* 5.6Hz); 5.322 (t, 2H, *J* 5.6Hz); 7.853 (m, 2H, Ar-H), 7.926 (t, 1H, *J* 7.2Hz), 8.123 (t, 1H, *J* 7.2Hz), 8.209 (d, 1H, *J* 8.52Hz), 8.313 (d, 1H, *J* 8.12 Hz), 8.580 (d, 1H, *J* 8.38 Hz), 8.662 (d, 1H, *J* 7.29Hz), 9.767 (s, 1H). ^{13}C NMR (D_2O:100 MHz) δ 28.99 (C-1), 58.47 (C-2), 118.5 (Ar-CH), 122.56(Ar-CH), 122.90(Ar-C_q), 124.69(Ar-CH), 126.14 (Ar-C_q), 130.29, 130.42, 132.16 (Ar-CH), 132.35(Ar-C_q), 132.77(Ar-CH), 135.15(Ar-C_q), 138.59(Ar-CH), 154.87(C-3); IR (KBr, cm^{-1}) 2946 (w), 1626 (s), 765 (s); M.S. (FAB+ mode):286.1 (M-Br) (100), 206.1 (10), 154.1 (37), 137.1 (23);Anal Calcd. For $C_{15}H_{13}Br_2N$: C, 49.08; H, 3.57; N, 3.82. Found: C, 49.06; H, 3.56; N, 3.73.

8.4.2 2,3-Dihydro-1-(2-pyridyl-methyl)-imidazo[1,2-f]phenathridinium bromide. (22)

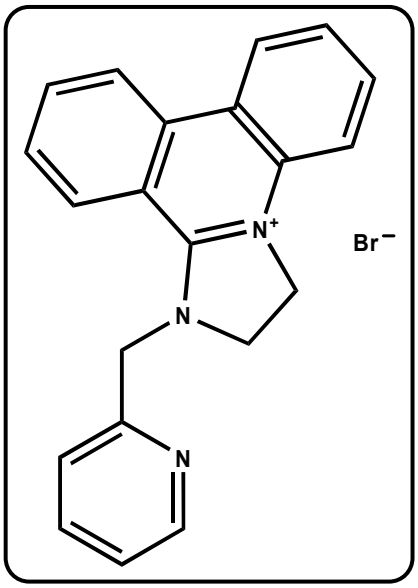

2-(aminomethyl)-pyridine (237 mg, 2.20 mmol) was dissolved in ethyl acetate (40 mL), to which was added a 5% aqueous Na_2CO_3 solution (40 mL). The biphasic mixture was cooled to 0˚C and 2-bromoethyl phenanthridinium bromide, **3** (700 mg, 1.91 mmol) was added. The above reaction mixture was allowed to warm to room temperature and kept stirring for 2h. The organic layer was separated, washed with water and transferred to a separate round bottomed flask covered with aluminium foil, to which was added *N*-bromosuccinimide (373 mg, 2.10 mmol). The reaction was then stirred for another 1 hour, during which time a white precipitate formed. The precipitate was isolated by filtration and recrystallised from MeOH to give **22** (681 mg, 1.74 mmol) as a white powder. The ligand (30 mg) was dissolved in MeOH (30 mL), to which a methanolic solution of $NaBPh_4$ (10 mL) was added. Small amount of precipitates were filtered and slow evaporation of the filtrate resulted in the formation of white crystals of **22**·BPh_4.

Yield: 91%; ^{1}H NMR (d_6-DMSO, 400 MHz): δ 4.44 (t, 2H, *J*=10.4 Hz), 4.85 (t, 2H, *J*=10.6 Hz), 5.57 (s, 2H), 7.45 (t, 1H, *J*=6.0 Hz), 7.63 (t, 1H, *J*=7.6 Hz), 7.71 (m, 2H), 7.78 (d, 1H, *J*=8.0 Hz), 7.86 (t, 1H, *J*=7.8 Hz), 7.98 (t, 1H, *J*=7.7 Hz), 8.07 (t, 1H, *J*=7.7 Hz), 8.38 (d, 1H, *J*=8.4 Hz), 8.60 (d, 1H, *J*=4.3 Hz), 8.72 (d, 1H, *J*=8.3 Hz), 8.86 (d, 1H, *J*=8.3 Hz); ^{13}C NMR (DMSO, 100 MHz): δ 46.2 (CH_2), 52.13 (CH_2), 54.2 (CH_2), 115.3 (Cq),

116.0 (CH), 119.9 (Cq), 122.4 (CH), 123.5 (CH), 123.9 (CH), 124.1 (CH), 125.4 (CH), 127.5 (CH), 129.1 (CH), 131.4 (CH), 132.6 (Cq), 134.7 (Cq), 135.3 (CH), 138.2 (CH), 149.1 (CH), 153.6 (Cq), 154.0 (Cq). MS(ESI): 312.3 (M^+). Calcd for ($C_{21}H_{18}BrN_3$): C 64.30, H 4.62, N 10.71; Found C 64.26, H 4.44, N 10.21.

8.4.3 1-Pyridin-4-ylmethyl-2,3-dihydro-1H-imidazo[1,2-f]phenanthridin-4-ylium bromide. (23)

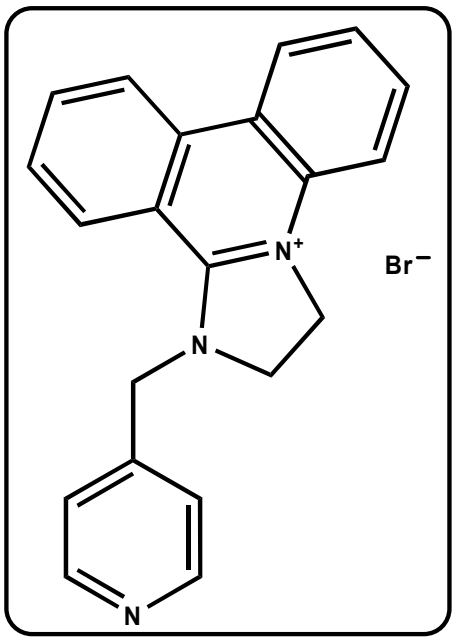

4-(aminomethyl)-pyridine (237mg, 2.20mmol) was dissolved in ethyl acetate (40ml) to which was added a 5% aqueous Na_2CO_3 solution (40ml). The biphasic mixture was cooled to 0˚C and **3** (700mg, 1.91mmol) added. the reaction mixture was allowed to warm to room temperature and stirred for 2h. The layers were separated and the organic layer washed with water and transferred to a separate round bottomed flask covered in aluminium foil. To this was added NBS (373mg, 2.10mmol). the reaction was then stirred for a further hour during which time a white precipitate formed. The precipitate was isolated by filtration and recrystallised from MeOH to give **23** (644 mg, 1.64 mmol) as a white powder.

Yield: 86%; ^{1}H NMR (d_6-DMSO, 400 MHz): δ 4.40 (t, 2H, *J*=10.8 Hz), 4.85 (t, 2H, *J*=9.6 Hz), 5.50 (s, 2H), 7.63 (d, 2H, *J*=6 Hz), 7.70 (m, 3H), 7.90 (t, 1H, *J*=7.2 Hz), 8.10 (t, 2H, *J*=8 Hz), 8.47 (d, 1H, *J*=8 Hz), 8.64 (d, 1H, *J*=6 Hz), 8.79 (t, 1H, *J*=8 Hz); ^{13}C NMR (DMSO, 100 MHz): δ 46.3 (CH_2), 52.0 (CH_2), 52.5 (CH_2), 115.3 (Cq), 116.0 (CH), 120.0 (Cq), 121.5 (CH), 124.0 (CH), 124.2 (CH), 125.4 (CH), 127.2 (CH), 129.2 (CH), 131.5 (CH), 132.7 (Cq), 134.9 (Cq), 135.3 (CH), 144.1 (Cq), 150.0 (CH), 154.1 (Cq). MS (ESI): 312.2 (M^+). Calcd for ($C_{21}H_{18}BrN_3$): C 64.30, H 4.62, N 10.71; Found C 64.54, H 4.40, N 10.47.

8.4.4 $[Cu(22\text{-}Br_{0.05})_2Br_2](22\text{-}Br_{0.45})_2(BF_4)_4$. (24)

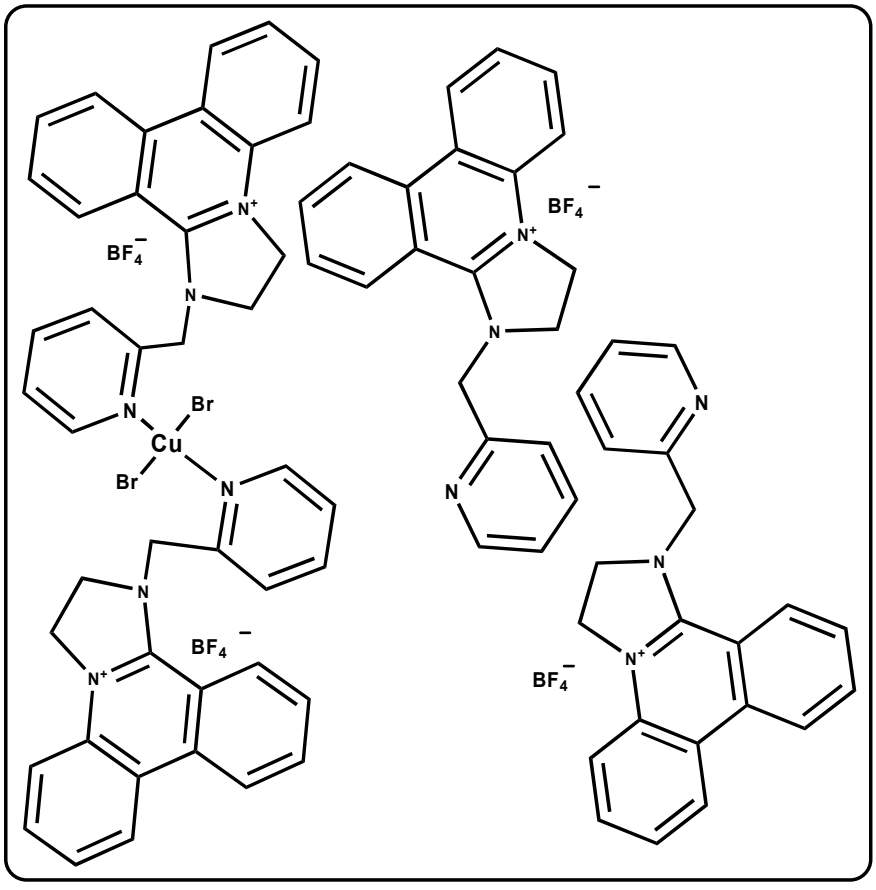

2,3-dihydro-1-(2-pyridyl-methyl)-imidazo[1,2-f]phenathridinium bromide **22** (100 mg, 0.25 mmol) was dissolved in 5 mL of MeOH which was added dropwise to a solution of $Cu(BF_4)_2{\cdot}6H_2O$ (175 mg, 0.50 mmol) in 5 mL of MeOH. A colour change of the solution

was observed from originally transparent blue to dark green. A few drops of dilute Et_3N (triethylamine) in 10 mL of MeOH was added. The solution was filtered and dark green crystals of **24** (35 mg, 0.018 mmol) were formed after slow evaporation.

Yield: 30%; IR (KBr, cm^{-1}): 1578.4 (s), 1555.3 (s), 1434.8 (s), 1359.6 (m), 1307.5 (s), 1056.8 (vs), 749.2 (m), 716.4 (w), 670.1 (w), 521.6 (w);Calcd for ($CuC_{84}H_{71}B_4Br_3F_{16}N_{12}$): C 53.13, H 3.77, N 8.85; Found C 52.87, H 3.33, N 8.97.

8.4.5 Cu(22)$Br_2(NO_3)$. (25)

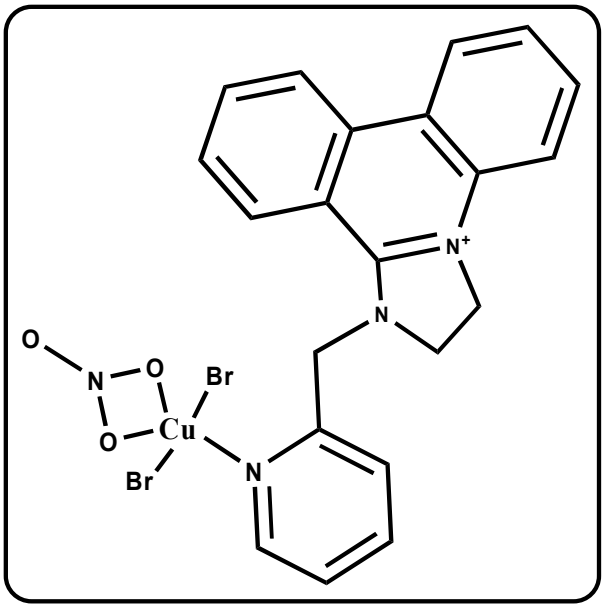

A solution of 2,3-dihydro-1-(2-pyridyl-methyl)-imidazo[1,2-f]phenathridinium bromide **22** (100 mg, 0.25 mmol) in 5 mL of MeOH was added to $Cu(NO_3)_2 \cdot 3H_2O$ (123 mg, 0.50 mmol) in 10 mL of MeOH. A colour change was observed from an opaque, straw yellow colour to a transparent bright green solution. The solution was filtered and the filtrate was allowed to evaporate slowly, yielding well formed green crystals of **25** (55 mg, 0.092 mmol), suitable for X-ray single crystal diffraction measurement.

Yield: 37%; IR (KBr, cm^{-1}): 1608.3 (s), 1577.5 (s), 1428.0 (s), 1282.4 (s), 1014.4 (w), 760.8 (s), 717.4 (m), 670.1 (w); Calcd for ($CuC_{21}H_{18}Br_2N_4O_3$; 597.7 g/mol): C 42.20, H 3.04, N 9.37; Found C 41.72, H 2.94, N 9.04.

8.4.6 Cu(22)Br_3. (26)

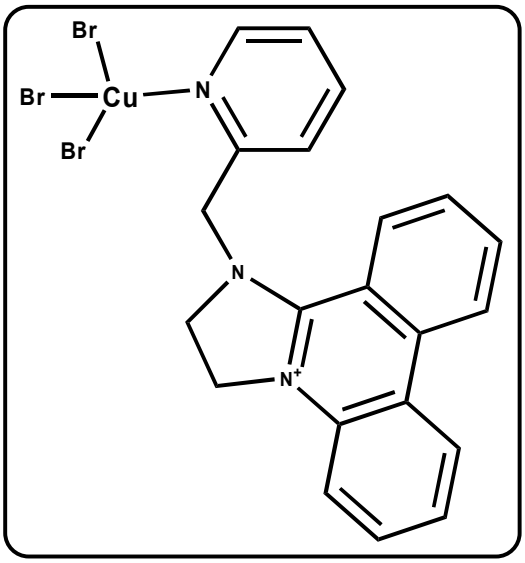

2,3-dihydro-1-(2-pyridyl-methyl)-imidazo[1,2-f]phenathridinium bromide **22** (100 mg, 0.25 mmol) in 5 mL of MeOH was added dropwise to a solution of $CuBr_2$ (113.8 mg, 0.50 mmol) in 10 mL of MeOH. A colour change was observed from transparent blue to dark brown solution, from which a dark brown precipitate was formed. The solution was filtered and the filtrate was allowed to evaporate slowly yielding more of the dark crystalline powder, which was isolated by filtration and combined with the previous sample. The precipitate was dried under vacuum and recrystallisation of the product from a MeOH/MeCN (2:1) solution led to the formation of brown crystals of **26** (54 mg, 0.088 mmol).

Yield: 35%; IR (KBr, cm^{-1}): 3433.6 (m), 1609.1 (s), 1573.1 (s), 1551.0 (s), 1309.2 (w), 780.5 (w), 761.5 (m), 743.6 (m), 720.3 (w), 668.2 (m); Calcd for ($CuC_{21}H_{18}N_3Br_3$): C 40.97, H 2.95, N 6.83; Found C 40.75, H 2.78, N 6.64.

8.4.7 $Cu_2(22)_2(N_3)_6$. (28)

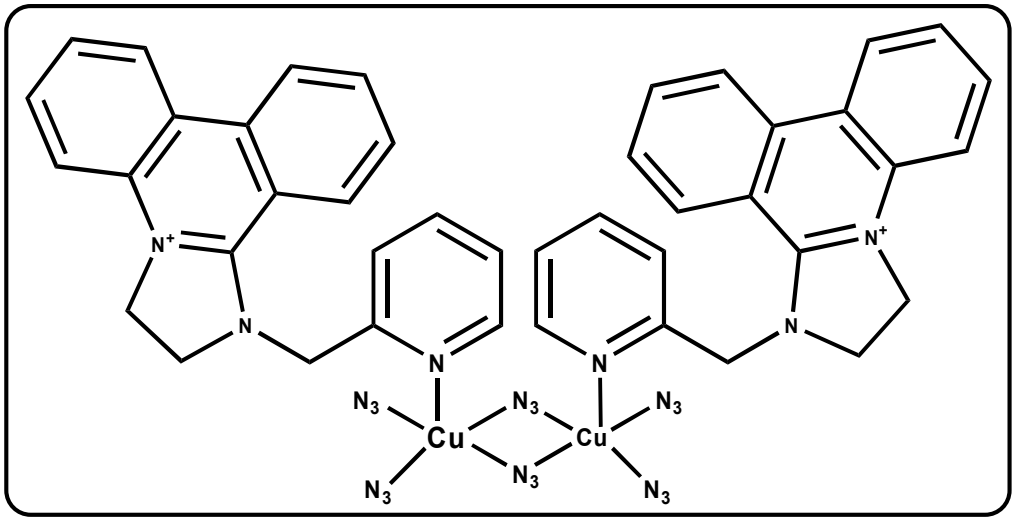

2,3-dihydro-1-(2-pyridyl-methyl)-imidazo[1,2-f]phenathridinium bromide **22** (100 mg, 0.25 mmol) in 5 mL of MeOH was added to $Cu(NO_3)_2 \bullet 3H_2O$ (123 mg, 0.50 mmol) in 5 mL of MeOH, to which NaN_3 (132. 5mg, 2.00 mmol) was added dropwise. The colour of the solution changed from green to brown and brown precipitates were formed after stirring for 30 mins. The solution was heated to 50^{o}C and 15 mL of DMF was added to aid solvation. The solution was cooled down to room temperature and filtered. Slow evaporation of the filtrate led to the formation of brown crystals of **28** (33 mg, 0.033 mmol).

Yield: 26%; IR (KBr, cm^{-1}): 3427.4 (w), 2125.2 (s), 2101 (s), 1625.3 (s), 1436.0 (w), 1625.6 (s), 1296.2 (w), 1273.7 (w), 694.9 (m); Calcd for ($Cu_2C_{42}H_{36}N_{24}$): C 50.24, H 3.61, N 33.48; Found C 49.95, H 3.27, N 33. 70.

8.4.8 $Cu_2(22)_2(NCS)_4(OCH_3)_2$. (29)

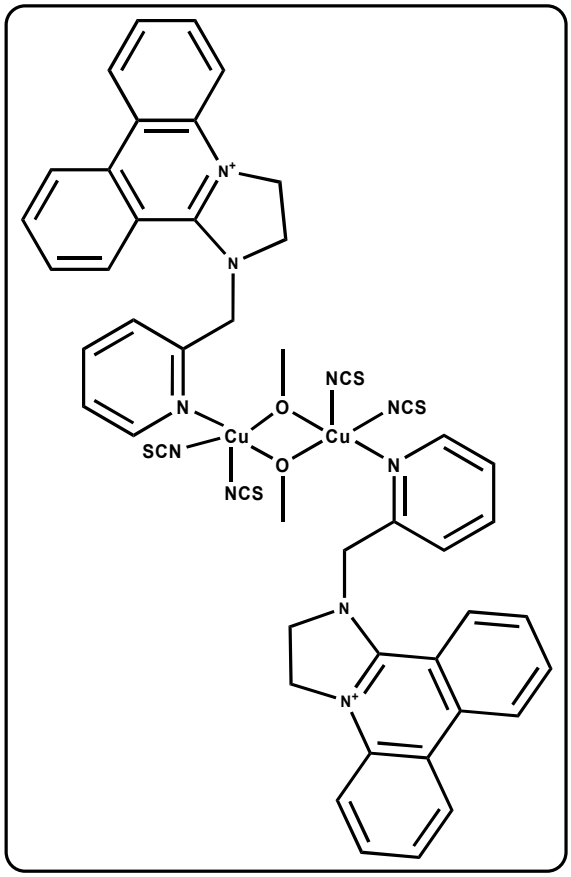

2,3-Dihydro-1-(2-pyridyl-methyl)-imidazo[1,2-f]phenathridinium bromide **22** (50 mg, 0.13 mmol) in 5 mL of MeOH was added to $Cu(NO_3)_2 \cdot 3H_2O$ (61 mg, 0.25 mmol) in 5 mL of MeOH, to which NaSCN (82.7 mg, 1.02 mmol) was added. The colour of the solution was changed from green to brown and some brown precipitates were formed. Several drops of Et_3N were added till the solution colour became blue green and the solution was filtered. Slow evaporation of the solution resulted in the formation of green crystals of **29** (17 mg, 0.016 mmol), suitable for X-ray diffraction measurement.

Yield: 25%; IR (KBr, cm^{-1}): 3429.5 (m), 2077.2 (vs), 1598.7 (m), 1576.7 (s), 1554.6 (m), 1433.6 (w), 1305.6 9m), 749.7 (m), 713.3 (w), 662.7 (w); Calcd for ($Cu_2C_{48}H_{42}N_{10}O_2S_4$): C 55.10, H 4.00, N 13.39; Found C 55.03, H 3.51, N 13.20.

8.4.9 $Cu(Br)_3(23)_2]Br$. (27)

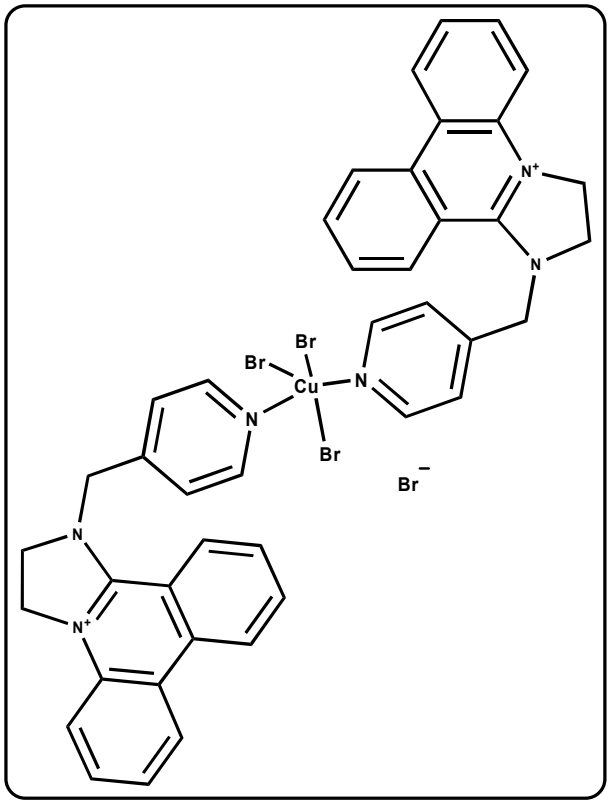

2,3-Dihydro-1-(4-pyridyl-methyl)-imidazo[1,2-f]phenathridinium bromide **23** (200 mg, 0.51mmol) was dissolved in MeOH. This solution was added dropwise to a solution of $CuBr_2$ (110 mg, 0.51mmol) in MeOH and dark green precipitates were produced immediately. The precipitate was collected, dried and suspended in MeOH, to which water was added until the suspension was dissolved forming a pale green solution. This solution was filtered and yellow crystals of **27** (136 mg, 0.13 mmol) suitable for X-Ray diffraction measurement were formed after slow evaporation of the filtrate for two weeks.

Yield: 26%; IR (KBr, cm^{-1}) 3432.2 (m), 1612.4(m), 1597.9 (m), 1578.5 (s), 1549.7 (w), 1459.3 (w), 1424.6(m), 1306.8 (m), 755.7 (w), 718.1(w); Calcd for ($C_{42}H_{38}Br_4CuN_6O$): C 49.17, H 3.73, N 8.19; Found C 49.25, H 3.88, N 8.61.

8.4.10 2-chloro[4,6-(dipyridin-2-ylamino)]-1,3,5triazine. (32)

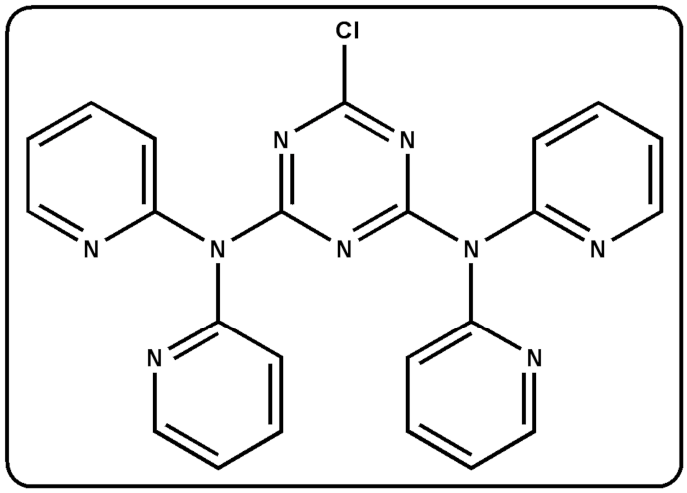

2-chloro[4,6-(dipyridin-2-ylamino)]-1,3,5-triazine was synthesized by literature procedures:[122] To a solution of 2,4,6-trichloro-[1,3,5]-triazine **30** (5.00 g, 27.11 mmol) in THF (50 mL) were added two equivalents of N-ethyl diisopropylamine (7.01g, 54.22 mmol) and the two-necked round-bottomed flask was cooled to 0°C. Dipyridin-2-ylamine **31** (9.28 g, 54.22 mmol) was added to the reaction mixture. After the completion of the addition, the clear reaction mixture was warmed to room temperature and then heated to reflux for 48 h. The yellow precipitate was isolated by filtration and washed with cold THF (3×20 mL) and ethanol (3×25 mL) to remove *N*-ethyldiisopropylamine hydrochloride and yield **32** as a light yellow powder (8.017 g, 17.70 mmol).

Yield: 65%; ^{1}H NMR ($CDCl_3$, 400 MHz): δ 7.05 (t, 2H, *J*=6.1 Hz), 7.39 (d, 2H, *J*=8.0 Hz), 7.58 (t, 2H, *J*=7.6 Hz), 8.31 (d, 2H, *J*=4.6 Hz); ^{13}C NMR ($CDCl_3$, 100 MHz): δ 121.7 (CH), 122.7 (CH), 137.6 (CH), 148.8 (CH), 154.1 (C_q), 165.5 (C_q), 170.2 (C_q); MS (FAB^+): 454.12 (100) ($[MH]^+$), 418.15 (23), 248.11 (17), 170.51 (56); Anal. Calcd. for ($C_{23}H_{16}N_9Cl$): C 60.86, H 3.55, N 27.77; Found C 60.24, H 3.66, N 27.40.

8.4.11 1-(2-Amino-ethyl)-2,3-dihydro-1H-imidazo[1,2-f]phenanthridin-4-ylium bromide hydrobromide. (34)

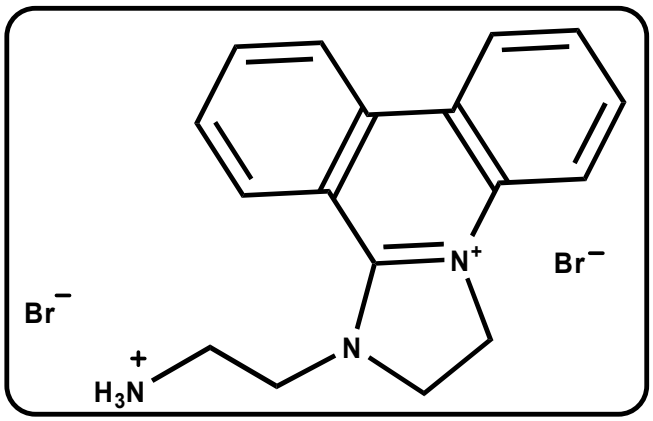

Mono-Boc ethylene diamine **33** (0.33 g, 2.1 mmol) was dissolved in ethyl acetate (40 ml), to which was added 5% aqueous Na_2CO_3 (40 ml). 5-(2-Bromo-ethyl)-phenanthridinium bromide (0.70 g, 1.76 mmol) was added to the stirred biphasic mixture. The reaction mixture was allowed to stir under nitrogen atmosphere for two hours. The organic layer was then separated, washed three times with water and transferred to a round-bottomed flask covered with aluminium foil. The reaction mixture was then cooled to 0 ˚C with an ice bath and *N*-bromo succinimide (0.41 g, 2.30 mmol) was added. The reaction mixture was then stirred for another hour under a nitrogen atmosphere, during which time a white precipitate formed. The precipitate was filtered off to give the Boc protected DIP ethyl amine derivative as a white powder. The white powder was suspended in MeOH and HBr (44% in H_2O) was added dropwise until all the solid had dissolved. The reaction mixture was stirred for 1 hour at room temperature, during which time a white precipitate formed. Diethyl ether was added to the mixture to complete precipitation and the precipitate was filtered off and washed in diethyl ether to give compound **34** (0.71 g, 1.67 mmol) as a white powder.

Yield: 90%. mp: >400˚C; ^{1}H NMR (d_6-DMSO, 400 MHz): δ 3.39 (m, 2H, *J*=5.2Hz), 4.39 (m, 4H), 4.76 (t, 2H, *J*=8.4 Hz), 7.67 (t, 1H, *J*=7.2 Hz), 7.73 (d, 1H, *J*=8.0 Hz), 8.20 (t, 3H, *J*=7.4Hz), 8.61 (d, 1H, *J*=8.4 Hz), 8.79 (d, 1H, *J*=7.6 Hz), 8.96 (d, 1H, *J*=8.4 Hz); ^{13}C NMR ((d_6-DMSO, 100 MHz): δ 36.3 (CH_2), 46.2 (CH_2), 47.1 (CH_2), 51.4 (CH_2), 115.3

(Cq), 116.0 (CH), 119.9 (Cq), 123.9 (CH), 124.3 (CH), 125.4 (CH), 127.8 (CH), 129.5 (CH), 131.5 (CH), 132.6 (Cq), 134.7 (Cq), 135.3 (CH), 153.6 (Cq); IR (KBr, cm^{-1}): 3434.60 (m), 2858.95 (m), 1599.66 (s), 1577.49 (s), 1454.06 (m), 1302.68 (m), 744.38 (w), 716.43 (w); MS (FAB^+): 264.2 (100) ($[MH]^+$) Calcd for ($C_{17}H_{19}Br_2N_3$): C 48.02, H 4.50, N 9.88; Found C 49.01, H 4.22, N 10.11.

8.4.12 1-{2-[4,6-Bis-(di-pyridin-2-yl-amino)-[1,3,5]triazin-2-ylamino]-ethyl}-2,3-dihydro-1H-imidazo[1,2-f]phenanthridin-4-ylium bromide. (35)

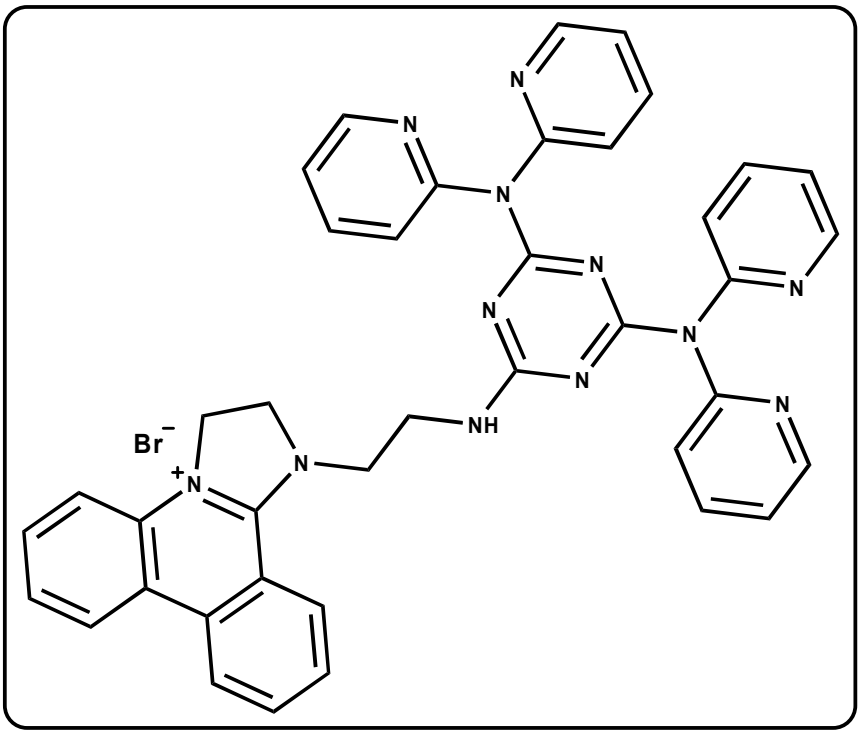

To a stirred solution of 2-chloro[4,6-(dipyridin-2-ylamino)]-1,3,5-triazine **32** (500 mg, 1.01 mmol) and N-ethyl diisopropylamine (285 mg, 2.21 mmol) in MeCN (80 ml) was added compound (2) (468 mg, 1.01 mmol). The reaction mixture was then heated to 80 ˚C under a nitrogen atmosphere for 48 hours. The reaction mixture was then filtered to remove unreacted compound **34** and the solvent was removed under reduced pressure. The resulting residue was then washed with diethyl ether and acetone to yield compound **35** (448 mg, 0.59 mmol) as a white powder.

Yield: 58%. mp: >400 °C; ^{1}H NMR (d_1-$CDCl_3$, 400 MHz): δ 3.1 (m, 2H), 4.24 (m, 2H), 4.38 (t, 2H, J=10.8 Hz), 4.83 (t, 2H, J=11.2 Hz), 7.01 (m, 4H), 7.08 (t, 2H, J=6.4 Hz), 7.15 (d, 2H, J=8.4 Hz), 7.383 (d, 1H, J=8.4 Hz), 7.448 (t, 1H, J=7.6 Hz), 7.53 (t, 2H, J=7.6 Hz), 7.632 (m, 3H), 7.743 (t, 1H, J=7.6 Hz), 7.818 (t, 1H, J=7.6 Hz), 8.26 (d, 2H, J=3.6 Hz), 8.31 (d, 1H, J=8.0 Hz), 8.44 (d, 1H, J=8.4 Hz), 8.478 (d, 1H, J=8.4 Hz), 8.527 (m, 2H); ^{13}C NMR (d_1-$CDCl_3$, 100 MHz): δ 38.1 (CH_2), 46.5 (CH_2), 50.2 (CH_2), 50.9 (CH_2), 115.2 (Cq), 115.9 (CH), 120.5 (Cq), 121.2 (CH), 122.6 (CH), 123.5 (CH), 123.6 (CH), 125.5 (CH), 128.0 (CH), 129.6 (CH), 131.4 (CH), 132.8 (Cq), 135.2 (CH), 137.4 (CH), 148.4 (CH), 153.8 (Cq), 154.9 (Cq), 165.1 (Cq); IR (KBr, cm^{-1}): 3433.64 (s), 1576.52 (s), 1461.78 (s), 1429.96 (s), 1372.10 (s), 1308.46 (m), 779.10 (w); ESI-MS (positive mode): 681.31 ($[M]^+$); Anal. Calcd for $C_{40}H_{33}BrN_{12}H_2O$: C 61.62; H 4.52; N 21.56; Found: C 61.28; H 4.41; N 20.94.

8.4.13 $C_{96}H_{92}Br_2N_{24}O_{18}Pd_5$. (36)

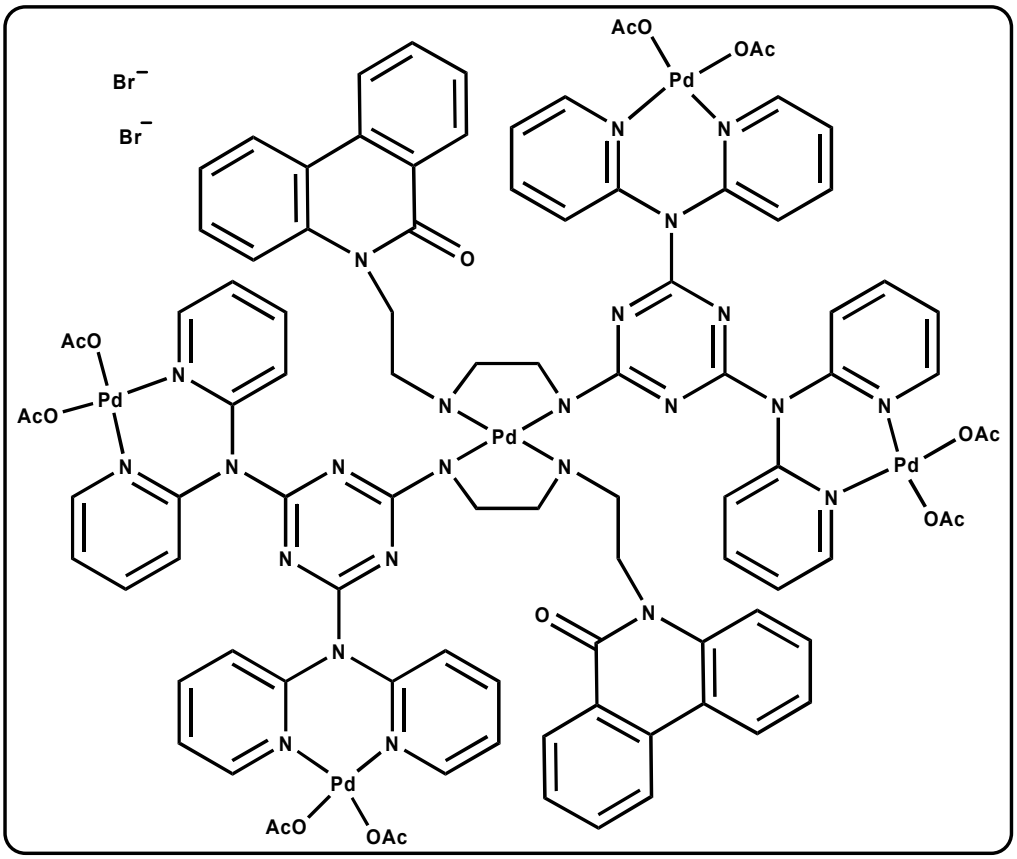

Toluene (5 ml) and a solution of $Pd(OAc)_2$ (29.5mg, 0.13 mmol) in THF (5 ml) were successively layered over a solution of compound (**35**) (50 mg, 0.066 mmol) in dichloromethane (5ml) and allowed to diffuse over two weeks yielding yellow single crystals of **36** (26.6 mg, 0.010 mmol) of sufficient quality for X-Ray diffraction studies.

Yield: 38%; IR (KBr, cm^{-1})**:** 3433.64 (m), 1716.34 (w), 1606.41 (s), 1556.27 (s), 1468.53 (m), 1378.85 (s), 1330.64 (m), 1267.97 (m), 1159.97 (w), 754.03 (w), 690.39 (w); Anal. Calcd for $C_{96}H_{92}Br_2N_{24}O_{18}Pd_5.5H_2O$: C 43.48; H 3.88; N 12.68; Found: C 43.77; H 3.58; N 12.17.

8.4.14 $(35)_2Cu_2Br_2(ClO_4)_4 \cdot 10(CH_3CN)$. (37)

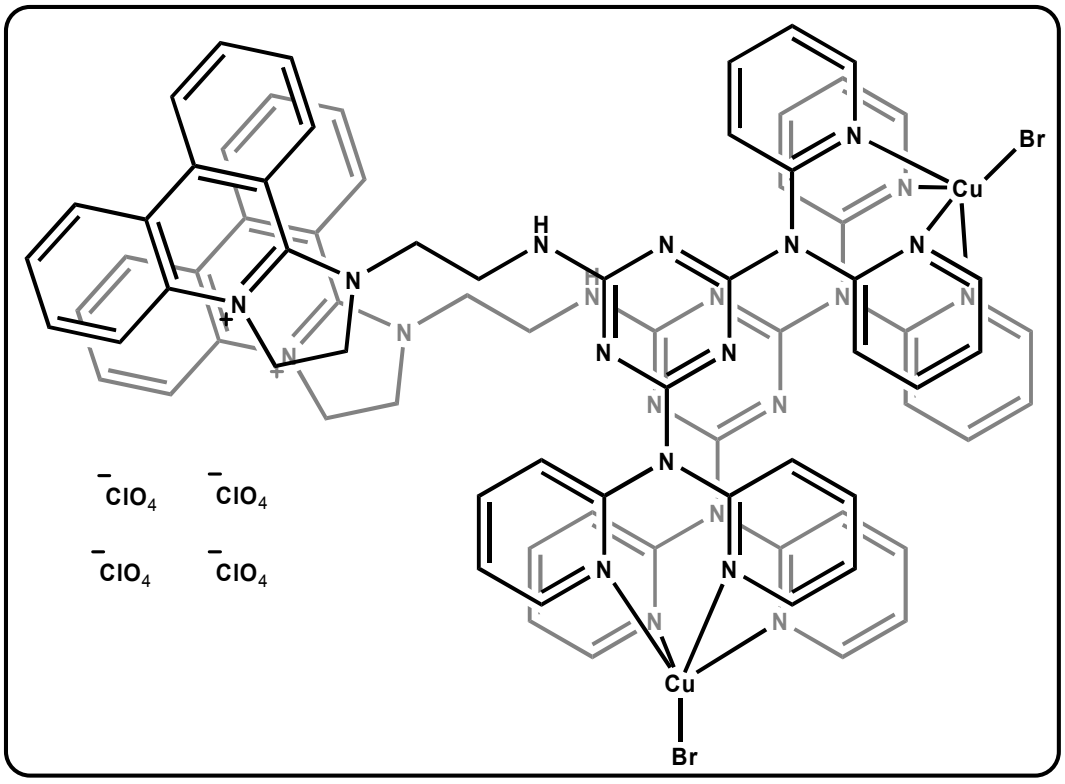

A solution of compound **35** (20 mg, $2.63x10^{-5}$ mol) in MeCN was added dropwise to a stirred solution of $Cu(ClO_4)_2.6H_2O$ (19.5 mg, $5.25x10^{-5}$ mol., 2 eq.). The solution then changed colour from pale blue to a much deeper blue/green colour. This solution was then filtered and set up for crystallization by Diethyl ether diffusion. Blue needle shaped crystals of **37** (14.2 mg $5.80x10^{-6}$ mmol) formed over 1-2 weeks.

Yield: 44%; IR (KBr, cm^{-1})**:** 3694.94 (w), 3619.73 (w), 3433.64 (m, b), 3083.62 (w), 2924.52 (w), 1609.31 (s), 1574.59 (s), 1484.92 (m), 1428.03 (m), 1376.93 (s), 1302.68 (m), 1266.04 (w), 1096.33 (s), 912.165 (w), 621.93 (m), 539.01 (m), 431.01 (w); Anal. Calcd for $(C_{80}H_{66}Br_2Cu_2N_{24})(ClO_4)_4$: C 46.91; H 3.25; N 16.41; Found: C 46.08; H 3.46; N 15.165.

8.4.15 5-(2-Oxo-2-pyridin-2-yl-ethyl)-phenanthridinium bromide. (39)

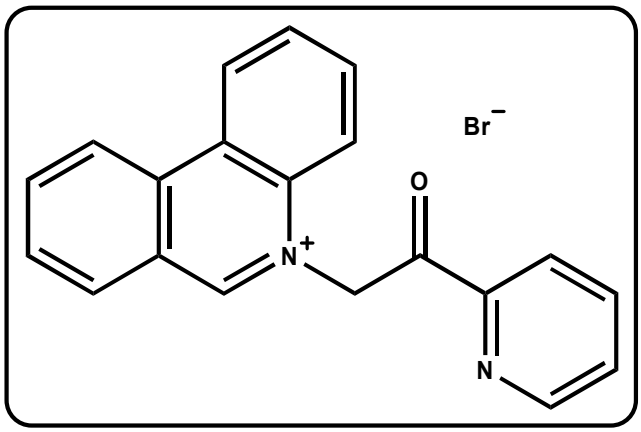

To a solution of 5% aqueous Na_2CO_3 (10ml) was added 2-(bromoacetyl) pyridine hydrobromide (2 g, 7.12 mmol). The solution was then extracted with Ethyl acetate (5x10ml). The organic layers were then collected, dried over $MgSO_4$ and transferred to a round-bottomed flask, to which was added phenanthridine(1.53 g, 8.54 mmol). The reaction mixture was then refluxed under nitrogen for 18hours. The resulting precipitate was filtered and washed once with ethyl acetate and triturated with diethyl ether yielding **39** as a beige powder (2.32 g, 6.12 mmol).

Yield: 86% mp: >300˚C ^{1}H NMR (DMSO, 400 MHz): δ 7.06 (s, 2H), 7.89 (m, 1H), 8.06 (m, 2H), 8.16 (m, 3H), 8.50 (m, 2H), 8.60 (d, 1H, *J*=8.0 Hz), 8.97 (d, 1H, *J*=4.4 Hz), 9.26 (d, 2H, *J*=6.8 Hz), 10.38 (s, 1H,); ^{13}C NMR (DMSO, 100 MHz): δ 120.4 (CH), 122.2 (CH), 123.2 (CH), 123.5 (CH), 124.8 (CH), 125.4 (C_q), 129.2 (CH), 130.4 (CH), 130.7 (CH), 132.1 (CH), 133.1 (CH), 134.1 (C_q), 134.8 (C_q), 138.1 (CH), 138.8 (CH), 145.5 (C_q), 149.6 (CH), 150.7 (C_q), 157.2 (CH), 191.7 (CO);

8.4.16 2-Pyridin-2-yl-imidazo[1,2-f]phenanthridine. (40)

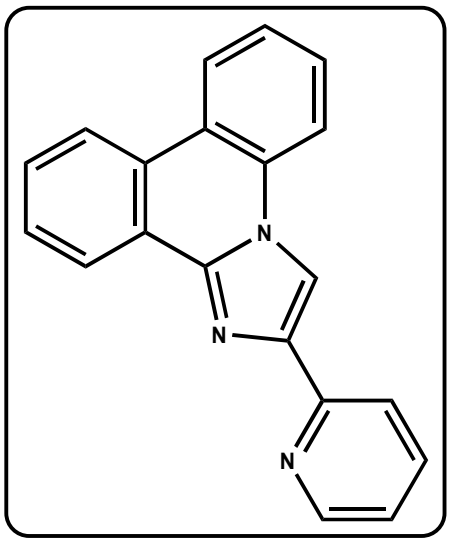

To a suspension of MnO_2 (6.912g, 79.50mmol, 10eq) in dioxane (50ml) was successively added under stirring at room temperature, ammonium acetate (3.063g, 39.75mmol, 5eq), and 5-(2-Oxo-2-pyridin-2-yl-ethyl)-phenanthridinium bromide **39** (3.015g, 7.95mmol). The reaction mixture was refluxed under nitrogen for four hours. To the hot reaction mixture was added slowly Na_2CO_3 (8.426g, 79.50mmol, 10eq). The reaction mixture was then left to cool to room temperature before addition of diethyl ether (50ml). The reaction mixture was then filtered to remove the resulting precipitate, and the precipitate was triturated and washed extensively with acetone to remove any adsorbed organic material. The organic washings were collected and the solvent removed under reduced pressure. The resulting residue was taken into chloroform and washed successively with water and brine. The combined organic layers were then collected and the solvent removed under reduced pressure to yield 2-pyridin-2-yl-imidazo[1,2-f]phenanthridine **40** as a beige powder (2.113 g, 7.16 mmol).

Yield: 90%; ^{1}H NMR ($CDCl_3$, 400 MHz): δ 7.18 (m, 1H), 7.48 (t, 1H, *J*=7.2 Hz), 7.61 (m, 3H), 7.76 (dt, 1H, J_1=7.6 J_2=1.6 Hz), 7.92 (d, 1H, *J*=7.6 Hz), 8.25 (d, 1H, *J*=8.0 Hz), 8.34 (m, 1H), 8.46 (d, 1H, *J*=7.6 Hz), 8.60 (d, 1H, *J*=4.0 Hz), 8.64 (s, 1H), 8.72 (m, 1H); ^{13}C NMR ($CDCl_3$, 100 MHz): δ 111.7 (CH), 116.2 (CH), 120.8 (CH), 122.0 (C_q), 122.5 (CH), 123.4 (C_q), 124.2 (CH), 124.5 (CH), 125.6 (CH), 127.9 (C_q), 128.6 (CH), 129.1 (CH), 129.2 (CH), 131.7 (C_q), 138.0 (CH), 142.9 (C_q), 148.2 (CH), 152.3 (CH); IR (KBr,

cm^{-1}): 3434.6 (s), 1631.48 (w), 1590 (s), 1570.74 (w), 1528.31 (w), 1460.81 (s), 1424.17 (s), 1396.21 (m), 1209.15 (w), 1122.37 (w), 771.39 (m), 740.53 (s), 719.32 (m), 612.288 (w); MS (EI+): 295.1 (100) (M+), 267.1 (14), 190.1 (3), 178.1 (8), 147.5 (11), 44.0 (12); Anal. Calcd for $C_{20}H_{13}N_3$: C, 81.34; H, 4.44; N, 14.23; Found: C, 80.08; H, 4.32; N, 13.91.

8.4.17 (40)$CuBr_2(C_3H_7NO)$. (41)

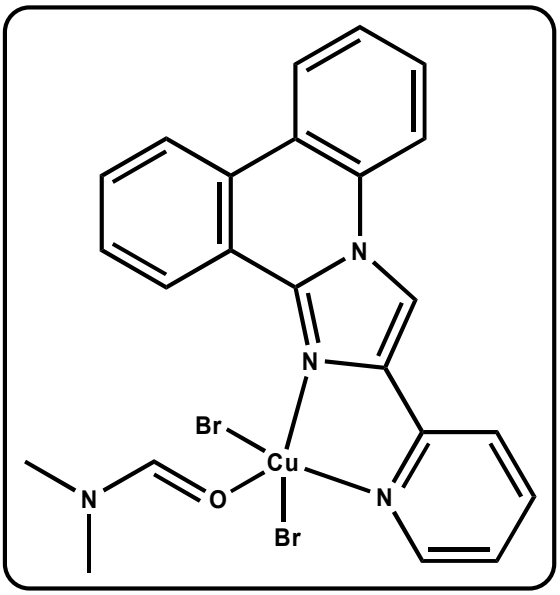

2-Pyridin-2-yl-imidazo[1,2-f]phenanthridine **40** (20mg, $6.772x10^{-5}$mol) was dissolved in methanol and added dropwise to a solution of $CuBr_2$ (30 mg, $1.35x10^{-4}$ mmol) in methanol under stirring. The resulting dark brown precipitate was filtered off, dried and suspended in methanol. Dimethyl formamide was added dropwise until the precipitate had completely dissolved giving a yellow solution. This solution was filtered and allowed to evaporate slowly yielding compound **41** as yellow block crystals (28.9mg, $2.44x10^{-5}$mol). These crystals showed a tendency to twin, however it was possible to break the crystals in order to obtain a single crystal suitable of X-Ray diffraction studies.

Yield: 36%; IR (KBr, cm^{-1})**:** 3433.64 (b, w), 3098.08 (w), 2937.06 (w), 1642.08 (s), 1533.13 (m), 1440.56 (m), 1380.78 (s), 1124.30 (w), 779.10 (m), 749.21 (m), 410.76 (w);

Anal. Calcd for $C_{46}H_{40}Br_4Cu_2N_8O_2$: C 46.68; H 3.41; N 9.47; Found: C 46.89; H 3.30; N 9.26.

8.4.18 (40)$PdCl_2$·$(CH_3)_2SO$. (42)

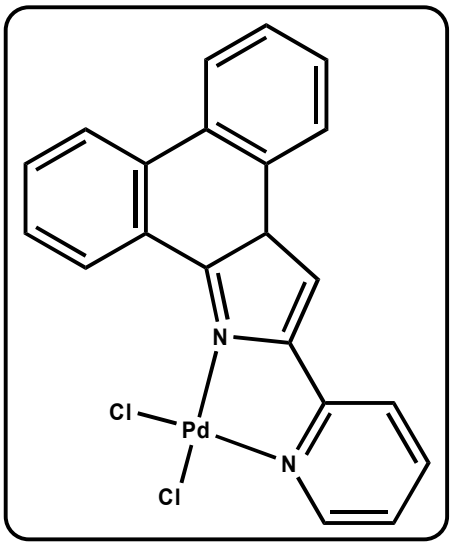

2-Pyridin-2-yl-imidazo[1,2-f]phenanthridine **40** (5mg, $1.69x10^{-5}$mol) was dissolved in DMSO (3.0ml), to which was added $PdCl_2$. the solution was then heated until the $PdCl_2$ had entirely dissolved. The solution was then filtered and left overnight, by which time compound **42** had formed as red block single crystals (4.9 mg, $9.46x10^{-6}$mmol) suitable for X-ray diffraction studies.

Yield: 56%; IR (KBr, cm^{-1})**:** 3433 (b, s), 3118.33 (w), 1614.13 (m), 1528.31 (m), 1458.89 (s), 1033.66 (m), 755.00 (s), 716.43 (m), 427.16 (w); Anal. Calcd for $C_{22}H_{19}Cl_2N_3OPdS$: C 47.97; H 3.48; N 7.63; Found: C 46.94; H 3.26; N 7.23.

8.4.19 $(40)_2AgNO_3 \cdot 3(CH_3OH)$. (43)

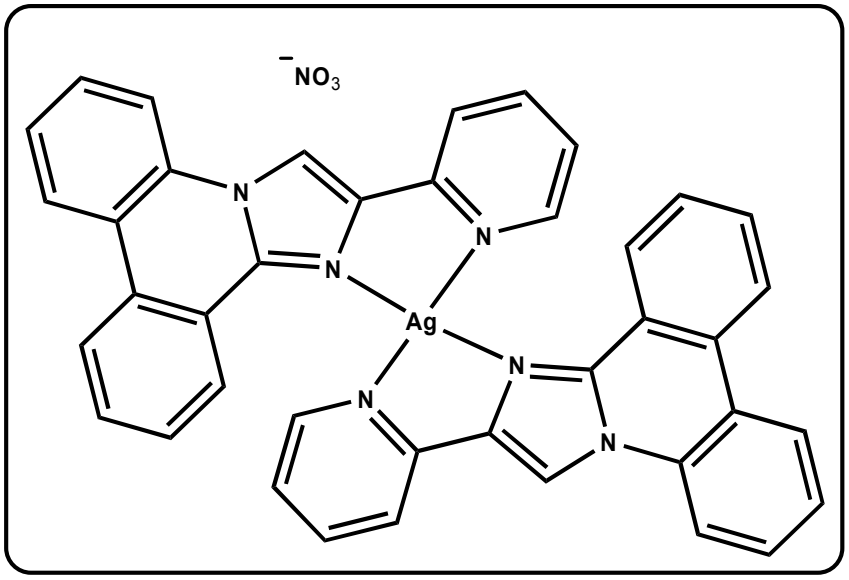

2-Pyridin-2-yl-imidazo[1,2-f]phenanthridine **40** (20mg, 6.772×10^{-5}mol) was dissolved in methanol. To this was added a solution of $AgNO_3$ (11.5mg, 6.772×10^{-5}mol) in methanol. The solution was protected from UV light by wrapping the vial in aluminium foil. The resulting solution was then filtered and crystallised by slow diffusion of diethyl ether into the methanolic solution, yielding compound **43** as colourless block crystals (9.9mg, 1.15×10^{-5}mmol).

Yield: 17%; IR (KBr, cm^{-1}): 3434.60 (b, m), 3100.97 (w), 1598.70 (m), 1567.84 (m), 1536.99 (m), 1459.85 (s), 1440.56 (s), 1384.64 (s), 1275.68 (s), 1159.01 (w), 748.245 (s); Anal. Calcd for $(C_{40}H_{26}N_6Ag)(NO_3)$: C 63.17; H 3.45; N 12.89; Found: C 64.06; H 3.74; N 13.21.

8.4.20 $(40)_4Co_20H(BF_4)_3.2MeCN$ (44)

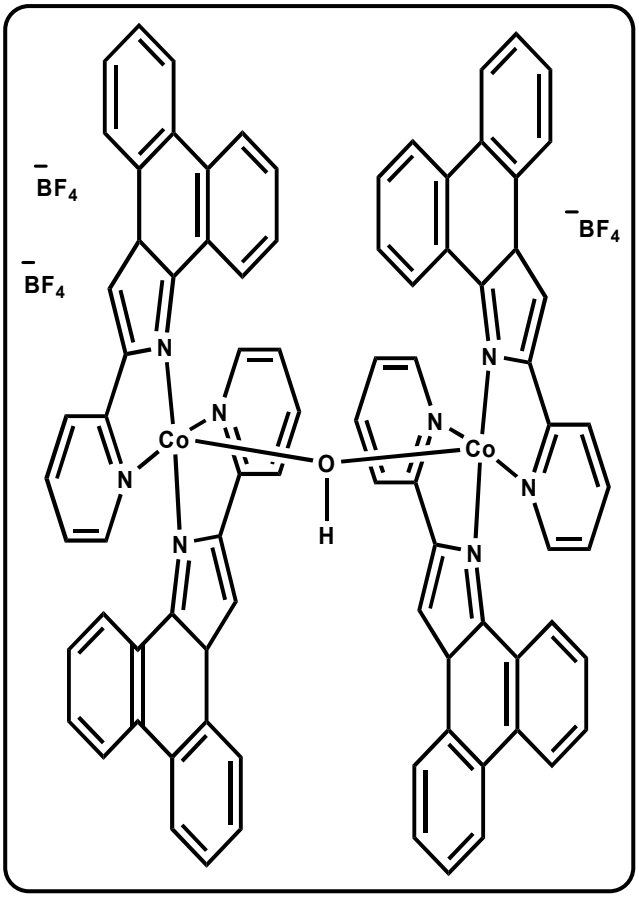

A solution of 2-Pyridin-2-yl-imidazo[1,2-f]phenanthridine **40** (20mg, $6.772x10^{-5}$mol) in MeCN (2ml) was added dropwise to a solution of $Co(BF_4)_2 \cdot 3H_2O$ (38.8mg, $1.35x10^{-4}$mol) also in MeCN. The reaction mixture was then heated to 80ºC for 2 hours. The resulting green solution was filtered and set up for crystallisation by slow diffusion of ether, yielding red/green block crystals of **44** (30.9 mg, $1.86x10^{-5}$mmol) after 1-2 weeks.

Yield: 55%; IR (KBr, cm^{-1}): 3433.64 (b, m), 312.97 (w), 2360.44 (w), 2248.59 (w), 1612.20 (s), 1580.38 (m), 1058.73 (b, s), 750.17 (s), 676.89 (w), 648.93 (w), 613.25 (w), 520.69 (w); Anal. Calcd for $(C_{80}H_{53}Co_2N_{12}O)(BF_4)_3(C_2H_3N)_2$: C 60.82; H 3.59; N 11.82; Found: C 60.49; H 3.35; N 11.39.

8.4.21 2,3-Dihydro-12H-pyrrolo[1,2-f]phenanthridine-1,1-dicarbonitrile. (47)

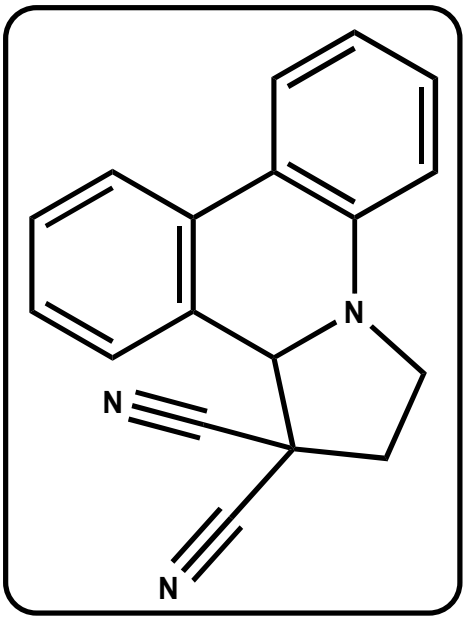

To a stirred solution of Malonnonitrile **45** (1.00g, 15.10mmol) in MeOH (30 ml) was added 5-(2-Bromo-ethyl)-phenanthridinium bromide **3** (5.56g, 15.10mmol). To the reaction mixture was then added triethylamine (7.659g, 7.57mmol). The reaction mixture was then stirred under a N_2 atmosphere for 1 hour, during which time a white precipitate had formed. The precipitate was isolated by filtration and washed with cold MeOH (5ml) to yield 2,3-Dihydro-12H-pyrrolo[1,2-f]phenanthridine-1,1-dicarbonitrile **47** as a white microcrystalline powder (3.57g, 13.60mmol). Single crystals suitable for X-Ray crystal analysis were obtained by recrystallising the product from hot MeOH.

Yield: 87%; mp: 45.3-46.1 ˚C ; ^{1}H NMR ($CDCl_3$, 400 MHz): δ 2.82 (ddd, 1H, J_1=6.5 Hz, J_2=10.2 Hz, J_3=13.6 Hz), 3.06 (ddd, 1H, J_1=4.2 Hz, J_2=8.6 Hz, J_3=13.4 Hz), 3.51 (ddd, 1H, J_1=4.3 Hz, J_2=J_3=10.0 Hz), 3.85 (ddd, 1H, J_1=6.6 Hz, J_2=8.8 Hz, J_3=9.6 Hz), 6.65 (d, 1H, J=8.1 Hz), 5.14 (s, 1H,), 6.96 (t, 1H, J=7.58 Hz), 7.27 (t, 1H, J=7.7 Hz), 7.43 (dt, 1H, J_1=1.24 Hz, J_2=7.52 Hz), 7.50 (t, 1H, J=7.38 Hz), 7.65 (d, 1H, J=7.6 Hz), 7.78 (dd, 1H, J_1=1.28 Hz, J_2=8.0 Hz), 7.89 (d, 1H, J=8.0 Hz); ^{13}C NMR ($CDCl_3$, 100 MHz): δ 35.9 (CH_2), 38.4 (C_q), 44.26 (CH_2), 68.6 (CH), 112.7 (CH), 113.7 (C_q), 115.1 (C_q), 110.0 (CH), 121.1 (C_q), 123.2 (CH), 123.6 (CH), 124.8 (CH), 127.9 (C_q), 128.2 (CH), 129.7 (CH), 129.8 (CH), 131.6 (C_q), 142.0 (C_q); IR (KBr, cm^{-1}): 2930.31 (m), 2874.34 (m), 2788.56

(m), 2248.59 (w), 1602.56 (m), 1493.6 (s), 1451.17 (s), 1377.89 (m), 1294.00 (m), 1218.79 (m), 778.14 (m), 741.50 (s), 613.25 (w); MS (FAB+): 271.13 (33) (M+), 219.22 (12), 179.10 (100); Anal. Calcd for $C_{18}H_{13}N_3$: C, 79.68; H, 4.83; N, 15.49; Found: C, 79.72; H, 4.91; N, 15.62.

8.4.22 5-(3,3-Dicyano-propyl)-phenanthridinium chloride. (49)

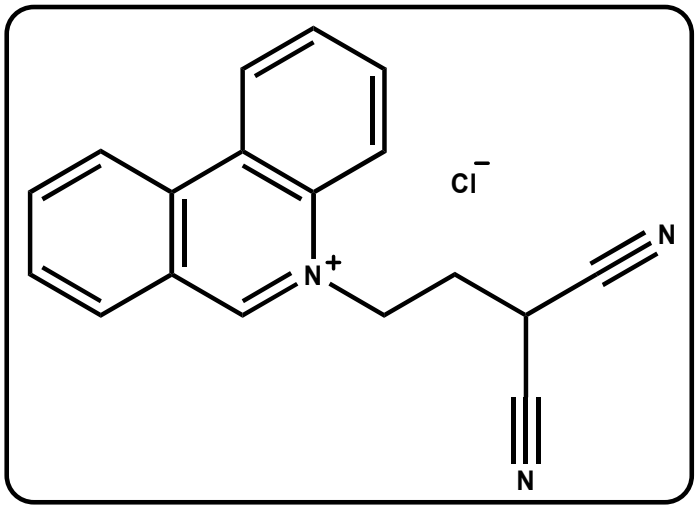

2,3-Dihydro-12H-pyrrolo[1,2-f]phenanthridine-1,1-dicarbonitrile **47** (100mg, 0.37mmol) was suspended in MeOH (10 ml). To this concentrated hydrochloric acid was added dropwise until all the starting material had dissolved. The reaction mixture was then stirred for one hour. The product was then precipitated by addition of diethyl ether and isolated by filtration to yield (**49**) as a white powder (111mg, 0.36mmol).

Yield: 99 %; ^{1}H NMR (MeOD, 400 MHz): δ 3.01 (m, 2H), 5.45 (m, 2H), 8.18 (m, 2H), 8.25 (ddd, 1H, J_1=1.4 Hz, J_2=7.1 Hz, J_3=8.6 Hz), 8.47 (ddd, 1H, J_1=1.28 Hz J_2=7.2 Hz, J_3=8.44 Hz), 8.60 (d, 1H, J=8.6 Hz), 8.65 (d, 1H, J=8.1 Hz), 9.15 (d, 1H, J=8.5 Hz), 9.22 (dd, 1H, J_1=1.4 Hz, J_2=9.6 Hz), 10.30 (s, 1H); ^{13}C NMR (MeOD, 100 MHz): δ 30.6 (CH_2), 56.0 (CH_2), 114.1 (C_q), 120.5 (CH), 124.4 (CH), 125.4 (C_q), 126.5 (CH), 128.1 (C_q), 131.8 (CH), 132.0 (CH), 133.8 (CH), 134.5 (CH), 134.7 (C_q), 137.1 (CH), 140.1 (CH), 157.6 (CH); IR (KBr, cm^{-1}): 3419.17 (b, m), 3010.34 (w), 2798.21 (w), 2256.31 (w), 1626.66 (s), 1534.10 (m), 1451.17 (m), 1423.21 (w), 1262.18 (w), 760.78 (s), 720.28 (m); MS (CI+):

272.13 (16) (M+), 207.25 (8), 193.25 (28), 179.26 (100), 75.23 (82); Anal. $C_{18}H_{14}ClN_3$: C, 70.24; H, 4.58; N, 13.65; Found: C, 69.03; H, 4.62; N, 13.44.

8.4.23 2,3-Dihydro-12H-pyrrolo[1,2-f]phenanthridine-1-indan-1,3-dione.(48)

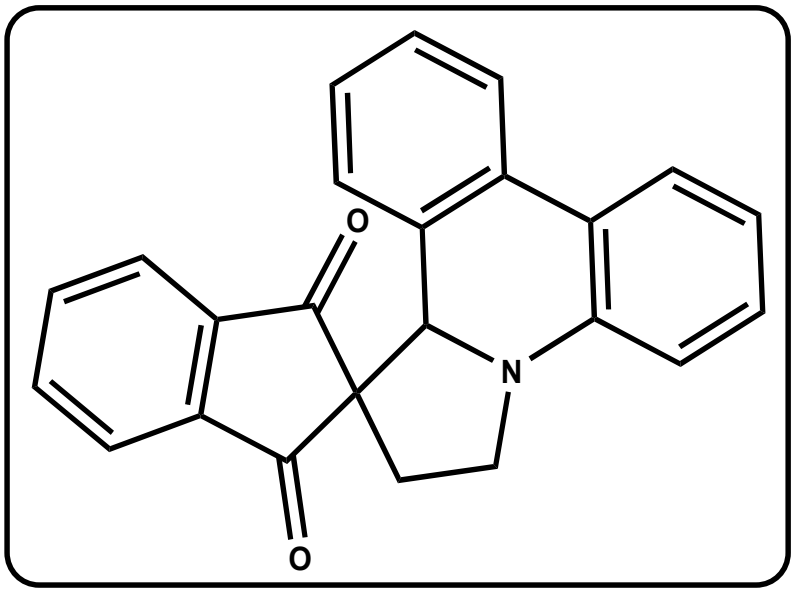

To a stirred solution of indan-1,3-dione (1.00g, 6.80mmol) in EtOAc (40 ml), was added 5% aqueous Na_2CO_3 (40ml) followed by 5-(2-bromo-ethyl)-phenanthridinium bromide **3** (2.51g, 6.80mmol). The reaction mixture was then stirred for 3 hours under N_2 during which time the mixture turned a deep orange colour. The EtOAc layer was then separated, washed three times with water and dried over $MgSO_4$. The EtOAc was then removed under vacuum and the crude product recrystallised from warm MeOH to yield 2,3-dihydro-12H-pyrrolo[1,2-f]phenanthridine-1-indan-1,3-dione **48** as an orange microcrystalline powder (1.76g, 5.00mmol). Single crystals suitable for X-Ray chrystallography were grown by recrystallising the product from MeOH.

Yield: 73%; mp: 86.4-87.4 °C; ^{1}H NMR ($CDCl_3$, 400 MHz): δ 2.30 (t, 2H, *J*=7.18 Hz), 3.74 (t, 2H, *J*=7.2 Hz), 5.36 (s, 1H), 6.30 (d, 1H, *J*=7.6 Hz), 6.62 (d, 1H, *J*=8.1 Hz), 6.66 (t, 1H, *J*=7.5 Hz), 6.72 (t, 1H, *J*=7.5 Hz), 7.0437 (t, 1H, *J*=7.7 Hz), 7.14 (t, 1H, *J*=7.7 Hz), 7.58 (dd, 1H, J_1=1.12 Hz, J_2=7.8 Hz), 7.641 (d, 1H, *J*=8.0 Hz), 7.75 (m, 2H), 7.84 (m, 2H), ^{13}C NMR ($CDCl_3$, 100 MHz): δ 32.4 (CH_2), 48.0 (CH_2), 64.0 (C_q), 68.1 (CH), 112.5 (CH),

118.0 (CH), 119.8 (C_q), 122.6 (CH), 122.9 (CH), 123.4 (CH), 123.3 (C_q), 124.9 (CH), 126.6 (CH), 128.2 (CH), 129.3 (C_q), 129.6 (CH), 131.6 (C_q), 135.7 (CH), 142.4 (C_q), 201.2 (C_q); IR (KBr, cm^{-1}): 3424.96 (b, m), 2844.49 (w), 1737.55 (m), 1703.80 (s), 1602.56 (m), 1494.56 (m), 1242.90 (s), 736.67 (s); MS (FAB+): 351.13 (21) (M+), 275.10 (15), 247.11 (23), 219.11 (58), 179.13 (100); Anal. Calcd for $C_{24}H_{17}NO_2$: C, 82.03; H, 4.88; N, 3.99; Found: C, 81.88; H, 4.76; N, 4.11.

8.4.24 5-(3,-(indan-1,3-dione)-propyl)-phenanthridinium chloride. (50)

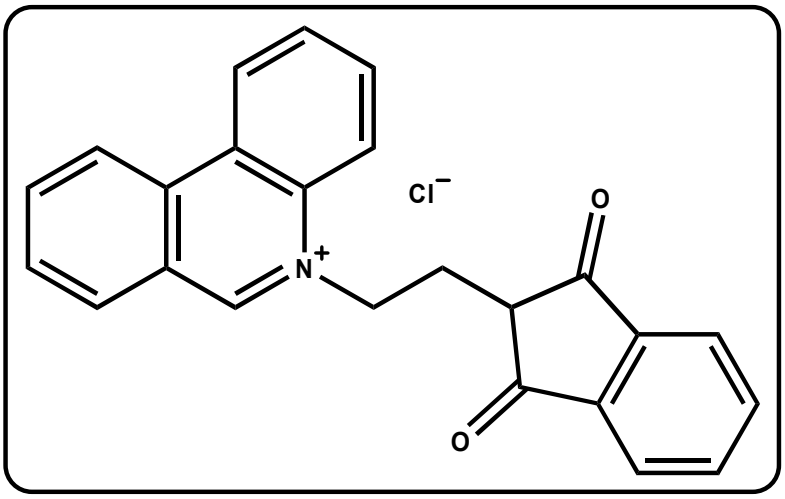

2,3-dihydro-12H-pyrrolo[1,2-f]phenanthridine-1-indan-1,3-dione **48** (100mg, 0.28mmol) was suspended in MeOH (10ml). To this concentrated hydrochloric acid was added dropwise until all the starting material had dissolved. The reaction mixture was then stirred for one hour. The product was then precipitated by addition of diethyl ether and isolated by filtration to yield 5-(3,-(indan-1,3-dione)-propyl)-phenanthridinium chloride **50** as a bright yellow powder (101mg, 0.26mmol).

Yield: 91%; ^{1}H NMR (MeOD, 400 MHz): δ 1.03 (t, 2H, *J*=7.5 Hz), 3.83 (t, 2H, *J*=7.6 Hz), 6.25 (m, 4H), 6.46 (m, 3H), 6.73 (t, 1H, *J*=8.0 Hz), 6.89 (d, 1, *J*=8.2 Hz), 6.99 (d, 1H, *J*=8.6 Hz), 7.42 (d, 1H, *J*=8.4 Hz), 7.48 (d, 1H, *J*=8.2 Hz), 8.55 (s, 1H); ^{13}C NMR (MeOD, 100 MHz): δ 27.2 (CH_2), 57.7 (CH_2), 120.8 (CH), 120.8 (CH), 124.3 (CH), 124.3 (CH), 125.5 (C_q), 126.4 (CH), 128.1 (C_q), 131.6 (CH), 131.8 (CH), 132.6 (C_q), 133.6 (CH), 134.2 (CH), 134.9 (C_q), 137.8 (CH), 139.7 (CH), 143.3 (C_q), 157.0 (CH), 200.7 (C_q); IR (KBr,

cm^{-1}): 3425.96 (m), 2486.76 (w), 1683.55 (m), 1624.73 (s), 1586.16 (s), 1455.99 (w), 1310.39 (w), 1260.25 (s), 1157.08 (w), 956.52 (w), 767.53 (m), 733.78 (m); MS (CI+): 352.13 (26) (M+), 207.16 (67), 179.08 (89), 145.06 (100); Anal. Calcd for $C_{24}H_{18}ClNO_2$: C, 74.32; H, 4.68; N, 3.61; Found: C, 73.56; H, 4.52; N, 3.70.

8.5 pH Dependant Behaviour of DPP Derivatives

8.5.1 ^{1}H NMR Experiment on (47)

A ^{1}H NMR spectrum was recorded of a suspension of **47** in d_4-methanol, to this suspension was added one drop of conc. DCL (36% in D_2O). Upon addition the material became fully dissolved and a second ^{1}H NMR was recorded. To this same NMR sample was then added two drops of TEA. Upon addition a suspension of white crystalline product was formed and a third ^{1}H NMR was recorded. All NMR spectra were collected at 400 MHz over 16 scans.

8.5.2 UV and Emission Spectra of Compounds 47, 48, 49 and 50 condidtions.

Stock solutions of each compound to be studied were prepared at $5x10^{-5}$ M concentrations and UV spectra were recorded for each sample. Conditions for the emission spectra of each compound are given below:

(**47**): $5x10^{-5}$M, excitation wavelength: 347nm, scan range: 350-520nm, slit (ex) 3nm, slit (em) 1.5nm.

(**49**): $5x10^{-5}$M, excitation wavelength: 347nm, scan range: 350-520nm, slit (ex) 3nm, slit (em) 1.5nm.

(**48**): $5x10^{-5}$M, excitation wavelength: 315nm, scan range: 350-520nm, slit (ex) 5nm, slit (em) 5nm.

(**50**): $5x10^{-5}$M, excitation wavelength: 322nm, scan range: 350-520nm, slit (ex) 5nm, slit (em) 3nm.

8.6 Cryospray Mass Spectrometry of 36

CS-MS measurements were made at -40ºC. The Mass Spectrum of a crystalline sample of complex **36** was collected in an Acetonitrile/DCM solvent mixture, to which had been added a small quantity of solid NaCl. This solution was infused into the electrospray at 180 µL/h. The mass spectrometer used for the measurements was a Bruker microTOFQ and the data was collected in negative ion mode. The spectrometer was previous calibrated with the standard tune mix to give a precision of ca. 1.5 ppm in the region of 500-5000 m/z. The standard parameters for a medium mass data acquisition were used and the end plate voltage was set to -500 V and the capillary to +4500 V. The collision cell was set to a collision energy of -8.0 eV/z with a gas flow rate at 25% of maximum and the cell RF was set at 600 Vpp.

.

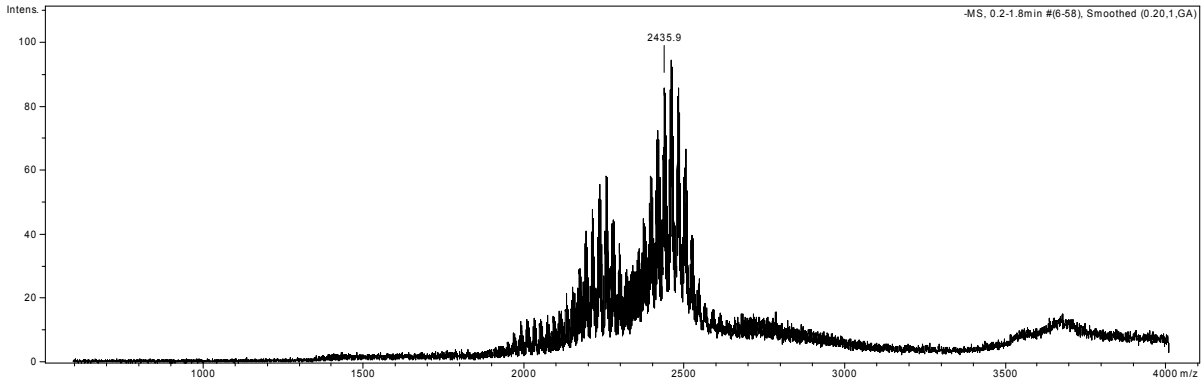

Figure 70: Full CSI-MS of 36.

Crystallographic Section

9 CRYSTALLOGRAPHY

15 single-crystal X-ray diffraction datasets are presented in this thesis. This section contains the only the refinement details of each structure. For full bonding distances and angles the reader is referred to the supplementary data which is deposited with this thesis and can be obtained from the University of Glasgow. Structures were solved using Patterson or Direct methods with SHELXS-97[162] or SIR-92[163] using WinGX[164] routines. Refinement was accomplished by full matrix least-squares on F^2 *via* SHELXL-97. All non-hydrogen atoms were refined anisotropically unless stated otherwise. Hydrogen atom positions were calculated using standard geometric criteria and refined using a riding model. All data manipulation and presentation steps were performed using WinGX. Details of interest about the structure refinement are given in the tables. The following quantities are given in the information for each structure and were calculated as follows:

$$\text{Goodness-of-fit (GooF)} = \left(\sqrt{\sum \frac{w(F_0^2 - F_c^2)^2}{(n-p)}} \right)$$

$$\text{Weighting scheme } w = \frac{1}{[\sigma^2(\mathrm{F_0})^2 + (\mathrm{A\,P})^2 + (\mathrm{BP})]}$$

$$\text{With } P = \frac{[\max(I_{obs,O}) + 2F_c^2]}{3}$$

and p: number of parameters; n: number of data; A, B: weighting scheme parameters

$$\mathrm{R1} = \frac{\Sigma \,||\,\mathrm{F_0}\,| - |\,\mathrm{F_c}\,||}{\Sigma\,|\,\mathrm{F_o}\,|}$$

$$\mathrm{wR2} = \sqrt{\frac{\Sigma[\mathrm{w}(\mathrm{F_0^2} - \mathrm{F_c^2})^2]}{\Sigma \mathrm{w}(\mathrm{F_0^2})^2}}$$

$$\mathrm{R(int)} = \frac{\Sigma\left|F_0^2 - F_c^2(mean)\right|}{\Sigma\left|F_0^2\right|}$$

where both summation involve reflections for which more than one symmetry equivalent is averaged.

9.1 2,3-Dihydro-1-(2-pyridyl-methyl)-imidazo[1,2-f]phenathridinium tetraphenyl borate 22·BPh_4

Empirical formula	$C_{45}H_{38}BN_3$
Formula weight	631.59
Temperature	100(2) K
Wavelength	0.71073 Å
Crystal system, space group	Monoclinic, P21/n
Unit cell dimensions	*a* = 10.3685(7) Å α = 90º
	b = 18.5863(11) Å β = 104.445(3)º
	c = 18.5508(11) Å γ = 90º
Volume	3461.9(4) $Å^3$
Z, Calculated density	4, 1.212 Mg/m^3
Absorption coefficient	0.070 mm^{-1}
F(000)	1336
Crystal size	0.30 x 0.20 x 0.20 mm
Theta range for data collection	1.58 to 22.00º
Limiting indices	-10<=h<=10, -19<=k<=19, -18<=l<=19
Reflections collected / unique	45379 / 4248 [R(int) = 0.0736]
Completeness to theta =	22.00 100.0 %
Absorption correction	Empirical
Max. and min. transmission	0.9861 and 0.9793
Refinement method	Full-matrix least-squares on F^2
Data / restraints / parameters	4248 / 0 / 443
Goodness-of-fit on F^2	1.029
Final R indices [I>2sigma(I)]	R1 = 0.0466, wR2 = 0.1128
R indices (all data)	R1 = 0.0794, wR2 = 0.1334
Largest diff. peak and hole	0.43 and -0.13 $e.Å^{-3}$

9.2 $[Cu(22\text{-}Br_{0.05})_2Br_2](22\text{-}Br_{0.45})_2(BF_4)_4$. (24)

Empirical formula	$C_{84}H_{71}B_4Br_3CuF_{16}N_{12}$	
Formula weight	1899.04	
Temperature	100(2) K	
Wavelength	0.71073 Å	
Crystal system, space group	Monoclinic, P21/c	
Unit cell dimensions	*a* = 28.553(2) Å	α = 90º
	b = 8.2201(6) Å	β = 100.746(3)º
	c = 16.7163(13) Å	γ = 90º
Volume	3854.7(5) $Å^3$	
Z, Calculated density	2, 1.636 Mg/m^3	
Absorption coefficient	1.934 mm^{-1}	
F(000)	1914	
Crystal size	0.14 x 0.12 x 0.08 mm	
Theta range for data collection	1.45 to 22.18º	
Limiting indices	-29<=h<=30, -7<=k<=8, -17<=l<=17	
Reflections collected / unique	23213 / 4747 [R(int) = 0.0676]	
Completeness to theta =	22.18 98.1 %	
Absorption correction	Empirical	
Max. and min. transmission	0.8606 and 0.7735	
Refinement method	Full-matrix least-squares on F^2	
Data / restraints / parameters	4747 / 0 / 562	
Goodness-of-fit on F^2	1.145	
Final R indices [I>2sigma(I)]	R1 = 0.0590, wR2 = 0.1068	
R indices (all data)	R1 = 0.0805, wR2 = 0.1137	
Largest diff. peak and hole	0.55 and -0.42 e.$Å^{-3}$	

9.3 Cu(22)$Br_2(NO_3)$. (25)

Empirical formula	$C_{21}H_{18}Br_2CuN_4O_3$	
Formula weight	597.75	
Temperature	100(2) K	
Wavelength	0.71073 Å	
Crystal system, space group	Triclinic, P-1	
Unit cell dimensions	*a* = 8.8546(5) Å	α = 63.335(3)º
	b = 11.6779(7) Å	β = 76.612(3)º
	c = 12.0660(7) Å	γ = 78.007(3)º
Volume	1076.90(11) $Å^3$	
Z, Calculated density	2, 1.843 Mg/m^3	
Absorption coefficient	4.756 mm^{-1}	
F(000)	590	
Crystal size	0.40 x 0.22 x 0.06 mm	
Theta range for data collection	1.91 to 25.00º	
Limiting indices	-10<=h<=9, -13<=k<=13, -14<=l<=14	
Reflections collected / unique	16793 / 3787 [R(int) = 0.0378]	
Completeness to theta = 25.00	99.4 %	
Absorption correction	Empirical	
Max. and min. transmission	0.7634 and 0.2521	
Refinement method	Full-matrix least-squares on F^2	
Data / restraints / parameters	3787 / 0 / 286	
Goodness-of-fit on F^2	1.018	
Final R indices [I>2sigma(I)]	R1 = 0.0425, wR2 = 0.0975	
R indices (all data)	R1 = 0.0581, wR2 = 0.1056	
Largest diff. peak and hole	2.23 and -0.65 $e.Å^{-3}$	

9.4 Cu(22)Br_3. (26)

Empirical formula	$C_{21}H_{18}Br_3CuN_3$	
Formula weight	615.65	
Temperature	273(2) K	
Wavelength	0.71073 Å	
Crystal system, space group	Triclinic, P-1	
Unit cell dimensions	*a* = 11.867(4) Å	α = 106.773(8)º
	b = 13.477(5) Å	β = 104.342(8)º
	c = 14.980(5) Å	γ = 100.370(8)º
Volume	2139.1(12) $Å^3$	
Z, Calculated density	4, 1.912 Mg/m^3	
Absorption coefficient	6.637 mm^{-1}	
F(000)	1196	
Crystal size	0.26 x 0.20 x 0.06 mm	
Theta range for data collection	1.50 to 23.00º	
Limiting indices	-8<=h<=12, -9<=k<=14, -14<=l<=14	
Reflections collected / unique	5690 / 4038 [R(int) = 0.0435]	
Completeness to theta = 23.00	67.8 %	
Absorption correction	Empirical	
Max. and min. transmission	0.6915 and 0.2773	
Refinement method	Full-matrix least-squares on F^2	
Data / restraints / parameters	4038 / 0 / 266	
Goodness-of-fit on F^2	1.054	
Final R indices [I>2sigma(I)]	R1 = 0.0810, wR2 = 0.2231	
R indices (all data)	R1 = 0.1098, wR2 = 0.2489	
Largest diff. peak and hole	2.21 and -0.94 $e.Å^{-3}$	

9.5 $Cu_2(22)_2(N_3)_6$. (28)

Empirical formula	$C_{42}H_{36}Cu_2N_{24}$	
Formula weight	1004.03	
Temperature	100(2) K	
Wavelength	0.71073 Å	
Crystal system, space group	Monoclinic, C2/c	
Unit cell dimensions	*a* = 31.917(2) Å	α = 90º
	b = 8.5868(5) Å	β = 107.844(2)º
	c = 15.9626(10) Å	γ = 90º
Volume	4164.3(4) $Å^3$	
Z, Calculated density	4, 1.601 Mg/m^3	
Absorption coefficient	1.089 mm^{-1}	
F(000)	2056	
Crystal size	0.28 x 0.16 x 0.10 mm	
Theta range for data collection	2.46 to 25.78º	
Limiting indices	-38<=h<=38, -10<=k<=10, -19<=l<=19	
Reflections collected / unique	18504 / 3981 [R(int) = 0.0602]	
Completeness to theta = 25.78	99.6 %	
Absorption correction	Empirical	
Max. and min. transmission	0.8989 and 0.7502	
Refinement method	Full-matrix least-squares on F^2	
Data / restraints / parameters	3981 / 0 / 307	
Goodness-of-fit on F^2	1.034	
Final R indices [I>2sigma(I)]	R1 = 0.0381, wR2 = 0.0782	
R indices (all data)	R1 = 0.0611, wR2 = 0.0885	
Largest diff. peak and hole	0.63 and -0.44 $e.Å^{-3}$	

9.6 $Cu_2(22)_2(NCS)_4(OCH_3)_2$. (29)

Empirical formula	$C_{49}H_{46}Cu_2N_{10}O_3S_4$	
Formula weight	1078.28	
Temperature	100(2) K	
Wavelength	0.71073 Å	
Crystal system, space group	Triclinic, P-1	
Unit cell dimensions	*a* = 9.2344(7) Å	α = 65.526(3)º
	b = 11.5240(9) Å	β = 88.615(3)º
	c = 12.4542(9) Å	γ = 80.281(3)º
Volume	1187.40(16) $Å^3$	
Z, Calculated density	1, 1.508 Mg/m^3	
Absorption coefficient	1.126 mm^{-1}	
F(000)	556	
Crystal size	0.25 x 0.24 x 0.12 mm	
Theta range for data collection	1.80 to 24.20º	
Limiting indices	-10<=h<=10, -13<=k<=13, -14<=l<=13	
Reflections collected / unique	18035 / 3771 [R(int) = 0.0501]	
Completeness to theta = 24.20	98.6 %	
Absorption correction	Empirical	
Max. and min. transmission	0.8767 and 0.7660	
Refinement method	Full-matrix least-squares on F^2	
Data / restraints / parameters	3771 / 0 / 308	
Goodness-of-fit on F^2	1.030	
Final R indices [I>2sigma(I)]	R1 = 0.0455, wR2 = 0.1056	
R indices (all data)	R1 = 0.0720, wR2 = 0.1210	
Largest diff. peak and hole	1.54 and -0.49 $e.Å^{-3}$	

9.7 $Cu(Br)_3(X2)_2]Br$. (27)

Empirical formula	$C_{42}H_{38}Br_4CuN_6O$	
Formula weight	1025.96	
Temperature	100(2) K	
Wavelength	0.71073 Å	
Crystal system, space group	Monoclinic, C2/c	
Unit cell dimensions	*a* = 13.1236(6) Å	α = 90º
	b = 22.2503(11) Å	β = 101.917(2)º
	c = 13.7765(10) Å	γ = 90º
Volume	3936.1(4) $Å^3$	
Z, Calculated density	4, 1.731 Mg/m^3	
Absorption coefficient	4.658 mm^{-1}	
F(000)	2036	
Crystal size	0.20 x 0.20 x 0.10 mm	
Theta range for data collection	1.83 to 23.29º	
Limiting indices	-14<=h<=14, -24<=k<=24, -15<=l<=11	
Reflections collected / unique	13804 / 2829 [R(int) = 0.0561]	
Completeness to theta = 23.29	99.6 %	
Absorption correction	Empirical	
Max. and min. transmission	0.6530 and 0.4560	
Refinement method	Full-matrix least-squares on F^2	
Data / restraints / parameters	2829 / 0 / 254	
Goodness-of-fit on F^2	1.056	
Final R indices [I>2sigma(I)]	R1 = 0.0553, wR2 = 0.1384	
R indices (all data)	R1 = 0.0776, wR2 = 0.1513	
Largest diff. peak and hole	2.32 and -0.70 $e.Å^{-3}$	

9.8 $C_{96}H_{92}Br_2N_{24}O_{18}Pd_5$. (36)

Empirical formula	$C_{102}H_{114}Br_2C_{112}N_{24}O_{23}Pd_5$	
Formula weight	3161.39	
Temperature	100(2) K	
Wavelength	0.71073 Å	
Crystal system, space group	Triclinic, P-1	
Unit cell dimensions	*a* = 11.9704(6) Å	α = 84.276(2)º
	b = 15.7849(6) Å	β = 86.994(2)º
	c = 21.4407(10) Å	γ = 83.200(2)º
Volume	3999.3(3) $Å^3$	
Z, Calculated density	1, 1.313 Mg/m^3	
Absorption coefficient	1.310 mm^{-1}	
F(000)	1582	
Crystal size	0.20 x 0.10 x 0.10 mm	
Theta range for data collection	1.54 to 25.73º	
Limiting indices	-14<=h<=14, -18<=k<=16, -26<=l<=24	
Reflections collected / unique	34772 / 14352 [R(int) = 0.0389]	
Completeness to theta = 25.73	93.9 %	
Absorption correction	Empirical	
Max. and min. transmission	1.000 and 0.766	
Refinement method	Full-matrix least-squares on F^2	
Data / restraints / parameters	14352 / 2 / 792	
Goodness-of-fit on F^2	1.058	
Final R indices [I>2sigma(I)]	R1 = 0.0869, wR2 = 0.2489	
R indices (all data)	R1 = 0.1335, wR2 = 0.2879	
Largest diff. peak and hole	2.23 and -1.01 $e.A^{-3}$	

9.9 $(35)_2Cu_2Br_2(ClO_4)_4 \cdot 10(CH_3CN)$. (37)

Empirical formula	$C_{100}H_{96}Br_2C_{l4}Cu_2N_{34}O_{16}$
Formula weight	2458.81
Temperature	150(2) K
Wavelength	0.71073 Å
Crystal system, space group	Monoclinic, C2/c
Unit cell dimensions	a = 30.5136(19) Å α = 90º
	b = 13.1914(5) Å β = 106.045(2)º
	c = 29.0711(10) Å γ = 90º
Volume	11245.8(9) $Å^3$
Z, Calculated density	4, 1.452 Mg/m^3
Absorption coefficient	1.262 mm^{-1}
F(000)	5032
Crystal size	0.24 x 0.15 x 0.09 mm
Theta range for data collection	3.17 to 24.50º
Limiting indices	-35<=h<=35, -15<=k<=15, -33<=l<=33
Reflections collected / unique	63979 / 9332 [R(int) = 0.1455]
Completeness to theta = 24.50	99.4 %
Absorption correction	Semi-empirical from equivalents
Max. and min. transmission	0.8949 and 0.7516
Refinement method	Full-matrix least-squares on F^2
Data / restraints / parameters	9332 / 36 / 643
Goodness-of-fit on F^2	0.863
Final R indices [I>2sigma(I)]	R1 = 0.0887, wR2 = 0.1605
R indices (all data)	R1 = 0.1944, wR2 = 0.1938
Largest diff. peak and hole	1.08 and -1.15 $e.Å^{-3}$

9.10 (40)$CuBr_2(C_3H_7NO)$. (41)

Empirical formula	$C_{46}H_{40}Br_4Cu_2N_8O_2$	
Formula weight	1183.58	
Temperature	150(2) K	
Wavelength	0.71073 Å	
Crystal system, space group	Triclinic, P-1	
Unit cell dimensions	*a* = 9.7488(5) Å	α = 72.531(2)º
	b = 9.7736(3) Å	β = 70.911(2)º
	c = 12.7109(6) Å	γ = 85.395(2) º
Volume	1091.51(8) A^3	
Z, Calculated density	1, 1.801 Mg/m^3	
Absorption coefficient	4.685 mm^{-1}	
F(000)	586	
Crystal size	0.20 x 0.20 x 0.16 mm	
Theta range for data collection	2.38 to 25.00º	
Limiting indices	-11<=h<=11, -11<=k<=11, -15<=l<=15	
Reflections collected / unique	15111 / 3834 [R(int) = 0.1354]	
Completeness to theta = 25.00	99.7 %	
Absorption correction	Empirical	
Max. and min. transmission	0.5211 and 0.4543	
Refinement method	Full-matrix least-squares on F^2	
Data / restraints / parameters	3834 / 0 / 282	
Goodness-of-fit on F^2	1.005	
Final R indices [I>2sigma(I)]	R1 = 0.0571, wR2 = 0.0633	
R indices (all data)	R1 = 0.1561, wR2 = 0.0813	
Largest diff. peak and hole	0.70 and -0.76 $e.Å^{-3}$	

9.11 (40)$PdCl_2$·$(CH_3)_2SO$. (42)

Empirical formula	$C_{22}H_{19}C_{l2}N_3OPdS$
Formula weight	550.76
Temperature	100(2) K
Wavelength	0.71073 Å
Crystal system, space group	Monoclinic, P2(1)/c
Unit cell dimensions	*a* = 8.3924(4) Å α = 90º
	b = 28.1425(16) Å β = 100.234(2)º
	c = 8.8627(5) Å γ = 90º
Volume	2059.92(19) $Å^3$
Z, Calculated density	4, 1.776 Mg/m^3
Absorption coefficient	1.282 mm^{-1}
F(000)	1104
Crystal size	0.20 x 0.12 x 0.08 mm
Theta range for data collection	1.45 to 26.00º
Limiting indices	-10<=h<=10, -34<=k<=25, -10<=l<=10
Reflections collected / unique	16645 / 4031 [R(int) = 0.0218]
Completeness to theta = 26.00	99.6 %
Absorption correction	Empirical
Max. and min. transmission	0.9044 and 0.7835
Refinement method	Full-matrix least-squares on F^2
Data / restraints / parameters	4031 / 0 / 347
Goodness-of-fit on F^2	1.127
Final R indices [I>2sigma(I)]	R1 = 0.0213, wR2 = 0.0503
R indices (all data)	R1 = 0.0229, wR2 = 0.0513
Largest diff. peak and hole	0.46 and -0.47 $e.Å^{-3}$

9.12 $(40)_2AgNO_3 \cdot 3(CH_3OH)$. (43)

Empirical formula	$C_{43}H_{38}AgN_7O_6$	
Formula weight	856.67	
Temperature	150(2) K	
Wavelength	0.71073 Å	
Crystal system, space group	Triclinic, P-1	
Unit cell dimensions	a = 9.2718(8) Å	α = 106.440(5)º
	b = 14.6570(14) Å	β = 100.856(5)º
	c = 15.2653(15) Å	γ = 102.997(5)º
Volume	1866.9(3) $Å^3$	
Z, Calculated density	2, 1.524 Mg/m^3	
Absorption coefficient	0.601 mm^{-1}	
F(000)	880	
Crystal size	0.18 x 0.13 x 0.10 mm	
Theta range for data collection	1.44 to 18.89º	
Limiting indices	-8<=h<=8, -13<=k<=13, -13<=l<=13	
Reflections collected / unique	12363 / 2932 [R(int) = 0.0775]	
Completeness to theta = 18.89	99.2 %	
Absorption correction	Empirical	
Max. and min. transmission	0.9423 and 0.8995	
Refinement method	Full-matrix least-squares on F^2	
Data / restraints / parameters	2932 / 3 / 408	
Goodness-of-fit on F^2	1.079	
Final R indices [I>2sigma(I)]	R1 = 0.0634, wR2 = 0.1661	
R indices (all data)	R1 = 0.0985, wR2 = 0.1893	
Largest diff. peak and hole	1.09 and -0.42 $e.Å^{-3}$	

9.13 $(40)_4Co_20H(BF_4)_3.2MeCN$ (44)

Empirical formula	$C_{84}H_{59}B_3Co_2F_{12}N_{14}O$	
Formula weight	1658.74	
Temperature	150(2) K	
Wavelength	0.71073 Å	
Crystal system, space group	Monoclinic, Cc	
Unit cell dimensions	*a* = 26.6212(9) Å	α = 90º
	b = 16.3359(5) Å	β = 121.898(3)º
	c = 19.8259(5) Å	γ = 90º
Volume	7319.9(4) $Å^3$	
Z, Calculated density	4, 1.505 Mg/m^3	
Absorption coefficient	0.545 mm^{-1}	
F(000)	3384	
Crystal size	0.20 x 0.16 x 0.13 mm	
Theta range for data collection	3.25 to 26.00º	
Limiting indices	-32<=h<=18, -18<=k<=20, -23<=l<=24	
Reflections collected / unique	14700 / 8959 [R(int) = 0.0378]	
Completeness to theta = 26.00	96.3 %	
Absorption correction	Semi-empirical from equivalents	
Max. and min. transmission	0.9326 and 0.8989	
Refinement method	Full-matrix least-squares on F^2	
Data / restraints / parameters	8959 / 24 / 1026	
Goodness-of-fit on F^2	0.990	
Final R indices [I>2sigma(I)]	R1 = 0.0507, wR2 = 0.1204	
R indices (all data)	R1 = 0.0675, wR2 = 0.1287	
Absolute structure parameter	0.006(16)	
Largest diff. peak and hole	1.08 and -0.50 $e.Å^{-3}$	

9.14 2,3-Dihydro-12H-pyrrolo[1,2-f]phenanthridine-1,1-dicarbonitrile. (47)

Empirical formula	$C_{18}H_{13}N_3$	
Formula weight	271.31	
Temperature	150(2) K	
Wavelength	0.71073 Å	
Crystal system, space group	Monoclinic, P2(1)/c	
Unit cell dimensions	*a* = 17.8112(8) Å	α = 90º
	b = 6.4552(3) Å	β = 99.737(4)º
	c = 11.8419(5) Å	γ = 90º
Volume	1341.91(10) $Å^3$	
Z, Calculated density	4, 1.343 Mg/m^3	
Absorption coefficient	0.082 mm^{-1}	
F(000)	568	
Crystal size	0.13 x 0.09 x 0.05 mm	
Theta range for data collection	3.48 to 25.04º	
Limiting indices	-21<=h<=21, -7<=k<=7, -14<=l<=14	
Reflections collected / unique	7905 / 2354 [R(int) = 0.0743]	
Completeness to theta =	25.04 99.0 %	
Absorption correction	Analytical	
Max. and min. transmission	0.997 and 0.992	
Refinement method	Full-matrix least-squares on F^2	
Data / restraints / parameters	2354 / 0 / 190	
Goodness-of-fit on F^2	0.775	
Final R indices [I>2sigma(I)]	R1 = 0.0421, wR2 = 0.0671	
R indices (all data)	R1 = 0.0960, wR2 = 0.0746	
Largest diff. peak and hole	0.14 and -0.16 $e.Å^{-3}$	

9.15 2,3-Dihydro-12H-pyrrolo[1,2-f]phenanthridine-1-indan-1,3-dione.(48)

Empirical formula	$C_{24}H_{17}NO_2$	
Formula weight	351.39	
Temperature	150(2) K	
Wavelength	0.71073 Å	
Crystal system, space group	Triclinic, P-1	
Unit cell dimensions	*a* = 6.2544(4) Å	α = 98.758(4)º
	b = 11.5568(8) Å	β = 97.634(4)º
	c = 11.9526(6) Å	γ = 97.453(3)º
Volume	836.33(9) $Å^3$	
Z, Calculated density	2, 1.395 Mg/m^3	
Absorption coefficient	0.089 mm^{-1}	
F(000)	368	
Crystal size	0.28 x 0.14 x 0.14 mm	
Theta range for data collection	1.75 to 25.48º	
Limiting indices	-7<=h<=7, -13<=k<=13, -14<=l<=14	
Reflections collected / unique	10103 / 3106 [R(int) = 0.0427]	
Completeness to theta = 25.48	99.6 %	
Absorption correction	Empirical	
Max. and min. transmission	0.9877 and 0.9756	
Refinement method	Full-matrix least-squares on F^2	
Data / restraints / parameters	3106 / 0 / 244	
Goodness-of-fit on F^2	1.061	
Final R indices [I>2sigma(I)]	R1 = 0.0481, wR2 = 0.0909	
R indices (all data)	R1 = 0.1007, wR2 = 0.1075	
Largest diff. peak and hole	0.20 and -0.23 $e.Å^{-3}$	

Publications

The following articles and communications were published, or are in preparation as a result of work undertaken over the course of this Ph.D. programme.

- "A New C-C Bond Forming Annulation Reaction Leading to pH Switchable Organic Materials" P. J. Kitson, A. D. C. Parenty, D.-L. Long, C. J. Richmond and L. Cronin, **2009,** *in press.*
- "The Design and Synthesis of a New Imidazo-Phenanthridine Based 2,2'-Bipyridine Analogue for Inorganic Crystal Engineering" P. J. Kitson, Y.-F. Song, D.-L. Long, A. D. C. Parenty, and L. Cronin **2009** *in preparation*
- "Metal-Mediated Transformation of a Triazinephenanthridinium Ligand Leading to a {Pd5} Coordination Complex Observed Crystallographically and by Cryospray Mass Spectrometry" P. J. Kitson, Y.-F. Song, P. Gamez, P. de Hoog, D.-L. Long, A. D. C. Parenty,J. Reedijk, and L. Cronin, *Inog. Chem.* **2008**, 47, (6), 1883-1885.
- "Supramolecular self-assembly and anion-dependence of copper(II) complexes with cationic dihydro-imidazo phenanthridinium (DIP)-containing ligands" Y.-F. Song, P. J. Kitson, D.-L. Long, A. D. C. Parenty, R. J. Thatcher and L. Cronin, Crystengcomm, **2008**, 10, 1243-1251.

Appendix – ^{1}H NMR of Selected Compounds

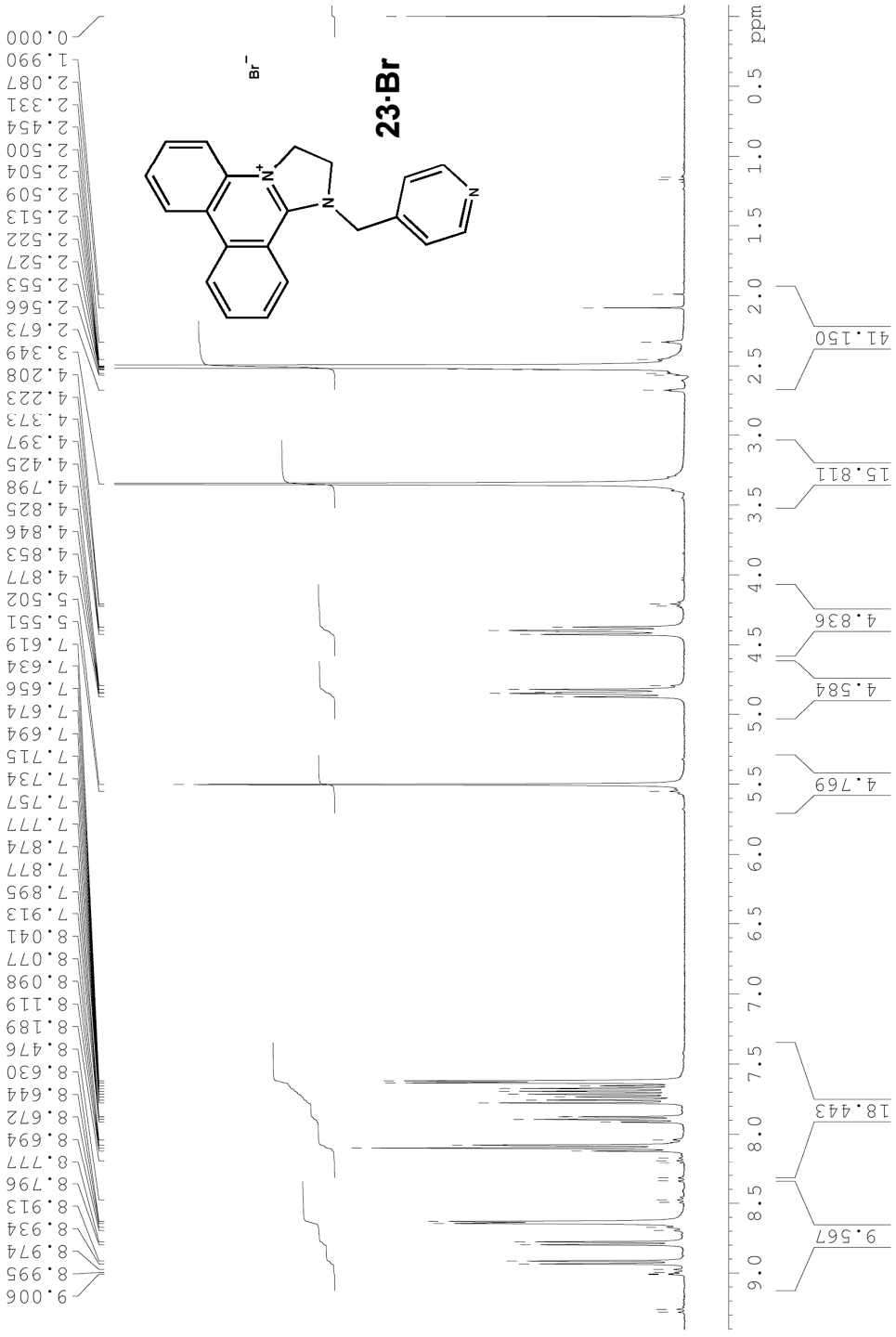
23·Br
Br⁻
ppm
41.150
15.811
4.836
4.584
4.769
18.443
9.567

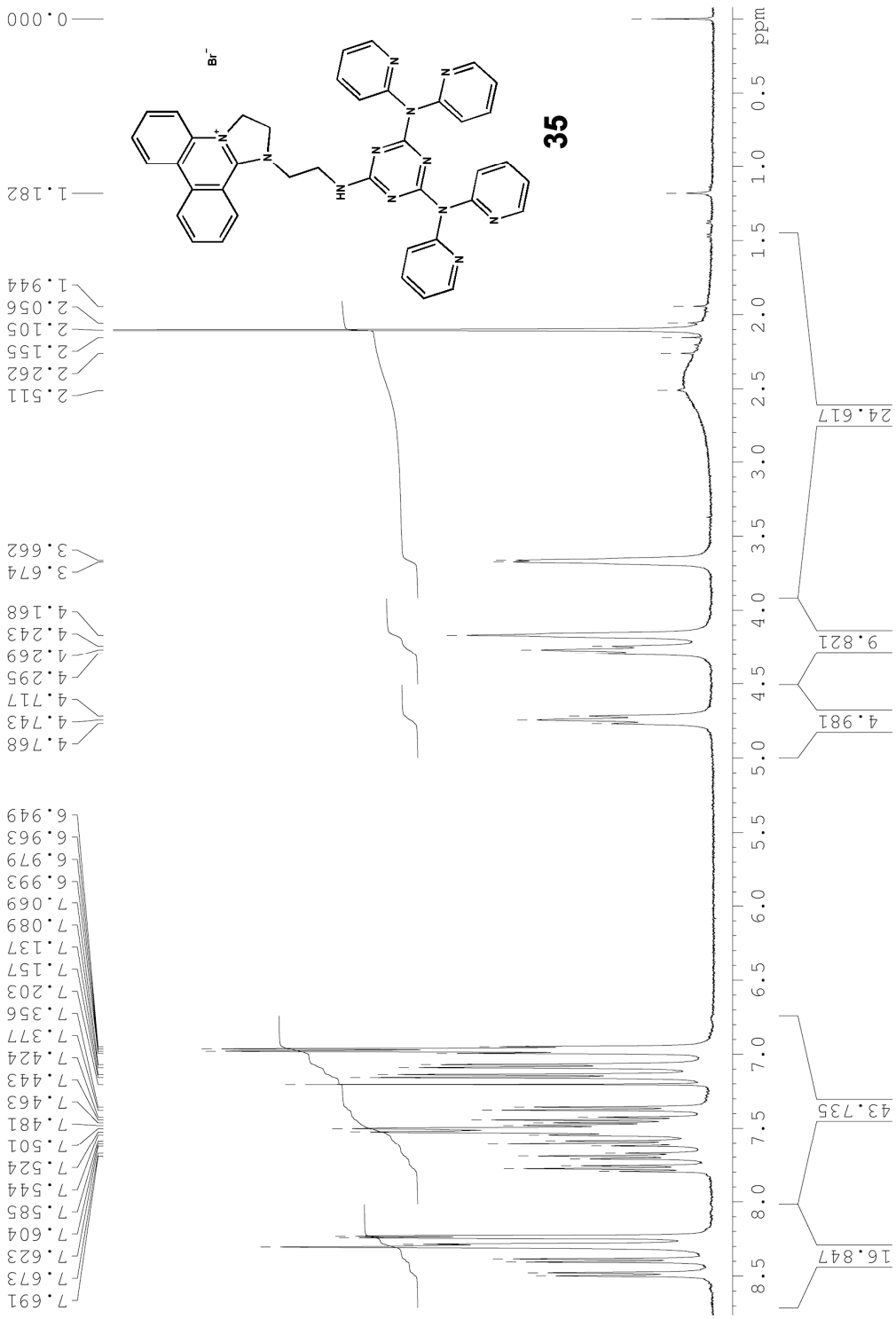
35
Br⁻
HN
ppm
0.000
1.182
1.944
2.056
2.105
2.155
2.262
2.511
3.662
3.674
4.168
4.243
4.269
4.295
4.717
4.743
4.768
6.949
6.963
6.979
6.993
7.069
7.089
7.137
7.157
7.203
7.356
7.377
7.424
7.443
7.463
7.481
7.501
7.524
7.544
7.585
7.604
7.623
7.673
7.691
24.617
9.821
4.981
43.735
16.847

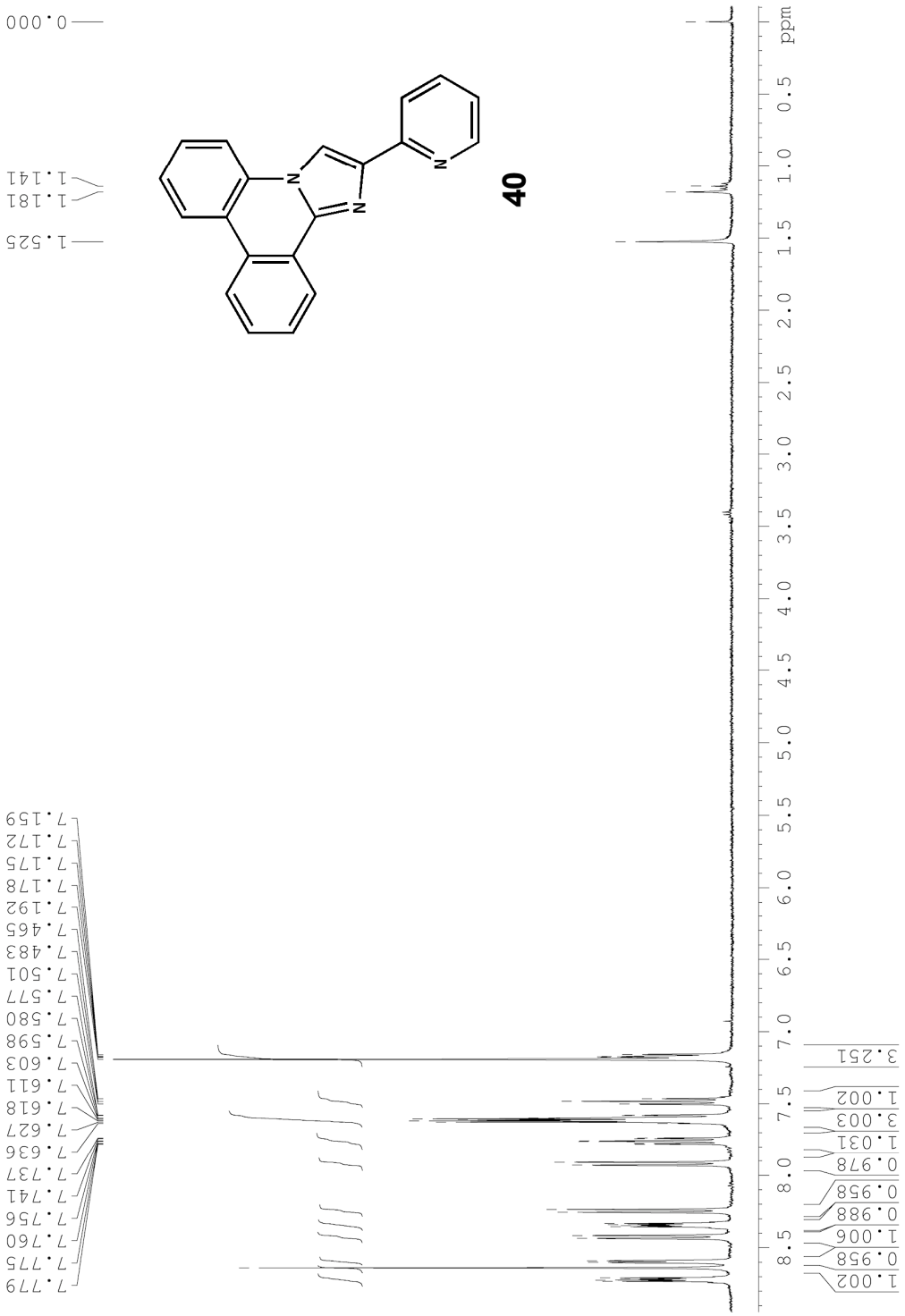
40
ppm
0.000
1.141
1.181
1.525
7.159
7.172
7.175
7.178
7.192
7.465
7.483
7.501
7.577
7.580
7.598
7.603
7.611
7.618
7.627
7.636
7.737
7.741
7.756
7.760
7.775
7.779
1.002
0.958
1.006
0.988
0.958
0.978
1.031
3.003
1.002
3.251

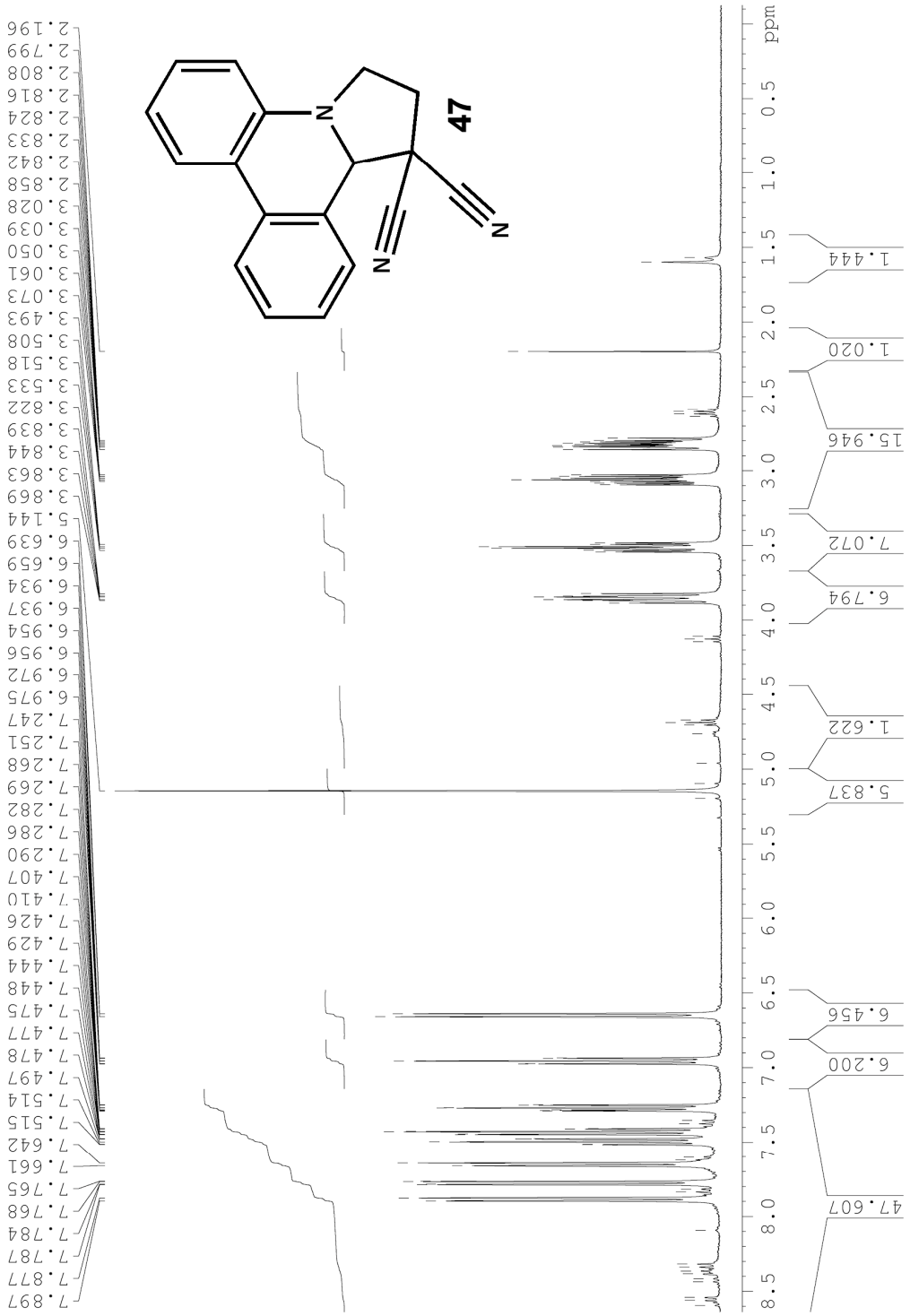
47
N
N
N
ppm
0.5
1.0
1.5
2.0
2.5
3.0
3.5
4.0
4.5
5.0
5.5
6.0
6.5
7.0
7.5
8.0
8.5
1.444
1.020
15.946
7.072
6.794
1.622
5.837
6.456
6.200
47.607
2.196
2.799
2.808
2.816
2.824
2.833
2.842
2.858
3.028
3.039
3.050
3.061
3.073
3.493
3.508
3.518
3.533
3.822
3.839
3.844
3.863
3.869
5.144
6.639
6.659
6.934
6.937
6.954
6.956
6.972
6.975
7.247
7.251
7.268
7.269
7.282
7.286
7.290
7.407
7.410
7.426
7.429
7.444
7.448
7.475
7.477
7.478
7.497
7.514
7.515
7.642
7.661
7.765
7.768
7.784
7.787
7.877
7.897

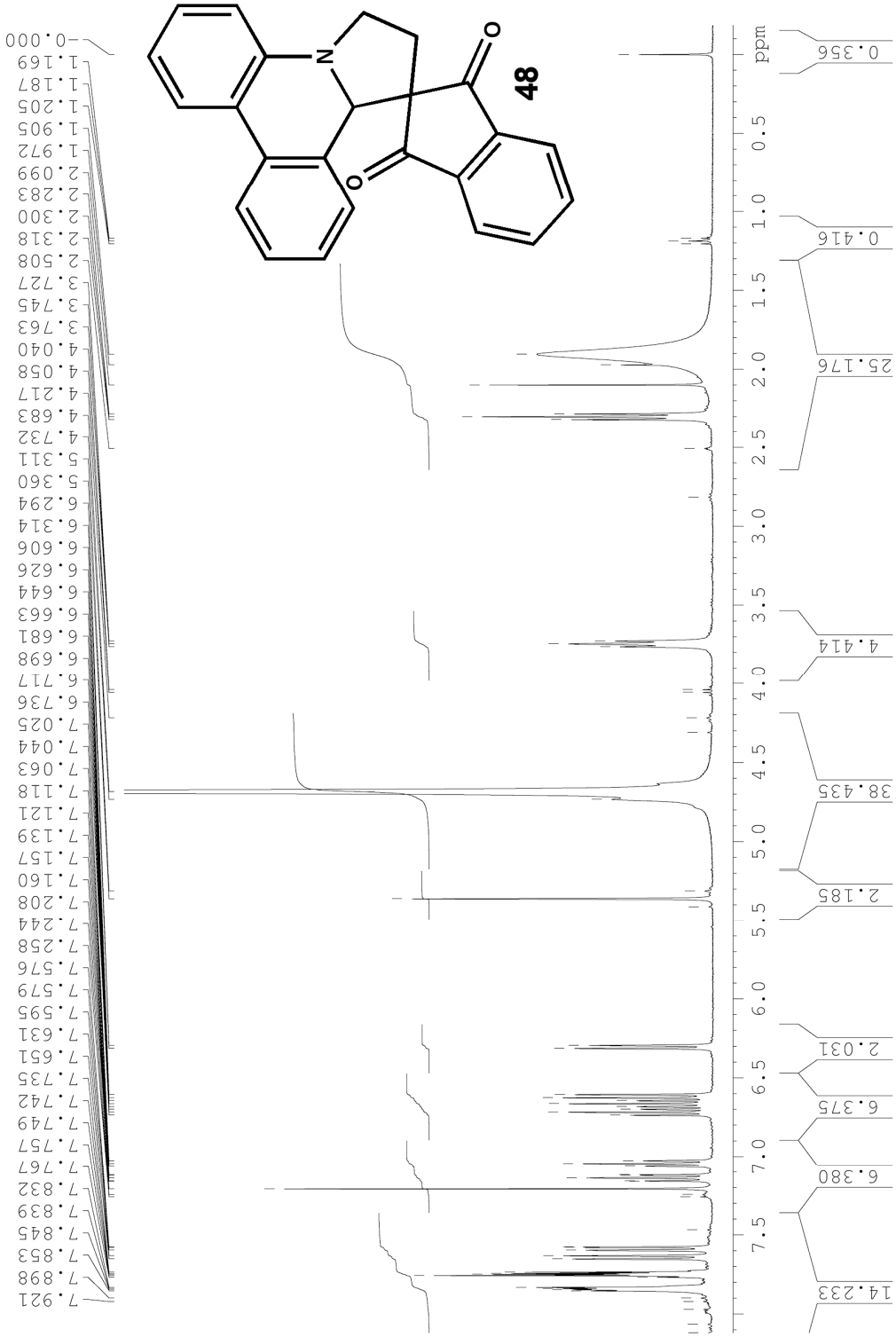
48
N
O
O
ppm
0.5
1.0
1.5
2.0
2.5
3.0
3.5
4.0
4.5
5.0
5.5
6.0
6.5
7.0
7.5
0.356
0.416
25.176
4.414
38.435
2.185
2.031
6.375
6.380
14.233
0.000
1.169
1.187
1.205
1.905
1.972
2.099
2.283
2.300
2.318
2.508
3.727
3.745
3.763
4.040
4.058
4.217
4.683
4.732
5.311
5.360
6.294
6.314
6.606
6.626
6.644
6.663
6.681
6.698
6.717
6.736
7.025
7.044
7.063
7.118
7.121
7.139
7.157
7.160
7.208
7.244
7.258
7.576
7.579
7.595
7.631
7.651
7.735
7.742
7.749
7.757
7.767
7.832
7.839
7.845
7.853
7.898
7.921


49
Br⁻
N⁺
N
N
ppm
1
2
3
4
5
6
7
8
9
10
1.208
2.997
3.016
3.035
3.161
3.330
3.334
3.338
3.342
3.346
3.377
3.510
3.867
4.856
4.908
4.957
4.987
5.221
5.428
5.447
5.466
8.148
8.150
8.168
8.173
8.176
8.186
8.188
8.191
8.194
8.212
8.214
8.232
8.236
8.251
8.254
8.258
8.272
8.276
8.454
8.457
8.472
8.475
8.478
8.493
8.496
8.593
9.178
0.210
23.429
0.223
17.897
8.940
13.148
13.498
9.030
4.448

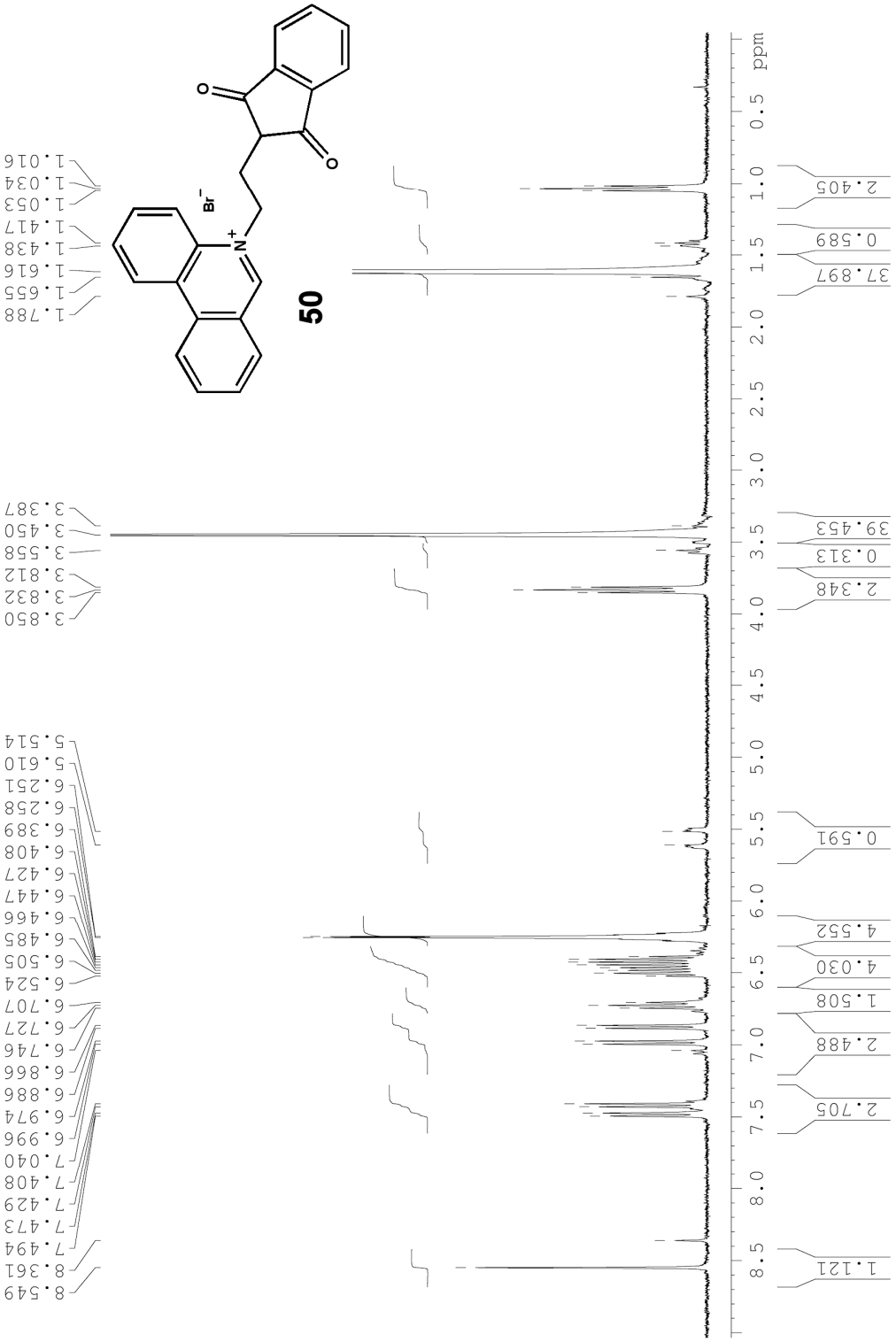
50
Br⁻
N⁺
O
O
ppm
0.5
1.0
1.5
2.0
2.5
3.0
3.5
4.0
4.5
5.0
5.5
6.0
6.5
7.0
7.5
8.0
8.5
2.405
0.589
37.897
39.453
0.313
2.348
0.591
4.552
4.030
1.508
2.488
2.705
1.121
1.016
1.034
1.053
1.417
1.438
1.616
1.655
1.788
3.387
3.450
3.558
3.812
3.832
3.850
5.514
5.610
6.251
6.258
6.389
6.408
6.427
6.447
6.466
6.485
6.505
6.524
6.707
6.727
6.746
6.866
6.886
6.974
6.996
7.040
7.408
7.429
7.473
7.494
8.361
8.549

References

1. Fisher, E. *Ber. Deutsch. Chem. Ges.* **1894,** 27, 2985.
2. Lehn, J. M. *Pure Appl. Chem.* **1978,** 50, (9-10), 871-892.
3. Lagona, J.; Mukhopadhyay, P.; Chakrabarti, S.; Isaacs, L. *Angew. Chem. Int. Ed.* **2005,** 44, (31), 4844-4870.
4. Smejkal, T.; Breit, B. *Angew. Chem. Int. Ed.* **2008,** 47, (21), 3946-3949.
5. Pedersen, C. J. *J. Am. Chem. Soc.* **1967,** 89, (26), 7017-&.
6. Dietrich, B.; Lehn, J. M.; Sauvage, J. P. *Tetrahedron Lett.* **1969**, (34), 2889-&.
7. Lehn, J. M., *Supramolecular Chemistry: Concepts and Perspectives*. VCH: Weinheim, 1995.
8. Richman, J. E.; Atkins, T. J. *J. Am. Chem. Soc.* **1974,** 96, (7), 2268-2270.
9. Blake, A. J.; Champness, N. R.; Hubberstey, P.; Li, W. S.; Withersby, M. A.; Schröder, M. *Coord. Chem. Rev.* **1999,** 183, 117-138.
10. Janiak, C. *Dalton Trans.* **2003**, (14), 2781-2804.
11. Balzani, V.; Gomez-Lopez, M.; Stoddart, J. F. *Acc. Chem. Res.* **1998,** 31, (7), 405-414.
12. Fyfe, M. C. T.; Stoddart, J. F. *Acc. Chem. Res.* **1997,** 30, (10), 393-401.
13. Steed, J. W., Atwood J. L., *Supramolecular Chemistry*. John Wiley & Sons, Ltd: Chichester, 2000.
14. Housecroft, C. E., Sharpe, A.G., *Inorganic Chemistry*. Pearson Education Limited: Harlow, 2001.
15. Orgel, L. E., *An introduction to Transition Metal Chemistry*. Methuen & Co Ltd: London, 1966.
16. Cotton, F. A.; Wilkinson, G., *Advanced Inorganic Chemistry*. John Wiley & Sons, Ltd: Chichester, 1988.
17. Wilkinson, G.; Rosenblum, M.; Whiting, M. C.; Woodward, R. B. *J. Am. Chem. Soc.* **1952,** 74, (8), 2125-2126.
18. Dougherty, D. A. *Science* **1996,** 271, (5246), 163-168.
19. Ma, J. C.; Dougherty, D. A. *Chem. Rev.* **1997,** 97, (5), 1303-1324.
20. Sunner, J.; Nishizawa, K.; Kebarle, P. *J. Phys. Chem.* **1981,** 85, (13), 1814-1820.
21. Lee, J. Y.; Lee, S. J.; Choi, H. S.; Cho, S. J.; Kim, K. S.; Ha, T. K. *Chem. Phys. Lett.* **1995,** 232, (1-2), 67-71.

22. Schneider, H. J. *Angew. Chem. Int. Ed.* **1991,** 30, (11), 1417-1436.
23. Kim, K. S.; Lee, J. Y.; Lee, S. J.; Ha, T. K.; Kim, D. H. *J. Am. Chem. Soc.* **1994,** 116, (16), 7399-7400.
24. Mecozzi, S.; West, A. P.; Dougherty, D. A. *J. Am. Chem. Soc.* **1996,** 118, (9), 2307-2308.
25. Gotz, R. J.; Robertazzi, A.; Mutikainen, I.; Turpeinen, U.; Gamez, P.; Reedijk, J. *Chem. Commun.* **2008**, (29), 3384-3386.
26. de Hoog, P.; Gamez, P.; Mutikainen, H.; Turpeinen, U.; Reedijk, J. *Angew. Chem. Int. Ed.* **2004,** 43, (43), 5815-5817.
27. Demeshko, S.; Dechert, S.; Meyer, F. *J. Am. Chem. Soc.* **2004,** 126, (14), 4508-4509.
28. Desiraju, G. R. *Acc. Chem. Res.* **2002,** 35, (7), 565-573.
29. Kobayashi, Y.; Saigo, K. *J. Am. Chem. Soc.* **2005,** 127, (43), 15054-15060.
30. Meyer, E. A.; Castellano, R. K.; Diederich, F. *Angew. Chem. Int. Ed.* **2003,** 42, (11), 1210-1250.
31. Muller-Dethlefs, K.; Hobza, P. *Chem. Rev.* **2000,** 100, (1), 143-167.
32. Calhorda, M. J. *Chem. Commun.* **2000**, (10), 801-809.
33. Malone, J. F.; Murray, C. M.; Charlton, M. H.; Docherty, R.; Lavery, A. J. *J. Chem. Soc.-Faraday Trans.* **1997,** 93, (19), 3429-3436.
34. Pickering, A. L.; Seeber, G.; Long, D. L.; Cronin, L. *Crystengcomm* **2005,** 7, 504-510.
35. Desiraju, G. R. *Science* **1997,** 278, (5337), 404-405.
36. McGaughey, G. B.; Gagne, M.; Rappe, A. K. *J. Biol. Chem.* **1998,** 273, (25), 15458-15463.
37. Steiner, T.; Koellner, G. *J. Mol. Biol.* **2001,** 305, (3), 535-557.
38. Burley, S. K.; Petsko, G. A. *Science* **1985,** 229, (4708), 23-28.
39. Watson, J. D.; Crick, F. H. C. *Nature* **1953,** 171, (4356), 737-738.
40. Hunter, C. A.; Lawson, K. R.; Perkins, J.; Urch, C. J. *J. Chem. Soc.-Perkin Trans. 2* **2001**, (5), 651-669.
41. Blanchard, M. D.; Hughes, R. P.; Concolino, T. E.; Rheingold, A. L. *Chem. Mat.* **2000,** 12, (6), 1604-1610.
42. Breault, G. A.; Hunter, C. A.; Mayers, P. C. *J. Am. Chem. Soc.* **1998,** 120, (14), 3402-3410.

43. Hunter, C. A.; Sanders, J. K. M. *J. Am. Chem. Soc.* **1990,** 112, (14), 5525-5534.
44. Janiak, C. *J. Chem. Soc.-Dalton Trans.* **2000**, (21), 3885-3896.
45. Hobza, P.; Selzle, H. L.; Schlag, E. W. *J. Phys. Chem.* **1996,** 100, (48), 18790-18794.
46. Desiraju, G. R. *Acc. Chem. Res.* **1996,** 29, (9), 441-449.
47. MacGillivray, L. R.; Atwood, J. L. *Nature* **1997,** 389, (6650), 469-472.
48. Hof, F.; Craig, S. L.; Nuckolls, C.; Rebek, J. *Angew. Chem. Int. Ed.* **2002,** 41, (9), 1488-1508.
49. Rebek, J. *Angew. Chem. Int. Ed.* **1990,** 29, (3), 245-255.
50. Harada, A.; Li, J.; Kamachi, M. *Nature* **1992,** 356, (6367), 325-327.
51. Harada, A.; Li, J.; Kamachi, M. *Nature* **1994,** 370, (6485), 126-128.
52. Choi, H. J.; Suh, M. P. *J. Am. Chem. Soc.* **1998,** 120, (41), 10622-10628.
53. Robson, R. *J. Chem. Soc.-Dalton Trans.* **2000**, (21), 3735-3744.
54. Caulder, D. L.; Raymond, K. N. *J. Chem. Soc.-Dalton Trans.* **1999**, (8), 1185-1200.
55. Kondo, M.; Okubo, T.; Asami, A.; Noro, S.; Yoshitomi, T.; Kitagawa, S.; Ishii, T.; Matsuzaka, H.; Seki, K. *Angew. Chem. Int. Ed.* **1999,** 38, (1-2), 140-143.
56. Saalfrank, R. W.; Bernt, I.; Uller, E.; Hampel, F. *Angew. Chem. Int. Ed.* **1997,** 36, (22), 2482-2485.
57. Leininger, S.; Olenyuk, B.; Stang, P. J. *Chem. Rev.* **2000,** 100, (3), 853-907.
58. Stricklen, P. M.; Volcko, E. J.; Verkade, J. G. *J. Am. Chem. Soc.* **1983,** 105, (8), 2494-2495.
59. Fujita, M. *Chem. Soc. Rev.* **1998,** 27, (6), 417-425.
60. Baxter, P. N. W.; Lehn, J. M.; Kneisel, B. O.; Baum, G.; Fenske, D. *Chem.-Eur. J.* **1999,** 5, (1), 113-120.
61. Fujita, M.; Umemoto, K.; Yoshizawa, M.; Fujita, N.; Kusukawa, T.; Biradha, K. *Chem. Commun.* **2001**, (6), 509-518.
62. Umemoto, K.; Tsukui, H.; Kusukawa, T.; Biradha, K.; Fujita, M. *Angew. Chem. Int. Ed.* **2001,** 40, (14), 2620-2622.
63. Yoshizawa, M.; Takeyama, Y.; Kusukawa, T.; Fujita, M. *Angew. Chem. Int. Ed.* **2002,** 41, (8), 1347-1349.
64. Yoshizawa, M.; Tamura, M.; Fujita, M. *Science* **2006,** 312, (5771), 251-254.
65. Blake, A. J.; Brooks, N. R.; Champness, N. R.; Hanton, L. R.; Hubberstey, P.; Schröder, M. *Pure Appl. Chem.* **1998,** 70, (12), 2351-2357.

66. Casellas, H.; Gamez, P.; Reedijk, J.; Massera, C. *Polyhedron* **2006,** 25, (15), 2959-2966.

67. Miller, P.; Nieuwenhuyzen, M.; Charmant, J. P. H.; James, S. L. *Crystengcomm* **2004,** 6, 408-412.

68. Yu, Y. F.; Wei, Y. Q.; Broer, R.; Sa, R. J.; Wu, K. C. *J. Solid State Chem.* **2008,** 181, (3), 539-551.

69. Gamez, P.; de Hoog, P.; Roubeau, O.; Lutz, M.; Driessen, W. L.; Spek, A. L.; Reedijk, J. *Chem. Commun.* **2002**, (14), 1488-1489.

70. Dunitz, J., *Perspectives in Supramolecular Chemistry: The Crystal as a Supramolecular Entity*. John Wiley & Sons, Ltd: Chichester, 1996.

71. Berman, H. M.; Battistuz, T.; Bhat, T. N.; Bluhm, W. F.; Bourne, P. E.; Burkhardt, K.; Iype, L.; Jain, S.; Fagan, P.; Marvin, J.; Padilla, D.; Ravichandran, V.; Schneider, B.; Thanki, N.; Weissig, H.; Westbrook, J. D.; Zardecki, C. *Acta Crystallogr. Sect. D-Biol. Crystallogr.* **2002,** 58, 899-907.

72. Vyas, N. K.; Vyas, M. N.; Quiocho, F. A. *Science* **1988,** 242, (4883), 1290-1295.

73. Allen, F. H. *Acta Crystallogr. Sect. B-Struct. Sci.* **2002,** 58, 380-388.

74. Belsky, A.; Hellenbrandt, M.; Karen, V. L.; Luksch, P. *Acta Crystallogr. Sect. B-Struct. Sci.* **2002,** 58, 364-369.

75. Dunitz, J. D.; Gavezzotti, A. *Acc. Chem. Res.* **1999,** 32, (8), 677-684.

76. Gavezzotti, A. *Synlett* **2002**, (2), 201-214.

77. Parkin, A.; Barr, G.; Dong, W.; Gilmore, C. J.; Jayatilaka, D.; McKinnon, J. J.; Spackman, M. A.; Wilson, C. C. *Crystengcomm* **2007,** 9, (8), 648-652.

78. Desiraju, G. R., *Crystal engineering: the design of organic solids*. Elsevier: Amsterdam, 1989.

79. Cox, E. G.; Cruickshank, D. W. J.; Smith, J. A. S. **1958,** 247, (1248), 1-21.

80. Desiraju, G. R.; Gavezzotti, A. *Acta Crystallogr. Sect. B-Struct. Commun.* **1989,** 45, 473-482.

81. Ebel, A.; Donaubauer, W.; Hampel, F.; Hirsch, A. *Eur. J. Org. Chem.* **2007**, (21), 3488-3494.

82. Du, M.; Li, C. P.; Zhao, X. J.; Yu, Q. *Crystengcomm* **2007,** 9, (11), 1011-1028.

83. Wang, X. J.; Gui, L. C.; Ni, Q. L.; Liao, Y. F.; Jiang, X. F.; Tang, L. H.; Zhang, Z.; Wu, Q. *Crystengcomm* **2008,** 10, (8), 1003-1010.

84. Chang, Y. C.; Chen, Y. D.; Chen, C. H.; Wen, Y. S.; Lin, J. T.; Chen, H. Y.; Kuo, M. Y.; Chao, I. *J. Org. Chem.* **2008,** 73, (12), 4608-4614.

85. Alcock, N. W.; Barker, P. R.; Haider, J. M.; Hannon, M. J.; Painting, C. L.; Pikramenou, Z.; Plummer, E. A.; Rissanen, K.; Saarenketo, P. *J. Chem. Soc.-Dalton Trans.* **2000,** 9, (9), 1447-1461.

86. Roesky, H. W.; Andruh, M. *Coord. Chem. Rev.* **2003,** 236, (1-2), 91-119.

87. Munakata, M.; Dai, J.; Maekawa, M.; Takayoshi, K. S.; Fukui, J. T. *J. Chem. Soc.-Chem. Commun.* **1994**, (20), 2331-2332.

88. Biradha, K.; Sarkar, M.; Rajput, L. *Chem. Commun.* **2006**, (40), 4169-4179.

89. Zaworotko, M. J. *Chem. Commun.* **2001**, (01), 1-9.

90. Yaghi, O. M.; Li, H. L.; Groy, T. L. *Inorg. Chem.* **1997,** 36, (20), 4292-4293.

91. Chen, X. M.; Liu, G. F. *Chem.-Eur. J.* **2002,** 8, (20), 4811-4817.

92. Katritzky, A. R.; Rees, C. W., *Comprehensive Heterocyclic Chemistry*. Pergamon Press: New York, 1984.

93. Pozharskii, A. F.; Soldatenkov, A. T.; Katritzky, A. R., *Heterocycles in Life and Society*. John Wiley & Sons, Ltd: Chichester, 1997.

94. Davies, D. T., *Aromatic Heterocyclic Chemistry*. Oxford University Press: Oxford, 1992.

95. Maxwell, J. C.; Caughey, W. S. *Biochemistry* **1976,** 15, (2), 388-396.

96. Katritzky, A. R.; Lam, J. N. *Heterocycles* **1992,** 33, (2), 1011-1049.

97. Dupriest, M. T.; Schmidt, C. L.; Kuzmich, D.; Williams, S. B. *J. Org. Chem.* **1986,** 51, (11), 2021-2023.

98. Yamanaka, H.; Ohba, S. *Heterocycles* **1990,** 31, (5), 895-909.

99. Hanessian, S.; Kagotani, M. *Synthesis* **1987**, (4), 409-411.

100. Weber, H. *Adv. Heterocycl. Chem.* **1987,** 41, 275-317.

101. Thiessen, L. M.; Lepoivre, J. A.; Alderwei.Fc. *Tetrahedron Lett.* **1974**, (1), 59-62.

102. Lunn, G.; Sansone, E. B. *J. Org. Chem.* **1986,** 51, (4), 513-517.

103. Anderson, P. S.; Krueger, W. E.; Lyle, R. E. *Tetrahedron Lett.* **1965**, (45), 4011-&.

104. Lodish, H.; Baltimore, D.; Berk, A.; Zipursky, S. L.; Matsudaira, P.; Darnell, J., *Molecular Cell Biology*. W.H. Freeman: New York, 2000.

105. Whittaker, J.; McFadyen, W. D.; Wickham, G.; Wakelin, L. P. G.; Murray, V. *Nucleic Acids Res.* **1998,** 26, (17), 3933-3939.

106. Whittaker, J.; McFadyen, W. D.; Baguley, B. C.; Murray, V. *Anti-Cancer Drug Des.* **2001,** 16, (2-3), 81-89.

107. Brana, M. F.; Cacho, M.; Gradillas, A.; de Pascual-Teresa, B.; Ramos, A. *Curr. Pharm. Design* **2001,** 7, (17), 1745-1780.

108. Nicolaou, K. C.; Huang, X.; Giuseppone, N.; Rao, P. B.; Bella, M.; Reddy, M. V.; Snyder, S. A. *Angew. Chem. Int. Ed.* **2001,** 40, (24), 4705-+.

109. Lerman, L. S. *J. Mol. Biol.* **1961,** 3, (1), 18-&.

110. Smith, L. V.; Parenty, A. D. C.; Guthrie, K. M.; Plumb, J.; Brown, R.; Cronin, L. *Chembiochem* **2006,** 7, (11), 1757-1763.

111. Parenty, A. D. C.; Cronin, L. *Synthesis-Stuttgart* **2008**, (1), 155-160.

112. Yang, L.; Powell, D. R.; Houser, R. P. *Dalton Trans.* **2007**, (9), 955-964.

113. Addison, A. W.; Rao, T. N.; Reedijk, J.; Vanrijn, J.; Verschoor, G. C. *J. Chem. Soc.-Dalton Trans.* **1984**, (7), 1349-1356.

114. Neumann, R.; Assael, I. *J. Chem. Soc.-Chem. Commun.* **1988**, (19), 1285-1287.

115. Mohan, K.; Narender, N.; Srinivasu, P.; Kulkarni, S. J.; Raghavan, K. V. *Synth. Commun.* **2004,** 34, (12), 2143-2152.

116. Ganchegui, B.; Leitner, W. *Green Chem.* **2007,** 9, (1), 26-29.

117. Conte, V.; Floris, B.; Galloni, P.; Silvagni, A. *Pure Appl. Chem.* **2005,** 77, (9), 1575-1581.

118. Pickardt, J. *Z.Naturforsch.(B)* **1982,** 37, (1), 110-111.

119. Fenske, D.; Steiner, K.; Dehnicke, K. *Z. Anorg. Allg. Chem.* **1987,** 553, (10), 57-63.

120. Morgan, R. S.; Tatsch, C. E.; Gushard, R. H.; McAdon, J. M.; Warme, P. K. **1978,** 11, (3), 209-217.

121. Tchertanov, L.; Pascard, C. *Acta Crystallogr., Sect. B: Struct. Sci* **1996,** 52, 685-690.

122. de Hoog, P.; Gamez, P.; Driessen, W. L.; Reedijk, J. *Tetrahedron Lett.* **2002,** 43, (38), 6783-6786.

123. Gamez, P.; Reedijk, J. *Eur. J. Inorg. Chem.* **2006**, (1), 29-42.

124. Seward, C.; Jia, W. L.; Wang, R. Y.; Wang, S. *Inorg. Chem.* **2004,** 43, (3), 978-985.

125. Okabe, N.; Mizubayashi, Y.; Odoko, M. *Acta Crystallogr. Sect. E.-Struct Rep. Online* **2006,** 62, M2747-M2749.

126. Macdougall, J. J.; Nelson, J. H.; Fultz, W. C.; Burmeister, J. L.; Holt, E. M.; Alcock, N. W. *Inorg. Chim. Acta* **1982,** 63, (1), 75-83.

127. Newkome, G. R.; Frere, Y. A.; Fronczek, F. R.; Gupta, V. K. *Inorg. Chem.* **1985,** 24, (7), 1001-1006.

128. Thalladi, V. R.; Boese, R.; Brasselet, S.; Ledoux, I.; Zyss, J.; Jetti, R. K. R.; Desiraju, G. R. *Chem. Commun.* **1999**, (17), 1639-1640.

129. Gamez, P.; Mooibroek, T. J.; Teat, S. J.; Reedijk, J. *Acc. Chem. Res.* **2007,** 40, (6), 435-444.

130. Frontera, A.; Quinonero, D.; Costa, A.; Ballester, P.; Deya, P. M. *New J. Chem.* **2007,** 31, (4), 556-560.

131. Quinonero, D.; Frontera, A.; Garau, C.; Ballester, P.; Costa, A.; Deya, P. M. *ChemPhysChem* **2006,** 7, (12), 2487-2491.

132. Sakamoto, S.; Fujita, M.; Kim, K.; Yamaguchi, K. *Tetrahedron* **2000,** 56, (7), 955-964.

133. Park, S. J.; Shin, D. M.; Sakamoto, S.; Yamaguchi, K.; Chung, Y. K.; Lah, M. S.; Hong, J. I. *Chem.-Eur. J.* **2005,** 11, (1), 235-241.

134. Kaes, C.; Katz, A.; Hosseini, M. W. *Chem. Rev.* **2000,** 100, (10), 3553-3590.

135. Mukkala, V. M.; Kankare, J. J. *Helv. Chim. Acta* **1992,** 75, (5), 1578-1592.

136. Kato, M.; Sasano, K.; Kosuge, C.; Yamazaki, M.; Yano, S.; Kimura, M. *Inorg. Chem.* **1996,** 35, (1), 116-123.

137. Malkov, A. V.; Baxendale, I. R.; Bella, M.; Langer, V.; Fawcett, J.; Russell, D. R.; Mansfield, D. J.; Valko, M.; Kocovsky, P. *Organometallics* **2001,** 20, (4), 673-690.

138. Ito, K.; Tabuchi, S.; Katsuki, T. *Synlett* **1992**, (7), 575-576.

139. Parenty, A. D. C.; Song, Y. F.; Richmond, C. J.; Cronin, L. *Org. Lett.* **2007,** 9, (12), 2253-2256.

140. Parenty, A. D. C.; Guthrie, K. M.; Song, Y. F.; Smith, L. V.; Burkholder, E.; Cronin, L. *Chem. Commun.* **2006**, (11), 1194-1196.

141. Parenty, A. D. C.; Cronin, L. *Synthesis-Stuttgart* **2008**, (9), 1479-1485.

142. Wendelstorf, C.; Kramer, R. *Angew. Chem. Int. Ed.* **1997,** 36, (24), 2791-2793.

143. Kitajima, N.; Hikichi, S.; Tanaka, M.; Morooka, Y. *J. Am. Chem. Soc.* **1993,** 115, (13), 5496-5508.

144. Harada, H.; Kodera, M.; Vuckovic, G.; Matsumoto, N.; Kida, S. *Inorg. Chem.* **1991,** 30, (6), 1190-1194.

145. Maggard, P. A.; Kopf, A. L.; Stern, C. L.; Poeppelmeier, K. R. *Acta Crystallogr. Sect. C-Cryst. Struct. Commun.* **2002,** 58, M207-M209.

146. Seitz, M.; Stempfhuber, S.; Zabel, M.; Schutz, M.; Reiser, O. *Angew. Chem. Int. Ed.* **2005,** 44, (2), 242-245.

147. Mamula, O.; von Zelewsky, A.; Bark, T.; Stoeckli-Evans, H.; Neels, A.; Bernardinelli, G. *Chem.-Eur. J.* **2000,** 6, (19), 3575-3585.

148. Boyd, R. H.; Wang, C. H. *J. Am. Chem. Soc.* **1965,** 87, (3), 430-&.

149. Freeman, F. *Chem. Rev.* **1969,** 69, (5), 591-&.

150. Trotzki, R.; Hoffmann, M. M.; Ondruschka, B. *Green Chem.* **2008,** 10, (8), 873-878.

151. Mowry, D. T. *J. Am. Chem. Soc.* **1945,** 67, (7), 1050-1051.

152. Guan, X. Y.; Shi, M. *Org. Biomol. Chem.* **2008,** 6, (19), 3616-3620.

153. Yavari, I.; Mirzaei, A.; Moradi, L.; Hosseini, N. *Tetrahedron Lett.* **2008,** 49, (15), 2355-2358.

154. Ryabukhin, S. V.; Plaskon, A. S.; Volochnyuk, D. M.; Shivanyuk, A. N.; Tolmachev, A. A. *Synthesis* **2007**, (18), 2872-2886.

155. Sigalov, M.; Krief, P.; Shapiro, L.; Khodorkovsky, V. *Eur. J. Org. Chem.* **2008**, (4), 673-683.

156. Karplus, M. *J. Am. Chem. Soc.* **1963,** 85, (18), 2870-&.

157. Ahmed, M.; Vernon, J. M. *J. Chem. Soc.-Perkin Trans. 1* **1977**, (6), 601-605.

158. Hitchings, G. J.; Thomas, M. D.; Vernon, J. M. *J. Chem. Soc.-Perkin Trans. 1* **1992**, (7), 895-898.

159. Hitchings, G. J.; Vernon, J. M. *J. Chem. Soc.-Perkin Trans. 1* **1990**, (6), 1757-1763.

160. Richmond, C. J.; Parenty, A. D. C.; Song, Y. F.; Cooke, G.; Cronin, L. *J. Am. Chem. Soc.* **2008,** 130, (39), 13059-13065.

161. Armarego, W. L. F.; Perrin, D. D., *Purification of Laboratory Chemicals*. Butterworth Heinemann: Oxford, 1996.

162. Sheldrick, G. M. *Acta Crystallogr. Sect. A* **2008,** 64, 112-122.

163. Altomare, A.; Cascarano, G.; Giacovazzo, C.; Guagliardi, A. *J. Appl. Crystallogr.* **1993,** 26, 343-350.

164. Farrugia, L. J. *J. Appl. Crystallogr.* **1999,** 32, 837-838.